Control over Colloidal Particle Morphology by Dispersion Polymerization

Cover:
front: various shaped particles swimming in a fish tank backgrounded with a traditional Chinese landscape painting. These particles are present in this thesis.
back: a random-hexagonal close packed structure discussed in Chapter 8.

Control over Colloidal Particle Morphology by Dispersion Polymerization

Controle over de Morfologie van Colloïdale Deeltjes

door middel van

Dispersie Polymerisatie

(met een samenvatting in het Nederlands)

Proefschrift

ter verkrijging van de graad van doctor aan de Universiteit Utrecht op gezag van de rector magnificus, prof. Dr. G. J. Van der Zwaan, ingevolge het besluit van het college voor promoties in het openbaar te verdedigen op maandag 11 maart 2013 des middags te 2.30 uur

door

Bo Peng

geboren op 9 februari 1983 te Dezhou, P.R.China

Promotor: Prof. dr. A. van Blaaderen

Co-promotor: Dr. A. Imhof

To my grandmother Xiuzhi Jiang

Contents

1

Introduction

ABSTRACT

In this prefatory chapter, we concisely introduce colloids and their use in fundamental research and industrial applications. Then, we focus on sketching the synthesis strategy of spherical and non-spherical particles mainly by dispersion polymerization, and their behaviors in self-assembly or in the presence of an external field. We also give an outline of our experimental work described throughout the thesis. A more specialized introduction to each of the different topics is given in the subsequent research chapters.

1.1 COLLOIDS

The term colloid was coined by Graham in 1861, [1] from the Greek word for glue-like. He defined a colloid in terms of its inability to pass through a fine membrane. Actually, Overbeek [2] suggested the birth of colloid science was in the 1840s, 20 years earlier than Graham, with aggregation studies of pseudo-solutions of sulfur and silver iodide in water, by the toxicologist Francesco Selmi. [3] Later came the development of the famous gold dispersion by Faraday which can still be observed in the Royal Institution in London. [4]

Traditionally, a colloid is defined as a particle with dimensions ranging from a few nanometers to a few micrometers. The most important considerations behind this definition are that these particles are much larger than the surrounding solvent molecules, but much smaller than macroscopic objects (granular matter). The colloids in this size range experience forces from fluctuations in time in the number of collisions by solvent molecules. The intensity of bombardment varies from moment to moment on one side or other of the particle and this leads to an irregular motion of the particle through the solvent, known as Brownian motion. The discovery of this phenomenon is now attributed to Robert Brown, an English botanist, who examined pollen grains. [10] It was at first thought that the phenomenon was a characteristic only of living cells but it was soon shown to be more general and occurred with any particles as long as they were small enough. Albert Einstein [5] and William Sutherland [6] put those ideas into quantitative terms in the early 1900s and that made it possible for Jean Baptiste Perrin [7] to test the fundamental notions of the kinetic theory.

Colloids are ubiquitous in our daily life. A non-exhaustive list of fields in which colloids are involved includes, but is not restricted to, food, paints, cosmetics, detergents, inks and medical applications. [8-11] They are also frequently seen and studied in materials science, chemistry, and biology. Generally, colloidal dispersions are a class of materials, in which the kinetic units that are dispersed through the dispersion medium are very much larger than the molecules of this medium. The disperse phase and medium can be either solids, liquids, or gases. The nomenclature of various types of colloid dispersion has been given by Ostwald, [12] e.g., aerosol is defined having a gaseous dispersion medium, while the word sol, or dispersion corresponds to solid particles dispersed in a liquid dispersion medium. In this thesis, we focus on solid colloidal particles dispersed in a liquid.

As just mentioned, a system of solid particles dispersed in a liquid medium is called dispersion, and the most studied and best established examples of such solid particles are spherical inorganic silica particles [13] and polymer latexes. [14] This is mainly because of the conveniently high quantity and quality (uniform in size and distribution) of the preparation methods of such solid particles. In the 1960s, Stöber and co-workers [15] pioneeringly

introduced a method to prepare highly monodisperse spherical silica particles in the submicron range from tetraethyl orthosilicate (TEOS), in a solvent consisting of water, ammonia and an alcohol. Later, a variety of extensions based on the Stöber method flourished in this domain, for example, dispersion of silica in apolar solvents was achieved amongst many others by van Helden *et al.* [16] and Philipse *et al.*, [17] and organo- or fluorescent silica particles were successfully prepared through the incorporation of TEOS using dyes coupled to silane coupling agents by van Blaaderen *et al.* [18, 19] The further growth of silica particles, initially prepared from the Stöber method, to several micrometers, has also been extensively investigated. [20-22] For systems of polymers, there are many methods that can be used to make the polymers synthetically and these include condensation, free radical and ionic, and emulsion polymerization methods. Since this thesis concentrates on the polymer particles, the five main types of liquid-phase heterogeneous free-radical polymerizations are introduced here.

1.2 HETERGENEOUS FREE-RADICAL POLYMERIZATION

Polymer particles are prepared extensively as synthetic latexes, which are applied as binders in the industrial fields of paint, paper and inks, and as films such as adhesive and coating materials. [8, 9, 23] In general, polymer particles can be produced from nano- to micrometer size by mainly using five types of liquid-phase heterogeneous free-radical polymerizations: emulsion polymerization, microemulsion polymerization, miniemulsion polymerization, dispersion polymerization and suspension polymerization. [23, 24]

A typical emulsion polymerization formulation comprises solvent-insoluble monomer, solvent, surfactant and solvent-soluble initiator. The reaction system is characterized by emulsified monomer droplets dispersed in the continuous solvent phase with the aid of a surfactant at the very beginning of polymerization. Monomer swollen micelles may also exist in the reaction system provided that the concentration of surfactant in the dispersion medium is above its critical micelle concentration (CMC). Only a small fraction of the monomer is present in the micelles or dissolved in the dispersion medium. Most of the monomer molecules dwell in the emulsion droplets, which act as giant monomer reservoirs. The polymerization is initiated by the release of free radicals from the initiator, caused by an elevation of the temperature. Particle formation takes place via the effective capture of free radicals by micelles, which exhibit an extremely large oil-water interfacial area, compared to monomer droplets. The growth of newly born particle nuclei is achieved by molecular diffusion of monomer from monomer droplets to particle nuclei. In the end, submicron-sized latex particles are present. Note that this is also possible in the absence of a surfactant, which

gives rise to so-called emulsifier-free emulsion polymerization. In this kind of polymerization, the reaction is initiated by the thermal decomposition of initiator and the particles can grow in size via a propagation reaction with the small fraction of monomer molecules dissolved in the dispersion medium. When a critical chain length is reached, the oligomers precipitate and form a particle nucleus stabilized by the electric charges on the residue left over from the decomposition of the initiator. Then, a growth stage similar to the emulsion polymerization takes place in this system and, finally, leads to submicron sized monodisperse polymer particles. [25, 26]

One of the best definitions of microemulsions is by Danielsson and Lindman: [27] "a microemulsion is a system of water, oil and an amphiphile which is a single optically isotropic and thermodynamically stable liquid solution". In some respects, microemulsions can be considered small-scale versions of emulsions, with the droplets having a radius in the order of 5-50 nm. However, an emulsion is thermodynamically unstable, while a microemulsion is stable. This stems from one of the most fundamental properties of microemulsions, namely an ultra-low interfacial tension between the oil and water phase. A relatively large amount of surfactant is crucial to sufficiently reduce the interfacial tension. Correspondingly, the surface area increases, so that a thermodynamically stable system is formed. The three basic types of microemulsions are direct (oil dispersed in water, o/w), reversed (water dispersed in oil, w/o) and bicontinuous microemulsions. [23] Over the past two decades, free radical polymerization studies have mainly been carried out in both o/w and w/o microemulsions. The enormous number of nano-globules are loci for fast polymerization, producing microlatex particles less than 50 nm in radius.

Miniemulsion polymerization began with a single paper in 1973 by Ugelstad *et. al.* [28] Subsequently, the number of contributions in this field rose rapidly. This probably mainly relates to a specific characteristic of miniemulsion polymerization, namely that the amount of surfactant required to form a miniemulsion is comparatively small (below the CMC), which is promising both for fundamental research and industry applications. Miniemulsions are produced by high-energy homogenization, and usually yield stable and narrowly distributed droplets with a size ranging from 50 to 500 nm. Since the concentration of surfactant is below the CMC, almost no surfactant micelles are present, which leads to the subsequent polymerization only taking place in a 'confined reactor'. Based on this unique property, hybrid composites, polymer particles and functional copolymeric particles have been successfully prepared. [29, 30]

Dispersion polymerization is defined as a polymerization reaction in which the monomer is soluble, but the polymer is not. The starting reaction mixture of dispersion polymerization is a

clear, single-phased solution. The polymer begins to precipitate as it is formed and protected by a stabilizer. The stabilizer is usually a polymer that adsorbs or grafts onto the polymer that is be formed. The initial particles absorb both monomer and initiator to grow until all of the monomer has been consumed. [31] Dispersion polymerization may be regarded as a type of precipitation polymerization. It is an attractive and promising method because it results in micron-sized monodisperse polymer particles in a single batch process. Traditional dispersion polymerization involves a single-step reaction with a simple synthesis protocol in which all the reactants are mixed and heated, and often leads to particles with an exceptionally narrow size distribution. [23, 31] The preparation of uniform micron-sized polymer particles has been extensively studied, especially for polystyrene (PS) [32-34] and poly(methyl methacrylate) (PMMA). [35, 36] However, copolymerization is much more troublesome, especially copolymerization with a cross-linker. An effective way to alleviate the problems will be described in detail in chapter 2 and 4.

Suspension polymerization describes a process in which monomers, relatively insoluble in solvents, are dispersed as liquid droplets with or without steric stabilizer and vigorous stirring to produce polymer particles as a dispersed solid phase. Initiators soluble in the liquid monomer phase are employed in this polymerization. The major aim in suspension polymerization is the formation of an as uniform as possible dispersion of monomer droplets in the solvent phase with controlled coalescence of these droplets during the polymerization process. The interfacial tension, the degree of agitation, and the design of the stirrer/reactor system govern the dispersion of monomer droplets, typically with diameters in the range of 10 μm to 5 mm. [24, 37, 38]

1.3 ANISOTROPIC COLLOIDS

To date, most studies of colloids have been limited to spherical particles or particles with simple shapes, such as rods and plates, which is mainly caused by the convenient preparation methods of these particles and the uniformity of the final products in size and shape. Both rod and plate systems have been well established theoretically and experimentally. [39-43] For extending the spectrum of colloidal particles, considerable effort has been devoted to research, ranging from the anisotropic shape design to surface chemical anisotropic control. The interest in these anisotropic particles stems from their high potential in optical, electrical, and chemical applications. [44-46] For example, Li *et al.* computationally predicted that it is easier to achieve a full photonic band gap in both face-centered-cubic (*fcc*) and body-centered-cubic (*bcc*) lattices of dumbbell shaped particles than those of spherical particles. [47]

In general, three types of dumbbell-shaped particles are defined in terms of their composite materials: inorganic, [48] organic, [49] or mixed inorganic-organic particles. [50] They all take spheres as starting particles. Johnson *et al.* [48] devised a way to destabilize the silica sphere dispersion by introducing a high concentration of salt. The subsequent shell growth permanently fixed the resulting aggregates, and multiple purifications allowed separation from spheres and larger aggregates. In principle, this method can also be extended to other systems. [49] Organic dumbbell particles (usually PS) have been widely prepared through the so-called seeded over-swollen polymerization method. [50-53] By swelling cross-linked seed particles with a monomer and by a subsequent heating step, elastic stress build-up causes the excess monomer to phase separate in the form of a protrusion which can be polymerized. [50, 52, 53] Upon simply repeating the swelling-polymerization process or allowing the liquid protrusions to merge, various shaped particles were synthesized. [54-56] If the cross-linked polymer network is constructed on an inorganic core (such as a silica core, [51] or a magnetic silica core [57]) prior to the swelling and de-swelling procedure, hybrid inorganic-organic dumbbell particles are, finally, obtained by the aid of such a seeded emulsion polymerization method.

1.4 COLLOIDS AS A MODEL SYSTEM

As mentioned at the beginning of this chapter, colloid particles undergo Brownian motion due to the fluctuations in their random collisions with solvent molecules. Consequently, they exhibit a similar phase behavior as that of atoms and molecules, but the colloid particles are sufficiently large and slow to be straightforwardly observed using microscopes. [58]

Compared to conventional light microscopy, confocal microscopy is an advanced technique, which was pionneered by Marvin Minsky in 1955. [59] The main difference is that the confocal microscope contains two pinholes, one of which is placed in front of the detector to eliminate out-of-focus light, while the other is used to limit the excitation light to a diffraction limited point. [60] If micrometer sized particles are refractive index-matched with the solvent, and combined with fluorescent dyes, one can directly observe them on a single-particle level and study the behavior of even concentrated colloidal structures and dynamics by using confocal microscopy. [61-67]

The two frequently used materials for 3D confocal microscopy studies of colloids are silica and PMMA colloids, because it is relatively easy to eliminate the interference from the scattering by means of refractive index-matching between the particles and solvents. If the mass density of the particles also matches that of the solvent, the effects of gravity on the system can be limited. This is very important for some studies using large particles as building

blocks, in which the sedimentation of particles needs to be prevented or slowed. PMMA is much easier to density match than silica. [68, 69]

On the other hand, the interactions between the PMMA particles can be manipulated by means of chemical and physical modification of the particles, or by the choice of various dispersion media. For example, sterically stabilized PMMA particles that are also refractive index matched with the solvent can serve as an ideal hard-sphere model system; [70] the range of repulsive interactions for soft PMMA particle systems can be tuned by the addition of a salt; [68, 71] the addition of polymer to a colloidal suspension generally induces short-ranged attractive depletion forces. [72, 73] Moreover, the interactions between the colloidal particles can be altered by external fields such as electric fields, [68, 71, 74] magnetic fields, [75] and optical fields. [76]

1.5 SELF-ASSEMBLY OF COLLOIDAL PARTICLES IN CONFINEMENT

As previously mentioned, an emulsion can not only lead to monodisperse particles, but also can be used as a micro- or nano- reactor. For example, Manoharan *et al.* [77] introduced a novel emulsion template method to confine spherical particles in the emulsion droplets, and subsequent controlled evaporation of the emulsion droplets led to self-assembly of the polymer particles, yielding a large quantity of unique colloidal complexes. This study opened a window to a better understanding of how finite groups of spheres organize themselves at a colloidal scale. Later, Yang's group [78, 79] extended this method to a binary colloidal system – combining spherical particles on the nanometer and micrometer scales, and making use of various materials as building blocks.

This evaporation-driven self-assembly method has also been applied to prepare clusters constructed by nanoparticles. Li's group [80] contributed a paper, in which almost monodisperse clusters built by nanoparticles were obtained through the microemulsion technique. The success of microfluidics [81] suggests that the aim of crystals of crystals of nanocrystals may be reached when these techniques are combined.

1.6 OUTLINE OF THIS THESIS

The preparation of monodisperse anisotropic colloids using dispersion polymerization is highly desired, especially for PMMA system, because the convenience in density and refractive index matching with solvent makes them a good model system on the research of phase behavior at a visual scale. Constructing the polymer particles with a fluorescent dye allows the real space recording possible for these particles by using a confocal. In this thesis,

topics ranging from preparation methods to phase behavior of anisotropic particles are described in the following.

This thesis consists of nine chapters, in which the topic of how we exploit the preparation of anisotropic polymer particles is explored. The self-assembly and the behavior of these anisotropic particles in the presence of an external field is investigated as well. In chapter 2, we present a linear successive addition method of cross-linker, as well as dyes, to produce homogeneously cross-linked- or core-shell-structured fluorescent PMMA spheres in the micron size range by dispersion polymerization. [82] We show that the absence or very low concentration level of 'troublesome' reagents during the nucleation stage is crucial for successful preparation of monodisperse PMMA in a one-step dispersion polymerization in a polar medium (mixture of methanol and de-ionized water). The swelling behavior of these particles in a good solvent (Tetrahydrofuran, THF) is investigated as well. A significant feature of this chapter is that the swelling ratio increased when the addition of cross-linker was postponed. In chapter 3, we apply a variation of this method to the formation of hollow particles by using a crucial reagent DVB (divinylbenzene) at a high content (> 10 wt% based on the monomer mass). The method is quite universal, being applicable to various organic monomers (styrene, methyl methacrylate, *N*-isopropylacrylamide and a mixture of them), to diverse preparation strategies (surfactant-free emulsion, dispersion and precipitation polymerization), and to various differently shaped particles (e.g., snowman, dumbbell, hamburger shaped particles.). We also precisely controlled the thickness of the shell, and the size of both the cavities and particles. In chapter 4, we exploit variation of the cross-link morphology of lightly cross-linked PMMA particles (< 5 wt% based on the monomer mass) to prepare dimpled and rough particles with dispersion polymerization. A slight change in the experimental conditions leads to a significant variation in the surface structure of the particles. A potential formation mechanism is proposed as well in this chapter.

Inspired by the key feature mentioned in chapter 2, in chapter 5 we extend the seeded emulsion polymerization method to synthesize dumbbell-shaped PMMA particles, aided by using the aforementioned core-shell cross-linked PMMA spheres, [83] while homogeneously cross-linked PMMA spheres only result in snowman-shaped particles. In chapter 6, we present an adaptation of the method in chapter 5. In order to yield multiple protrusions via the seeded emulsion polymerization technique, big (~ 2 μm in diameter), yet highly cross-linked (2 wt%) PMMA particles are used as seeds and give rise to linear trimer structured particles under optimized conditions. Moreover, variously shaped clusters that appeared during the synthesis and their reconstruction are shown in this chapter as well.

In chapter 7 and 8, we shift the research focus from synthesis to manipulation of

anisotropic particles (dumbbell or snowman shaped PMMA particles). In chapter 7, we show results, in which the asymmetric or symmetric dumbbell particles are used as components for building clusters of these particles by the evaporation-driven self-assembly method proposed by Manoharan *et al.* [77] For given values of *n* (the number of particles in cluster), the packing process is reproducible and the conformation of clusters is uniform. A series of intricate colloidal molecules [84, 85] can be prepared from not only symmetric, but also asymmetric units. Computer simulations support our results. In chapter 8, the success of transferring PVP (polyvinylpyrrolidone) stabilized dumbbell PMMA particles from a polar to an apolar solvent with the aid of a non-ionic surfactant (Span 85) results in the formation of a so-called plastic crystal, which exhibits long-ranged positional order but no orientational order. High-frequency electric fields (1MHz) are used to partially restore long-ranged order (crystallinity) to the orientation of the particles.

In chapter 9, we research the anisotropic growth of polymers (PMMA and polystyrene) on silica rods. We find that the combination of chemical anisotropy and the geometry of the rods influences the growth site of polymer, which only takes place at the flat tip of the rods in dispersion polymerization. The tendency of the rods to attach end-on to the polymer is used to produce porcupine-like hybrid particles, in which the rods function as a stabilizer and stick out of surface of the PMMA particles perpendicularly.

1.7 REFERENCES

[1] Graham T. *Liquid diffusion applied to analysis*. Philosophical transactions of the royal society of London, **1861**, *151*, 183-224.

[2] Overbeek, J. Th. G. *Colloidal Dispersions*, in: Goodwin, J. W. (Ed.), The Royal Society of Chemistry, London, **1983**.

[3] Selmi, F. *Nuvi Ann. Science Nature. Di Bologna 2* **1845**, *24*, 225.

[4] Faraday, M. *Phil. Trans. Roy. Soc.* **1857**, *147*, 145-181.

[5] Einstein, A. *Ann. Phys.* **1905**, *322*, 549-560.

[6] Sutherland, W. *Phil. Mag.* **1905**, *9*, 781-785.

[7] Perrin J. *Ann. Chim. Phys.* **1909**, *18*, 5-114.

[8] Caruso, F. *Colloids and Colloid Assemblies*, Wiley-VCH Verlag GmbH & Co. KGaA, Weinheim, **2004**.

[9] Xia, Y.; Gates, B.; Yin, Y.; Lu, Y. *Adv. Mater.* **2000**, *12*, 693-713.

[10] Russel, W. B.; Saville, D. A. *Colloidal dispersions*, Cambridge Univ. Press, Cambridge, **1999**.

[11] Hunter, R. J. *Foundations of colloid Science*, 2nd ed., Oxford Univ. Press, Oxford, **2001**.

[12] Ostwald, W. *Z. Phys. Chem.* (Leipzig), **1907**, *34*, 295.

[13] Iler, R. K. *The chemistry of silica*, Wiley, New York, **1979**.

[14] Piirma, I. Emulsion polymerization, Academic, New York, **1982**.

[15] Stöber, W.; Fink, A.; Bohn, E. *J. Colloid Interface Sci.* **1968**, *26*, 62-69.

[16] van Helden, A.; Jansen, J.; Vrij, A. *J. Colloid Interface Sci.* **1981**, *81*, 354-368.

[17] Philipse, A.; Vrij, A. *J. Colloid Interface Sci.* **1989**, *128*, 121-128.

[18] van Blaaderen, A.; Vrij, A. Langmuir **1992**, *8*, 2921-2931.

[19] van Blaaderen, A.; Vrij, A. *J. Colloid Interface Sci.* **1993**, *156*, 1-18.

[20] Philipse, A. PhD thesis, 1987.

[21] Bogush, G.; Zukoski-IV C. F. *J. Colloid Interface Sci.* **1991**, *142*, 1-18.

[22] Giesche, H. *J. Eur. Ceram. Soc.* **1994**, *14*, 205-214.

[23] Okubo, M. *Polymer particles*, Springer Berlin Heidelberg, New York, **2005**.

[24] Arshady, R. *Colloid Polym. Sci.* **1992**, *270*, 717-732.

[25] Gilbert, R. G. *Emulsion polymerization: A mechanistic approach*, Academic, London, **1995**.

[26] Lovell, P. A.; El-Aasser, M. S. *Emulsion polymerization and emulsion polymers*, Wiley, New York, **1997**.

[27] Danielsson, I.; Lindman, B. *Colloids Surf. A* **1981**, *3*, 391-392.

[28] Ugelstad, J.; El-Aasser M. S.; Vanderhoff, J. W. *J. Polym. Sci. Pol. Lett.* **1973**, *11*, 503-513.

[29] Landfester, K. *Angew. Chem. Int. Ed.* **2009**, *48*, 4488-4507.

[30] Mailander, V.; Landfester, K. *Biomacromolecules* **2009**, *10*, 2379-2400.

[31] Barret, K. E. J. Dispersion polymerization in organic media. Wiley, London, **1975**.

[32] Tseng, C. M.; Lu, Y. Y.; El-Aasser, M. S.; Vanderhoof, J. W. *J. Polym. Sci., Part A: Polym. Chem.* **1986**, *24*, 2995-3007.

[33] Lok, K. P.; Ober, C. K. *Can. J. Chem.* **1985**, *63*, 209-216.

[34] Paine, A. J.; Luymes, W.; McNulty, J. *Macromolecules* **1990**, *23*, 3104-3109.

[35] Shen, S.; Sudol, E. D.; El-Aasser, M. S. *J. Polym. Sci., Part A: Polym. Chem.* **1993**, *31*, 1393-1402.

[36] Shen, S.; Sudol, E. D.; El-Aasser, M. S. *J. Polym. Sci., Part A: Polym. Chem.* **1994**, *32*, 1087-1100.

[37] Brooks, B. W. *Makromol. Chem-M. Symp.* **1990**, *35-36*, 121-140.

[38] Brooks, B. W. *Chem. Eng. Technol.* **2010**, *33*, 1737-1744.

[39] Bolhuis, P.; Frenkel, D. *J. Chem. Phys.* **1997**, *106*, 666-687.

[40] Bates, M. A.; Frenkel, D. *J. Chem. Phys.* **2000**, *112*, 10034-10041.

[41] van der Kooij, F.; Kassapidou, K.; Lekkerkerker, H. N. W. *Nature*, **2000**, *406*, 868-871.

[42] Veerman, J. A. C.; Frenkel, D. *Phys. Rev. A* **1992**, *45*, 5632-5648.

[43] Kuijk, A. Ph.D. thesis, Utrecht University, **2012**.

[44] Perro, A.; Reculusa, S.; Ravaine, S.; Bourgeat-Lami, E.; Duguet, E. *J. Mater. Chem.* **2005**, *15*, 3745-3760.

[45] Glotzer, S.; Solomon, M. *Nat. Mater.* **2007**, *6*, 557-562.

[46] Yan, S.; Kim, S.; Lim, J.; Yi, G. *J. Mater. Chem.* **2008**, *18*, 2177-2190.

[47] Li, Z.; Wang, J.; Gu, B. *J. Phys. Soc. Jpn.* **1998**, *67*, 3288-3291.

[48] Johnson, P. M.; van Kats, C. M.; van Blaaderen, A. *Langmuir* **2005**, *21*, 11510-11517.

[49] Yake, A. M.; Panella, R. A.; Snyder, C. E.; Velegol, D. *Langmuir* **2006**, *22*, 9135-9141.

[50] Sheu, H. R.; El-Aasser, M. S.; Vanderhoff, J. W. *J. Polym. Sci., Part A: Polym. Chem.* **1990**, *28*, 629-651.

[51] Nagao, D.; Hashimoto, M.; Hayasaka, K.; Konno, M. *Macromol. Rapid Commun.* **2008**, *29*, 1484-1488.

[52] Mock, E. B.; De Bruyn, H.; Hawkett, B. S.; Gilbert, R. G.; Zukoski, C. F. *Langmuir* **2006**, *22*, 4037-4043.

[53] Kim, J. -W.; Larsen, R. J.; Weitz, D. A. *J. Am. Chem. Soc.* **2006**, *128*, 14374-14377.

[54] Kim, J. -W.; Larsen, R. J.; Weitz, D. A. *Adv. Mater.* **2007**, *19*, 2005-2009.

[55] Park, J. -G.; Forster, J. D.; Dufresne, E. R. *Langmuir* **2009**, *25*, 8903-8906.

[56] Kraft, D. J.; Vlug, W. S.; van Kats, C. M.; van Blaaderen, A.; Imhof, A.; Kegel, W. K. *J. Am. Chem. Soc.* **2009**, *131*, 1182-1186.

[57] Ge, J.; Hu, Y.; Zhang, T.; Yin, Y. *J. Am. Chem. Soc.* **2007**, *129*, 8975-8975.

[58] Elliot, M.; Poon, W. *Adv. Colloid Inter. Sci.* **2001**, *92*, 133-194.

[59] Minsky, M. *Scanning* **1988**, *10*, 128-138.

[60] Wilson, T. *Confocal Microscopy*, Academic Press, London, **1990**.

[61] van Blaaderen, A.; Imhof, A.; Hage, W.; Vrij, A. *Langmuir* **1992**, *8*, 1514-1517.

[62] van Blaaderen, A.; Wiltzius, P. *Science* **1995**, *270*, 1177-1179.

[63] Kegel, W.; van Blaaderen, A. *Science* **2000**, *287*, 290-293.

[64] van Blaaderen, A. *Prog. Colloid Polym. Sci.* **1997**, *104*, 59-65.

[65] Jenkins, M. C.; Egelhaaf, S. U. *Adv. Colloid Interface Sci.* **2008**, *136*, 65-92.

[66] Prasad, V.; Semwogerere, D.; Weeks, E. R. *J. Phys.: Condens. Matter* **2007**, *19*, 113102.

[67] Besseling, R.; Isa, L.; Weeks, E. R.; Poon, W. C. K. *Adv. Colloid Interface Sci.* **2009**, *146*, 1-17.

[68] Yethiraj, A.; van Blaaderen, A. *Nature* **2003**, *421*, 513-517.

[69] Royall, C. P.; Dzubiella, J.; Schmidt, M.; van Blaaderen, A. *Phys. Rev. Lett.* **2007**, *98*, 188304.

[70] van Megen, W.; Underwood, S. M. *Nature* **1993**, *362*, 616−618.

[71] Leunissen, M. P.; Christova, C. G.; Hynninen, A. P.; Royall, C. P.; Campbell, A. I.; Imhof, A.; Dijkstra, M.; van Roij, R.; van Blaaderen, A. *Nature* **2005**, *437*, 235-240.

[72] Kraft, D. J.; Ni, R.; Smallenburg, F.; Hermes, M.; Yoon, K.; Weitz, D. A.; van Blaaderen, A.; Groenewold, J.; Dijkstra, M.; Kegel, W. K. *Proc. Natl. Acad. Sci. U. S. A.* **2012**, *209*, 10787-10792.

[73] Badaire, S.; Cottin-Bizonne, C.; Stroock, A. D. *Langmuir* **2008**, *24*, 11451-11463.

[74] Leunissen, M. E.; Vutukuri, H. R.; van Blaaderen, A. *Adv. Mater.* **2009**, *21*, 3116-3120.

[75] Hu, Y.; He, L.; Yin, Y. *Angew. Chem. Int. Ed.* **2011**, *50*, 3747-3750.

[76] Ashkin, A.; Dziedzic, J. M.; Bjorkholm, J. E.; Chu, S. *Opt. Lett.* **1986**, *11*, 288-290.

[77] Manoharan, V. N.; Elsesser, M. T.; Pine, D. J. *Science* **2003**, *301*, 483-487.

[78] Cho, Y.-S.; Yi, G. -R.; Lim, J. -M.; Kim, S. -H.; Manoharan, V. N.; Pine, D. J.; Yang, S. -M. *J. Am. Chem. Soc.* **2005**, *127*, 15968-15975.

[79] Yi, G.-R.; Manoharan, V. N.; Klein, S.; Brzezinska, K. R.; Pine, D. J.; Langes, F. F.; Yang, S.-M. *Adv. Mater.* **2002**, *14*, 1137-1140.

[80] Bai, F.; Wang, D.; Huo, Z.; Chen, W.; Liu, L.; Liang, X.; Chen, C.; Wang, X.; Peng, Q.; Li, Y. *Angew. Chem. Int. Ed.* **2007**, *46*, 6650-6653.

[81] Utada, A. S.; Lorenceau, E.; Link, D. R.; Kaplan, P. D.; Stone, H. A.; Weitz, D. A. *Science* **2005**, *308*, 537-541.

[82] Peng, B.; van der Wee, E.; Imhof, A.; van Blaaderen, A. *Langmuir* **2012**, *28*, 6775-6785.

[83] Peng, B.; Vutukuri, H. R.; van Blaaderen, A.; Imhof, A. *J. Mater. Chem.* **2012**, *22*, 21901-21908.

[84] van Blaaderen, A. *Science* **2003**, *301*, 470-471.

[85] Duguet, E.; Desert, A.; Perro, A.; Ravaine, S. *Chem. Soc. Rev.* **2011**, *40*, 941-960.

2

Synthesis of Monodisperse, Highly Cross-Linked Fluorescent PMMA Particles by Dispersion Polymerization

ABSTRACT

We describe a facile method to synthesize sterically stabilized monodisperse fluorescent poly(methyl methacrylate) (PMMA) colloids in the polar solvent mixture water/methanol with either a core-shell or a homogeneously cross-linked structure, by dispersion polymerization. The particles were sterically stabilized by the polymer poly (vinylpyrrolidone) (PVP). The morphology of the particles was controlled by varying the moment at which the gradual addition of cross-linker and dye was started. The absence of these extra agents at a time when the particle nuclei formed reduced the negative effects on this important process to a minimum and produced a core-shell structure, whereas an essentially homogeneously cross-linked fluorescent polymer colloid structure could be obtained by reducing the starting time of the addition of dye and cross-linker to zero. Three different dyes were chemically incorporated into the polymer network. Such dyes are important for the use of the particles in confocal scanning laser microscopy studies aimed at characterizing concentrated dispersions quantitatively in real space. A series of PMMA particles with different sizes were obtained through the variation of the weight ratio of solvents and the content of cross-linker. Furthermore, the swelling properties of the cross-linked PMMA particles in a good solvent (tetrahydrofuran) were investigated. The particles were stable in polar solvents (water and formamide), but could also successfully be transferred to apolar solvents such as decahydronaphthalene (decalin). The PVP stabilizer also allowed the particles to be permanently bonded in flexible strings by the application of an external electric field.

2.1 INTRODUCTION

The preparation of monodisperse, spherical colloidal particles has received a great deal of attention because they can be used as model systems for studying crystallization, melting, freezing, gelation, vitrification, and the rheology of colloidal materials. For recent reviews, see ref. 1-4. If monodisperse particles of micrometer size are combined with fluorescent dyes, one can directly observe them on a single-particle level and study the behavior of even concentrated colloidal dispersions in real space to obtain insight into colloidal structures and dynamics using confocal scanning laser microscopy. [1-7] Almost all investigations on quantitative 3D confocal microscopy have been performed using either fluorescently labeled silica or sterically stabilized poly(methyl methacrylate) (PMMA) colloids. Sterically stabilized PMMA particles under refractive-index-matching conditions are a well-established hard-sphere model system. [8] The variety of possible interaction potentials has been significantly extended by controlling particle charges and the use of external electric fields, which can even be combined with index and density matching. [9, 10] The range of the repulsive interactions for even micrometer-sized particles can be varied from many times the particle diameter to almost hard-sphere-like, and by the use of external electric fields with frequencies high enough that the double-layer ions cannot follow the field; a dipolar interaction can be superimposed on the soft or hard interaction as well. [9] For many model studies that use large (micrometer-sized) particles, it is also important that the density of PMMA particles is much easier to match than that of silica. [9, 11] Although non-cross-linked PMMA particles are used often, these particles have the disadvantage that they cannot be dispersed in many solvents because the particles swell or even fall apart. In addition, there has been a particularly strong demand for highly cross-linked polymer beads in applications because they have superior heat resistance, solvent resistance, and mechanical strength to serve as spacers for display panels, electronic paper, reverse-phase high-performance liquid chromatography fillers, medical and chemical applications such as absorbents, and in polymer-supported catalysis. [12-15] Finally, spherical, often cross-linked, polymer colloids have recently regained interest for their ability to be used as the starting point for making more complex colloids. [16-21] For instance, by heating and stretching, spherical PMMA particles can be turned into ellipsoids, the interactions of which can be modified in interesting ways, giving rise to monodisperse patchy anisotropic particles. [20] PMMA particles can be turned into regular clusters by the use of an emulsion templating method (ref 21 and cited work). They have also been used for the synthesis of 2D sheets [22] and 1D strings through the application of an external electric field. [23] In addition, several groups have taken up

older methods [16] that make use of a swelling step of already-synthesized cross-linked particles with monomer for a second polymerization step that could result in many different morphologies. [16-19]

However, the preparation of sterically stabilized fluorescent and monodisperse, micrometer-sized (~1 μm) PMMA particles, preferably with core-shell morphology is still a major challenge. [24-26] So far, micrometer-sized particles could be made by the successive seeded emulsion polymerization developed by Vanderhoff [27] or the activated swelling and suspension polymerization methods developed by Ugelstad. [28] The dispersion polymerization method has received a great deal of attention over the years for the synthesis of model colloids [21, 24-26, 29-41] because of the simplicity of the process of making larger micrometer-sized spheres in one step, the fact that sterically stabilized particles can be dispersed in apolar solvents, making index and density matching a possibility, and the wide variety of monomers that can be successfully polymerized. [29]

As mentioned, dispersion polymerization is typically carried out in a nonpolar organic medium. There are many publications describing the preparation of PMMA particles in nonpolar media via dispersion polymerization; however, almost all of the sterically stabilized PMMA particles used as a colloidal model system follow the synthesis path developed by researchers at ICI and the Bristol group. [26, 30-39] It involves a somewhat difficult to reproduce, lengthy synthesis of a comb graft copolymer called PHSA-*g*-PMMA (a poly (12-hydroxystearic acid) (PHSA) graft PMMA copolymer) [26, 30] and a final locking step of the stabilizer after the dispersion polymerization in a higher-boiling alkane. Bosma *et al.* [32] synthesized fluorescently dyed monomers 2-(methyl(7-nitrobenzo[*c*][1,2,5]oxadiazol-4-yl) amino) ethyl methacrylate (also known as   4-(*N*-methyl-*N*-(methacryloyloxyethyl)-amino) -7 -nitrobenzo-2-oxa-1,3-diazol, NBD) and *N*-(9-(2-carboxy-4-(3-(4-vinylphenyl) thioureido) phenyl)-6-(diethylamino)-3*H*-xanthen-3-ylidene)-*N*-ethylethanaminium chloride (also known as (rodamine b isothiocyanate)-aminostyrene,   RAS) and copolymerized them with plain monomers to obtain fluorescent particles using this ICI/Bristol recipe. The particles were uniform in size and suitable for microscopy. Dullens *et al.* [34, 35] adopted a similar approach in which they prepared cross-linked fluorescent PMMA using ethylene glycol dimethacrylate (EGDMA) to be able to make fluorescent core-shell particles. Dullens noticed that having dye and a cross-linking agent present during particle nucleation had a negative effect on the results, and he started adding these components slowly during the synthesis. However, when the amount of cross-linker was increased to 1.5 wt% of the total monomer mass, the PMMA particles deformed into nonspherical objects. [40] This same problem is also known in the dispersion polymerization of styrene. [41] Others also made modifications to the original

recipe to try to improve several difficulties, which are the length of the total procedure, the reproducibility of making the stabilizer, the final particle size, and the fact that the fluorescent monomers degrade (bleach) at the relatively high temperature used. [26, 36-39] Several of these difficulties were also experienced by Winnik's group, [24, 25] when they tried to make fluorescent particles of polystyrene (PS) using the more polar ethanol/water solvent mixture with a stabilizer more suited to this environment: polyvinylpyrrolidone (PVP). This group found, similarly to Dullens *et al.* for the dispersion polymerization of PMMA, [34, 35] that the nucleation stage was much more sensitive to the additions of dye, cross-linker and other monomers and therefore started adding these only after nucleation was complete (which they termed two-stage dispersion polymerization).

In this chapter we describe how we adopted the more polar dispersion polymerization of PMMA [24, 25, 42] to two-stages. Through this alternative route we circumvent the difficult-to-reproduce PHSA-*graft*-PMMA copolymer as a stabilizer and obtain a sterically stabilized system that can also be used in more polar solvents. Three key features of this approach are the following: (1) By keeping the heterogeneous reagents (dye, cross-linker and comonomer) at low concentrations either during the partial or whole reaction process, the final obtained particles stay spherical and stable. (2) By starting the addition of cross-linker (EGDMA) and/or dye later during the reaction, the homogeneously cross-linked structure can be continuously changed to a core-shell cross-linked structure. We used three fluorescent monomers {2-(methyl(7-nitrobenzo[*c*][1,2,5]oxadiazol-4-yl)amino)ethyl methacrylate (NBD), *N*-(9-(2-carboxy-4-(3-(4-vinylphenyl)thioureido)phenyl)-6-(diethylamino) -3*H*-xanthen-3-ylid ene)-*N*-ethylethanaminium chloride (RAS) and 7-(diethylamino) -2-oxo-*N*-(4-vinylphenyl)- 2*H*-chromene-3-carboxamide (previously known as (7-(diethylamino)-coumarin-3-carboxylic acid)-aminostyrene, CAS)} whose chemical structures are shown in Scheme 2.1. (3) The size of the PMMA particles could be controlled in the micrometer range by varying the ratio of polar solvents or the high concentration of cross-linker. Moreover, we also explored the properties of the resulting cross-linked particles in good solvent tetrahydrofuran (THF), and thanks to the fluorescent dyes incorporated into the polymer network, we were able to study their internal structure by confocal scanning laser microscopy. Additionally, even although the synthesized PVP-stabilized PMMA particles are not sterically stabilized in more apolar solvents such as decalin and cyclohexyl bromide, in which most of the earlier density and index-matching earlier studies were performed, we found and describe that a recently published method of transferring such particles from a more polar environment to an apolar solvent, developed by Behrens *et al.* [35] using a nonionic surfactant, also worked for the particles described in this chapter. Finally, a recently developed method from our group [23]

that makes use of external electric fields and sterically stabilized polymer particles was used to turn the PVP-stabilized fluorescent beads into flexible strings dispersed in the polar formamide solvent.
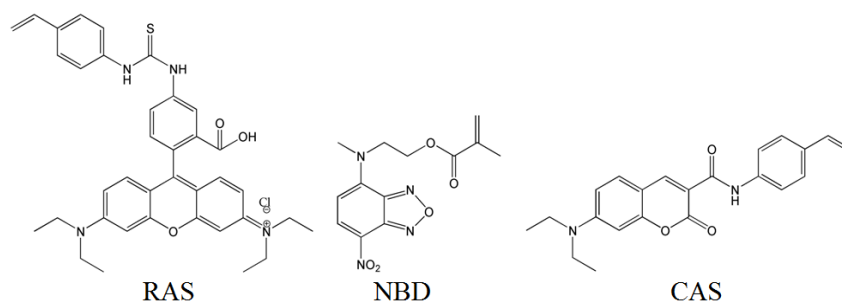
Scheme 2.1. Chemical structures of *N*-(9-(2-Carboxy-4-(3-(4-vinylphenyl)thioureido) phenyl)-6-(diethylamino)-3*H*-xanthen-3-ylidene)-*N*-ethylethanaminium chloride (RAS), 2-(Methyl(7-nitrobenzo[*c*][1,2,5]oxadiazol-4-yl)amino)ethyl methacrylate (NBD), and 7-(Diethylamino)-2-oxo-*N*-(4-vinylphenyl)-2*H*-chromene-3-carboxamide (CAS)

2.2 MATERIALS AND METHODS

2.2.1 Materials

Methyl methacrylate (MMA, Aldrich) was passed over an inhibitor removal column (Aldrich) at room temperature. After the inhibitor had been removed, MMA was stored in a refrigerator at +5 $^{\circ}$C for not longer than 1 month. Azo-bis-isobutyronitrile (AIBN, Janssen Chimica) was recrystallized from ethanol before use. Ethylene glycol dimethacrylate (EGDMA, Sigma-Aldrich) was used as the cross-linking agent. Poly (vinylpyrrolidone) (PVP, K-90, Sigma) with a molecular weight of 360000 g/mol was used as the stabilizer. Fluorescent monomers 2-(methyl(7-nitrobenzo[*c*][1,2,5] oxadiazol-4-yl)amino)ethyl methacrylate (NBD), *N*-(9-(2-carboxy-4-(3-(4-vinylphenyl)thioureido)phenyl)-6-(diethylamino)-3*H*-xanthen-3-ylid ene)-*N*-ethylethanaminium chloride (RAS), 7-(diethylamino)-2-oxo-*N*-(4-vinylphenyl)-2*H*-chromene-3-carboxamide (CAS) were prepared following the methods described by Bosma *et al.* [32] and Jones *et al.* [49] Nonionic surfactant sorbitan trioleate (span 85) was purchased from Sigma. Tetrahydrofuran (THF, Biosolve, chemical grade), methanol (Biosolve, chemical grade), pentanol (Sigma, chemical grade), hexane (Biosolve, chemical grade), formamide (Baker, analytical grade), decahydronaphthalene (mixture of *cis* and *trans*, decalin, Fluka, $\geqslant$ 98%) and cyclohexyl bromide (CHB, Fluka, chemical grade) were used as supplied. Deionized water was used in all experiments.

2.2.2 Procedure for Particle Synthesis

As mentioned, our method is an adaptation of the work of Shen *et al.* [42] and Song *et al.* [24, 25] In detail, the solvent mixture consisted of methanol and water containing 8.3 wt% PVP stabilizer. Two thirds of this mixture, all of the monomer (MMA), and all the initiator (AIBN) were placed in a 250-ml, three-necked flask equipped with a gas supply, a condenser, and a Teflon-coated stir bar. After a homogeneous solution had formed at room temperature, nitrogen was bubbled through the reaction system at room temperature for 30 min. Then, the flask was immersed in a silicon oil bath, which was maintained at 55 ^{o}C and stirred at 100 rpm. Different amounts of cross-linker (EGDMA) and fluorescent dyes were dissolved in the remaining one third of the solvent mixture. (The total volume of the solvent mixture was about 13 mL.) The mixture was fed into the reaction vessel dropwise above the reaction system at a constant rate (for example, if the total addition time was 2 h, then the addition rate of the solvent mixture was about 6.5 mL/h, and the addition rate of the dye and cross-linker can be calculated similarly) with the aid of a peristaltic pump. The addition was started after the polymerization reaction had run for a certain period of time, which is listed in Table 2.1. After the addition was complete, the reaction mixture was maintained at 55 ^{o}C for 24 h before cooling. The final particles were washed about three times with methanol using a centrifuge (Hettich Rotina 46 S centrifuge, at 315 g for 20 min) to remove the free stabilizer.

By using the same method as described above, multiple batches of fluorescent and nonfluorescent latexes were prepared. The details of these preparations are summarized in Table 2.1.

2.2.3 Characterization of the Latex Particles

To determine the size and polydispersity of the particles, static Light Scattering (SLS) was performed on highly dilute suspensions in methanol with home-built equipment using a He-Ne laser as a light source (632.8 nm, 10 mW). The logarithm of the scattering intensity was plotted against the scattering vector $k = 4\pi n \sin(\theta/2)/\lambda$, where n is the solvent refractive index, θ is the scattering angle, and λ is the wavelength in vacuum. The SLS profiles were compared with theoretical curves calculated with the full Mie solution for the scattering form factor for (polydisperse) particles with a core-shell or a homogeneous structure. [44]

Table 2.1. Details for the Highly Cross-Linked Fluorescent Latexes[a]

batch no.	1	2	3	4	5	6	7	8	9	10	11	12	13	14	15	16	17
methanol: water (wt)[b]	10:0	9:1	8:2	8:2	8:2	8:2	8:2	8:2	8:2	8:2	8:2	8:2	8:2	8:2	8:2	8:2	8:2
EGDMA (wt%)[c]	2	2	2	1	2	2	2	2	2	2	2	3	4	5	6	8	10
dye[d]	-	-	-	-	NBD	CAS	RAS	-	RAS	RAS	RAS	-	-	-	-	-	-
addition start time (h)	1.5	1.5	1.5	1.5	1.5	1.5	1.5	0	0	0.33	1	1.5	1.5	1.5	1.5	1.5	1.5
total addition time (h)	2	2	2	2	2	2	2	3.5	3.5	3.17	2.5	2	2	2	2	2	2
SLS radius (R_0) (nm)	880	630	550	625	500	540	500	430	385	430	415	550	540	515	480	530	545
SLS polydispersity (%)	5	3	6	4	5	5	5	6	8	7	7	5	5	6	5	5	5
SEM radius (R) (nm)	-	-	533	617	502	465	469	-	-	-	-	518	514	472	428	501	509
SEM polydispersity (%)	-	-	3.6	5.2	3.7	4.9	5.1	-	-	-	-	3.4	4.0	3.0	4.1	3.4	3.0
R_s (nm)	-	-	870	1060	-	-	809	-	533	618	640	845	780	746	666	705	718

[a] Other chemicals: PVP, 3 g; AIBN, 0.025 g; MMA: 2.5 g.

[b] Solvents : 30.71 g.

[c] Based on the MMA mass.

[d] RAS: 0.5 wt% based on the MMA mass. NBD and CAS did not dissolve well in the mixture of methanol, water, and cross-linker; therefore, they were dissolved in methanol first and then added to the mixture that was slowly added to the growing particles.

The radius of the PMMA particles after synthesis was first assessed by SLS in a solvent in which the particles do not swell (methanol). Subsequently, the swelling ratio was determined in THF, a good solvent for PMMA. The degree of swelling was quantified by the swelling

ratio α

$$\alpha = R_s / R_o \qquad (2.1)$$

where the particle radius in methanol (inferred from the SLS data) was taken to be R_o. R_s is the radius of swollen particles. To account for the penetration of solvent into the particles and the dissolution of the uncross-linked core in the good solvent in the case of core-shell-structured particles, an effective refractive index n_e, was used in the calculations of the form factors. n_e is a function of the swelling ratio α and the uncross-linked radius fraction of the particles β

$$\beta = R_{ou} / R_o \qquad (2.2)$$

Here, the uncross-linked core radius in methanol was taken to be R_{ou}. The effective refractive index n_e was obtained by multiplying the refractive indices of PMMA n_p, and the solvent n_s with their respective volume fractions in the swollen particles, while keeping the volume occupied by PMMA constant:

$$n_e = \frac{1}{\alpha^3}\left[n_p(1-\beta^3) + n_s\left(\alpha^3 - 1 + \beta^3\right)\right] \qquad (2.3)$$

Alternatively, distinct refractive indices were used for the core and the shell. In this model it is assumed that the uncross-linked core is completely dissolved and replaced by THF. Also, it assumes that the inner and outer radius of the shell swell by the same factor β. It can then easily be shown that the refractive index of the shell is given by:

$$n_{es} = \frac{n_p(1-\beta^3) + n_s\left[\alpha^3 - (\alpha\beta)^3 - 1 + \beta^3\right]}{\alpha^3 - (\alpha\beta)^3} \qquad (2.4)$$

Scanning electron microscopy (SEM) was done with a Philips XL30FEG microscopy to measure the size of the particles and their polydispersity. The samples were prepared by placing a drop of dispersion on a grid and allowing the solvent to evaporate at room temperature. The samples then were sputter-coated with a layer of gold (Au) of about 5 nm. A number-averaged particle radius (R) and its standard deviation (σ) were calculated on the basis of the surface area of the spheres (more than 100 particles have been counted). The polydispersity (δ) of the colloidal systems was defined as $\delta = \sigma / R$.

Confocal scanning laser microscopy (CSLM) was used to help assess the particle morphology of the fluorescently labeled PMMA particles in real space. To change the solvent, a small amount of particles (about 0.01 g) was sedimentated by using a Beckman Coulter Spinchron centrifuge, and the supernatant was removed. We modified the transfer approach from Espinosa *et al.* [43] In brief, the PMMA particles were first transferred from

methanol/water to pentanol as the intermediate solvent and then further to a solvent of span 85 (50 mM) in decalin or CHB. If we dispersed the PMMA particles into apolar solvent (decalin or CHB) without span 85, then the particles aggregated immediately. After this procedure had been repeated for the fourth time, the solvent was considered to be completely changed. The sample was put into a small vial (contents ~1 mL). To be able to use the cell in a CSLM setup, the bottom of the vial was removed and replaced with a thin cover glass, which was glued to the vial using epoxy glue. A Nikon confocal scanning laser scan head (Nikon C1) was operated in fluorescent mode on a Leica (DM IRB) inverted microscope. Measurements were performed with a Leica 63 × oil confocal immersion lens with a numerical aperture of 1.4. The fluorescent particles were excited at around 543 nm (RAS), 488 nm (NBD), and 408 nm (CAS), and their images were observed at emission wavelengths of around 605 nm (RAS), 515 nm (NBD), and 450 nm (CAS), respectively.

To prepare flexible strings, a rectangular sample cell consisting of a 0.1 mm × 1.0 mm capillary (VitroCom, U.K.) with two 50-μm-thick nickel alloy wires (Goodfellow, U.K.) threaded along the side walls was used, as mentioned in our previous work. [23] To be brief, the suspension containing fluorescent core-shell particles was separated from the mixture of methanol and water by a centrifuge and dispersed in formamide through sonication. The resulting solid content of particles was about 0.5 wt%. Then, the two ends of the cell were sealed using no. 68 UV-curing optical adhesive (Norland) under a UV lamp. Subsequently, a 75 V root-mean-square sinusoidal signal with a frequency of 1 MHz was applied for 2 h. Before the electric field was turned off, a thermal annealing process was carried out by using a stream of hot air (about 70-75 $^{\circ}$C) that was much wider than the sample cell, lasting 2 min.

2.3 RESULTS AND DISCUSSION

2.3.1 Synthesis of Cross-Linked, Fluorescent PMMA Particles

Highly cross-linked, fluorescent PMMA particles were successfully fabricated by slowly feeding the cross-linker into the reaction vessel after the dispersion polymerization of the monomer had started. Before describing our results in more detail, we first give a brief recap of the generally accepted formation mechanism of particles in dispersion polymerization that is based on the original work of Barrett [29] and others and as represented in Figure 1. At the beginning of the process, monomer, stabilizer, and initiator are present homogeneously in the medium. After being hearted, the initiator decomposes, and the free radicals liberated start to react with monomers to form oligomer radicals. When these reach a critical chain length, the oligomers precipitate to form primary nuclei, which adsorb stabilizer on their surfaces. If a

cross-linker and/or a dye is added at the beginning at a relatively low concentration (typically less than 0.5 wt%), this does not have a significant negative effect on nucleation. Fairly soon after the first nuclei appear, the monomer, dye monomer, and cross-linker are incorporated from the continuous phase onto/into existing particles only and nucleation stops. From this stage on, polymerization mainly takes place within the monomer-swollen particles until all of the monomer has been consumed. By timing the start of the additions during the growth stage, core-shell structures can be obtained without too much interference from both the final particle size and the polydispersity.

Different reaction conditions and starting times of the addition were tried, as summarized in Table 2.1. At first, two kinds of polar solvents, ethanol and methanol, were used. It was found that the reaction did not yield particles when pure ethanol was used as the solvent, probably because the poly(methyl methacrylate) does not reach the critical chain length to precipitate from the ethanol to form nuclei. To remedy this, a poor solvent for PMMA (20 wt%)was introduced into the system to shorten the critical chain length at which the precipitation of PMMA occurs. Unfortunately, a dispersion of particles with a broad size
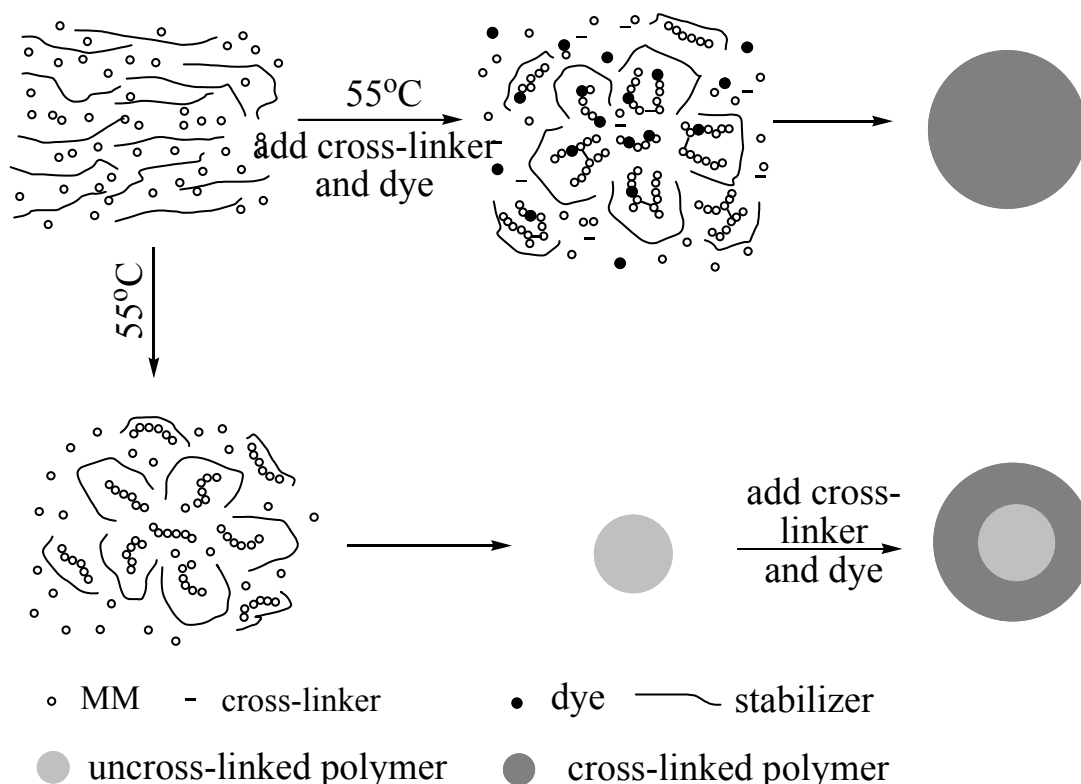
Figure 2.1. Schematic diagram proposed for homogeneous and core-shell cross- linked particle formation and growth in the dispersion polymerization of methyl methacrylate.

distribution was obtained. Therefore, we modified the method, which was put forward by Shen *et al.* [42] using methanol as solvent, AIBN as the initiator, PVP (K-90) as the stabilizer.

In Shen's case, when the concentration of cross-linker was below 0.3 wt% on the basis of the monomer, spherical particles with a low polydispersity were obtained, but on further increasing the concentration of cross-linker, partial flocculation of the dispersion took place, and total flocculation was observed at 0.6 wt%. Various other research groups have also found that when they added cross-linker, or even a dye, to a dispersion polymerization recipe in which all the ingredients were added at the beginning, poor results were obtained. [34, 35, 41, 45, 46] The final particle size was affected significantly, the size distribution became much broader, and sometimes coagulation occurred. We encountered similar difficulties when we added a small amount of cross-linker to the reaction. For example, although the addition of less than 0.3 wt% cross-linker (EGDMA) to a traditional one-step dispersion polymerization of MMA in methanol led to PMMA particles that were spherical and uniform in size, a larger amount of cross-linker (1 wt%) led to polydisperse particles. Fluorescent dyes had a similar negative effect; we even observed that dyes could inhibit the dispersion polymerization altogether if added at the beginning of the reaction. The same phenomenon was described by Horak. [47] Therefore, we adapted the methodology used by Dullens *et al.* [34, 35] and Song *et al.* [24, 25] to try not to affect the nucleation stage of our dispersion polymerization and to determine if, in our case, the particle growth stage would be more robust. Moreover, by changing the addition start time we obtained monodisperse core-shell or homogeneously cross-linked fluorescent PMMA particles, as we will show in the following text.
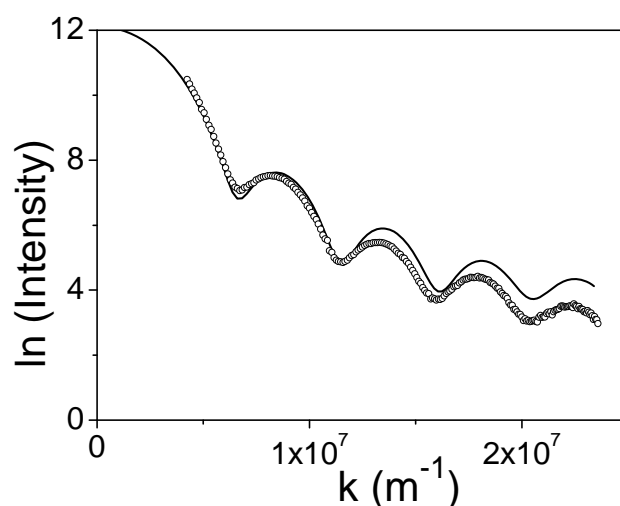
Figure 2.2. Static light scattering data (open circles) and theoretical curve (solid line) of batch 4 (having a core-shell cross-linked structure with 1 wt% cross-link density) measured in methanol. The curve was calculated using Mie theory (625 nm radius and 4% polydispersity).
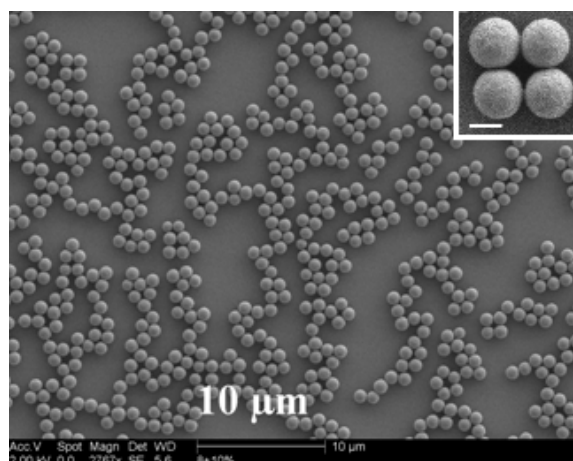
Figure 2.3. SEM image of batch 17 (having a core-shell structure with a 10 wt% cross-link density). The scale bar in the main image is 10 μm, and that in the inset is 500 nm (509 nm radius with 3% polydispersity).

Indeed, this methodology produced good results. Figure 2.2 shows an experimental SLS curve together with a calculated curve using the quoted parameters that we obtained for batch 4 with a cross-link density of 1 wt%. The locations of the minima and maxima on the *k*-axis depend sensitively on the particle size, whereas the depth of the minima gives an estimate of the polydispersity. Using the refractive index of PMMA (1.49), we find a particle radius of 625 nm. The deep minima indicate a small polydispersity of 4.0% (or lower). A convenient method of obtaining direct information about the particle shape, size, and polydispersity is scanning electron microscopy. In Figure 2.3a, an SEM image of batch 17 with a cross-link density of 10 wt% is given. The polydispersity of sample 17 is 3.0% as determined by SEM, confirming that the particles indeed maintain a uniform size even when highly cross-linked. It is obvious from Table 1 that both the particle size and polydispersity obtained by SEM are slightly smaller than those obtained by SLS. This is because particles tend to shrink in vacuum (SEM) whereas multiple scattering and background scattering tend to reduce the depth of the scattering minima, leading to a polydispersity that is slightly overestimated.

2.3.2 Core-shell or Homogeneous Structure

To find the optimal addition start time and total addition time, we first measured the growth stage of particles in time. During the synthesis of batch 3, addition was started at 1.5 h and samples were taken from the reaction flask at intervals. The samples were quenched in a large amount of room temperature methanol to prevent the further growth of particles. Subsequently, SLS was used to obtain the radii of the particles after different reaction times. The detailed data are shown in Figure 2.4. It is observed that after 3.5 h about 82% of the final radius is reached. After 5 h, more than 92% of the final radius is reached. Because of the delay between

cross-linker addition and its becoming part of the particles, we chose 3.5 h as the point at which the addition was finished for all preparation. In this way, cross-linker was present during a significant part of particle growth but not during particle nucleation.

As just mentioned, to avoid disturbing the nucleation stage, the second solution containing cross-linker and dye was added to the reaction flask after the reaction had run for 1.5 h. Some as-synthesized PMMA particles are shown in Figure 2.5. The inset images in Figure 2.5 a-c show confocal microscopy images of particles dispersed in methanol, which are labeled by RAS, CAS, NBD, respectively, and cross-linked at 2 wt%. The corresponding SEM images are also shown in Figure 2.5 (a-c). It is clearly seen that the particles are uniform and fluorescent. The radii of the particles were in the range from 540 to 500 nm, which is slightly smaller than particles without dye (batch 3). It is indeed a strong indication that the nucleation stage has finished after the reaction has run for 1.5 h. This is also seen by comparing batches 8 and 9, where addition was started at the beginning. This shows that even very small amounts of dye can have a serious effect on the nucleation phase of free-radical polymerization. [47] On close inspection of Figure 2.5a, it appears that the dye is inhomogeneously dispersed in the PMMA particles, being more concentrated in an outer shell. To observe this more clearly, the fluorescent particles were dispersed in cyclohexyl bromide (CHB), which almost matches the refractive index of PMMA. The result is shown in Figure 2.6a, where the core-shell structure is now clearly apparent. It is to be noticed that the simple centrifugation and sonication process resulted in aggregation of the particles in this solvent (Figure 2.6a). However, Espinosa *et al.* [43] proposed an intriguing set of steps to transfer particles stable in polar solvents such as water to apolar solvents like hexane where they are charge-stabilized by surfactant span 85. We used and adapted their method to transfer our particles as charged-stabilized systems in decalin and CHB; results of colloidal crystals with a lattice spacing larger than the particle size are clearly visible in Figure 2.6c. By reducing the addition start time from 1.5 to 1 h and then to 20 min (batches 11 and 10) after starting the reaction (always keeping the end of the total addition time fixed at 3.5 h), the fluorescent shell became thicker. Unfortunately, we were not able to measure the exact thickness of the shell because the resolution of confocal microscopy (roughly 250 nm in the plane and 500 nm along the optical axis) is not sufficient for this. However, it is clear that the dye gets incorporated into the shell that grows around the particles only from the moment that the addition is started. Because the cross-linker was added along with the dye, it stands to reason that it was also incorporated into a shell. Nevertheless, we found that it is still possible to produce homogeneously cross-linked dyed particles by reducing the addition start time all the way to zero (batch 9, see Figure 2.6b). To observe the detailed fluorescent structure of batch 9,

we dropped the diluted particle suspension onto a thin glass slide and let it dry at room temperature and then covered it with a refractive-index-matching solvent (CHB), as shown in Figure 2.6b. Because of the slow feed, the concentrations of cross-linker and dye present at the time of nucleation were too low to disturb the formation of uniform particles polydispersity, but the number of nuclei and therefore the final size were already reduced significantly.
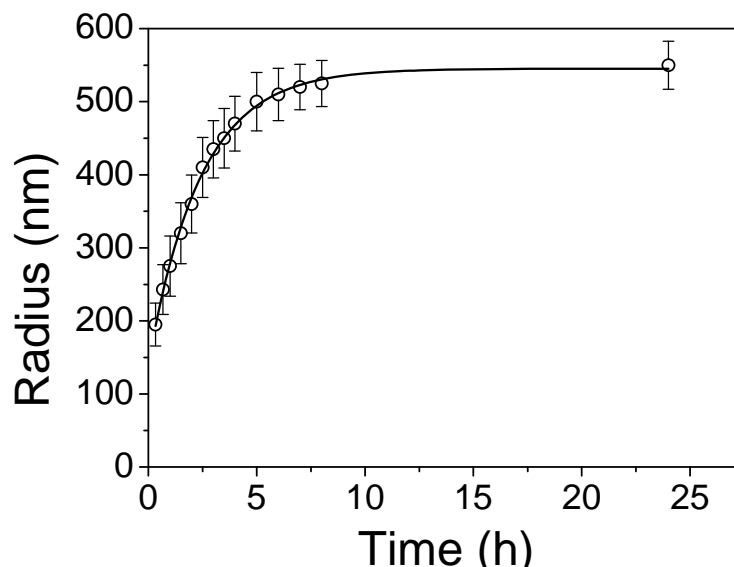

Figure 2.4. Radius of particles in batch 3 (having the core-shell cross-linked structure with a 2% cross-link density) as a function of time. Open circles are the experimental data points, and the solid line is a guide to the eye.
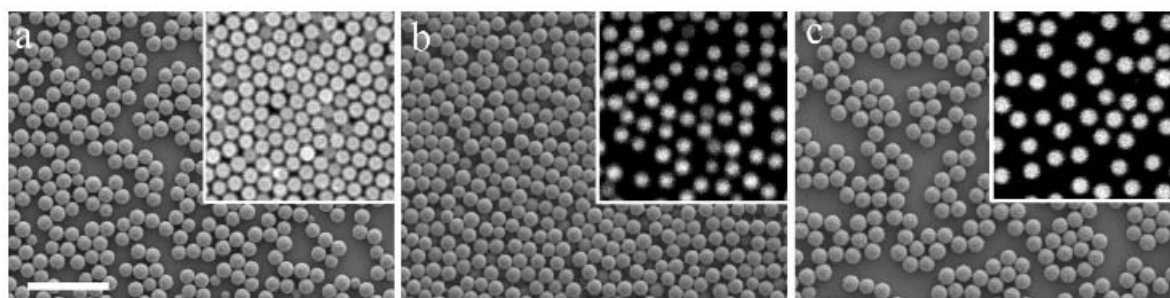
Figure 2.5. SEM and inset confocal fluorescence microscopy images of PMMA particles (having a core-shell cross-linked structure with a 2% cross-link density) labeled by different dyes in methanol. (a) RAS (batch 7, radius is 469 nm and polydispersity is 5.1%); (b) CAS (batch 6, radius is 465 nm and polydispersity is 4.9%); and (c) NBD (batch 5, radius is 502 nm and polydispersity is 3.7%). All samples were measured with SEM.   The scale bar is 5 μm and is also applicable to the confocal images.
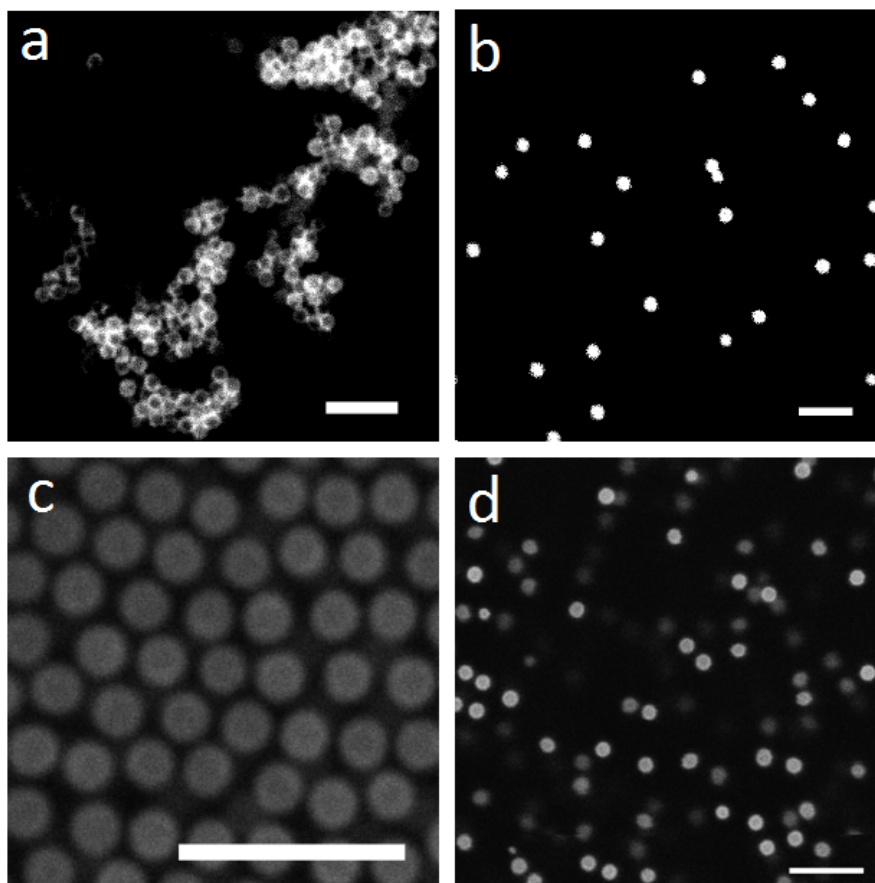
Figure 2.6. Confocal images of PMMA particles labeled by RAS in apolar solvents with different addition times of cross-linker and dye: (a) 1.5 h (batch 7; the confocal image shows that the particles were not stable when they lacked the extra surfactant in CHB); (b) 0 h (batch 9; particles were first dried on a glass slide and then immersed in CHB); (c) soft colloidal crystals made from charged PMMA particles (batch 7) in decalin (stabilized by span 85, 50 mM); (d) confocal image of dyed PMMA in CHB stabilized by span 85 (50 mM, batch 7). The scale bars are 5 μm.

2.3.3 Effect of the Cross-Linker Content

The cross-linker has a significant influence on the morphology of the PMMA particles if added at the beginning of the reaction, but after the nucleation stage has finished, it has less effect. The effects of the concentrations of EGDMA on the particle size and polydispersity can be read in Table 1. All particles had a narrow size distribution, even when the concentration of the cross-linker was increased to 10 wt% (based on the monomer), which gives the potential to fabricate more highly cross-linked fluorescent polymer particles. The open circles in Figure 2.7 show the particle radii measured with SLS as obtained for the nonfluorescent particles as a function of the EGDMA concentration. There is a clear initial tendency for the radius to decrease with increasing concentration of cross-linker. When the concentration is higher

than 6 wt%, however, the radius slightly increases again, although this is hardly significant in view of the measurement errors in the data. We believe that because the addition was started so long after the nucleation stage the number of nuclei is not affected by the cross-linker. Therefore, the final size of the particles is determined by the density of the shell and the amount of cross-linker, assuming also that the conversion of cross-linker and monomer does not change significantly. Six weight percent is apparently the turning point at which the density increase is offset by the increasing cross-linker content. [48]
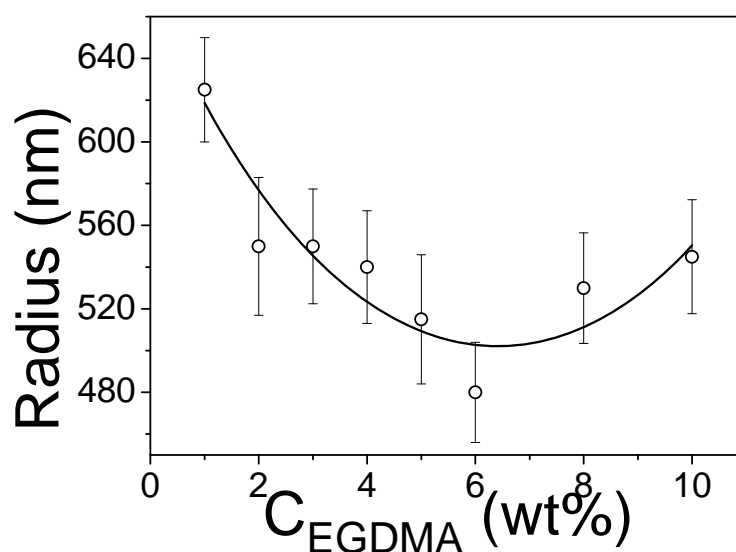
Figure 2.7. Particle radii measured with SLS of the nonfluorescent polymer particles in methanol as a function of the cross-linker concentration, C_{EGDMA}. Cross-linker addition was started after 1.5 h. The open circles are the experimental data (batches 4, 3, and 12-17), and the solid line is a guide to the eye.

2.3.4 Effect of the Ratio of the Water/Methanol Solvent Mixture

The polarity of the solvent plays an important role in the preparation of polymer particles by dispersion polymerization. Therefore, we fixed the weight ratio of monomer to the other components, such as the stabilizer, initiator, total solvent mixture, and cross-linker, and other experimental parameters and changed only the weight ratio of the solvent mixture (methanol/water). As shown in Figure 2.8, the measured SLS curves are well fit by the theoretical curves. Curves a-c in Figure 2.8 belong to as-synthesized PMMA with cross-linker content of 2 wt% prepared in solvents mixtures of 10:0, 9:1 and 8:2 (weight ratio of methanol and water), respectively. When comparing the three Mie fitting curves in a-c, one observes a shift in the minima to a higher scattering vector (k). Furthermore, the number of minima becomes smaller, implying that the as-synthesized PMMA particles become smaller with

decreasing weight ratio of methanol and water. The Mie calculations give 880, 630 and 550 nm as the particle radii. It should be noted that the filling up of the minima at low wave vectors is mainly due to some multiple scattering at small angles, which is hard to prevent for such large particles. At higher wave vectors, the minima tend to fill up mainly because of the system's polydispersity. When the water content of the solvent mixture was increased further, the system tended to become unstable and flocculated after the reaction had run for several minutes.

Because water is also a good solvent for PVP, the solubility of the latter would not be affected significantly by the presence of water, but water is a poorer solvent than methanol for PMMA. With increasing water content, the critical chain length is therefore expected to decrease, and thus the number of nuclei formed and the amount of adsorbed PVP would increase, resulting in smaller particles. With further increases in water content, the generation of more nuclei and the adsorption of more stabilizer would make it more difficult for existing particles to capture all of the nuclei and aggregates from the continuous phase before they become stable particles. Therefore, the particles tended to aggregate at some critical amount of water.
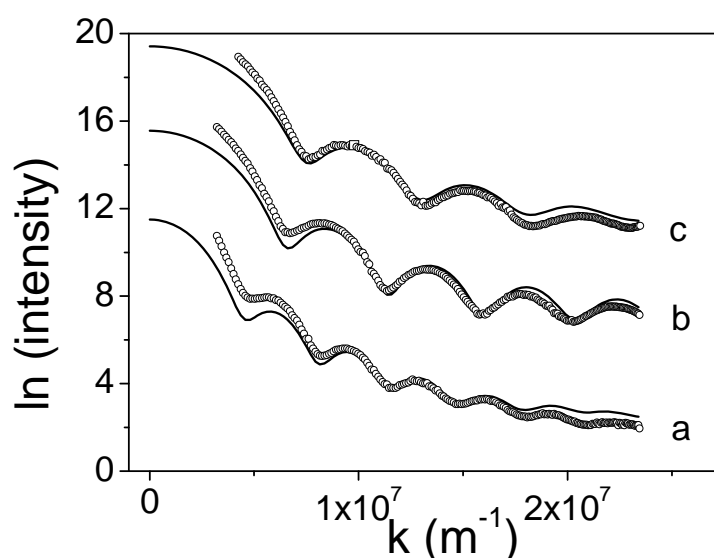
Figure 2.8. SLS experimental (open circles) and Mie theoretical (solid line) values of (a) batch 1 (radius 880 nm, polydispersity 5%), (b) batch 2 (630 nm, 3%) and (c) batch 3 (550 nm, 6%), showing the influence of the water content (0, 10 and 20 wt% correspond to curves a-c, respectively) of the solvent mixture on the particle size.

2.3.5 PMMA Particles in a Good Solvent

The cross-linking of the PMMA particles prevents their dissolution in a good solvent for PMMA such as THF. Instead, the particles merely swell. As mentioned in the Introduction,

such a swelling process performed with monomer is interesting in several schemes to arrive at more complex particles starting from cross-linked spheres. [16-19] Quantifying the swelling is therefore interesting. Particles were given 2 weeks to swell in THF to make sure they had reached their final sizes. [35] Broken and empty shells clearly show that material had exited the particle interiors in Figure 2.9a, which again confirms that the particles had a core-shell structure. The confocal image of Figure 2.9b further confirms this conclusion (We believe that the fragmentation and distortions of particle shapes shown in Figure 2.9a were partially due to drying effects; see also Figure 2.6 and 2.9b.) The size of the swollen particles was measured with SLS. To fit these data with calculated curves, we had to assume a model for the refractive indices of the core and the shell. The simplest model is to assume a homogeneous refractive index of n_e for the whole particle, as shown in equation 2.3. This will be good if the refractive index of THF-swollen PMMA is not very different from that of THF itself. It also assumes that the cross-linked shell of the particles is fully cross-linked without any un-cross-linked polymer chains and that the un-cross-linked core is fully dissolved and replaced by THF. The un-cross-linked radius fraction β in different systems was calculated on the basis of the particle growth data in Figure 2.4. The positions of the minima in Figure 2.10 show that the particles from batch 11 swelled significantly, from 415 nm in methanol to 640 nm in THF. This corresponds to a swelling factor α of 1.54, as calculated by equation 2.1. The deep minima imply that the polydispersity of the particles did not change much in the swelling process.
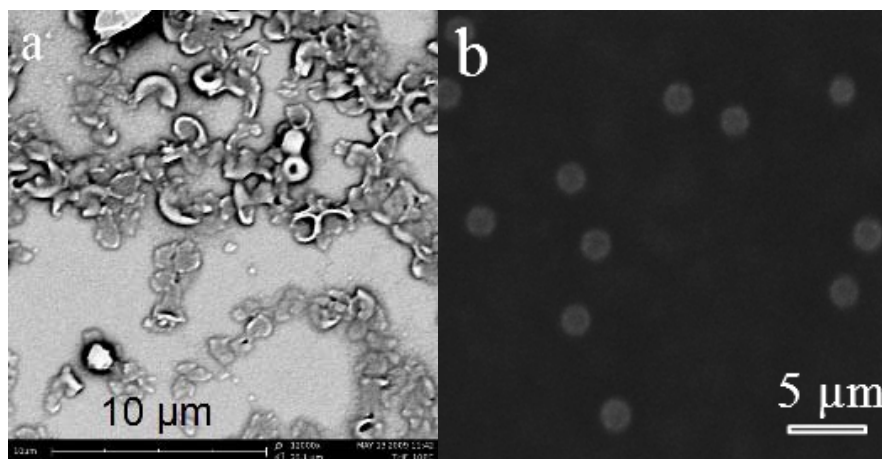
Figure 2.9. SEM and confocal images of swollen core-shell cross-linked PMMA particles (batch 7) (a) dried from THF at room temperature, as observed by SEM, and (b) in THF, as observed by confocal microscopy (20 times the averaged image).

Table 2.1 also shows the final radii of swollen PMMA particles with different cross-link densities, the addition start time, and the total addition time. For comparison, we also calculated the swelling ratios using an alternative model with different refractive indices for

the core and shell (equation 2.4). This model assumes that the inner radius of the shell increases by the same factor as the outer radius. The data are then fitted to the Mie theory for a core-shell sphere. From the fitted radius, a new swelling ratio and shell refractive index are
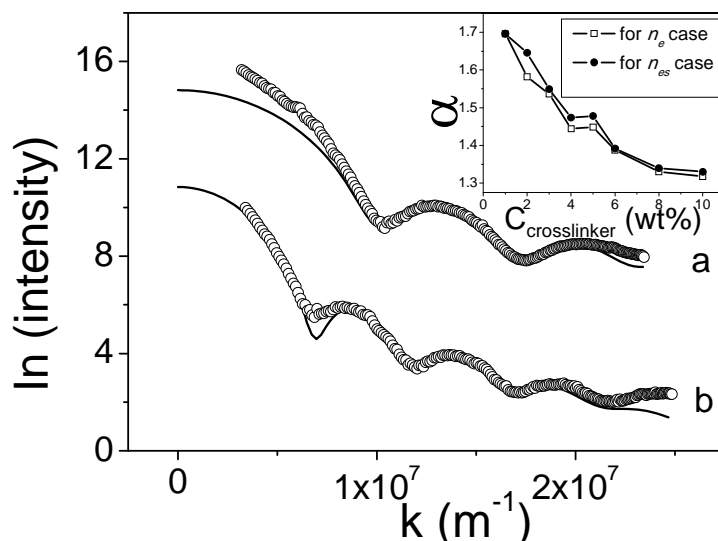

Figure 2.10. Experimental SLS data (open circles) and Mie theoretical fits (solid lines) of batch 11 in (a) methanol and (b) THF. The inset shows the swelling factor (α) as a function of the concentration of cross-linker ($C_{\text{cross-linker}}$) calculated from two models (batches 3, 4 and 12-17). The open squares are the data points from our first model mentioned in the Materials and Mathods section (equation 3), and the solid circles are our second model (equation 2.4).
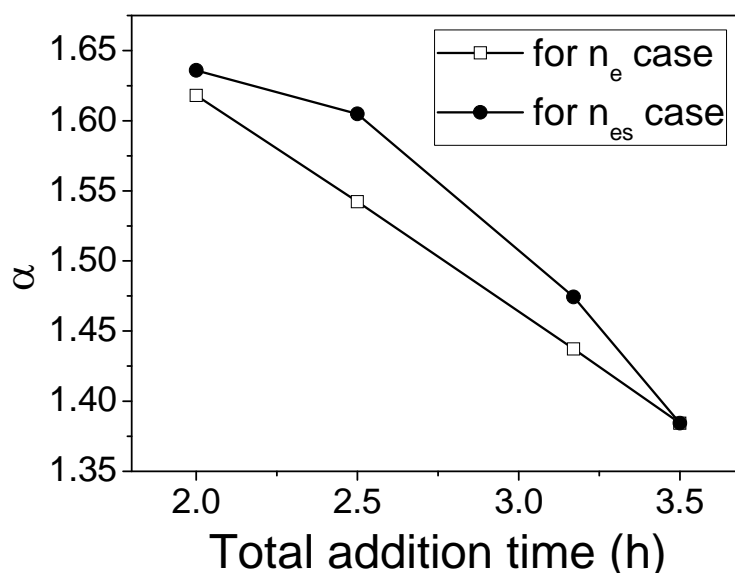
Figure 2.11. Effect of total addition time on the swelling factor α for PMMA at 2% cross-linking from two different models (batches 7 and 9-11 in Table 2.1).

calculated iteratively. The results from both models are shown in the inset of Figure 2.10. In comparing the two curves, there is not a significant difference between the two models. This is because the final effective indices of the particles are close to the refractive index of THF. It is seen that if the concentration of the cross-linker is increased then the swelling factor decreases because the rigidity of the polymer network increased (inset in Figure 2.10). Second, by fixing the cross-linker content while increasing the total addition time, we found that the swelling factor decreased (Figure 2.11). Apparently, the particles swell less if a larger portion of their volume is cross-linked. This time there is a larger difference between the two models, but both show the same trend.

2.3.6 Flexible Strings

In addition, a slightly modified procedure of a published strategy [23] was carried out in a polar solvent (formamide) by using the as-synthesized core-shell cross-linked PMMA particles (batch 7, cross-link density is 2 wt%) as building blocks. The high-frequency (1 MHz) ac electric field induced the dipole interaction of each particle without affecting the ions in the double layer and led to the assembly of the building blocks into strings. Subsequently, a thermal treatment of the strings fixed them permanently. Interestingly, the obtained strings were semiflexible, which makes these strings interesting as an experimental model system for (coarse-grained) polymer models. Details are shown in Figure 2.12.
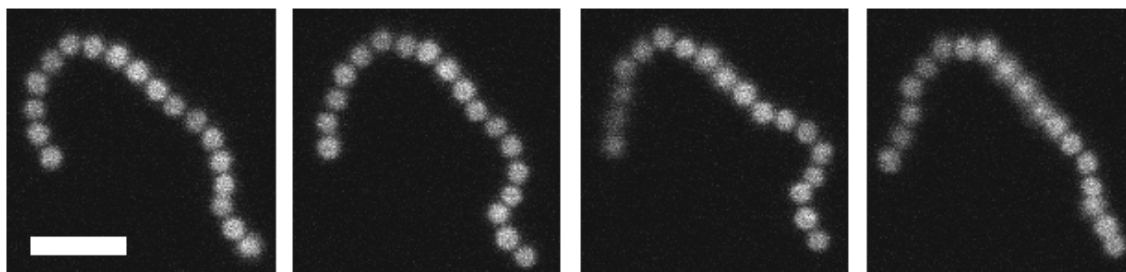
Figure 2.12. Time-lapse confocal images of semiflexible colloidal string (total recording time is about 34 s) made of core-shelled PMMA (batch 7) in formamide. The scale bar is 5 μm.

2.4 CONCLUSIONS

We described a straightforward procedure for the synthesis of monodisperse, highly cross-linked, fluorescent PMMA colloids with a core-shell or homogeneous structure. The preparation by dispersion polymerization was convenient and simple to carry out. This approach resulted in monodisperse particles ranging from submicron to micrometer size, depending on the concentration of cross-linker (EGDMA) in the range from 1 wt% to 10 wt%

with respect to the monomer (MMA) and on the weight ratio of polar solvents methanol and water. Controlling the addition start time of the cross-linker feed mixture offered a convenient way to interpolate between a heterogeneous (core-shell) to a homogeneous structure. Additionally, the cross-linked particles swelled significantly in good solvents (THF), with the swelling factor increasing with increasing addition start time or decreasing concentration of cross-linker. Moreover, the particles are sterically stabilized in more polar solvents but could nevertheless also be transferred to apolar solvents as charged-stabilized systems with double-layer thicknesses larger than the particle size. Finally, these PVP-stabilized particles could be transformed into flexible permanent strings by the application of a heating step in an external electric field. [23]

2.5 ACKNOWLEDGMENTS

2.6 REFERENCES

[1] Jenkins, M. C.; Egelhaaf, S. U. *Adv. Colloid Interface Sci.* **2008**, *136*, 65-92.

[2] Prasad, V.; Semwogerere, D.; Weeks, E. R. *J. Phys.: Condens. Matter* **2007**, *19*, 113102.

[3] Yethiraj, A. *Soft Matter* **2007**, *3*, 1099-1155.

[4] Besseling, R.; Isa, L.; Weeks, E. R.; Poon, W. C. K. *Adv. Colloid Interface Sci.* **2009**, *146*, 1-17.

[5] van Blaaderen, A. *Prog. Colloid Polym. Sci.* **1997**, *104*, 59-65.

[6] van Blaaderen, A.; Imhof, A.; Hage, W.; Vrij, A. *Langmuir* **1992**, *8*, 1514-1517.

[7] van Blaaderen, A.; Wiltzius, P. *Science* **1995**, *270*, 1177-1179.

[8] van Megen, W.; Underwood, S. M. *Nature* **1993**, *362*, 616-618.

[9] Yethiraj, A.; van Blaaderen, A. *Nature* **2003**, *421*, 513-517.

[10] Leunissen, M. P.; Christova, C. G.; Hynninen, A. P.; Royall, C. P.; Campbell, A. I.; Imhof, A.; Dijkstra, M.; van Roij, R.; van Blaaderen, A. *Nature* **2005**, *437*, 235-240.

[11] Royall, C. P.; Dzubiella, J.; Schmidt, M.; van Blaaderen, A. *Phys. Rev. Lett.* **2007**, *98*, 188304.

[12] Yu, D.; An, J. H.; Bae, J. Y.; Jung, D.; Kim, S.; Ahn, S. D.; Kang, S.; Suh, K. S. *Chem. Mater.* **2004**, *16*, 4693-4698.

[13] Ugelstad, J.; Soderberg, L.; Berge, A.; Bergstrom, J. *Nature* **1983**, *303*, 95-96.

[14] Chen, Y.; Au, J.; Kazlas, P.; Ritenour, A.; Gates, H.; Mc-Creary, M. *Nature* **2003**, *423*, 136.

[15] Comiskey, B.; Albert, J. D.; Yoshizawa, H.; Jacobson, J. *Nature* **1998**, *394*, 253-255.

[16] Sheu, H. R.; El-Aasser, M. S.; Vanderhoff, J. W. *J. Polym. Sci., Part A: Polym. Chem.* **1990**, *28*, 629-651.

[17] Mock, E. B.; De Bruyn, H.; Hawkett, B. S.; Gilbert, R. G.; Zukoski, C. F. *Langmuir* **2006**, *22*, 4037-4043.

[18] Kraft, D. J.; Vlug, W. S.; van Kats, C. M.; van Blaaderen, A.; Imhof, A.; Kegel, W. K. *J. Am. Chem. Soc.* **2009**, *131*, 1182-1186.

[19] Kim, J. -W.; Larsen, R. J.; Weitz, D. A. *J. Am. Chem. Soc.* **2006**, *128*, 14374-14377.

[20] Zhang, Z.; Pfleiderer, P.; Schofield, A. B.; Clasen, C.; Vermant, J. *J. Am. Chem. Soc.* **2011**, *133*, 392-395.

[21] Elsesser, M. T.; Hollingsworth, A. D.; Edmond, K. V.; Pine, D. J. *Langmuir* **2011**, *27*, 917-927.

[22] Leunissen, M. E.; Vutukuri, H. R.; van Blaaderen, A. *Adv. Mater.* **2009**, *21*, 3116-3120.

[23] Vutukuri, H. R.; Demirors, A.; Peng, B.; van Oostrum, P.; Imhof, A.; van Blaaderen, A. *Angew. Chem. Int. Ed.* **2002**, *51*, 11249-11253.

[24] Song, J. S.; Tronc, F.; Winnik, M. A. *J. Am. Chem. Soc.* **2004**, *126*, 6562-6563.

[25] Song, J. S.; Winnik, M. A. *Macromolecules* **2005**, *38*, 8300-8307.

[26] Elsesser, M. T.; Hollingsworth, A. D. *Langmuir* **2010**, *26*, 17989-19996.

[27] Branford, E. B.; Vanderhoff, J. W. Electron Microscopy of Monodisperse Latexes. *J. Appl. Phys.* **1955**, *26*, 864-871.

[28] Ugelstad, J.; Kaggerud, K. H.; Hansen, F. K.; Berge, A. *Makromol. Chem.* **1979**, *180*, 737-744.

[29] Barrett, K. E. J. *Dispersion Polymerization in Organic Media*; Wiley-Interscience: New York, **1975**.

[30] Antl, L.; Goodwin, J. W.; Hill, R. D.; Ottewill, R. H.; Owens, S. M.; Papworth, S.; Waters, J. A. *Colloids Surf.* **1986**, *17*, 67-78.

[31] Phan, S.-E.; Russel, W. B.; Cheng, Z.; Zhu, J.; Chaikin, P. M.; Dunsmuir, J. H.; Ottewill, R. H. *Phys. Rev. E* **1996**, *54*, 6633-6645.

[32] Bosma, G.; Pathmamanoharan, C.; de Hoog, E. H. A.; Kegel, W. K.; van Blaaderen, A.; Lekkerkerker, H. N. W. *J. Colloid Interface Sci.* **2002**, *245*, 292-300.

[33] Klein, S. M.; Manoharan, V. N.; Pine, D. J.; Lange, F. F. *Colloid Polym. Sci.* **2003**, *282*, 7–13.

[34] Dullens, R. P. A.; Claesson, M.; Derks, D.; van Blaaderen, A.; Kegel, W. K. *Langmuir* **2003**, *19*, 5963-5966.

[35] Dullens, R. P. A.; Claesson, E. M.; Kegel, W. K. *Langmuir* **2004**, *20*, 658-664.

[36] Hu, H.; Larson, G. R. *Langmuir* **2004**, *20*, 7436-7443.

[37] Hu, H.; Larson, G. R. *J. Am. Chem. Soc.* **2004**, *126*, 13894-13895.

[38] Jardine, R. S.; Bartlett, P. *Colloids Surf., A* **2002**, *211*, 127-132.

[39] Campbell, A. I.; Bartlett, P. *J. Colloid Interface Sci. 2002*, *256*, 325-330.

[40] Dullens, R. P. A; Kegel, W. K. *Phys. Rev. Lett.* **2004**, *19*, 195702.

[41] Tseng, C. M.; Lu, Y. Y.; El-Aasser, M. S.; Vanderhoff, J. W. *J. Polym. Sci., Part A: Polym. Chem.* **1986**, *24*, 2995-3007.

[42] Shen, S.; Sudol, E. D.; El-Aasser, M. S. *J. Polym. Sci., Part A: Polym. Chem.* **1993**, *31*, 1393-1402.

[43] Espinosa, C. E.; Guo, Q.; Singh, V.; Behrens, S. H. *Langmuir* **2010**, *26*, 16941-16948.

[44] Bohren, C. F.; Huffman, D. R. *Absorption and Scattering of Light by Small Particles*; John Wiley & Son: New York, **1983**.

[45] Paine, A. J.; Luymes, W.; McNulty, J. *Macromolecules* **1990**, *23*, 3104-3109.

[46] Yasuda, M.; Seki, H.; Yokoyama, H.; Ogino, H.; Ishimi, K.; Ishikawa, H. *Macromolecules* **2001**, *34*, 3261-3270.

[47] Horak, D.; Svec, F.; Frechet, J. M. J. *J. Polym. Sci., Part A: Polym. Chem.* **1995**, *33*, 2961-2968.

[48] Peebles, L. H. In *Polymer Handbook 4th ed.*; Brandrup, J.; Immergut, E. H.; Grulke, E. A.; Abe, A.; Bloch, D. R., Eds; Wiley-Interscience: New York, **1999**; Vol. 2, page II 348.

[49] Jones, II, G.; Rahman, M. A. *J. Phys. Chem.* **1994**, *98*, 13028-13037.

3

A General Approach towards Monodisperse Hollow Polymer Particles with Tunable Structures

ABSTRACT

We propose a general method to synthesize monodisperse polymer particles with hollow structures. In a typical polymerization system, the addition of a key agent divinylbenzene (DVB) is postponed to the time when the uncross-linked particles are growing rather than in the nucleation stage. By utilizing these 'pre-formed' monomer-swollen uncross-linked polymer particles as templates, the gradual feed of DVB enables the formation of cross-linked rigid shell. The polymerization induced a solidification of system, which further led to a outward shrinkage taking place. Therefore, the voids formed. Our method is applicable to surfactant-free emulsion, dispersion and precipitation polymerization in a polar environment, and a wide range of polymeric materials as well. Upon simply varying some experimental parameters (*e.g.,* the addition start time of DVB and cross-link density), both the inner and outer radii of the particles can be precisely controlled. Our method is quite simple, because hollow structured particles can be achieved in this so-called one-pot synthesis. No extra procedures of preparation or removal of templates are needed. Subsequently, we extended our method from spherical to non-spherical particle domains. Due to the incompatibility between TPM (3-(trimethoxysilyl)propyl methacrylate) modified silica and uncross-linked PMMA, adjusting either the size of the silica cores or the weight ratio between silica cores and monomer, particles ranging from snowman, dumbbell, inverted-snowman (silica core is smaller than PMMA lobe), hamburger to multi-pod like, can be successfully fabricated. This inspires us to make use of this series of non-spherical particles as templates to create unique hollow non-spherical particles. A void in the different lobes is achieved either by post nucleation addition of DVB or by hydrofluoric acid etching of silica. Given the advantages (simple, universal, tunable, robust) of our method, it has a high potential to add to a long list of desired functional materials with a site-specific character.

3.1 INTRODUCTION

A rapid increase in the number of scientific publications and patents on hollow particles in recent years reflects a considerable and growing interest from both scientific and technologic researchers in the fields of chemistry, biology, physics, optics, medicine, pharmaceutics, materials science and the paint industry, all due to their substantially different properties compared to those of solid particles in general, *e.g.*, their void interior, low density, large specific surface area stability and surface permeability. [1-6] These unique properties make hollow particles interesting for a wide range of promising applications in many fields, including in encapsulation of drugs, [7, 8] enzymes, [9] protein, [10] and genes, [11] and also in catalysis, [12, 13] chemical sensing, [14, 15] and as electrode materials, [16-18], reactors, [19, 20] and as building blocks of photonic crystals. [21] The large variety of specific physicochemical characteristics of hollow particles is directly determined by the preparation techniques. A non-exhaustive list of manners in which extensive and intensive research has been dedicated to the synthesis of hollow particles during the past century includes hard template, [12, 22-28] soft template, [29-34] and template-free methods. [16, 35-37] In spite of their impressive success, these methods either suffer from inherent disadvantages related to the high cost and tedious synthesis procedures or the difficulties in well-controlling the morphologies, monodisperisities, and scaling up the yield of the hollow particles. Ideally, one would prefer a well-controlled one-step template method for the preparation of hollow structures in a wide range of sizes. In this sense, it is highly desirable to explore simpler but more efficient and robust synthetic strategies for hollow particles synthesis. A sacrificial template method is a relatively simple and highly efficient approach in which the templates are used transiently and are also involved as a reactant in the synthetic process of the shell materials. [8, 38-43] Unfortunately, most of the sacrificial template methods focused on the specific inorganic materials via two famous ways: the Kirkendall effect [38, 44] and galvanic replacement. [39] Cases on organic polymer materials are scarce. [41-43] However, these so-called sacrificial template approaches on preparing hollow polymer particles [41-43] cannot be achieved in a single step. Hard template synthesis was necessary, prior to the preparation of the hollow spheres. Additionally, these sacrificial template strategies for polymeric materials were only restricted to specific material (polystyrene), simple template shape (spherical) and a narrow size range. A general synthesis method meeting the requirements of a broad universality, high efficiency, simplicity, flexibility and good size and shape uniformities of the obtained particles, is highly desired.

Recently, some groups have tried to enlarge the range of preparations of hollow particles

from spherical to non-spherical structures through simply applying the analogous preparation methods of hollow spheres, *e.g.,* the approaches of hard template, [17, 24, 45-49] soft template, [50, 51] and template free. [52-55] These remarkable achievements not only drove the progress in fundamental research but were also of tremendous potential in applications. Unfortunately, again, the majority of this research was devoted to inorganic materials. Few were focused on organic materials. [46-49] This may be related to many unpredictable barriers, one of which is templates refusing to be non-spherical in order to minimize the interfacial energy. Because of this, there is a lack of non-spherical templates available for synthesis. Additionally, forming a uniform coating around the surface of a non-spherical template with large variations in curvature also introduces additional challenges. Very recently, we reported a unique method for the preparation of asymmetrical dumbbell shaped hollow particles with diversely moveable cores. [49] The hard templates, which were made based on seed emulsion technique, [56-59] consisted of two interpenetrating lobes, one of which was a cross-linked seed, the other one was a newly formed protrusion. Upon silica coating and subsequent thermal treatments, a hollow structure resulted.

In this chapter, we describe a versatile approach to the synthesis of particles with a hollow structure in one step. First, the pre-formed, uncross-linked polymeric nuclei favor absorbing monomer to form a swollen polymer network. Then the postponed addition of crucial cross-linking agent DVB (divinylbenzene) induces a polymerization taking place close to the surface of the particles, forming a cross-linked rigid shell. Subsequently, the polymerization induced the solidification of monomer-swollen core materials shrinks outward, leaving an empty interior in the particles. Based on recent breakthroughs in non-spherical particle synthesis, [60-63] we extend our approach to non-spherical particles.

Key features of this approach are: (1) A broad universality of our method ranging from various organic monomers (styrene, methyl methacrylate, *N*-isopropyl acrylamide and a mixture of them) to diverse preparation strategies (surfactant-free emulsion, dispersion and precipitation polymerization); (2) By delaying the addition of the pivotal agent DVB, a hollow structure is created swiftly through the consumption of the cores as template in a one-pot batch; neither separate template production nor post process removal are necessary; (3) Through varying a series of experimental parameters, both the size of the particles and the size of their hollow cavities can be easily tailored,   and they are all monodisperse in size and shape; (4) No special care is required to prevent collapse of the shells due to the robustness of the highly cross-linked shells. Even drying them would not destroy their structures; (5) This method is not only restricted to hollow spheres, but also has a widespread use in the preparation of non-spherical particles (snowman, dumbbell, hamburger shaped particles, *etc.*)

Moreover, a larger amount of hollow particles is easily obtained by simply scaling up the reaction. We believe this flexible approach can be readily extended to fabricate other functional particles with well-controlled numbers of hollow cavities by rationally selecting materials or varying experimental environments.

3.2 MATERIALS AND METHODS

3.2.1 Chemicals

Unless mentioned otherwise, all reagents used were of reagent grade and commercially available. Methyl methacrylate (MM, Aldrich) was passed over an inhibitor removal column (Aldrich) at room temperature to remove the inhibitor, and was placed in a refrigerator at around 4 °C for no longer than one month. Styrene (Fluka) was passed through a homemade activated alumina filled column to remove the inhibitor and used immediately. *N*-isopropylacrylamide (NIPAM, 97%, Aldrich), divinylbenzene (DVB, 80%, technical grade, Aldrich), ethylene glycol dimethacrylate (EGDMA, 98%, Aldrich), methacrylic acid (MA, $\geq$ 98%, Fluka) and tetraethyl orthosilicate (TEOS, 98%, Aldrich) were used as received. Azo-bis-isobutyronitrile (AIBN, Janssen Chimica, was recrystallized from ethanol before use) and potassium peroxydisulfate (KPS, $\geq$ 99%, Sigma-Aldrich) were used as initiators. (Rhodamine b isothiocyanate)-aminostyrene (RAS) was prepared following the method described by Bosma and ourselves. [64, 65] Polyvinylpyrrolidone (PVP, K-90, Fluka) with an average molecular weight of 360,000 g/mol and PHSA-*g*-PMMA (a poly(12-hydroxystearic acid) (PHSA) grafted PMMA copolymer) were used as stabilizers for dispersion polymerization. The PHSA-*g*-PMMA stabilizer, dissolved in a mixture of ethyl acetate and butyl acetate, was homemade and its synthesis is described by Antl *et al.* [66] Hydrofluoric acid (HF, 48 wt% in H_2O, Sigmal-Aldrich) was diluted to about 5 wt% with de-ionized water before use. 1-Octanethiol (Aldrich), methanol (Biosolve), ethanol (Biosolve), hexane (Biosolve), dodecane (Sigma-Aldrich), tetrahydrofuran (THF, Biosolve) cyclohexyl bromide (CHB, Fluka), 3-(trimethoxysilyl)propyl methacrylate (TPM, Aldrich) and ammonia (NH$_3$, 29 wt% solution in water, Merck) were used as supplied. De-ionized water was used in all experiments and was obtained from a Millipore Direct-Q UV3 reverse osmosis filter apparatus.

3.2.2 Procedures for Particles Synthesis

3.2.2.1 Preparation of Hollow PMMA Spheres via Dispersion Polymerization in a Polar Solvent

The procedures for preparing micro-sized PMMA (poly (methyl methacrylate)) hollow

particles by dispersion polymerization are based on our previous recipe. [65] In detail, a solvent (34 g) of methanol containing 8.8 wt% of PVP (K-90) was prepared first. Then, two thirds of this mixture and 2.5 g of monomer (MM) containing 1 wt% (based on monomer mass) initiator (AIBN) were charged into a 250-ml three-necked flask equipped with a gas supply, a condenser, and a Teflon-coated magnetic stir bar. After approximately 2 min stirring at room temperature, a homogeneously transparent solution was obtained. Then, the reaction mixture was deoxygenated for at least 30 min by bubbling nitrogen through it. Subsequently, the flask was lowered into a silicon oil bath, maintained at 55 ^{o}C and stirred at 100 rpm. Different amounts of cross-linker (DVB) (if desired along with a dye or other kinds of monomers) were dissolved in the remaining one third of the PVP-methanol mixture. This mixture was fed into the reaction vessel dropwise at a constant rate with the help of a syringe pump. The addition was started after the polymerization reaction had run for a certain period. After the addition was complete, the reaction was maintained at 55 ^{o}C for 24 h before cooling to room temperature. The obtained particles were rinsed three times with methanol using a centrifuge (Hettich Rotina 46 S, at 315g for 20 min). By simply scaling up the reaction (*e.g.*, five times the initial quantities), a higher yield was achieved.

3.2.2.2 Preparation of Hollow PS Spheres via Dispersion Polymerization in a Polar Solvent

The fabrication procedures for hollow PS spheres are similar to those of PMMA. A homogeneously transparent mixture consisting of ethanol (25 g), PVP (1 g), styrene (2.5 g) and AIBN (0.025 g) was charged into a suitable flask, and N_2 was bubbled through the reaction system for at least 30 min to deoxygenate. Then, the temperature of the system was elevated to 65 ^{o}C for an hour, and a second homogeneously transparent mixture consisting of ethanol (12.5 g), PVP (0.5 g) and DVB (40 wt% based on the styrene mass) was fed into the reaction system at a constant rate with the aid of a syringe pump. Feeding was complete in 3 h, and the reaction was maintained for another 24 h before cooling down to room temperature. The final particles were washed about three times with ethanol by a centrifuge (Hettich Rotina 315 g, 20 min).

3.2.2.3 Preparation of Hollow PMMA Spheres via Surfactant-Free Emulsion Polymerization in Water

In a typical surfactant-free emulsion polymerization, a 250 ml flask containing a mixture of 3.5 g of MM, 0.03 g of KPS and 50 g of water was equipped with the same devices as mentioned before. The mixture was vigorously stirred and deoxygenated for about 1 h before being immersed into a silicon oil bath at a temperature of 65 ^{o}C. The reaction was maintained for 1.5 h, and then 20 wt% (based on monomer mass) of cross-linker (DVB) was charged into the reaction vessel for 2 h at a constant addition speed. After another 24 h, the flask was

removed from the oil bath, and allowed to cool down. Particles were washed three times with de-ionized water using a centrifuge (559 rpm for 30 min).

3.2.2.4 Preparation of Hollow PNIPAM Spheres via Precipitation Polymerization in Water

The DVB cross-linked hollow PNIPAM particles were synthesized by a precipitation polymerization method according to ref. [67] 1.2 g of NIPAM and 0.042 g of KPS were dissolved in 40 g of water in a flask equipped with the same devices mentioned above. This mixture was deoxygenated with nitrogen at room temperature for 30 min and then heated to 65 ^{o}C under a constant stirring at 150 rpm for about 1 h, followed by a constant addition of cross-linker (DVB, 10 wt% based on monomer mass) for 2 h. The reaction was allowed to continue for 24 h at 65 ^{o}C, and then reaction was terminated by stopping the N_2 flow. It should be noted that the resulting sample was always stored in an oven at 70 ^{o}C unless mentioned otherwise.

3.2.2.5 Preparation of Silica Core Spheres

To synthesize silica core particles, a 1 L round bottom flask was used, and first loaded with ammonia (89.3 g), ethanol (776 g) and a stir bar and vigorously stirred for a few minutes before TEOS (37.8 g) was added. The mixture was stirred overnight to allow for the reaction to complete. The silica core particles were washed in ethanol several times, and a diameter of 322 nm and polydispersity of 2.6 % was measured by using Scanning electron microscopy (SEM). The size of silica core particles could be readily increased to 661 nm by simply adopting a method originally described by Giesche. [68] A suspension consisting of as-synthesized silica core particles (about 1 g), ethanol (70 g) and ammonia (10 g) was placed in a 500 ml flask. A mixture of ethanol (70 g) and TEOS (30 g) was fed to the flask constantly in 5 h. The reaction continued overnight, and resulted in bigger silica particles with a diameter of 661 nm and polydispersity of 2.7% (determined by SEM).

To provide a good basis for PMMA to grow on, silica core particles were coated using the coupling agent 3-(trimethoxysilyl) propyl methacrylate (TPM). Typically, 0.3 g of silica core particles was dispersed in 5 ml of ethanol after which 1ml ammonia and 3 ml TPM were added, respectively. The mixture was then stirred for 30 min, at a moderate stirring rate at room temperature. After this procedure, the suspension was transferred to a 50 ml round bottom flask and vacuum distilled at room temperature to promote the condensation reaction. [68] After about 30 min, 1-2 ml bright, gel-like suspension remained at the bottom of the flask, and the distillation was stopped. This TPM grafted silica (named TPM-SiO$_2$) was purified by 3 cycles of centrifugation/re-dispersion in ethanol. The final samples were dispersed in ethanol and stored at +4 ^{o}C for no longer than a week.

3.2.2.6 Preparation of Non-Spherically Hybrid Particles in a polar solvent

In order to be able to anisotropically grow a cross-linked PMMA layer on the TPM modified silica core particles, a procedure similar to the preparation of hollow PMMA particles by dispersion polymerization was followed, except in the presence of TPM-SiO$_2$ at the beginning of the polymerization. The structure of the obtained particles mainly depended on the weight ratio between TPM-SiO$_2$ and monomer (MM), and on whether DVB was present. Note, if the coating reaction was done in the absence of DVB, no hollow structure was formed.

3.2.2.7 Preparation of Cross-linked PMMA Particles in Apolar Solvents

An experiment of comparison was carried out in an apolar solvent by dispersion polymerization. 0.07 g of initiator (AIBN) was dissolved in a mixture of 5.15 g of MM and MA (100:3 by weight), then mixed with a solvent mixture comprising hexane and dodecane (5 g, 2:1 by weight) and 0.6 g of stabilizer solution (PHSA-*g*-PMMA) in a flask. In a 5 ml syringe, 10 wt% (based on MM mass) of DVB dissolved in a mixture consisting of hexane and dodecane (2.1 g, 2:1 by weight) and 0.3 g of stabilizer solution (PHSA-*g*-PMMA) was placed. Then, the flask was given a short deoxygen process for about 2 min by using N$_2$. The subsequent heating (83 ^{o}C) led to the polymerization of the monomers. After about 30 min, the DVB mixture was fed into the flask at a constant addition rate. The feed completed in 30 min. The reaction was continued for another 3 h after which the flask was allowed to cool down. The sample was rinsed three times with hexane prior to observation.

3.2.2.8 Preparation of Hybrid Silica-PMMA Particles in Apolar Solvents

First, TPM modified silica particles (~ 0.3 g) in ethanol were sedimented in a small vial by centrifugation and the supernatant was removed. Next, 0.3 g stabilizer solution (PHSA-*g*-PMMA) was added first. After stirring for 30 min, 20 ml hexane was added, and the particles were dispersed by sonication. After the sediments had dispersed, the vial was placed in a sonicator for another minute, to ensure complete re-dispersion of all particles. Particles were then allowed to sediment under gravity overnight.

The next day the supernatant was removed, and clean hexane was added. The sample was sediment again and the supernatant was removed along with unadsorbed stabilizer. The sediment was used as cores to grow a PMMA layer. Typically, 0.05 g of stabilizer solution (PHSA-*g*-PMMA) was added to the sediment. Next, 0.05 g of initiator (AIBN) dissolved in a mixture of MM/MA (0.583 g, 100:3 by weight) was charged into the vessel. Subsequently, a solvents mixture of hexane and dodecane (0.724 g, 2:1 by weight) was added after which 0.118 g of acetone was added. This suspension was briefly sonicated to properly disperse the core particles in their new solvent. Finally, 5 μL of 1-octanethiol was added to the suspension and a constant stirring was carried out for 30 min. Then, the system was heated to 83 ^{o}C for at least 3 h before cooling down. The obtained sample was washed by centrifugation in clean

hexane at least three times.

3.2.3 Characterization

Transmission electron microscopy (TEM) was performed with a Philips Tecnai 10 (accelerating voltage ≤ 100 kV). A diluted sample suspension was deposited on a copper grid coated with a polymer membrane which had been carbon coated. The sample was allowed to dry at room temperature. The inner structure of particles could easily be observed. A number-averaged particle radius (R) and its standard deviation (σ) were calculated on the basis of the circumference of the spheres (more than 100 particles were counted). For non-spherical hollow particles these same parameters were measured manually. The polydispersity (δ) of the colloidal systems was defined as $\delta = \sigma / R$.

In order to check the surface and other characteristics (*e.g.*, the internal voids) of the hollow particles, images were obtained by using a scanning electron microscope (SEM, Philips Phenom microscope). The samples were deposited on a grid which was adhered to a SEM stub and dried at room temperature. Then they were sputter-coated with a layer of platinum (Pt) of about 5 nm.

Confocal scanning laser microscopy (CSLM) was used to help assess the morphology of the fluorescent particles. The sample was first dried on a glass slide by allowing the solvent to evaporate at room temperature, and then was covered with the refractive index matching solvent CHB.

The temperature-dependent variations of Z-average size (the average hydrodynamic particle size) of the obtained hollow PNIPAM spheres were determined by a Zetasizer Nano ZS (Malvern instruments, UK) in the temperature range from 10 ^{o}C to 40 ^{o}C. The incident wavelength was at 633 nm of a HeNe laser, and the measurement angle was 90°.

3.3 RESULTS AND DISCUSSION

3.3.1 Hollow Spheres Synthesis

Several types of highly cross-linked spherical polymer or organic-inorganic hybrid non-spherical hollow particles in a wide size range with good uniformities in shapes and sizes were successfully fabricated. The crucial step is feeding a cross-linking agent divinylbenzene (DVB) slowly into the reaction flask after the polymerization had been started for a varying period. Recently, we developed a straightforward approach towards fluorescently labeled cross-linked poly(methyl methacrylate) PMMA spherical particles in a one-pot experiment, in which EGDMA was used as cross-linker. [65] To avoid the disturbance of the polymerization

reaction it was necessary to delay the addition of cross-linker to a step in which nuclei were formed. This way, core-shell cross-linked structured PMMA particles have been prepared successfully. Inspired by this facile method, another trial for highly cross-linked PMMA particles was carried out by using DVB instead of EGDMA at a very high cross-link density level (10 wt% and higher based on the monomer MM mass). After the dispersion polymerization had run 1.5 h, a mixture of DVB and solvent comprising 8.8 wt % stabilizer (PVP) was fed into the reaction vessel gradually at a constant addition rate. Before cooling down, the particles were allowed to mature for another 24 h after completing the addition of DVB (for details, see experimental section). Surprisingly, all the monodisperse as-synthesized particles (diameter 1366 nm and polydispersity 2.1%) had a single void (772 nm in diameter and 4.3% in polydispersity), but the hollow cavity located a little bit eccentric (this will be discussed later), as shown in Figure 3.1a. To make sure that it was not simply a core-shell structure but really a hollow structure, a further confirmation was carried out by SEM observation. Results are shown in Figure 3.1b. A clear cavity is present inside broken particles, which implies that the post-addition of DVB enables PMMA particles to become hollow. It would be extremely useful if this promising one-step method could readily be applied to other polymer, yet useful materials. Therefore, we attempted to extend this method to a variety of homo- and co-polymeric materials synthesized by a variety of polymerization strategies, *e.g.,* PS (see Fig. 3.1e, dispersion polymerization), PNIPAM (see Fig. 3.1f, precipitation polymerization), and PMMA-*co*-PNIPAM (see supplementary figure 3.1, SF-3.1, dispersion polymerization). The obtained particles are all monodisperse in size and shape, and possess a single empty cavity. This implies that the generality of our method extends not only to diverse materials but also to various polymerization methods.

Note that PNIPAM is a temperature sensitive material, which can shrink and/or swell in water in response to changes in the temperature and even undergo a large volume change at a temperature of ~32 °C. This is called the volume-phase-transition temperature (VPTT) in cross-linked polymers or lower critical solution temperature (LCST) in linear polymers. [67] Upon a slight change in the temperature, it undergoes a transition from a hydrophilic structure to a hydrophobic structure. Water can be expelled from the gel matrix as a result of the disruption of hydrogen bonds and hydrophobic interactions of isopropyl groups of neighboring polymer chains. At the same time, the particles can undergo a morphological transition from a loosely swollen network to rigid spheres. In other words, at temperatures below LCST, water is a good solvent, and the spheres are highly swollen. At elevated temperatures, the solvent quality changes, and above the LCST, water is a non-solvent; this leads to the collapse of the particles. Qiang *et al.* [69] adopted a smart way to use this LCST

to synthesize hollow PNIPAM spheres via a one-pot process by a well-known precipitation polymerization in aqueous environment. The post addition of cross-linker led to a core-shell cross-linked structure. The removal of cores took place simultaneously once the temperature decreased to below LCST: The uncross-linked PNIPAM cores simply dissolved in water and only the cross-linked shell remained. To prevent this and in consideration of the LCST of PNIPAM, the as-synthesized PNIPAM particles by our method were always stored in an oven
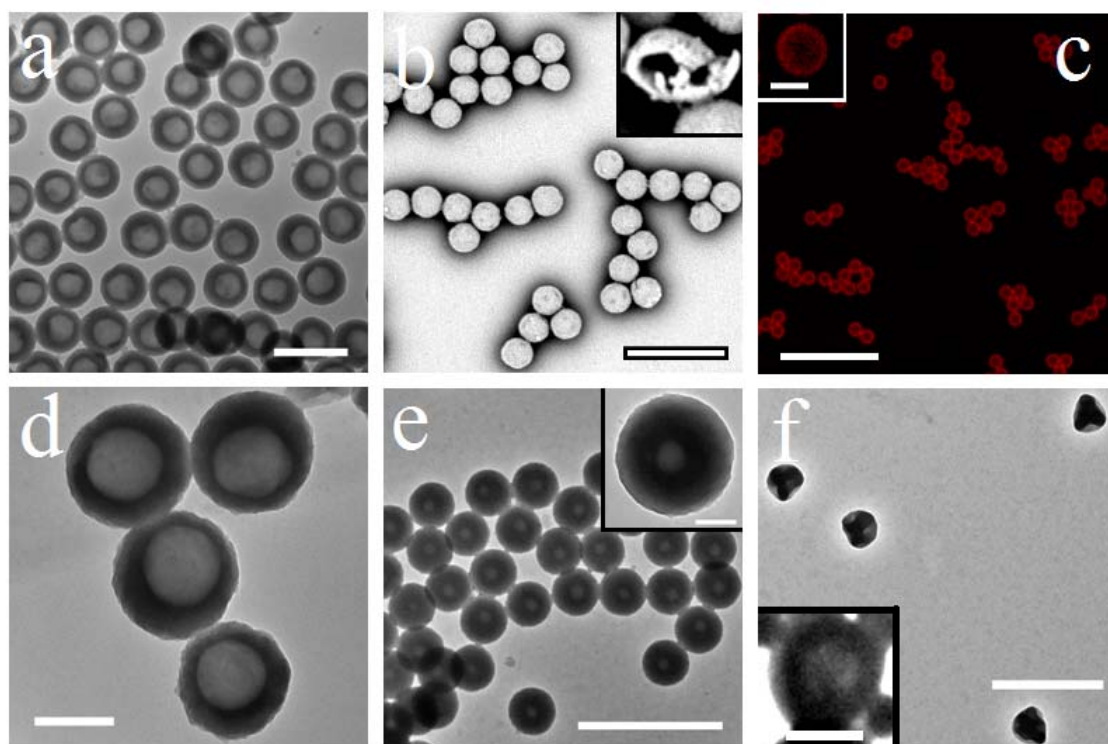
Figure 3.1. Micrographs of hollow particles a) TEM image of hollow PMMA particles made by dispersion polymerization in methanol. Cross-linker (DVB) density is 10 wt%, D_{inner} = 772 nm, PD = 4.3%, D_{outer} = 1366 nm, PD = 2.1% and the scale bar is 2 μm), b) SEM image of the same hollow PMMA particles. The inset is a broken hollow particle. The scale bar is 5 μm, c) confocal image of fluorescently labeled hollow PMMA particles in an index matching solvent (cyclohexyl bromide). The scale bar is 10 μm and the inserted one is 1 μm, d) TEM image of hollow PMMA particles made by surfactant-free emulsion polymerization in water. Cross-linker density is 20 wt%, D_{inner} = 221 nm, PD = 4.3%, D_{outer} = 361 nm, PD = 3.6% and the scale bar is 200 nm, e) TEM image of hollow PS particles made by dispersion polymerization in ethanol. Cross-linker density is 40 wt%, D_{inner} = 156 nm, PD = 3.4%, D_{outer} = 626 nm, PD = 3.4%. The scale bar is 2 μm and the inserted one is 200 nm, f) TEM image of hollow PNIPAM particles made by precipitation polymerization in water. Cross-linker density is 10 wt%, D_{outer} = 302 nm, PD = 3.7%. Due to the beam irradiation, most of the hollow PNIPAM spheres collapsed, so it is very hard to get the accurate size of the voids. The scale bar is 1 μm and the inserted one is 200 nm.

at 70 °C. Even during the preparation of samples for TEM observation, the sample loaded

grids were dried at a high temperature (~70 ^{o}C). A clear hollow architecture was observed nevertheless in TEM images, which signifies that the hollow structure of PNIPAM is not caused by the dissolution of the uncross-linked core. In addition, the hollow PNIPAM spheres exhibited a typical temperature-response, but the highly cross-linked network provoked a shift in the VPTT of the microgels (compared with the data in ref. 67) based on the normalized diameter as a function of temperature to 23 ^{o}C (see SF-3.2). Succeeding in fabricating this thermally sensitive PNIPAM is another convincing example that demonstrates that our method can be applied to both a variety of materials and a diversity of polymerization tactics.

The surfactant-free emulsion polymerization combined with our post nucleation addition of DVB was also successful in producing smaller hollow PMMA particles (in submicron size range). The obtained PMMA spheres (diameter 361 nm and polydispersity 3.6%, obtained from TEM images) indicated an clear hollow cavity (diameter 221 nm and polydispersity 4.3%), and both the particles and hollow cavities were monodisperse in size and shape (see Fig.3.1d). Combined with the previous success of micron-sized hollow PMMA particles made by dispersion polymerization, these are all strong proofs that our method is capable of preparing uniform hollow PMMA spheres in a wide size range, from sub-micron to micron scale.

If DVB was added along with a dye (RAS), fluorescent core-shell-structured particles were easily obtained, as shown in Figure 3.1c. They are monodisperse in size and shape, and the thickness of the fluorescently labeled shell is homogeneous. This is different from the previous eccentric cases (*e.g.*, Fig. 3.1a and 3.1d). The homogeneous distribution of dye among the shell sheds some light on the formation mechanism of these hollow particles. This will be discussed in detail in the next section.

3.3.2 Formation Mechanism

Insight into the formation mechanism can be obtained by sampling the reaction mixture at different times. For this we chose the preparation of hollow PMMA spheres with a cross-link density of 10 wt% via dispersion polymerization in methanol, the addition start time and total addition time were 1.5 and 2 h, respectively. Samples (~ 0.01 ml) were immediately mixed with 0.5 ml of a 'cold' (room temperature) solution (methanol) to quench the polymerization reaction. The detailed growth data of hollow cavity and particles were collected in a graph based on TEM observation as shown in Figure 3.2. Before the addition of DVB, the particles were solid with a smooth surface. When the feed of DVB was complete (at 3.5 h, see Fig.3.2-2), we observed an irregular hollow cavity in most particles. As polymerization proceeded, the shape of the hollow cavity became spherical, and their size increased. Meanwhile, the size of particles and thickness of the shell increased as well. Based on these

observations, and inspired by ref. [36, 42, 70], one can conclude that: In this system, DVB is a good solvent for uncross-linked polymer cores, and a cross-linker as well. [42, 70] As shown schematically in Figure 3.3, when DVB was added into the system, the polymerization of DVB along with monomer preferentially took place close to the particle-solvent interface and formed a rigid cross-linked shell. [69] Subsequently, the polymerization induced the attachment of monomer-swollen uncross-linked core material to the 'fixed' cross-linked particles' shell. Gradually, the monomer-swollen uncross-linked core moved from the center of the particles to the newly formed cross-linked shell together with DVB where it became immobilized, and the polymerization induced the density increase (from liquid to solid) of particles led to a outward shrinkage as well. Finally, a void was produced. In this case, we believe the DVB plays a similar role with the freezing behavior in the method mentioned in Ref. 36, in which the solidification (cause by the freezing) in the radial direction in a swollen polymer particle induced an outward shrinkage of the swollen polymer network, and finally, led to the formation of a void as well. A simple modal is set up to for our system. Assuming that the radius of particles do not change during the polymerization, while only their density changes. The radius ratio (α) of the voids (r) and particles (R) can be estimated as

$$\alpha = r/R = (1 - \rho_l / \rho_s)^{1/3} \tag{3.1}$$

where ρ_l and ρ_s are the density of liquid and solid, respectively. For PMMA system, the density increases from 0.94 g/cm^3 (ρ_{mm}) to 1.18 g/cm^3 (ρ_{PMMA}) as system polymerized (solidified). The values of α from Eq.3.1 (0.59) and from the PMMA sample (0.57) shown in Figure 3.1a agree reasonably well. Of course, the liquid-like monomer-swollen polymer cannot be ideally regarded as the pure monomer, the prefect fitting is extremely difficult. But it gives a rough impression that the shrinkage of polymer is significantly during the polymerization.

As more DVB was consumed, both the thickness and viscosity of the shell increased, all of which is expected to slow the further attachment of the uncross-linked core. Therefore, in the final stage, a core-shell-shell structure formed, consisting of a void, a swollen uncross-linked inner shell, and a cross-linked outer shell. Upon drying the particles, the swollen uncross-linked polymer piled onto the inner wall of the shell in-homogeneously, leaving a slightly eccentric cavity. The presence of some remaining uncross-linked polymer is confirmed by simply putting these hollow particles into a good solvent (THF) for a long time span (two days). Once the uncross-linked polymer chains were removed, a cross-linked shell of uniform but smaller thickness appeared (see SF-3.3, the average thickness of the shell decreased from 297 to 263.5 nm). This also indicates the hollow particles made by our method are robust against collapse even after drying from a good solvent. This process is

mainly accompanied by the polymerization induced shrinkage. DVB served as a cross-linker to anchor the cross-linked network at the surface of the particles, namely, from a rigid enough shell against collapse during the polymerization induced shrinking.
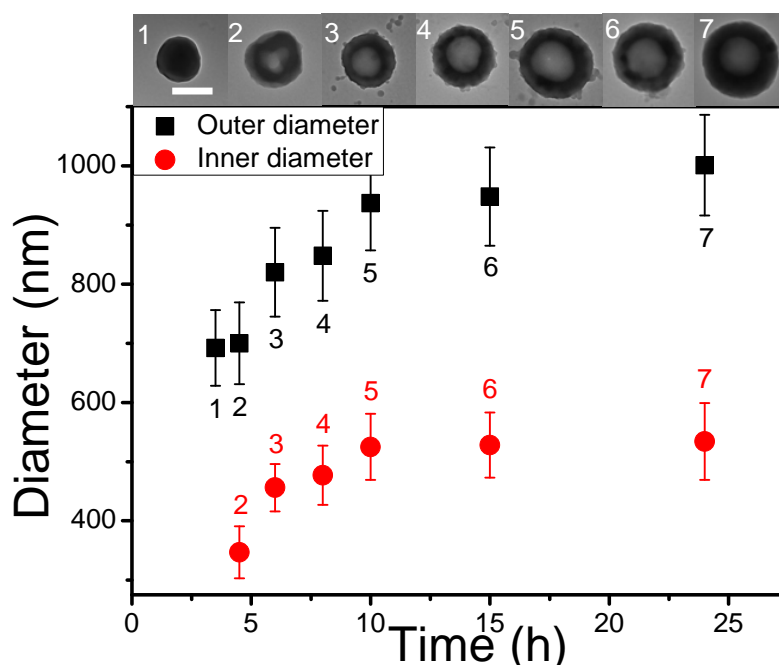
Figure 3.2. The outer and inner diameter growth and hollow cavity formation of hollow PMMA particles as a function of time. Cross-linker density is 10 wt %, addition start time and total addition time were 1.5 and 2 h, respectively. The scale bar is 500 nm.
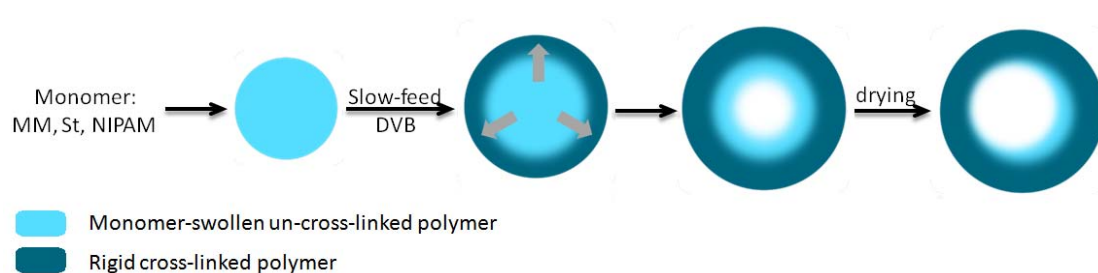
Figure 3.3. Schematic diagram of the proposed mechanism for the formation of hollow spheres in a polar environment. First, radical polymerization is started by the elevation of temperature. After a certain time, the cross-linker DVB was continuously fed into the reaction system. DVB swells the uncross-linked polymer core and co-polymerizes with the monomer at the place where is close to the surface of the particles. Gradually, a rigid cross-linked shell and a hollow void caused by the polymerization induced outward shrinkage are formed. When the resulting particles are dried, the residual uncross-linked polymer core material piles up to the inner surface of the particles, resulting in an eccentric void.

Moreover, we discovered that the formation of a void in the particles requires three essential elements. The first one is DVB, the second one is that polymerization should be

carried out in a polar solvent and the last one is that DVB needs to be added into the system after the seed particles have already partly formed. For instance, if an alternative cross-linker (EGDMA) was utilized rather than DVB in the dispersion polymerization of MM in a polar solvent (methanol), only solid particles were obtained (see SF-3.4). But interestingly, the obtained particles were non-spherical with some dents on the surface. This will be discussed elsewhere. On the other hand, if a dispersion polymerization of MM in the presence of DVB was carried out in non-polar solvents (hexane and dodecane), there were also no hollow particles (see SF-3.5). In addition, if DVB was added starting from the beginning of the polymerization, the same solid particles were obtained (see SF-3.6). Additionally, we also tried to add all DVB at once. The emulsion flocculated soon after the addition of DVB. To gain a stable hollow system, a slow feed is required.

3.3.3 Manipulation of the Sizes of the Particles and Voids

As mentioned, our method is applicable to a diversity of polymerization methods. In order to gain better understanding of our method, and obtain more control over the morphologies of these promising hollow particles, we investigated more closely system of dispersion polymerization of MM in a polar solvent (methanol). First, the growth of uncross-linked particles was monitored in time to guide the following experiments (see SF-3.7). Then, a series of batches with various addition start times of the cross-linker was carried out. The feed of mixture containing DVB was completed in 3 h in all batches. As shown in Figure 3.4A, delaying the addition time led to an increase of the relative cavity size (inner diameter/outer diameter), which can be easily explained by the growth of seed particles themselves. This also demonstrates that the size ratio of the hollow particles can be precisely controlled through simply adjusting the addition start time. According to the growth of uncross-linked plain PMMA particles (see SF-3.7), after 6 h, about 81% of the final radius is reached. Also, considering that it takes a while for DVB that is fed into the system (3 h) to become a part of the particles, we stopped further postponing the addition start time (later than 6 h).

The concentration of cross-linker plays an important role in the preparation of hollow particles. Therefore, we fixed the addition start time (1.5 h) and total addition (3 h) time, the recipe, and other experimental parameters, but only varied the amount of DVB. As shown in Figure 3.4B, the ratio of the thickness of the shell and the diameter of the particles decreases with increasing cross-link density, namely, the more cross-linker added, the thinner the shell of the resulting hollow particles. This can be explained by the formation mechanism of hollow particles, in which we proposed that the DVB could swell the polymer network. Logically, the more DVB added, the larger the swollen particle is. It directly leads to the formation of a larger hollow cavity. It is worth pointing out that when the cross-link density was higher than

40 wt% that the obtained particles would be polydisperse (see SF-3.8). Based on the results mentioned above, we believe the manipulation of hollow structures can be similarly extended to other polymerization methods, and other polymer materials as well.
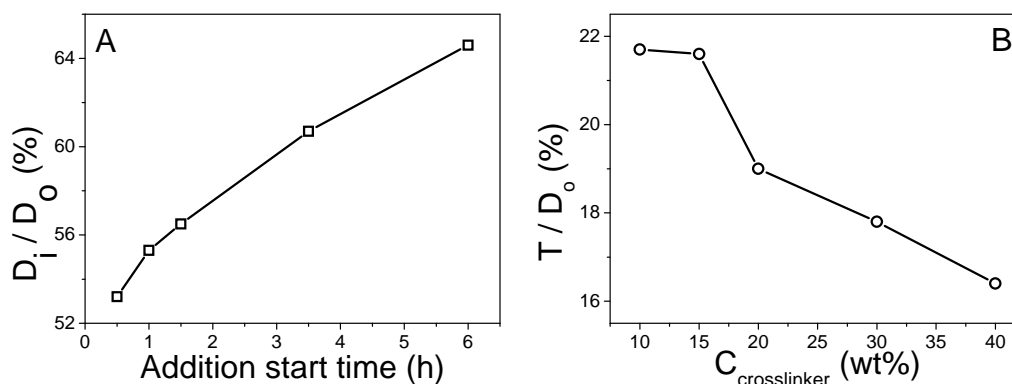
Figure 3.4. The effect of addition start time and cross-link density on the variation of hollow structures of PMMA particles, a) the ratio of inner (D_i) and outer (D_o) diameter of hollow PMMA particles as a function of addition start time (all additions finished in 3 h), b) the ratio of the thickness (T) of the shell and the size (D_o) of spheres as a function of cross-link density (based on MM mass). The addition start time and total addition time were 1.5 h and 3 h, respectively.

3.3.4 Non-Spherical Hollow Particles

Recently, Perro *et al.* [60-63] developed a unique approach for preparing non-spherical hybrid (PS-silica) particles. They consisted of one or more PS bulbs attached to a central silica particle. The morphology of these particles can be tuned from multipod-like to snowman-like. Here, we adapted this method and extended it to a PMMA-silica system. In the first system, small TPM modified silica (TPM-SiO$_2$) spheres with a diameter of 322 nm were used as cores (see SF-3.9). A PMMA layer was subsequently grown on them via a typical dispersion polymerization in methanol. Due to the incomplete wetting between the PMMA phase and TPM-SiO$_2$ spheres, the PMMA only partly engulfed the silica. Results are shown in Figure 3.5d. In a hybrid particle system, as shown in Figure 3.5d, the dark area is an original TPM-SiO$_2$ core, while the lighter area is the newly-formed PMMA. If the DVB is only added after the polymerization has run for 1.5 h, a void appeared in the PMMA. By simply adjusting the weight ratio between the monomer (MM) and silica cores, the size of the cavities could be readily tailored (see Fig. 3.5a-c). An interesting observation is made by comparing the particle in Figure 3.5b with those in Figure 3.5d. In the latter case, all conditions were the same except that DVB was not added. The silica clearly sticks out of the PMMA. However, if DVB was post-added to create a cavity the cross-linked polymer layer covered the silica (Fig. 3.5b), so that the silica appears to be attached to the cavity. Apparently, a secondary function of the

DVB is to immobilize the uncross-linked polymer onto the silica surface. Upon close
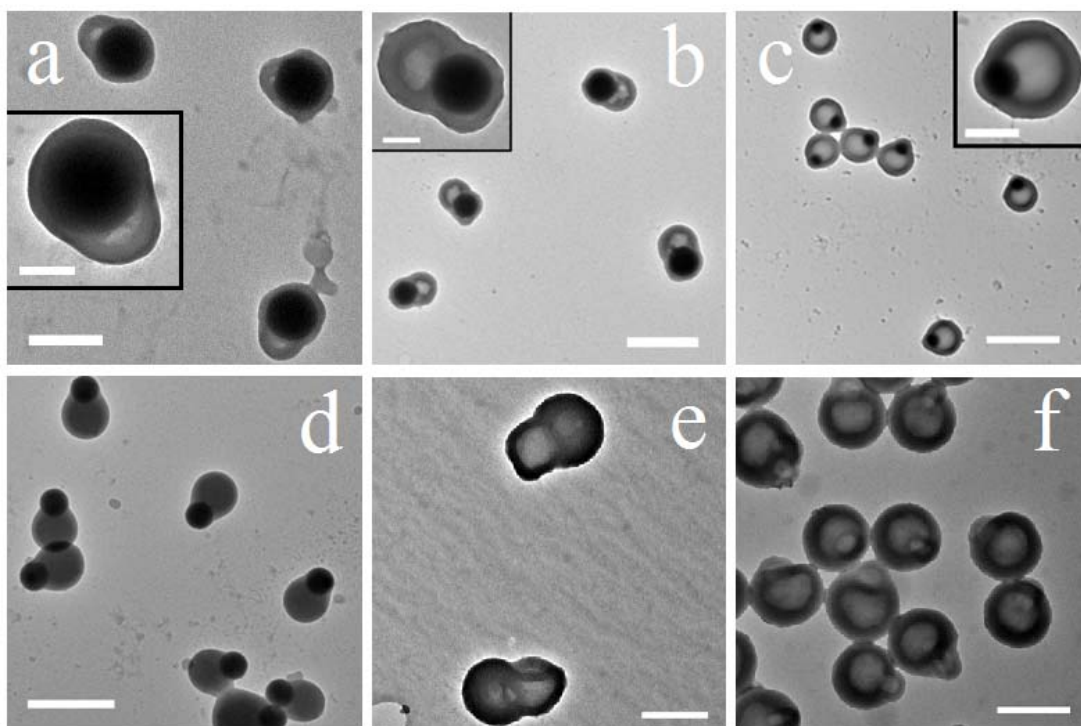
Figure 3.5. Non-spherical hollow or solid hybrid particles (TPM-SiO$_2$-core, cross-linked PMMA-shell) made by dispersion polymerization in methanol. Cross-linker density is 10 wt%, the addition start time and total addition time were 1.5 and 3 h, respectively. Small TPM-SiO$_2$ cores ($D = 322$ nm, $PD = 2.6\%$) were used. a) A mass ratio of MM and silica cores of 5:1. The scale bar is 500 nm and the inset 200 nm. b) A mass ratio of MM and silica core of 10:1. The scale bar is 1 μm and the inset 200 nm. c) A mass ratio of MM and silica core of 20:1, the scale bar is 2 μm and the inset 500 nm. d) The same recipe as in (b) except in the absence of DVB. The scale bar is 1 μm. e) The particles of (b) etched with HF. The scale bar is 500 nm. f) The sample of (c) etched with HF. The scale bar is 1 μm.

inspection of the shells of the hollow hybrid particles (see the images in the insets of Fig. 3.5a and c, and Fig. 3.5f, also see the inset in Fig. 3.6c and d), it can be seen that the thickness of the shells is again non-uniform. This can be seen better if the silica is first removed by etching in a dilute HF solution (Fig. 3.5e and f). The thickness of the part of a shell which links with a TPM-SiO$_2$ core is thinner than that of the other parts of a shell. This provides more evidence for the remaining uncross-linked PMMA polymer layer piling on the inner surface of the hollow particles.

When the small silica cores were replaced by big ones of 664 nm in diameter and 2.7 % in polydispersity, multiple PMMA bulbs were formed. A high mass ratio ($M_{MM}{:}M_{silica} = 20{:}1$) led to multipod-like particles (see Fig. 3.6a, most of them are asymmetric dimer and trimer). Decreasing the amount of MM ($M_{MM}{:}M_{silica} = 10{:}1$) induced a hamburger-like structure (see Fig. 3.6b). HF etching resulted in non-spherical particles with a single hollow cavity in their
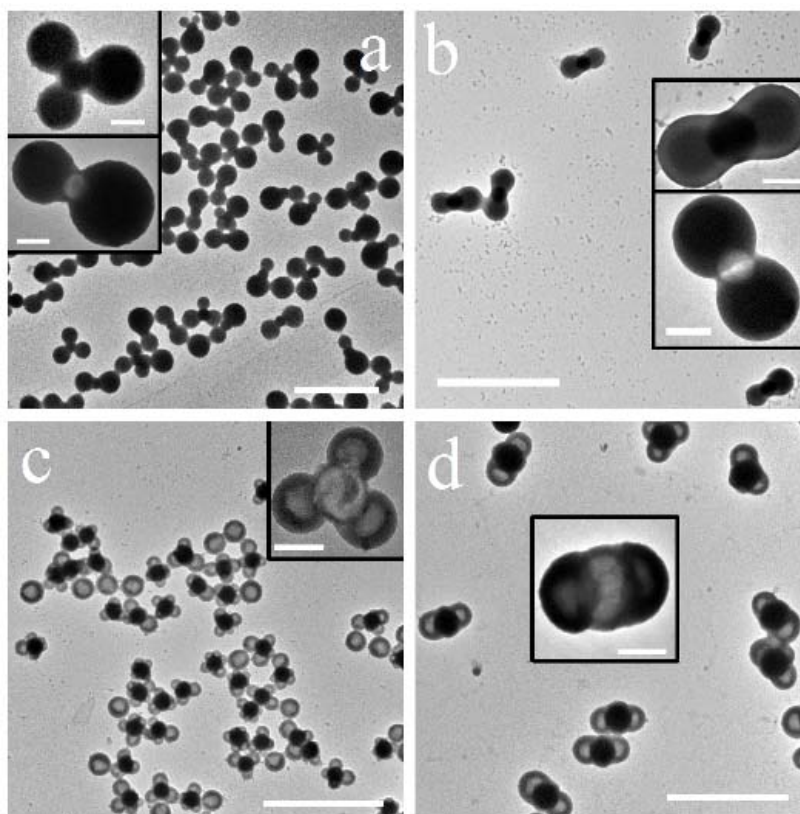
Figure 3.6. TEM micrographs of non-spherical hybrid particles made by dispersion polymerization in methanol with a TPM-SiO$_2$ core of 664 nm in diameter and 2.7% in polydispersity. a) A weight ratio of MM to silica of 20:1 and in the absence of DVB. The upper inset is a magnified image and the lower one shows the particles after the silica core was removed by HF. b) A weight ratio of MM to silica of 10:1, and in the absence of DVB. The upper inset is a magnified image and the lower one shows the particles after the silica core was removed by HF. c) Similar to (a), but with the post-addition of DVB. The cross-link density was 10 wt%, and the addition start time and total addition time were 1.5 and 3 h, respectively. The inset is a magnified image of particles after the silica core was removed by HF. d) Similar to (b), but with the post-addition of DVB. The cross-linker density was 10 wt%, and the addition start time and total addition time were 1.5 and 3 h, respectively. The inset is a magnified image of the particles after the silica core was removed by HF. All the scale bars are 5 μm and the insets 500 nm.

center (see the inset in Fig. 3.6a and b). Alternatively, the presence of DVB during the preparation of hybrid particles led to two or more hollow chambers. The number of hollow chambers mainly depended on the number of polymer protrusions attached on a TPM-SiO$_2$ core. Upon treatment with HF, a hollow multipod or hamburger –like structure could be obtained (see Fig. 3.6c and d). Alternatively, when this method was tried on a dispersion polymerization of MM onto silica in an apolar solvent (hexane and dodecane), it only resulted in uniform coated spherical core-shell structured particles (see SF-3.11).

3.4 CONCLUSIONS

In conclusion, we developed a facile one-step synthetic strategy for the preparation of polymer particles with hollow cavities. Our method bears several advantages, *e.g.*, it is a simple one-pot, self-template method, and no extra template removal or pre-production process is needed; it is universal: it is applicable to dispersion, surfactant-free emulsion and precipitation polymerization, and to a diversity of materials (PMMA, PS and PNIPAM) in a wide size range with a good monodispersity both in size and shape. It can also yield various shapes of particles (snowman, dumbbell and multipod like particles when used in combination with surface-modified silica seeds). The size of the particles and hollow cavities can be precisely controlled by first selecting a suitable preparation method, and then adjusting the timing and the amount of cross-linker addition. It is robust: the hollow structure always remained intact even after drying from a good solvent (THF), due to the highly cross-linked shells. Moreover, a diversity of organic-inorganic hybrid (PMMA-silica) particles with a controllable shape was synthesized successfully. Upon varying the size of the TPM-SiO$_2$ cores, and the weight ratio of MM and TPM-SiO$_2$ cores, the morphologies of hybrid particles ranged from snowman, dumbbell, inverted snowman (the silica core bigger than the PMMA lobe), hamburger, to multi-pod like. The lobes of the non-spherical particles can be selectively emptied by either the addition of the key agent DVB or HF etching. Based on this novel technique, we believe more species of functional particles with controllable cavities and outer structures can be produced, which will be useful for both fundamental research and applications.

3.5 ACKNOWLEDGEMENTS

3.6 SUPPLIEMENTARY INFORMATION
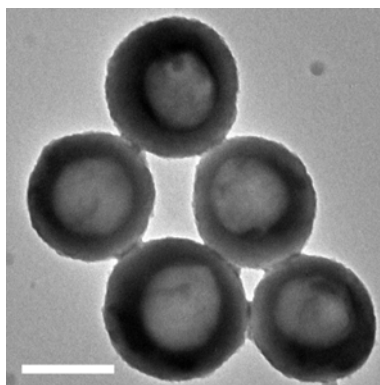
Supplementary Figure 3.1. TEM micrograph of hybrid hollow MMA-*co*-PNIPAM-*co*-DVB spheres. PNIPAM and DVB each are 10 wt%, based on total monomer mass. The addition start time and total addition time were 1.5 and 3 h, respectively. The scale bar is 500 nm.
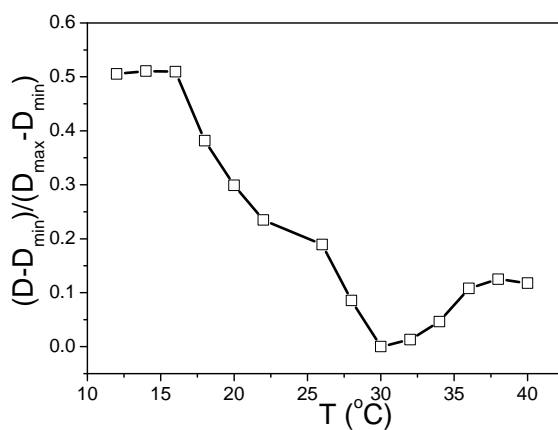
Supplementary Figure 3.2. Normalized diameter of the hollow PNIPAM spheres as a function of temperature. The VPTT was obtained from the temperature when the spheres were collapsed at half of the whole transition process. In this case, the VPTT is about 23 ^{o}C.
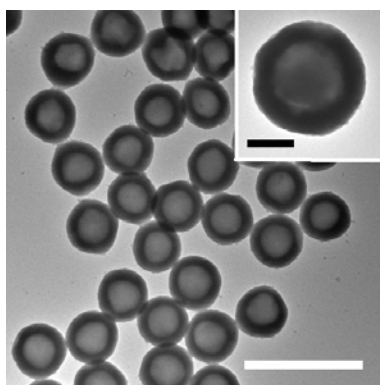
Supplementary Figure 3.3 TEM micrograph of hollow PMMA spheres, after being in a good solvent (THF) for 2 days. DVB was used as cross-linker, the cross-link density is 10 wt%, and

the addition start time and total addition time were 1.5 and 3 h, respectively. The outer and inner diameters are 1383 and 856 nm, respectively. The thinness of the shell decreased from 297 to 263.5 nm after the treatment of THF. The scale bar is 5 μm and the insert one is 500 nm.
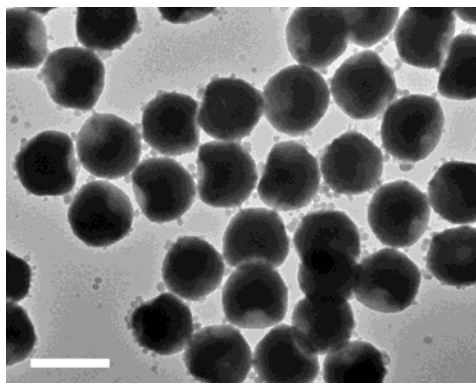
Supplementary Figure 3.4. TEM micrograph of buckled cross-linked PMMA particles. EGDMA (10 wt% based on MM) was used as cross-linker. The addition start time and total addition time were 1.5 and 3 h, respectively). A dimple instead of a void was obtained. The scale bar is 2 μm.
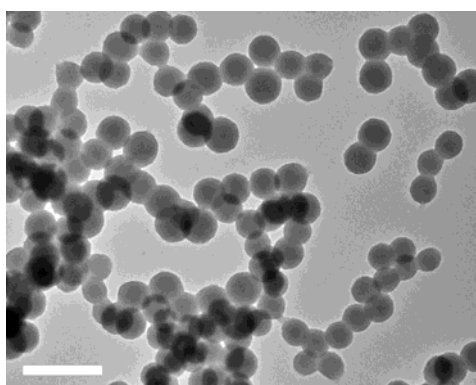
Supplementary Figure 3.5. TEM micrograph of solid cross-linked PMMA spheres made in apolar solvents (hexane and dodecane) via dispersion polymerization. DVB was used as cross-linker, 10 wt%, and the addition start time and total addition time both were about 30 min, and the reaction temperature was ~ 80 °C. No void was formed. The scale bar is 1 μm.
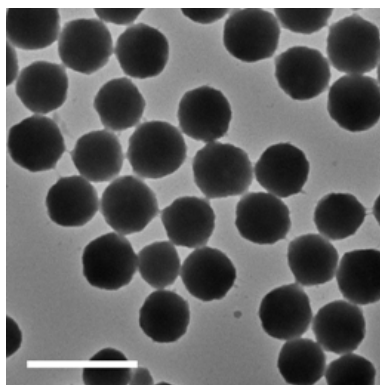
Supplementary Figure 3.6. TEM micrograph of cross-linked PMMA particles made by starting the addition of a cross-linker (DVB) at the beginning of the reaction. No void was formed. The total addition time was 5 h. The scale bar is 2 μm.
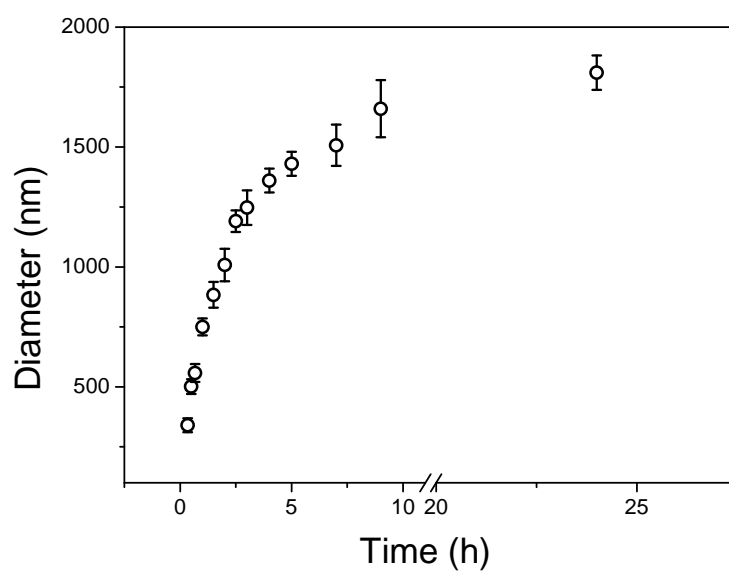
Supplementary Figure 3.7. The growth of uncross-linked PMMA particles as a function of time (in methanol).
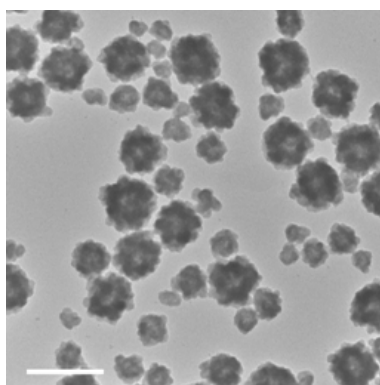
Supplementary Figure 3.8. TEM micrograph of PMMA particles with 50 wt% cross-linker. The addition start time and total addition time were 1.5 h and 3 h, respectively. The scale bar is 5 μm.
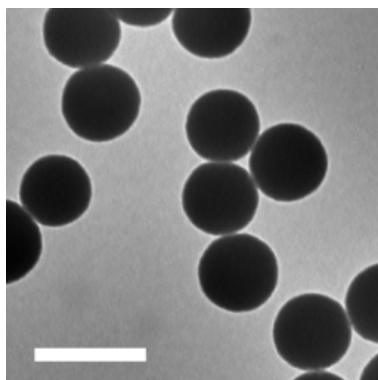
Supplementary Figure 3.9. TEM micrograph of small silica particles with a diameter of 322 nm and a low polydispersity of 2.6%. The scale bar is 500 nm.
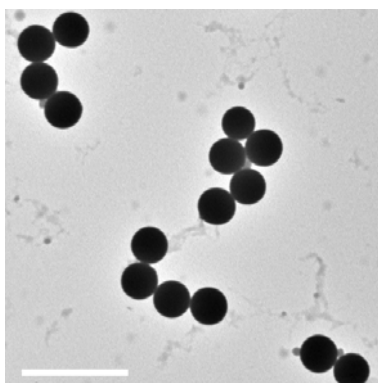
Supplementary Figure 3.10. TEM micrograph of big silica particles with a diameter of 661 nm and a low polydispersity of 2.7%. The scale bar is 2 μm.
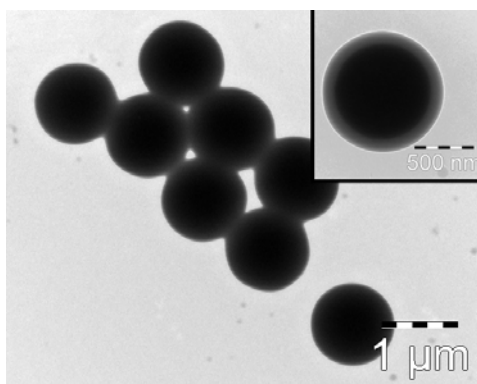
Supplementary Figure 3.11. TEM micrograph of core-shell silica-PMMA spherical particles made in apolar solvents (hexane and dodecane).

3.7 REFERENCES

[1] Luo, X. W.; Archer, L. A.; Yang, Z. *Adv. Mater.* **2008**, *20*, 1-33.

[2] Liu, J.; Liu, F.; Gao, K.; Wu, J.; Xue, D. *J. Mater. Chem.* **2009**, *19*, 6073-6084.

[3] Hu, J.; Chen, M.; Fang, X.; Wu. L. *Chem. Soc. Rev.* **2011**, *40*, 5472-5491.

[4] Fu, G.; Li, G. L.; Neoh, K. G.; Kang, E. T. *Prog. Polym. Sci.* **2011**, *36*, 127-167.

[5] Peyratout, C. S.; Dahne, L. *Angew. Chem. Int. Ed.* **2004**, *43*, 3762-3783.

[6] Chen, D.; Jiang, M. *Acc. Chem. Res.* **2005**, *38*, 494-502.

[7] Zhu, Y.; Shi, J.; Shen, W.; Dong, X.; Feng, J.; Ruan, M.; Li, Y. *Angew. Chem. Int. Ed.* **2005**, *44*, 5083-5087.

[8] Wang, Z.; Wu, L.; Chen, M.; Zhou, S. *J. Am. Chem. Soc.* **2009**, *131*, 11276-11277.

[9] Gill, I.; Ballesteros, A. *J. Am. Chem. Soc.* **1998**, *120*, 8587-8598.

[10] Lee, J. C.; Bermudez, H.; Discher, B. M.; Sheehan, M. A.; Won, Y.; Bates, F. S. Discher, D. E. *Biotechnol. Bioeng.* **2001**, *20*, 135-145.

[11] Sokolova, V. V.; Radtke, I.; Heumann, R. Epple, M. *Biomaterials* **2006**, *27*, 3147-3153.

[12] Kim, S.; Kim, M.; Lee, W. Y.; Hyeon, T. *J. Am. Chem. Soc.* **2002**, *124*, 7642-7643.

[13] Liang, H.; Zhang, H.; Hu, J.; Guo, Y.; Wan L.; Bai, C. *Angew. Chem. Int. Ed.* **2004**, *43*, 1540-1543.

[14] Martinez, C. J.; Hockey, B.; Montgomery, C. B.; Semancik, S. *Langmuir* **2005**, *21*, 7937-7944.

[15] Zhang, H.; Zhu, Q.; Zhang, Y.; Wang, Y.; Zhao, L.; Yu B. *Adv. Funct. Mater.* **2007**, *17*, 2766-2771.

[16] Luo, X. W.; Wang, Y.; Yuan, C.; Lee, J. Y.; Archer, L. A. *Adv. Mater.* **2006**, *18*, 2325-2329.

[17] Luo, X. W.; Archer, L. A. *Adv. Mater.* **2008**, *20*, 1853-1858.

[18] Cao, A.; Hu, J.; Liang, H.; Wan, L. *Angew. Chem. Int. Ed.* **2005**, *44*, 4391-4395.

[19] Luo, X. W.; Yuan, C.; Rhoades, E.; Zhang, Q.; Archer, L. A. *Adv. Funct. Mater.* **2006**, *16*, 1679-1684.

[20] Vriezema, D. M.; Garcia, P. M. L.; Oltra, N. S.; Hatzakis, N. S.; Kuiper, S. M.; Nolte, R. J. M.; Rowan, A. E.; van Hest, J. C. M. *Angew. Chem. Int. Ed.* **2007**, *46*, 7378-7382.

[21] Xu, X.; Asher, S. A. *J. Am. Chem. Soc.* **2004**, *126*, 7940-7945.

[22] Caruso, F.; Caruso, R. A.; Mohwald, H. *Science* **1998**, *282*, 1111-1114.

[23] Imhof, A. *Langmuir* **2001**, *17*, 3579-3585.

[24] Jiang, P.; Bertone, J. F.; Colvin, V. L. *Science*, **2001**, *291*, 453-457.

[25] Chen, M.; Wu, L.; Zhou, S.; You, B. *Adv. Mater.* **2006**, *18*, 801-806.

[26]Chen, X.; Chen, M.; Wu, L.; Gu, G. *Langmuir* **2006**, *22*, 3858-3863.

[27]Deng, Z.; Chen, M.; Zhou, S.; You, B.; Wu, L. *Langmuir* **2006**, *22*, 6403-6407.

[28]Deng, Z.; Chen, M; Gu, G.; Wu, L. *J. Phys. Chem. B* **2008**, *112*, 16-22.

[29]Zoldesi, C. I.; Imhof, A. *Adv. Mater.* **2005**, *17*, 924-928.

[30]Zoldesi, C. I.; van Walree, C. A.; Imhof, A. *Langmuir* **2006**, *22*, 4343-4352.

[31]Imhof, A.; Pine, D. J. *Nature* **1997**, *389*, 948-951.

[32]Wang, Z.; Chen, M.; Wu, L. *Chem. Mater.* **2008**, *20*, 3251-3253.

[33]Peng, B.; Chen, M.; Zhou, S.; Wu, L.; Ma, X. *J. Colloid Interface Sci.* **2008**, *321*, 67-73.

[34]Kim, S. S.; Zhang, W.; Pinnavaia, T. J. *Science* **1998**, *282*, 1302-1305.

[35]Li, J.; Zeng, H. C. *J. Am. Chem. Soc.* **2007**, *129*, 15839-15847.

[36]Im, S. H.; Jeong, U.; Xia, Y. *Nat. Mater.* **2005**, *4*, 671-675.

[37]Tartaj, P.; Gonzalez-Carreno, T.; Serna, C. J. *Adv. Mater.* **2001**, *13*, 1620-1624.

[38]Yin, Y.; Rioux, R. M.; Erdonmez, C. K.; Hughes, S.; Somorjai, G. A.; Alivisatos, A. P. *Science* **2004**, *304*, 711-714.

[39]Sun, Y. G.; Xia, Y. N. *Science* **2002**, *298*, 2176-2179.

[40]Jeong, U. Y.; Xia, Y. *Angew. Chem. Int. Ed.* **2005**, *44*, 3099-3103.

[41]Itou, N.; Masukawa, T.; Ozaki, I.; Hattori, M.; Kasai, K. *Colloid Surface A* **1999**, *153*, 311-316.

[42]Okubo, M.; Minami, H. *Colloid Polym. Sci.* **1995**, *274*, 433-438.

[43]Lv, H.; Lin, Q.; Zhang, K.; Yu, K.; Yao, T.; Zhang, X.; Zhang, J.; Yang, B. *Langmuir* **2008**, *24*, 13736-13741.

[44]Smigelskas, A. D.; Kirkendall, E. O. *Trans. Am. Inst. Min. Metall. Pet. Eng.* **1947**, *171*, 130.

[45]Luo, X. W.; Yuan, C.; Archer, A. *Adv. Mater.* **2007**, *19*, 3328-3332.

[46]Cheng, D.; Xia, H.; Chan, H. *Nanotechnology* **2006**, *17*, 1661-1667.

[47]Zhang, Z.; Sui, J.; Zhang, L.; Wang, M.; Wei, Y.; Yu, L. *Adv. Mater.* **2005**, *17*, 2854-2857.

[48]Hao, Y.; Zhu, C.; Jiang, W.; Chen, C.; Hu, Y.; Chen, Z. *J. Mater. Chem.* **2004**, *14*, 2929-2934.

[49]Nagao, D.; van Kats, C. M.; Hayasaka, K.; Sugimoto, M.; Konno, M.; Imhof, A.; van Blaaderen, A. *Langmuir* **2010**, *26*, 5208-5212.

[50]Lootens, D.; Vautrin, C.; van Damme, H.; Zemb, T. *J. Mater. Chem.* **2003**, *13*, 2072-2074.

[51]Wang, W.; Poudlel, B.; Wang, D.; Ren, Z. F. *Adv. Mater.* **2005**, *17*, 2110-2114.

[52] Lu, C.; Qi, L.; Yang, J.; Wang, X.; Zhang, D.; Xie, J.; Ma. J. *Adv. Mater.* **2005**, *17*, 2562-2567.

[53] Yang, H. G.; Zeng, H. C. *Angew. Chem. Int. Ed.* **2004**, *43*, 5930-5933.

[54] Cao, H.; Qian, X.; Wang, C.; Ma, X.; Yin, J.; Zhu, Z. *J. Am. Chem. Soc.* **2005**, *127*, 16024-16025.

[55] Yang, J.; Qi, L.; Lu, C.; Ma, M.; Cheng, H. *Angew. Chem. Int. Ed.* **2005**, *44*, 598-603.

[56] Sheu, H. R.; El-Aasser, M. S.; Vanderhoff, J. W. *J. Polym. Sci., Part A: Polym. Chem.* **1990**, *28*, 629-651.

[57] Mock, E. B.; De Bruyn, H.; Hawkett, B. S.; Gilbert, R. G.; Zukoski, C. F. *Langmuir* **2006**, *22*, 4037-4043.

[58] Kim, J. W.; Larsen, R. J.; Weitz, D. A. *J. Am. Chem. Soc.* **2006**, *128*, 14374-14377.

[59] Peng, B.; Vutukuri, H. R.; van Blaaderen, A.; Imhof, A. *J. Mater. Chem.* **2012**, *22*, 21893-21900.

[60] Perro, A.; Reculusa, S.; Ravaine, S.; Bourgeat-Lami, E.; Duguet, E. *J. Mater. Chem.* **2005**, *15*, 3745-3760.

[61] Duguet, E.; Desert, A.; Perro, A.; Ravaine, S. *Chem. Soc. Rev.* **2011**, *40*, 941-960.

[62] Perro, A.; Duguet, E. Lambert, O.; Taveau, J. C.; Bourgeat-Lami, E.; Ravaine, S. *Angew. Chem. Int. Ed.* **2009**, *48*, 361-365.

[63] Nguyen, D.; Ravaine, S.; Bourgeat-Lami, E.; Duguet, E. *J. Mater. Chem.* **2010**, *20*, 9392-9400.

[64] Bosma, G.; Pathmamanoharan, C.; de Hoog, E. H. A.; Kegel, W. K.; van Blaaderen, A.; Lekkerkerker, H. N. W. *J. Colloid Interface Sci.* **2002**, *245*, 292-300.

[65] Peng, B.; van der Wee, E.; Imhof, A.; van Blaaderen, A. *Langmuir* **2012**, *28*, 6776-6785.

[66] Antl, L.; Goodwin, J. W.; Hill, R. D.; Ottewill, R. H. *Colloids and Surface* **1986**, *17*, 67-78.

[67] Mackova, H.; Horak, D. *J. Polym. Sci., Part A: Polym. Chem.* **2006**, *44*, 968-982.

[68] Philipse, A. P.; Vrij, A. *J. Colloid Interface Sci.* **1989**, *128*, 121-136.

[69] Qian, J.; Wu, F. *Chem. Mater.* **2007**, *19*, 5839-5841.

[70] Okubo, M.; Minami, H. *Colloid Polym. Sci.* **1997**, *275*, 992-997.

4

Surface Morphology Control of Cross-Linked Polymer Particles via Dispersion Polymerization

ABSTRACT

Cross-linked polymer colloids (poly(methyl methacrylate and polystyrene) with diverse shapes were prepared in polar solvents (ethanol, methanol and water) via dispersion polymerization, in which a linear addition of cross-linker was used. Apart from spherical particles we found dented spheres or particles covered with nodules, or a combination of both. A comprehensive investigation was carried out, mainly concentrating on the effect of the experimental conditions (*e.g.*, the addition start time and total addition time, cross-linker density and the solvency of the solvents) on particle morphology. Consequently, we suggest some effective ways for the synthesis of regular (spherical) colloidal particles through maintaining a relatively low concentration of cross-linker during the entire reaction, or forcing the co-polymerization (of monomer and cross-linker) locus to the continuous medium, or using a high quality or quantity of stabilizer. Moreover, the size of the particles was also precisely manipulated by varying the polarity of the solvents, the concentration of the cross-linker, and the amount and average molecular weight of the stabilizer. In addition, the formation of the heavily dented particles with a very rough surface prepared under a pure or oxygen 'contaminated' nitrogen environment was monitored in time.

4.1 INTRODUCTION

Over the past quarter of a century there has been a strong interest in the synthesis of polymer particles with a narrow size distribution in the micro- or sub-micrometer range because they are used in many applications in a variety of fields that include inks and coatings, chromatography, protein synthesis, biomedical analysis, and medical diagnostics. [1-7] Particles with sub-micrometer dimensions are most commonly prepared by emulsion or surfactant-free emulsion polymerization. The second approach is particularly effective for preparing functional polymer particles with a very narrow size distribution, with typical diameters in the range of 400-800 nm. [8-10] Based on the uniform products from surfactant-free emulsion polymerization, micro-sized particles can be made either by the seeded emulsion polymerization developed by Vanderhoff [11] or the activated swelling and suspension polymerization method proposed by Ugelstad. [12] The 'dynamic swelling method' developed by Okubo [13] is also possible. However, these successful techniques suffer from tedious procedures, and are time-consuming and difficult to implement on a large scale. Dispersion polymerization is a relatively simple approach and the resulting products are monodisperse both in size and shape, and the yield can be readily scaled up. [14-21]

Dispersion polymerization is defined as a radical polymerization reaction in which the monomer is soluble, but the polymer is not. The starting reaction mixture of the dispersion polymerization system is a clear, single phase solution. The polymer begins to precipitate as it is formed. Its mechanism has been widely studied in 1960s and 1970s and well described in Barrett's book. [14] There are two major stages, that is, nucleation and growth. During nucleation, the mixture of the stabilizer, monomer, solvent, initiator and other components (like co-monomer) is maintained at a specific temperature. The initiator decomposes, and the free radicals liberated start to react with monomers to form oligomer radicals. When the oligomers become sufficiently large, they precipitate from the solvent to form nuclei that are protected by stabilizer. In the second stage, the initial particles swell slightly so that the monomer and initiator are absorbed into the particles. Each particle itself behaves like a small reactor. When all of the monomer has been consumed, the polymerization is complete. In principle, the nucleation stage sets the size distribution and the number of the particles, while in the particle growth stage, unless the reaction conditions are drastically changed, no more nuclei are generated and only particle growth occurs. Dispersion polymerization differs from precipitation polymerization in that it is carried out in the presence of a second soluble polymer as a steric stabilizer. The steric stabilizer becomes attached to the surface of the precipitating polymer, and stabilizes the precipitate in the form of micron size particles.

[14-16, 20] Traditional dispersion polymerization involves a single step reaction with a simple synthesis protocol in which all the reactants are mixed and heated, and often leads to particles with an exceptionally narrow size distribution. The preparation of monodisperse homo-polymer particles in dispersion polymerization has been extensively studied, especially for polystyrene (PS) [16-18] and poly(methyl methacrylate) (PMMA). [19, 20] Typical reaction conditions consist of monomer and poly(vinyl pyrrolidone) (PVP) as a polymeric stabilizer dissolved in ethanol for PS or methanol for PMMA, and the system is heated in the presence of a free radical initiator. As a result, monodisperse particles are obtained. However, the corresponding co-polymerization reactions are much more troublesome. [15, 16, 22] One of the biggest challenges is the synthesis of cross-linked particles, because the cross-linker has bi-functional vinyl groups (usually divinylbenzene (DVB) is used for PS system and ethylene glycol dimethacrylate (EGDMA) for PMMA system). [16, 19] The cross-linker enables the linear polymer chains to branch leading to a more rigid polymer network. This will hinder a 'healthy' growth of polymer particles. There are many articles in the literature to attest to the fact that dispersion polymerization fails when cross-linker is present. [16, 19, 23-27] Many factors from the standpoint of the reagents in dispersion polymerization, such as the choice and concentration of the monomer, co-monomer, stabilizer, solvent, and initiator, affect the morphology, size and size distribution of the resulting particles. Although several publications have pointed the way to improve this situation, no full solution has been demonstrated so far. [26, 28, 29] Thomson *et al.* [27, 28] reported that monodisperse cross-linked PS spheres could be obtained with less than 0.2 wt% of cross-linker (DVB) present in the initial charge. However, larger amounts of up to 1% DVB could be only incorporated by incremental addition during 7 h after the start of the polymerization. Then, by mainly varying the addition start time, a series of interestingly shaped stable PS particles was obtained: they contained one or more dimples, or were covered by nodules, or both. They explained the relationship between the diverse morphologies of the obtained particles and the variation of the addition start time, in terms of a more restricted mobility of the stabilizer when cross-linker is added. [27, 28] Moreover, Dullens *et al.* [25, 26] smartly circumvented this difficulty, which they believed was mainly caused by the interference of the cross-linker during the sensitive nucleation stage. They fed in the cross-linker (EGDMA) during the relatively robust particles growth stage. As a result, core-shell cross-linked (up to 6 wt% based on monomer mass) PMMA spheres of a good uniformity with a smooth surface were obtained. Odd shaped particles occasionally appeared when a high concentration (for example 6 wt%) of the cross-linker was used. A similar strategy was also adopted by Song *et al.* [23, 30] in the synthesis of core-shell cross-linked PS particles. However, most articles focused on the

synthesis of 'regular' spheres. Relatively few words were spent on the description of anomalous results. A particular and deep investigation on the variation of the shape and surface morphology of the polymer particles is still highly desired, not only because it will guide us to a better understanding of the formation of the polymer particles in dispersion polymerization, but also because particles with a more complex shape and structure can be designed this way. These particles are then used in various assembly methods. For example, particles with spherical dimples may spontaneously form chains when packed together, [31] or when an attractive depletion force is induced between the particles. [32] And controllable roughness has been shown to be a nice way to modulate depletion attractions between particles, [33, 34] or parts of particles. [35]

Recently, we developed a straightforward synthetic strategy for preparing monodisperse fluorescently labeled PMMA colloids with a heterogeneous or homogeneous cross-linked structure by simply varying the addition start time of the cross-linker. [24] We considered that the dispersion polymerization was a two-step reaction in which the fundamental hypothesis was that the nucleation stage was short-lived but very sensitive to perturbed, whereas the particles growth stage was more robust. We were able to prepare monodisperse fluorescently labeled PMMA particles with a core-shell cross-linked structure by delaying the addition until the nucleation stage has completed, and particles with a homogenously cross-linked structure by beginning to introduce the additives at a relatively low quantity before the nuclei had formed. Thus, highly cross-linked (as high as 10 wt% of cross-linker, based on the total monomer mass), stable PMMA spheres with a smooth surface were obtained in the end.

In this chapter, we describe the circumstances under which our technique reproducibly yields particles with a deviating morphology, such as dented or wrinkled spheres and particles covered with nodules. This yields insight into the particle formation mechanism and caters to the need for non-spherical particles in materials science. The shapes are reminiscent to those obtained by Thomson *et al.* [27, 28] for PS in dispersion polymerization and Xu, [36] and Huang *et al.* [37] for PS in emulsion polymerization, and probably have a common origin, although we arrive at a different formation mechanism.

4.2 MATERIALS AND METHODS

4.2.1 Materials

All reagents used were of chemical grade unless mentioned otherwise. Methyl methacrylate (MM, Aldrich) was passed over an inhibitor removal column (Aldrich). Styrene was eluted over a home-made inhibitor removal column which contained aluminum oxide (~ 150 mesh,

Aldrich). After the inhibitor had been removed, MM was stored in a refrigerator not longer than one month, while styrene was used at once. Azo-bis-isobutyronitrile (AIBN, Janssen Chimica) was re-crystallized from ethanol before use and was also stored in the refrigerator. Ethylene glycol dimethacrylate (EGDMA, Sigma-Aldrich) and divinylbenzene (DVB, 80% mixture of isomers, Aldrich) were used as cross-linking agents. Polyvinylpyrrolidone (PVP) with average molecular weights of 10,000 g/mol (K-15, Sigma-Aldrich), 40,000 g/mol (K-30, Sigma-Aldrich) and 360,000 g/mol (K-90, Sigma) was used as stabilizer. Methanol (Biosolve) and ethanol (J.T.Baker) were used as supplied. De-ionized water was used in all experiments.

4.2.2 Procedures for Particle Synthesis

The cross-linked PMMA colloidal particles with various surface morphologies were synthesized by a modified method on the basis of our previous work. [24] Briefly, a solvent (or solvent mixture) consisted of methanol or ethanol (or methanol and de-ionized water) containing about 5 wt% (based on the total solvent mass) of the stabilizer (PVP). All monomer (MM) together with 1 wt% (based on monomer) of initiator (AIBN), was added to two thirds of the solvent mixture (for detailed recipe, see Tab. 4.1). After bubbling nitrogen through the reaction system at room temperature for 30 min, the flask was immersed in a pre-heated silicon oil bath, maintained at 55 $^{\circ}$C, and stirred at 100 rpm. The remaining one third of the solvent mixture was mixed with different amounts of cross-linker (EGDMA or occasionally DVB) and fed into the reaction vessel at a constant rate with the aid of a peristaltic pump. The detailed addition start time and total addition time are listed in Table 4.1. After the feed was complete, the reaction was allowed to complete for 24 h before cooling to room temperature.

Cross-linked PS particles were prepared in a similar way as the PMMA particles. Typically, 25 g of ethanol, 1 g of PVP (K-30), 5 g of styrene and 0.1 g of AIBN were added to a 250 ml, three-necked flask equipped with a gas supply, a condenser, and a Teflon-coated stir bar. After a homogeneous solution had formed at room temperature by stirring at 250 rpm, a de-oxygenation process (N_2 was used) was carried out for at least half an hour. Subsequently, the temperature of the system was increased to 70 $^{\circ}$C and the stirring speed was slowed to 100 rpm. Various amounts of cross-linker (DVB) were dissolved in a mixture of 25 g of ethanol and 0.5 g of PVP (K-30). The addition of these mixtures started after the polymerization reaction had run for a certain period (the details can be found in Tab. 4.2). The reaction was allowed to maintain at 70 $^{\circ}$C for 24 h after the addition had finished.

In order to remove the unreacted stabilizer and monomer, all products were washed by three cycles of centrifugation (a Hettich Rotina 46 S centrifuge, at 315 g for 20 min) and re-dispersion (a ultrasonic bath, Bransonic 40 L) with methanol (for PMMA) or ethanol (for

PS) , and finally dispersed in methanol (for PMMA) or ethanol (for PS) at room temperature.

4.2.3 Characterization of the Latex Particles

In order to determine the size, polydispersity and surface morphology of the particles, scanning electron microscopy (SEM) was performed with a FEI Phenom scanning electron microscope. The samples were prepared by depositing a droplet of a diluted sample onto a glass slide and allowing the solvent to evaporate at room temperature. The samples were then

Table 4.1. Preparation Details of the Cross-Linked PMMA Latex

Batch	Methanol (ml)	Addition start time (h)	Total addition time (h)	EGDMA (wt %)[a]	PVP (g) [c]	Remark
1	38.76	1.5	2	1	1.5	Dented spheres with nodules
2	38.76	0.5	4	1	1.5	Lightly rough spheres
3	38.76	1.5	4	1	1.5	Spheres
4	38.76	1.5	4	1 (DVB)[b]	1.5	Rough spheres
5	38.76	0	4	1	1.5	Rough spheres
6	38.76	0	10	1	1.5	Dented spheres
7	31.02+6.14 (water)[d]	0	10	1	1.5	Spheres
8	38.76	1.5	2	2	1.5	Dented spheres with nodules
9	38.76	1.5	2	2	3	Rough spheres
10	38.76	1.5	10.5	2	1.5	Spheres
11	38.76	1.5	10.5	2	1.5 (K-30)	Wrinkled spheres
12	38.76 (ethanol)[e]	1.5	10.5	2	1.5 (K-30)	Wrinkled spheres
13	38.76	1.5	10.5	2 (DVB)[b]	1.5	Slightly rough spheres

[a] Based on MM mass.

[b] DVB was used as cross-linker in batch 4 and 13 instead of EGDMA.

[c] PVP with a average molecular weight of 40,000 g/mol (K-30) was used in batch 11 and 12, PVP with a molecular weight of 360,000 g/mol (K-90) was used in the rest batches.

[d] 6.14 ml of de-ionized water and 31.02 ml of methanol were used as solvent.

[e] Ethanol was used as solvent instead of methanol.

sputter-coated with a layer of gold (Au) of 10 nm. A number-averaged particle radius (R) and its standard deviation (σ) were calculated on the basis of the surface area of the spheres. The polydisperisty (δ) of the colloidal systems was defined as $\delta = \sigma / R$. For some cases of non-spherical particles, it is hard to determine their polydispersities. We just manually measured the size and standard deviation of the spherical particles whose outlines roughly fitted with those of non-spherical particles, and calculated the polydispersity of them.

Table 4.2. Preparation Details of the Cross-Linked PS Latex

Batch	Addition start time (h)	Total addition time (h)	DVB (wt%)	Remark
1	0	12	0.5	Spheres
2	0	12	1	Spheres
3	0	12	2	Spheres
4	0	12	4	Dented spheres
5	1	11	4	Lightly dented spheres
6	0	12	6	Heavily dented spheres

4.3 RESULTS AND DISCUSSION

As mentioned earlier, a dispersion polymerization in which the monomer co-polymerizes with the other monomer (co-monomer), in particular, a cross-linking monomer (cross-linker), will often lead to a poor result. In fact, the presence of cross-linker (usually > 0.5 wt% based on monomer mass) during the nucleation stage usually disturbs the formation of 'normal' nuclei. Nevertheless, our recent discoveries displayed that the presence of a cross-linker during the nucleation stage was possible, provided that the concentration of the cross-linker was maintained at a relatively low level. [24] As a result, homogeneously cross-linked PMMA particles were then successfully fabricated. Moreover, upon delaying the feed of the cross-linker to a point after the nucleation stage, highly cross-linked (as high as 10 wt%) spherical PMMA particles could also be prepared. Based on this knowledge, an adaptation of our previous method [24] was carried out not only on PMMA but also PS. In the following an exhaustive investigation on the varieties of morphologies of the cross-linked polymer particles obtained by varying different experimental parameters will be presented.

4.3.1 Effect of the Feeding Time

At first, in order to avoid a deleterious influence of the cross-linker on the initial nuclei, a polymerization was carried out by simply delaying the addition start time of the cross-linker to 1.5 h and continuing the feeding action for 2 h. Meanwhile, pure methanol was used as the solvent and the concentration of the stabilizer was maintained at ~5 wt% based on the solvent mass throughout the reaction. When 1 wt% (based on total monomer) of cross-linker was used (for details, see batch 1 in Tab. 4.1) in the reaction, particles with a number of large dents and covered with nodules were observed, as shown in Figure 4.1A. As mentioned before, the nucleation stage is short and sensitive. In this case, after 1.5 h, the reaction was in the process of particle growth (the evidence of particles in the growth stage can be found in the formation mechanism section), which implies that the addition of cross-linker during this period would lead to a core-shell structure. Indeed, the core-shell structure was confirmed by incorporation of a dye along with the cross-linker in our previous work. [24] If more cross-linker (2 wt%) was added into the system, fewer dents present on the surface of the particle as shown in Figure 4.1C. However, the roughness of the surface increased somewhat.

To avoid a deformed surface, we carried out two more experiments in which the EGDMA solution was added continuously over a longer period of time: 4 h for 1 wt% and 10.5 h for 2 wt% cases, keeping the addition start time at 1.5 h. In this way, the conversion of EGDMA is more evenly spread over the particle growth period (~24 h). As a result, cross-linked PMMA spheres with a smooth surface in a narrow size distribution were successfully synthesized (see Fig. 4.1B and 4.1D). At the same time, we observe reduction in particle size when the cross-linker is added over a longer period of time: At 1 wt% cross-linker the size decreased from 2.80 to 2.03 μm when the total addition time increased from 2 to 4 h. At 2 wt% cross-linker, the size decreased from 2.93 to 2.43 μm when this time went from 2 to 10.5 h.

For dispersion polymerization, all the chemicals are dispersed homogeneously in the medium (in our case methanol) in the beginning. The monomer and initiator concentrations in methanol are high, so that the alcohol phase is a major locus of the polymerization. The presence of the additive during the nucleation stage will play an unpredictable role on the formation of the nuclei. Therefore, we investigated the effect of the presence of the cross-linker in different stages through simply varying the addition start time. Figure 4.2A shows the morphologies of the particles which were prepared by starting to feed in the cross-linker when the polymerization reaction had started. The feed of the cross-linker lasted 4 h. It is observed that many tiny protrusions are randomly distributed on the particle surface (rough surface) (see Fig. 4.2A). According to our experience in making regular particles, we extended the total addition time to 10 h. This will lower the cross-linker concentration during
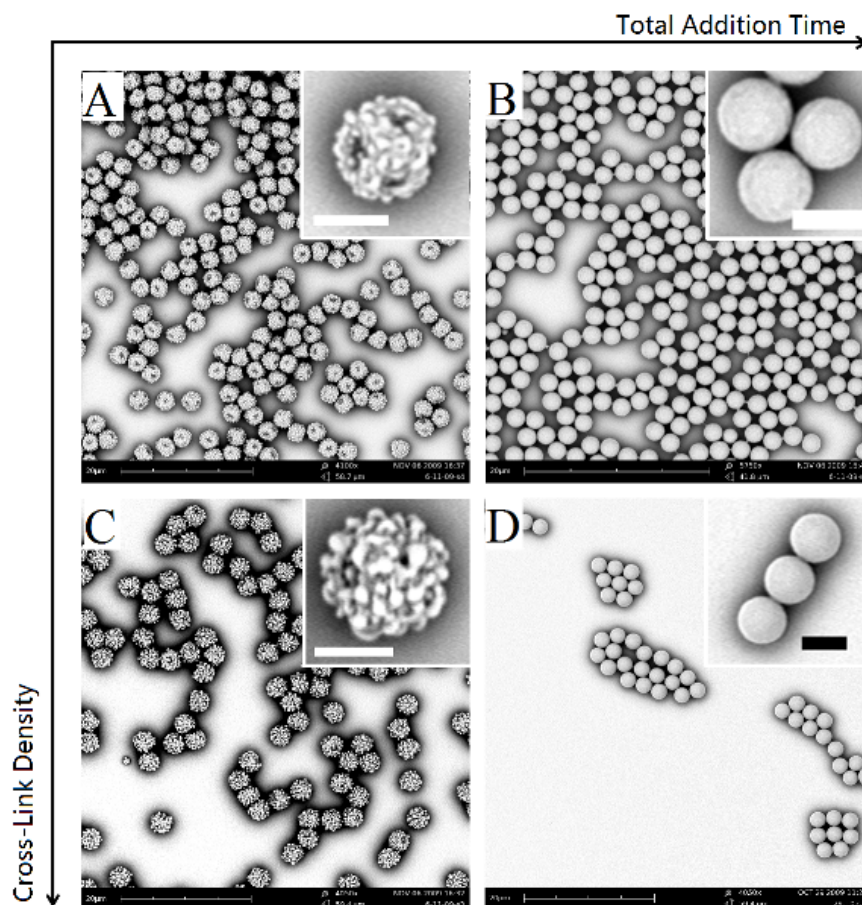
Figure 4.1. SEM micrographs of core-shell cross-linked PMMA particles prepared by the post-addition method, with different cross-link densities and total addition times according to Table 4.1 (the cross-link density and total addition time increased with the direct of the arrows). Key: (A) batch 1, (B) batch 3, (C) batch 8, (D) batch 10. The cross-link densities in A) and B) were 1 wt%, and in C) and D) were 2 wt%, respectively. The total addition times were 2 h in A) and C), 4 h in B) and 10.5 h in D), and the addition start time was 1.5 h in all the cases. The scale bars are 20 µm and the insets are 2 µm.

the nucleation stage while maintaining some degree of cross-linking in the cores of particles. The obtained particles had a smooth surface with a number of large dents, as shown in Figure 4.2B. Alternatively, in order to skip the perturbation of the sensitive nucleation stage altogether, the addition start time was postponed from 0 h to 0.5 h (see Fig. 4.2C), and then further to 1.5 h (see Fig. 4.2D). The surface of the particles became smoother as a later addition start time was used. In that case a 1.5 h addition start time the particle surface was even completely smooth. The occurrence of particles with a rough or a smooth surface apparently stems from the presence of a high concentration of the cross-linker during the sensitive nucleation stage. Therefore, one can infer that either a later addition time or a longer total addition time or both together are beneficial to producing spherical particles with a smooth surface. On the other hand, the occurrence of large dents in the particles seems to

correlated less well with the cross-linker concentration during nucleation as they may occur both at an addition start time of 1.5 h (see Fig. 4.1A, C) and at a long total addition time (Fig. 4.2B). The shape strongly resembles that after volume reduction of a soft sphere covered by a more rigid shell. [38, 39]
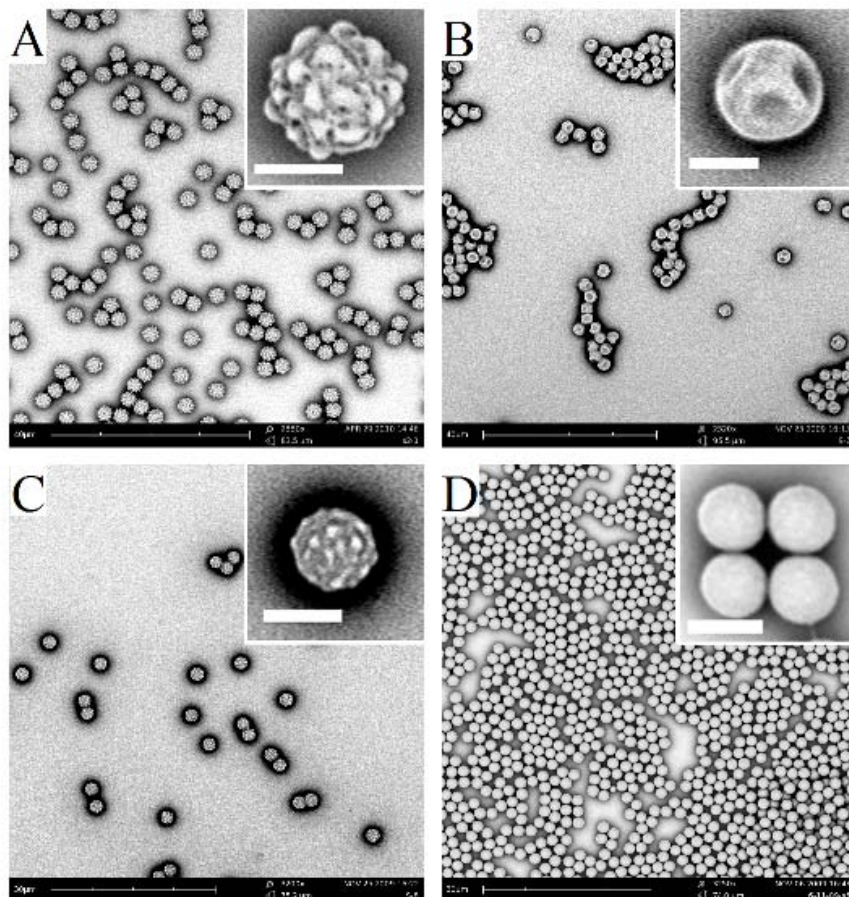
Figure 4.2. SEM micrographs of cross-linked PMMA particles with a cross-link density of 1 wt%, were prepared with different addition start time and total addition time according to Table 4.1. Key: (A) batch 5 (0-4 h), (B) batch 6 (0-10 h), (C) batch 2 (0.5-4 h), (D) batch 3 (1.5-4 h). The scale bars in A) and B) are 40 μm, in C) and D) are 30 μm, and the insets are 2 μm.

In order to test whether this behavior also applies to another polymer, we did the similar experiments on the preparation of polystyrene (PS) particles in dispersion polymerization. A series of homogeneously cross-linked polystyrene (PS) particles have been fabricated by the continuous addition method in which the sum of the addition start time and total addition time was kept fixed at 12 h. The recipes are summarized in Table 4.2. When the concentration of cross-linker was low (for instance 0.5 wt%, 1 wt%, 2 wt%, based on monomer mass), the obtained particles were smooth and spherical, and the size reduced with the increasing content of the cross-linker. As shown in Figure 4.3 (A, B and C), when the cross-link density of the PS particles increased from 0.5 wt% to 1 wt% and further to 2 wt%, the corresponding

diameter of the particles decreased from 1.26 μm to 1.20 μm and further to 1.01 μm, respectively. These results is in agreement with a conclusion mentioned in our previous work for PMMA system, [24] that is, the rise of the cross-link density of the particles results in the size reduction of the particles. Additionally, the success in producing these regular, yet homogeneously cross-linked PS particles reveals that the presence of the cross-linker at a low content level does not disturb the formation of the nuclei, which is probably also applicable to other co-monomers.
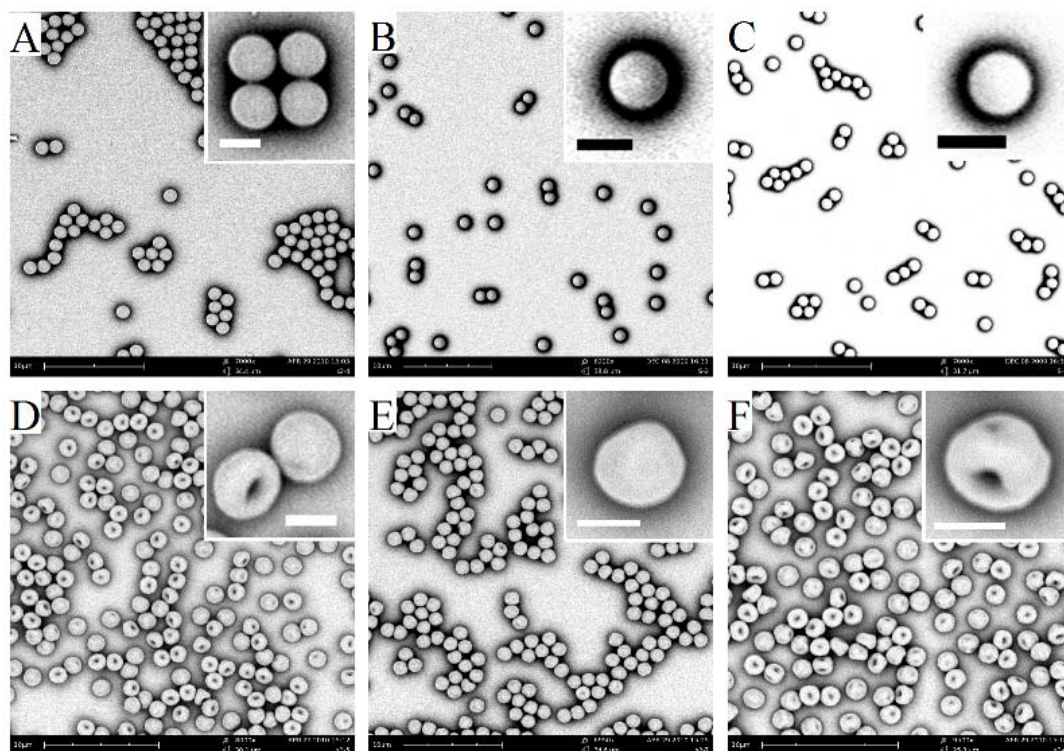
Figure 4.3. SEM micrographs of cross-linked PS particles with different cross-link densities, were prepared by a continuous addition of cross-linker (DVB) (details can be found in Table 4.2): (A) batch 1 (cross-link density was 0.5 wt%, based on the monomer mass); (B) batch 2 (1 wt%); (C) batch 3 (2 wt%); (D) batch 4 (4 wt%); (E) batch 5 (4 wt%); (F) batch 6 (6 wt%). The addition start time and total addition time were 0 and 12 h in all samples except in E) being 1 and 11 h, respectively. The scale bars are 10 μm and the insets are 1 μm.

However, further increasing the content of the cross-linker to 4 wt% led to PS particles with a large dent, as shown in Figure 4.3D. On a close inspection of Figure 4.3D, one can observe that very few particles have a secondary, but much more shallow dent. It implies that the ideal concentration of the cross-linker towards the cross-linked PS particles with a single dimple is somewhere between 2 to 4 wt%. In order to harvest regularly shaped particles, the long total addition time (12 h) cannot be further increased because there would be nearly no initiator left in the final stage. The alternative way is to delay the addition start time (1 h). The

obtained particles approach a spherical shape, as shown in Figure 4.3E. We expect that a later addition start time (> 1 h) would lead to regular shaped particles. On the other hand, when the concentration of the cross-linker was further increase to 6 wt%, the obtained particles were heavily deformed with a large dent and one or two other shallow dimples. In this case, it appears that if the cross-linker concentration is high at the end of the reaction (for example the addition lasted 12 h), a rigid shell will obtain. Then shrinkage of the monomer-swollen particles causes buckling of the surface. [38, 39]

4.3.2 Effect of the Stabilizer (PVP)

In dispersion polymerization, the stabilizer is usually regarded as an anti-coalescence barrier, which has an important role on the size and size distribution of the particles. Actually, it affects the morphology of the particles as well. For dispersion polymerization in polar media, polyvinylpyrrolidone (PVP) is a highly efficient stabilizer. Initially, three types of PVP were used: PVP K-15, K-30, and K-90. Their corresponding average molecular weighs are 10,000, 40,000 and 360,000 g/mol, respectively. The addition start time and total addition time were
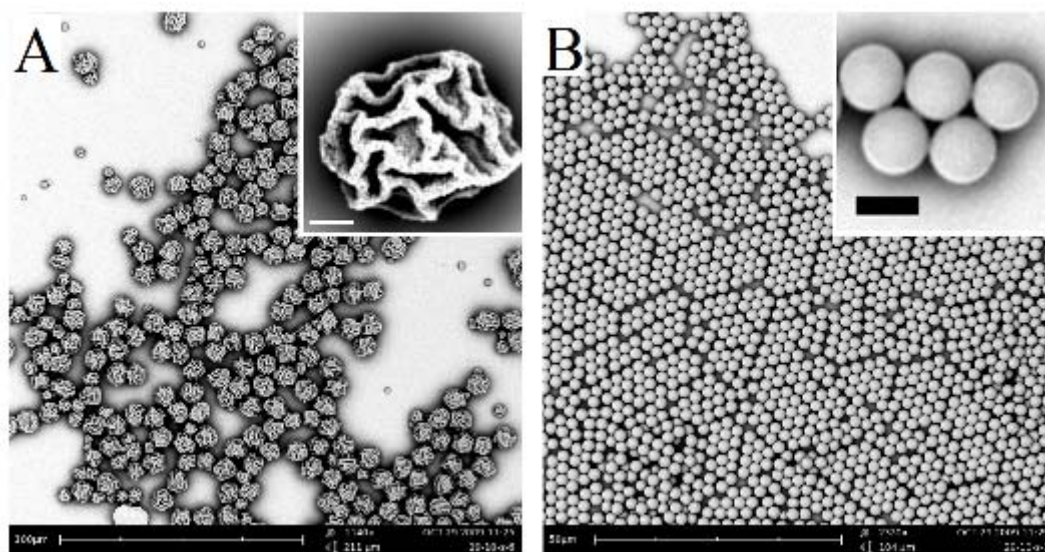
Figure 4.4. SEM micrographs of cross-linked PMMA particles (cross-linker density is 2 wt%) stabilized by different species of PVP: (A) PVP K-30 (batch 11 in Tab. 1); (B) PVP K-90 (batch 10 in Tab. 4.1). The addition start time and total addition time were 1.5 and 10.5 h, respectively. The scale bars are 100 μm in A) and 50 μm in B), respectively, and the insets are 2 μm.

fixed at 1.5 and 10.5 h, respectively. The batch in which PVP K-15 was used as stabilizer flocculated a few minutes after the addition of cross-linker. PVP K-30 and K-90 produced stable systems, the results are shown in Figure 4.4. The K-30 stabilized particles are polydisperse (PD = 26.0%) with a severely winkled surface, while the K-90 case is

monodisperse (PD = 2.1%) with a smooth surface, which directly reflects an increasing efficiency of PVP in stabilizing the system with increasing molecular weight. On the other hand, PVP influences the size of the particles too: the use of high molecular weight PVP led to a size decline of the particles (K-30: D = 7.89 μm; K-90: D = 2.43 μm). During the polymerization, the PVP-PMMA graft copolymers are absorbed by the immature particle, forming a steric barrier. If PVP is not efficient enough to sterically stabilize the particles, a polydisperse system will be obtained as shown in Figure 4.4A, or even worse, flocculation takes place as demonstrated in the batch of PVP K-15. On the other hand, for a given PVP concentration, increasing the molecular weight of the stabilizer increases the viscosity of the continuous phase, leading to smaller particles. The reason for the formation of wrinkled particles will be discussed in the 'effect of solvent' section.

Subsequently, we focused on investigating the effect of the concentration of PVP K-90 on the surface morphology of the cross-linked PMMA particles. In most earlier work, the particle size decreased with increasing concentration of the stabilizer. [16, 17, 19] This is because nuclei become stable at a earlier stage so that more nuclei are formed, leading to a smaller final particle size. Our results also showed this, which was reflected by the comparison of batch 8 with 9 in Table 4.1 (also see SEM images in Fig. 4.5). There was an obvious reduction in the size (from 2.93 μm to 1.75 μm) of the particle when the concentration of PVP K-90 was decreased from 1.5 to 3 g (the other experimental parameters were the same). Moreover, a high concentration of PVP helped to form spherical particles without heavy dents or a wrinkled surface, as shown in Figure 4.5, which was probably caused by the size of the particles. As mentioned before, a high concentration of stabilizer promotes the formation of smaller particles, which are more rigid than large particles. On the other hand, the chance of the cross-linker diffusing into the core of the small particles is much higher than the big particles, which will lead to a homogeneously cross-linked particle system. Therefore, the possibility of forming heavy dents decreases with increasing the concentration of the stabilizer. On a close inspection of batch 9 in Figure 4.5B, the roughness of the particles is non-uniform, some exotic (big) protrusions are present. This is reminiscent of the formation of the snowman-shaped particles developed by Sheu *et al.* [41] The cross-linked seed particles were swelled by a monomer, and then the elevation of the temperature led to the shrinkage of the cross-linked polymer network, compelling a part of the swelling monomer to form a large number of tiny droplets. Similarly, during the particle growth stage, the cross-linked immature particles absorbed the monomer from the medium, forming swollen particles. Then, more cross-linker was absorbed by the particles and built in the polymer network. The increase of the cross-link density of the system induced the shrinkage of the cross-linked polymer

network taking place, some swelling monomer extruded out in the form of relatively big liquid protrusions, and these big protrusions remained after the polymerization.
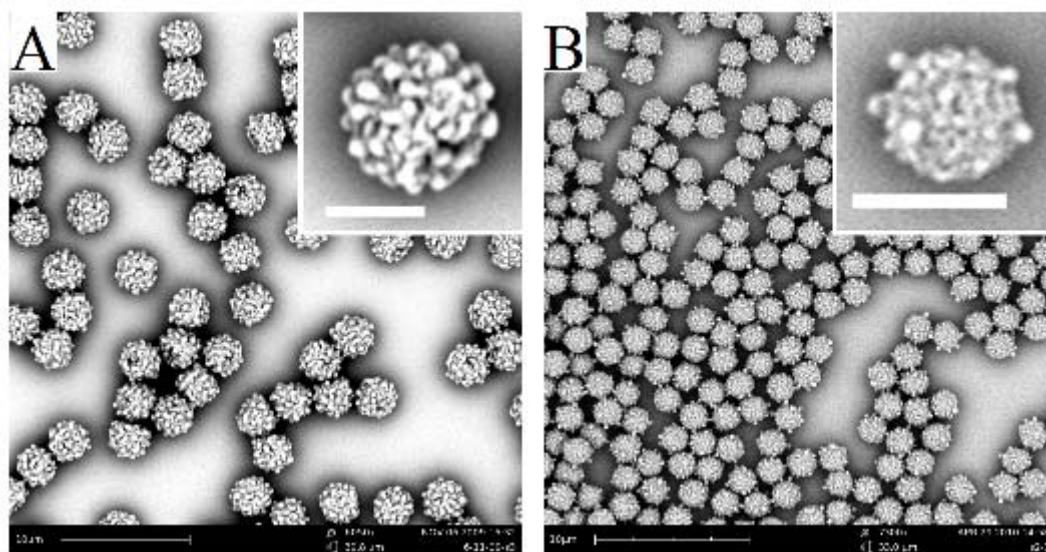
Figure 4.5. SEM micrographs of cross-linked PMMA particles with a cross-link density of 2 wt%, were prepared with different amounts of stabilizer (PVP K-90): (A) 1.5 g (batch 8 in Tab. 4.1); (B) 3 g (batch 9 in Tab. 4.1). The addition start time and total addition time were 1.5 and 2 h, respectively. The scale bars are 10 μm and the insets are 2 μm.

4.3.3 Effect of the Cross-Linker

Generally, the cross-linker interferes with the sensitive particle nucleation stage, causing flocculation and deformation. Therefore, in order to circumvent the problem that was caused by the presence of the cross-linker during the nucleation stage, we delayed the addition of the cross-linker to the particle growth stage (1.5 h), and it was successively fed into the reaction medium. Two kinds of reagents (EGDMA and DVB) were used as cross-linker for exploring their effect on the morphology of the particles. When 1 wt% of EGDMA was used, it took 4 h of slow addition to yield spherical particles with a smooth surface in a narrow size distribution (see Fig. 4.6A). However, the use of an alternative cross-linker DVB produced spherical particles but with a nodules surface (see Fig. 4.6B). To study, the cross-link density was increased to 2 wt%, as the case shown in Figure 4.6C. In order to obtain the same appearance (spherical shape and smooth surface) with the case owning cross-link density of 1 wt%, the total addition time had to be prolonged to 10.5 h. Again, slightly rough spheres were obtained as EGDMA was replaced by DVB. All results are shown in Figure 4.6. Thomson *et al.* [28] pointed out that commercial DVB was normally a mixture of *para* and *meta* isomers. For the *para* isomer in particular, the first double bond reacts faster than the second and also reacts more rapidly than monomer itself. The preferential consumption of *p*-DVB early in the
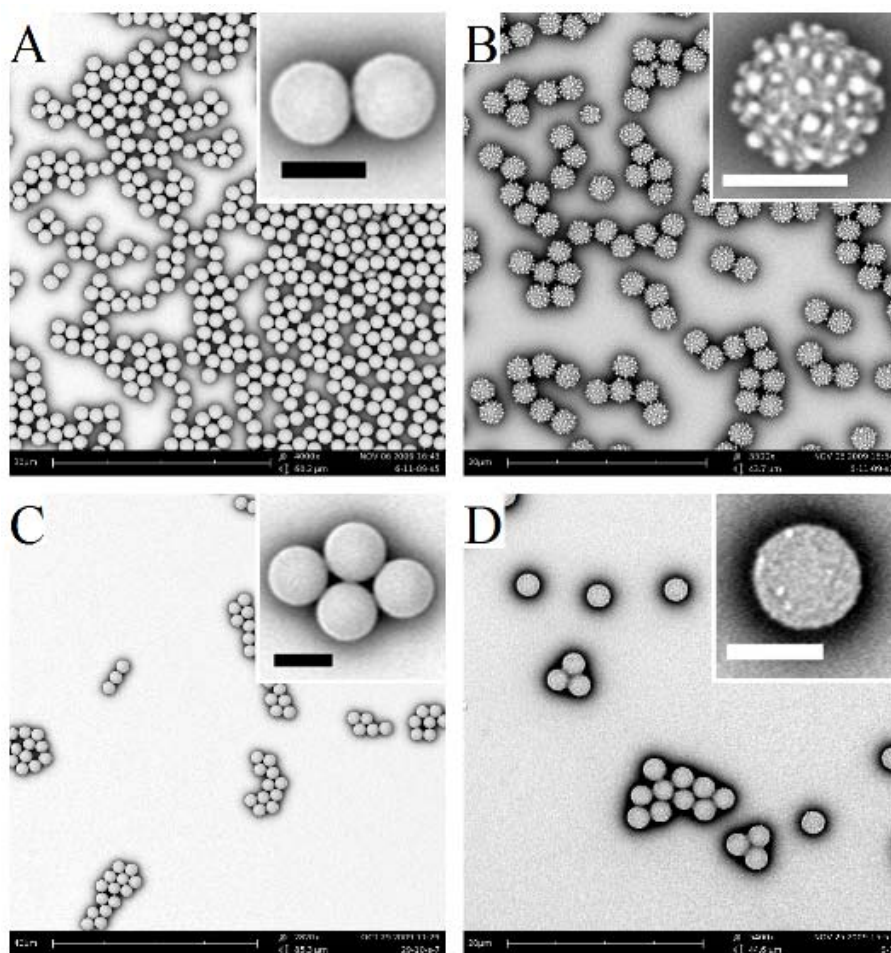
Figure 4.6. SEM micrographs of cross-linked PMMA particles prepared by different kinds of cross-linkers and cross-link densities: (A) 1 wt% of EGDMA (batch 3 in Tab. 4.1); (B) 1 wt% of DVB (batch 4 in Tab. 4.1); (C) 2 wt% of EGDMA (batch 10 in Tab. 4.1); (D) 2 wt% of DVB (batch 13 in Tab. 4.1). The addition start time and total addition time were 1.5 and 4 h in A) and B), 1.5 and 10.5 h in C) and D), respectively. The scale bars are 30, 20, 40 and 20 μm in A), B), C) and D), respectively, and the insets are 2 μm.

reaction can be a complicating feature of the use of DVB as a cross-linker. Therefore, the result of copolymerization of MM with DVB is a tendency toward the congregation of *p*-DVB units in the MM chains and a more even distribution of *m*-DVB isomers. [42] After a double bond of DVB has reacted, the pendant vinyl group is less reactive than either monomer. For example, in the copolymerization of styrene with pure *p*-DVB and *m*-DVB, Hild and Rempp [42] observed that the onset of gelation occurred much earlier and at lower conversion in the *p*-DVB system, strongly suggesting that such pendant groups in the *p*-DVB are more reactive than their meta-substituted equivalents. These results point to early consumption of *p*-DVB as the source of the deformation of the particle in the dispersion polymerization. In comparison with DVB, EGDMA has a slower reactivity in co-polymerization with MM, [40] and the

reactivities of the two methacrylate groups of EGDMA are essentially identical. As a consequence, one expects that many of the problems encountered when DVB is used as a cross-linker will be less serious for EGDMA.

4.3.4 Effect of the Solvent

Solvent plays an important role in the preparation of polymer particles in dispersion polymerization. [14, 16, 19, 24, 26] At first, two kinds of polar solvents, methanol and ethanol, were attempted. The obtained particles are shown in Figure 4.7. The sample (Fig. 4.7A) prepared in methanol is more heavily wrinkled than the one in ethanol (Fig. 4.7B). This probably associated with the difference of their solubility parameters. In principle, the degree of solubility of the precipitating polymer is inversely proportional to the difference of the solubility parameters of the dispersing medium and the polymer ($\delta_s - \delta_p$, where δ_s is the solubility parameter of the solvent and δ_p the solubility parameter of the polymer). [43, 44] The difference of solubility parameters between PMMA (δ_p = 19.0 MPa$^{1/2}$) and ethanol (δ_s = 26.2 MPa$^{1/2}$) is smaller than that of PMMA and methanol (δ_s = 29.7 MPa$^{1/2}$), [43] which implies that ethanol has a better solvency for PMMA, shifting the polymerization locus away from the particle phase into solution. Therefore, when methanol was used as the solvent, the bulk of the propagation of the polymerization took place within the particle phase, and more cross-linker was absorbed into the swollen particle where it contributes to a wrinkling of the surface. Using ethanol instead of methanol, moved the polymerization locus to the continuous
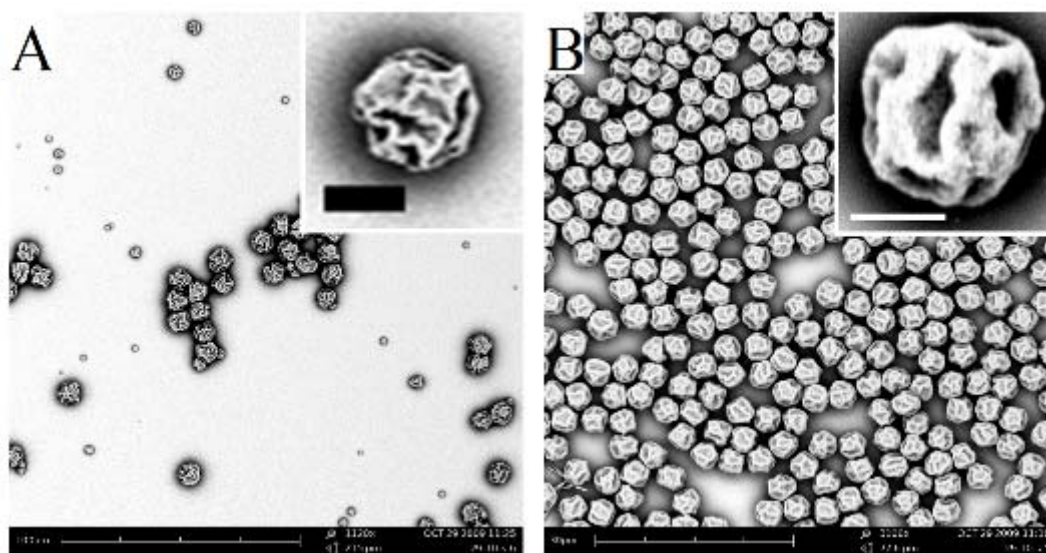
Figure 4.7. SEM micrographs of winkled cross-linked (cross-link density is 2 wt%) PMMA particles fabricated in different solvents: (A) methanol (batch 11 in Tab. 1); (B) ethanol (batch 12 in Tab. 1). The addition start and total addition time were 1.5 and 10.5 h, respectively. The scale bars are 100 μm in A) and 30 μm in B), and the insets are 5 μm in A) and 2 μm in B), respectively.

phase. Growth occurred as existing particles absorbed polymeric materials produced in the continuous phase, and opportunities for shape preservation rose as the material assimilated could be directed to those regions where expansion was still permitted.
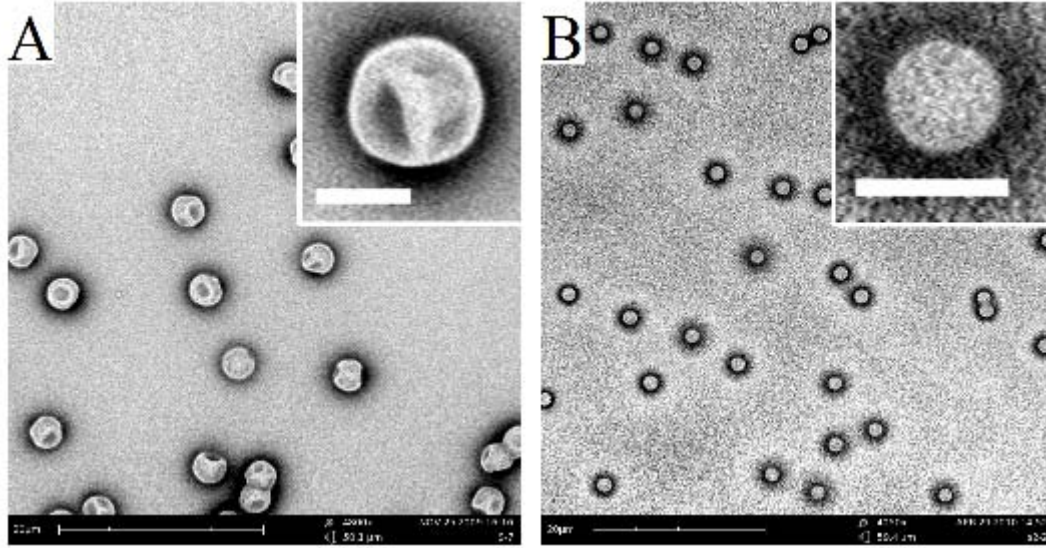
Figure 4.8. SEM micrographs of 1 wt% cross-linked PMMA particle at different methanol/water mass ratios: (A) 100/0 (batch 6 in Tab. 4.1); (B) 80/20 (batch 7 in Tab. 4.1). The addition start time and total addition time were 0 and 10 h, respectively. The scale bars are 20 μm, and the insets are 2 μm.

Mixtures of methanol and de-ionized water have also been tried in our experiments, for testing its influence on a variety of the morphologies of the particles. A pair of representative examples is shown in Figure 4.8. A difference in recipe between these two samples is: the sample in Figure 4.8A (batch 6 in Tab. 4.1) was prepared in a mixture of methanol/water (80:20 in weight), while the particles in Figure 4.8B (batch 7 in Tab. 4.1) were synthesized in the pure methanol environment. Due to the presence of the cross-linker during the nucleation stage, the particles in Figure 4.8B possess a heavily dented shape. The addition of a poorer [16, 19, 24] solvent (water) for PMMA led to smaller, but less deformed particle system. The addition of water further lowers the solubility of PMMA, inducing the critical chain length to decrease, directly resulting in smaller particles (see the inset in Fig. 4.8B). As mentioned before, in a system consisting of small particles, the occurrence of deformation was less likely because of its higher rigidity. On the other hand, from the point of solubility parameter, an empirical solubility parameter (δ) of the mixture of methanol/water can be calculated by: [45]

$$\delta = (\upsilon_m \delta_m^2 + \upsilon_w \delta_w^2)^{\frac{1}{2}} \tag{4.1}$$

where υ_m and υ_w are the volume fraction of methanol and water respectively. δ_m (29.7 MPa$^{1/2}$) and δ_w (48.0 MPa$^{1/2}$) [36] are the solubility parameters of methanol and water, respectively.

When the mass ratio between methanol and water is 80:20, the corresponding δ is 33.4 MPa$^{1/2}$, and the difference of the solubility parameter between the mixture and PMMA ($\delta - \delta_p$ =14.4 MPa$^{1/2}$) is larger than this between methanol and PMMA ($\delta_s - \delta_p$ = 8.9 MPa$^{1/2}$). It infers that the polymerization locus is away from the medium into particles in the case prepared in the methanol/water mixture, which further indicates more EGDMA will be absorbed along by the particle phase, and the potential for the formation of deformed particles is decreasing. Combining all factors, one can conclude that the addition of a poor solvent for PMMA results in smaller and less deformed particles. However, further decreasing the methanol/water mass ratio to 70/30 led to coagulation, mainly because of the fast nuclei generation rate. [24]

4.3.5 Formation Mechanism

Dispersion polymerization is used for the production of monodisperse polymeric particles in the micron size range. Both the size and size distribution of the particles can be well-controlled by varying the reaction parameters. Generally, the system is homogeneous prior to the polymerization. As soon as the polymerization is initiated by the decomposition of an initiator, oligomer chains grow in the continuous phase until they reach the critical chain length where they precipitate to form nuclei by a self aggregative mechanism. The nuclei are unstable and can aggregate with each other. Concurrently, nuclei absorb the PVP-monomer graft stabilizer and become stable particles, which capture oligo-radicals and nuclei from the continuous phase. As long as enough mature particles are formed to capture all the oligomers and nuclei, no new particle is formed and the formation of the particles is completed. However, the addition of the cross-linker would 'contaminate' the dispersion polymerization, leading to a diversity of irregular particles or bad results (*e.g.*, flocculation and agglomeration). In order to successfully harvest the regular shaped particles, Dullens *et al.* [25, 26] suggested to feed the cross-linker after the nucleation had finished for PMMA system in a polar medium. Song *et al.* [23, 30] used a similar approach for the preparation of cross-linked PS particles. Both of them assumed that the nucleation stage was much more sensitive, and complex than the particles growth stage. We circumvented the potential problems induced by the addition of the cross-linker prior to the formation of the nucleation, and selected the particle growth stage as the time during which the feeding of the cross-linker was carried out. The recipe and other experimental parameters are listed in Table 4.1, batch 1. During the synthesis of batch 1, the addition of the mixture containing cross-linker was started at 1.5 h and samples were taken from the reaction flask at intervals. The samples were quenched in a large amount of 'cold' (room temperature) methanol, to prevent further growth of the particles. Subsequently, SEM was used to obtain the details in morphology, size and size distribution of the particles at different time marks, and summarized in Figure 4.9 and 4.10.

In the first 1.5 hours (1.5 h is the addition start time), the particles could retain their spherical shape, which also implies the nucleation stage had been finished in 1.5 h of reaction. At the 2.5 h mark, particles seems slightly deformed, but still with a smooth surface. 1.5 hours later (at the 4 h mark), some dimples were visible. We believe this is the time when the formation of the heavy dents started. At this point the cross-linker addition is finished. At the 5.5 h mark, the dimples became deeper. Actually, this is induced by the addition of cross-linker, which copolymerized with monomer forming a cross-linked shell. The polymerization of swollen core induced self-shrinkage, pulling the cross-linked rigid shell and developing a deformed particles with dents. Meanwhile, we also observed a secondary structure comprising distinct bumps of uneven dimension dotted over the entire surface. Ultimately, the lava-texture-like particles were obtained.

In detail, after the addition started, the cross-linked network began to develop within each growing microsphere. As just mentioned, the cross-linker possessed much more reactivity than that of monomer, the cross-linker mostly reacted with each other in the swollen immature particles at initial stage, the core-shell cross-linked structures formed. [24] With a gradual increase in cross-link density, the cross-linked swollen core started to polymerize and pull the cross-linked more rigid shell, causing the macro-deformation (dents) of the cross-linked shell on the particles. On the other hand, the opportunity existed for some of the adsorbed stabilizer chains to join in the polymer structure due to the cross-linker having two vinyl groups. In this situation, radial growth could not be linearly sustained indefinitely because of the fixed cross-linked network, meanwhile graft production decreased with the reaction time as MM and PVP levels fall due to the reduction in concentration of cross-linker. Surface roughing commenced after most of the cross-linker was used up with the appearance of small dimples on the surface, presenting the low concentration of cross-linker did not enable to induce macro-deformation of the particles or the cross-linked shell was rigid enough to resist the formation of dents. Growth of the particles was still possible, only limited in the location whose surface was protected by the mobile graft. Nodules formed and became bigger, while the shape of them became less regular, indications that some merging has occurred. Note, small protrusions were also present on the inner walls of the dent, inferring that the shell is homogeneously cross-linked. This formation mechanism based on our observation was different with that in the work of Thomson *et al.*, [27, 28] who described the formation of these particles as being due to the inhomogeneity of the cross-linker among the shell of the particles.

In Thomson's paper, [27] it was suggested two ways for tolerating a high absolute quantity of DVB in a one-pot co-polymerization for PS system. Both of them were trying best to
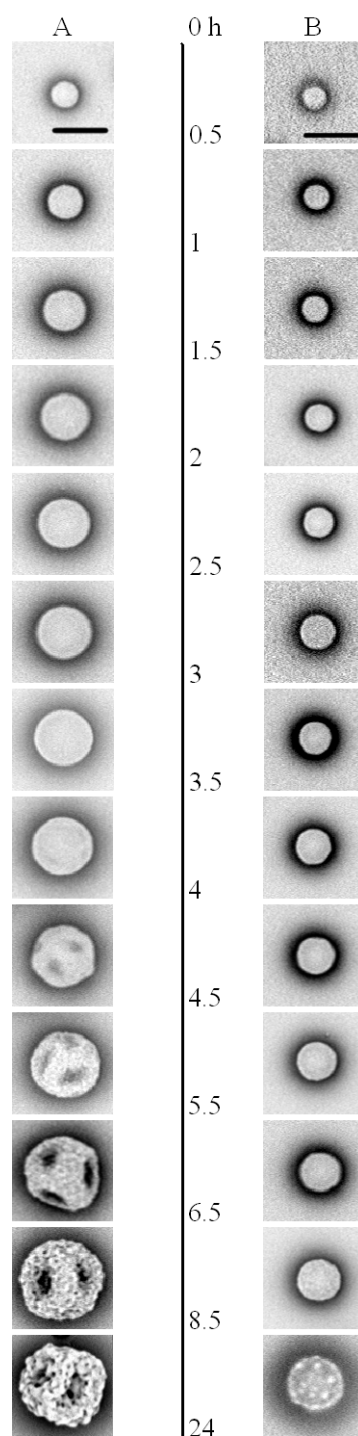
Figure 4.9. The SEM micrographs of the formation of cross-linked (1 wt%) PMMA particles in time (A) in a pure nitrogen atmosphere (batch 1 in Tab. 4.1), (B) in an un-pure nitrogen atmosphere (batch 1 in Tab. 4.1).

decrease the average length of the chains in essence. We were inspired by these suggestions, and brought in a tiny volume (which is hard to quantify) of air to 'pollute' the pure nitrogen
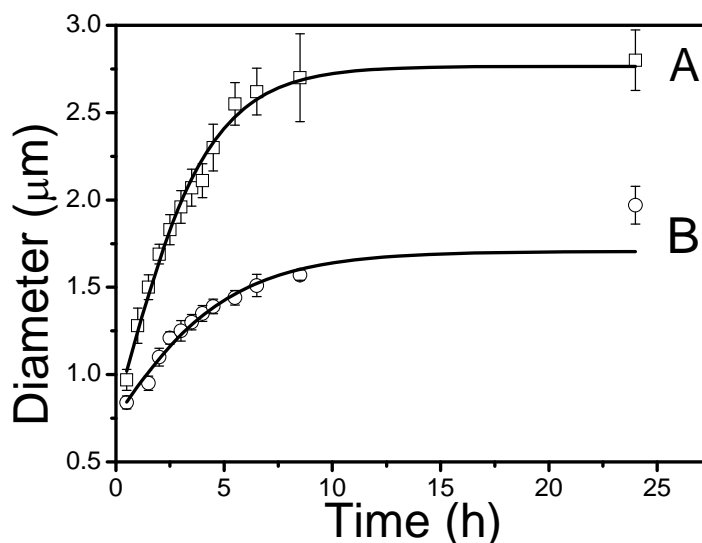
Figure 4.10. The growth of batch 1 in Table 4.1 in diameter as a function of time, (A) in a pure nitrogen atmosphere, corresponding to the case in Figure 4.9A, (B) in a un-pure nitrogen atmosphere, corresponding to the case in Figure 4.9B. The open squares and circles are the experimental date points, and the solid lines are a guide to the eye.

atmosphere during sampling. Air contains oxygen which can act as an inhibitor, hindering the radical polymerization. Sampling this batch at intervals exhibits a detailed formation process of it, and its SEM images were shown in Figure 4.9B and its diameters were summarized in Figure 4.10. We believe, the existence of the inhibitor disturbs the 'normal' process of the polymerization, in other words, it hinders the polymerization, which infers a chance that some oligmers cannot grow to the critical chain length to precipitate from the continuous medium. This directly results in smaller particles, and also hint that less cross-linker will join in the network construction of the cross-linked particles. Both of them restrain a macro-deformation (heavy dents) of the particles, but not the formation of a rugged surface.

4.4 CONCLUSIONS

The co-polymerization of the monomer and cross-linker led to the production of several new classes of polymer colloids with a variety of morphologies, which was prepared based on a successive linear addition method in dispersion polymerization. For the PMMA system, a high concentration of the cross-linker at the growth stage, or the presence of the cross-linker during the nucleation stage of the particles, led to the formation of heavy dents and/or many small nodules on the surface of the particles. Similar phenomena were also observed for the PS cases. A slow addition of the cross-linker or a high quantity (a high concentration of PVP) or quality (PVP with a long average molecular weight) of the stabilizer, could alleviate the

formation of the dents, and produce less irregular particles. Moreover, decreasing the difference of the solubility parameter between the polymer and solvent would compel the polymerization locus away the swollen immature particles, yielding less wrinkled particles. Additionally, the presence of a poor solvent for PMMA reduced the size of the particles, which has two functions in the synthesis of the regular shaped particles: one is, the smaller particles have a relatively higher rigidity which hinders the 'macro-deformation' of the particles; the other one is, the poor solvents force more cross-linker polymerizing in the particle phase, which would result in a more homogeneous dispersion of the cross-linker in the particle phase, decreasing the potential of the deformation. Following these suggestions, spherical cross-linked particles were successfully fabricated. Alternatively, dimpled and/or rough, yet monodisperse, polymer particle can be synthesized. At last, the clear formation mechanism was exploited by monitoring the maturing process of the particles either in a pure or impure nitrogen atmosphere. We believe these results provide insight into the formation of cross-linked polymer particles, and are also useful for constructing new monodisperse non-spherical particles reproducibly.

4.5 ACKNOWLEDGMENTS

4.6 REFERENCES

[1] Xia, Y.; Gates, B.; Yin, Y.; Lu, Y. *Adv. Mater.* **2000**, *12*, 693-713.

[2] Ugelstad, J.; Soderberg, L.; Berge, A.; Bergstrom, J. *Nature* **1983**, *303*, 95-96.

[3] Chen, Y.; Au. J.; Kazlas, P.; Ritenour, A.; Gates, H.; Mc-Creary, M. *Nature* **2003**, *423*, 136-136.

[4] Comiskey, B.; Albert, J. D.; Yoshizawa, H.; Jacobson, J. *Nature* **1998**, *394*, 253-255.

[5] Theodore, A. N.; Chattha, M. S. *J. Coat. Technol.* **1985**, *57*, 67.

[6] Yu, D.; An, J. H.; Bae, J. Y.; Jung, D.; Kim, S.; Ahn, S. D.; Kang, S.; Suh, K. S. *Chem. Mater.* **2004**, *16*, 4693-4698.

[7] Han, M.; Gao, X.; Su, J. Z.; Nie, S. *Nat. Biotechnol.* **2001**, *19*, 631-635.

[8] Chen, S. A.; Lee, S. T. *Macromolecules* **1991**, *24*, 3340-3351.

[9] Bourgeat-Lami, E.; Tissot, I.; Lefebvre, F. *Macromolecules* **2002**, *35*, 6185-6191.

[10] Nagao, D.; Sakamoto, T.; Konno, H.; Gu, S.; Konno, M. *Langmuir* **2006**, *22*, 10958-10962.

[11] Branford, E. B.; Vanderhoff, J. W. *J. Appl. Phys.* **1955**, *26*, 864-871.

[12] Ugelstad, J.; Kaggerud, K. H.; Hansen, F. K.; Berge, A. *Makromol. Chem.* **1979**, *180*, 737-744.

[13] Okubo M.; Tsujihiro M. US Patent 4, 996, 265; **1991**.

[14] Barrett, K. E. J. *Dispersion polymerization in organic media*; Wiley-Interscience: New York, **1975**.

[15] Kawaguchi, S.; Ito, K. *Adv. Polym. Sci.* **2005**, *175*, 299-328.

[16] Tseng, C. M.; Lu, Y. Y.; El-Aasser, M. S.; Vanderhoff, J. W. *J. Polym. Sci., Part A: Polym. Chem.* **1986**, *24*, 2995-3007.

[17] Lok, K. P.; Ober, C. K. *Can. J. Chem.* **1985**, *63*, 209-216.

[18] Paine, A. J.; Luymes, W.; McNulty, J. *Macromolecules* **1990**, *23*, 3104-3109.

[19] Shen, S.; Sudol, E. D.; El-Aasser, M. S. *J. Polym. Sci., Part A: Polym. Chem.* **1993**, *31*, 1393-1402.

[20] Shen, S.; Sudol, E. D.; El-Aasser, M. S. *J. Polym. Sci., Part A: Polym. Chem.* **1994**, *32*, 1087-1100.

[21] Antl, L.; Goodwin, J. W.; Hill, R. D.; Ottewill, R. H.; Owens, S. M.; Papworth, S.; Waters, J. A. *Colloids Surf.* **1986**, *17*, 67-78.

[22] Takahashi, K.; Miyamori, S.; Uyama, H.; Kobayashi, S. *J. Polym. Sci., Part A: Polym. Chem.* **1996**, *34*, 175-182.

[23] Song, J.-S.; Tronc, F.; Winnik, M. A. *J. Am. Chem. Soc.* **2004**, *126*, 6562-6563.

[24] Peng, B.; van der Wee, E.; Imhof, A.; van Blaaderen, A. *Langmuir* **2012**, *28*, 6776-6785.

[25] Dullens, R. P. A.; Claesson, M.; Derks, D.; van Blaaderen, A.; Kegel, W. K. *Langmuir* **2003**, *19*, 5963-5966.

[26] Dullens, R. P. A.; Claesson, M.; Kegel, W. K. *Langmuir* **2004**, *20*, 658-664.

[27] Thomson, B.; Rudin, A.; Lajoie, G. *J. Polym. Sci., Part A: Polym. Chem.* **1995**, *33*, 345-357.

[28] Thomson, B.; Rudin, A.; Lajoie, G. *J. Appl. Polym. Sci.* **1996**, *59*, 2009-2028.

[29] Elsesser, M. T.; Hollingsworth, A. D. *Langmuir* **2010**, *26*, 17989-17996.

[30] Song, J.-S.; Winnik, M. A. *Macromolecules* **2005**, *38*, 8300-8307.

[31] Marechal, M.; Kortschot, R. J.; Demirors, A. F.; Imhof, A.; Dijkstra, M. *Nano Lett.* **2010**, *10*, 1907-1911.

[32] Sacanna, S.; Irvine, W. T. M.; Chaikin, P. M.; Pine, D. J. *Nature* **2010**, *464*, 575-578.

[33] Badaire, S.; Cottin-Bizonne, C.; Stroock, A. D. *Langmuir* **2008**, *24*, 11451-11463.

[34] Zhao, K.; Mason, T. G. *Phys. Rev. Lett.* **2007**, *99*, 268301.

[35] Kraft, D. J.; Ni, R.; Smallenburg, F.; Hermes, M.; Yoon, K.; Weitz, D. A.; van Blaaderen, A.; Groenewold, J.; Dijkstra, M.; Kegel, W. K. *Pro. Natl. Acad. Sci. USA* **2012**, *109*, 10787-10792.

[36] Xu, L.; Li, H.; Jiang, X.; Wang, J.; Li, L.; Song, Y.; Jiang, L. *Macromol. Rapid. Commun.* **2010**, *31*, 1422-1426.

[37] Huang, Y.; Wang, J.; Zhou, J.; Xu, L.; Li, Z.; Zhang, Y.; Wang, J.; Song, Y.; Jiang, L. *Macromolecules* **2011**, *44*, 2404-2409.

[38] Vliegenthart, G. A.; Gompper, G. *New J. Phys.* **2011**, *13*, 045020.

[39] Yin, J.; Cao, Z.; Li, C.; Sheinman, I.; Chen, X. *Pro. Natl. Acad. Sci. USA* **2008**, *105*, 19132-19135.

[40] Wiley, R. H.; Sale, E. E. *J. Polym. Sci.* **1960**, *42*, 491-500.

[41] Sheu, H. R.; El-Aasser, M. S.; Vanderhoff, J. W. *J. Polym. Sci., Part A: Polym. Chem.* **1990**, *28*, 653-667.

[42] Hild, G.; Rempp, P. *Pure Appl. Chem.* **1981**, *53*, 1541-1556.

[43] Burke, J. *AIC Book Pap. Group Annu.* **1984**, *3*, 13-58.

[44] Almog, Y.; Reich, S.; Levy, M. *Br. Polym. J.* **1982**, *14*, 131-136.

[45] Paine, A. J. *Macromolecules* **1990**, *23*, 3109-3117.

<div style="text-align: right">

5

</div>

Synthesis of Fluorescent Monodisperse Non-Spherical Dumbbell-Like Model Colloids

ABSTRACT

We describe a facile and flexible approach for synthesizing uniform non-spherical micron sized PMMA (poly(methyl methacrylate)) colloids with well-controlled protrusions. When homogeneously cross-linked PMMA spheres were used as seeds in a swelling process using again methyl methacrylate monomer, they were found to transform into non-spherical particles with a single or multiple protrusions mainly depending on the cross-link density of the seeds. Alternatively, if core-shell PMMA spheres bearing a highly cross-linked shell around an uncross-linked 'soft' core were employed as seed particles, they always developed just a single protrusion. Precise control over the anisotropy of the particles was achieved by varying the amount and composition of the swelling mixture as well as the concentration of the stabilizer. Subsequently, the phase separation was enhanced and protrusions could be readily polymerized through temperature elevation of the system, yielding PMMA 'snowman'-like or dumbbell-like colloids. Furthermore, these particles could be labeled with fluorescent dyes either before or after the polymerization, and transferred into apolar, refractive index and density matching liquids (cyclohexyl bromide (CHB) and/or decalin), enabling their use in quantitative confocal fluorescence microscopy studies in concentrated systems. Some examples of the use of these particles as model system for real space analysis are given. These examples include the formation of plastic crystals, a special form of a colloidal crystal where the particles are positionally ordered but orientationally disordered. Additionally, the non-spherical particles could be organized into semi-flexibly bonded colloidal chains aided by an electric field in a polar solvent (formamide). Such chains of anisotropic particles are interesting as polymer analogs and for the preparation of new materials.

5.1 INTRODUCTION

Anisotropic colloidal particles and their self-assembly have been studied for a long time in the field of colloid science: see e.g. the review in ref [1]. However, the number of papers compared to those on spherical colloids has stayed relatively low until recently. As is apparent from some recent review papers [1-6] more complex colloids [7] made specifically with further self-assembly in mind are becoming a main stream topic. This is not only because it is realized that the extra degrees of freedom of anisotropic particles give rise to interesting new ways to tune materials' properties, such as in liquid crystal phases or photonic crystals, but also because new phenomena can be probed in model studies, such as the role of particle rotations in crystallization and the glass transition.

So many synthesis procedures have been developed for anisotropic inorganic, [8, 9] organic particles [10-12] or mixed inorganic-organic particles [13-15] that we can only give here some typical examples that focus on methods that also take spheres as starting material. In this paper we present a study on making anisotropic particles starting from spherical polymer particles through a method that is already several decades old and relies on swelling polymer seed particles with monomer and relying on the fact that for certain conditions a subsequent polymerization can result in anisotropic polymer particles. On swelling cross-linked seed particles with a monomer and by a subsequent heating step elastic stress build-up causes the excess monomer to phase separate in the form of a protrusion which can be polymerized. For instance Sheu et al. [16] demonstrated this method to produce several micrometer sized polystyrene (PS) particles with the shape of two interpenetrating spheres (now often called 'snowmen' particles or for equal sized sphere sections: dumbbells). Of much more interest in recent times is the extension of this method by Mock et al. [17, 18] to anisotropic particles of sub-micrometer size by the addition of a grafted hydrophilic layer on the surface of the seed particles to modify the surface tension and thus the wetting of the PS seed particles.

In addition, this method was also extended to hetero-phase dumbbell particles by using different monomers in the swelling stage. [13, 19] However, almost all the seed species were cross-linked PS particles. Developing new classes of seed particles and growing the size of the protrusions on the seed particles larger than the seeds, (in other words, inverted snowman shaped), are challenges, in this chapter we focus on the material of the seeds and the protrusions being poly(methyl methacrylate) (PMMA).

Sterically stabilized PMMA particles have received great attention in recent years in many model studies as both the refractive index and mass density of such particles can be matched

readily with organic solvent mixtures. [20-23] Furthermore, the solvent mixtures and polymeric stabilizers can be used to tune the particle interactions from very soft to nearly hard and with external electric fields of high enough frequency (MHz range) a dipolar interaction can be superimposed on top of the hard or long-ranged repulsions as well. [24-26] In addition, these kind of particles have also been shown to allow for the creation of systems with oppositely charged interactions that can form equilibrium structures like binary crystals. [27, 28] Also, anisotropic colloids have been made using a stretching method starting from spherical particles. [12] However, as far as we know, snowman or dumbbell shaped colloids of PMMA made using the above mentioned monomer swelling and second polymerization method have not yet been used in model studies on concentrated strongly interacting dispersions. This is probably related to the difficulties that arise in the preparation of uniform, highly cross-linked PMMA colloids as seeds and the subsequent swelling and protrusion formation. We, too, experienced such difficulties and often obtained very rough or polydisperse colloids, or found that the protrusion failed to form at all. Key to a solution is the preparation of seed spheres with an optimal cross-linked architecture. In previous work, [29] we succeeded in the production of either lightly or highly cross-linked PMMA seed spheres with a narrow size distribution by feeding the cross-linker slowly to the reaction vessel. By controlling the addition start time, either before or after the nucleation stage has finished, PMMA spheres could be obtained that were cross-linked either homogeneously or only in a shell . The slow cross-linker feed allowed us to obtain particles that were spherical and had a smooth surface up to a cross-link density as high as 10 wt%. With these particles used as seeds it turned out to be possible to produce monodisperse, dumbbell-shaped, all PMMA colloids using the swelling and protrusion method. The typical fabrication processes and some examples of obtained anisotropic particles are shown in Figure 5.1. Upon being in contact with methyl methacrylate (MMA), the cross-linked polymer PMMA network first swells by absorbing excess MMA and then expels some of it to form a protrusion (see the second bottom optical microscopy images in Fig. 5.1). The cross-linked PMMA seeds show similar swelling and protruding behaviors as with PS seeds. [30, 31] This was followed by a heating step in the presence of an initiator that polymerized the swelling monomer and increased the size of the protrusions (see the two bottom right images in Fig. 5.1). Our technique allows for tuning the shape from a dimeric colloid (snowman or dumbbell) to a colloid with multiple protrusions (rough particles) via adjustment of the swelling ratio and the cross-linking structure and density of the seeds, which control the rigidity and swelling capacity of the cross-linked polymer network. Furthermore, we could manipulate the radius ratio of the protrusion to the swollen seed (α, details see experimental section), which enables control
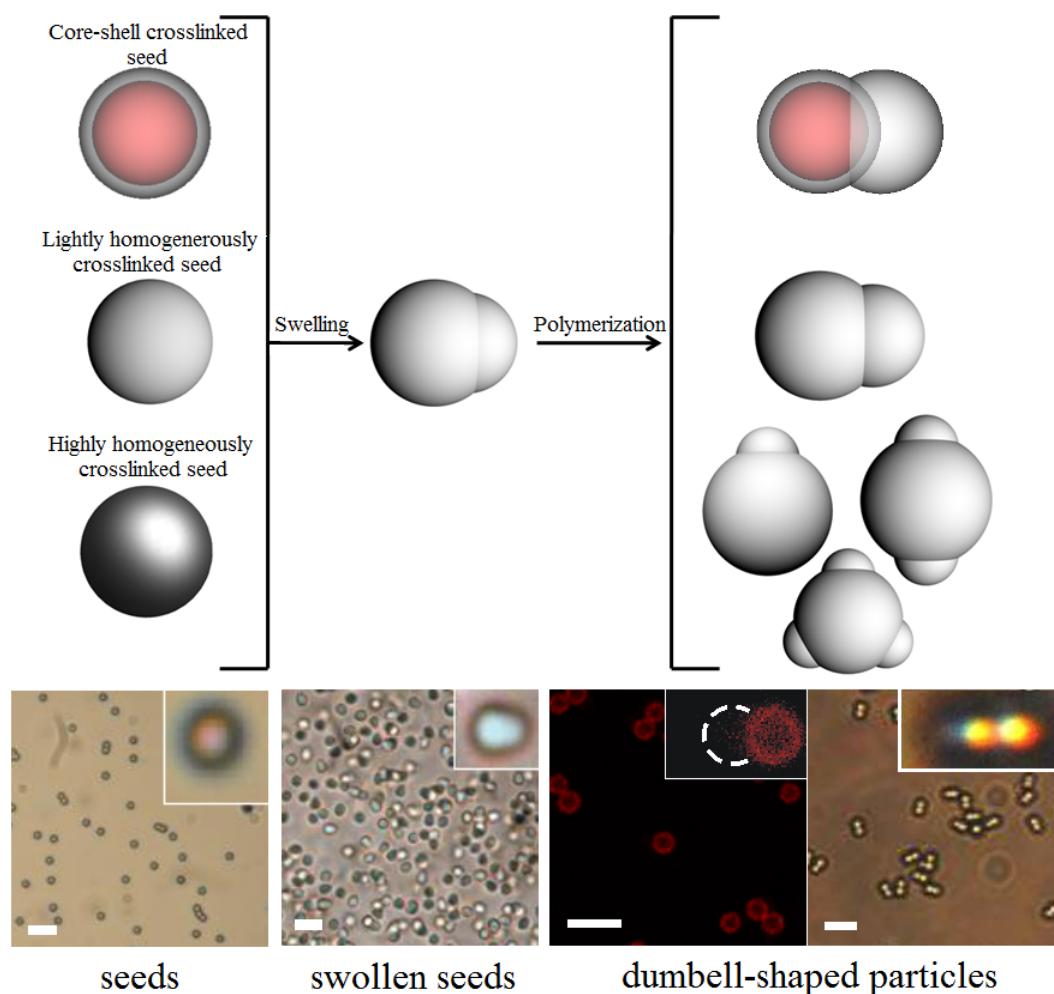
Figure 5.1. Schematic diagram showing the formation of the non-spherical homo-phase PMMA particles by the seeded emulsion polymerization technique. The optical and confocal micrographs exemplify the synthesis of non-spherical PMMA particles. The scale bars are 5 μm.

over the desired dumbbell or snowman shape of the particles.   In addition, to make these particles suitable for confocal fluorescence microscopy studies we labeled them with fluorescent dyes and demonstrated the possibility to transfer them into apolar solvents using a surfactant. Some examples of such dispersions and the consequences of our control over the range of the particles repulsions will be shown. Finally, we demonstrate assembly of these particles into semi-flexible chains using a method published by our group recently. [29, 32]

5.2 MATERIALS AND METHODS

5.2.1 Materials

Methyl methacrylate (MMA, Fluka and Aldrich, chemical grade) was passed over an inhibitor

removal column (Aldrich). After the inhibitor had been removed, MMA was stored in a refrigerator at 5 °C and not longer than one month. Azo-bis-isobutyronitrile (AIBN, Janssen Chimica) was re-crystallized in ethanol before use. Ethylene glycol dimethacrylate (EGDMA, Sigma-Aldrich, chemical grade) was used as the cross-linking agent. Polyvinylpyrrolidone (PVP, Sigma) with an average molecular weight of 360,000 g/mol (K-90) was used as the stabilizer. Hydroquinone (Fluka) was used as the inhibitor. The fluorescent monomers (rhodamine b isothiocyanate)-aminostyrene (RAS) and (7-(diethylamino)-coumarin-3-carboxylic acid N-succinimidyl ester)-aminostyrene (CAD) were prepared following the method described in our previous work. [29] Sorbitan trioleate (Span 85, Sigma, chemical grade), methanol (Biosolve, chemical grade), formamide (Fluka, chemical grade), decahydronaphthalene (mixture of *cis + trans*, decalin, Fluka, ≥ 98%), cyclohexyl bromide (CHB, Fluka, chemical grade) and hexane (Biosolve, chemical grade) were used as supplied. Deionized water was used in all experiments.

5.2.2 Procedure for Non-Spherical Particle Synthesis

Several series of monodisperse poly (methyl methacrylate) spheres with different cross-linked structures and cross-linked densities were prepared using the previously reported method. [29] The core-shell or homogeneously cross-linked structure of our PMMA seed spheres could be controlled by varying the addition start time of a mixture containing cross-linker; the addition end time was always kept fixed at 3.5 h. The obtained seeds were all monodisperse in size with a smooth surface and their diameters ranged from 770 nm to 1250 nm with polydispersities around 4%. Before carrying out further experiments, the seed spheres were rinsed twice with methanol, three times with a 1 wt% PVP aqueous solution, and finally stored in the 1 wt% PVP aqueous solution at a weight fraction of 0.7 % at room temperature no longer than one week. The seed particles needed to be dispersed homogeneously by sonication before further use.

Once the cross-linked seed spheres had been homogeneously dispersed in the 1wt% of PVP aqueous solution, non-spherical PMMA particles were prepared on the basis of our extension of the seeded emulsion polymerization technique. [16] Typically, 22 g of monomer oil-in-water emulsion (stabilized by 1 wt% PVP, based on total emulsion mass) consisting of 2 g of swelling monomer (MMA) was prepared in the presence of an initiator (AIBN) (1 wt% based on the swelling monomer mass) by homogenizing with a IKA MS2 minishaker at 2500 rpm for 5 min. Then all the monomer emulsion was added slowly to 20 g of seed suspension (0.7 wt%) with a constant stirring. The detailed recipes are summarized in Table 1. All samples were allowed to swell in a 250 ml, three-necked flask equipped with a condenser, and a Teflon-coated magnetic stirring bar with slow stirring (~100 rpm) for around 18 h.

Subsequently, nitrogen was bubbled through the reaction system for at least 30 min. Then the polymerization was carried out by temperature elevation to 70 °C. Addition of hydroquinone (0.5 wt% based on the amount of swelling monomer, a water soluble inhibitor) prior to the heating process inhibited secondary nucleation in the water phase at the early stage of the polymerization. The inhibiter (hydroquinone) compelled the polymerization to occur mainly in the protrusion and swollen seed phase. The reaction was maintained at 70 °C for 8 h before

Table 5.1. Detailed recipe for the Synthesis of Non-Spherical PMMA Particles

batch no.	1	2	3	4	5	6	7	8	9	10	11	12	13	14	15	16	17	18
Seeds System[a]																		
addition start time (h)	0	0	0	0	0	0.33	1.5	1.5	1.5	1.5	1.5	1.5	1.5	1.5	1.5	1.5	1.5	1.5
total addition time (h)	3.5	3.5	3.5	3.5	3.5	3.1	2	2	2	2	2	2	2	2	2	2	2	2
EGDMA (wt%)[b]	1	2	5	10	2	2	2	1	2	3	4	5	6	2	2	2	2	2
dye[c]	-	-	-	-	RAS	RAS	RAS	-	-	-	-	-	-	-	-	-	-	-
Swelling Monomer Dispersion[d]																		
amount of swelling monomer (g)	4	4	4	4	4	4	4	2	2	2	2	2	2	1	4	8	4	4
PVP (wt%)[e]	1	1	1	1	1	1	1	1	1	1	1	1	1	1	1	1	0.5	1
EGDMA (wt%)[f]	-	-	-	-	-	-	-	-	-	-	-	-	-	-	-	-	-	2

[a] Other chemicals: PVP, 3 g; AIBN, 0.025 g; MMA, 2.5 g; solvents, 30.71 g (methanol : water = 8 : 2 in weight).

[b] Based on the mass of the PMMA particle.

[c] RAS: 0.5 wt% based on the mass of the PMMA particle.

[d] Other Chemicals: deionized water, 20 g; 1 wt% of PVP, based on the mass of the deionzed water; 1 wt% of AIBN based on the mass of the swelling monomer.

[e] Based on the total mass of the suspension.

[f] Based on the mass of the swelling monomer.

cooling. The obtained particle suspension was washed about 4 times with deionized water by a centrifuge (Hettich Rotina 46S centrifuge, at 560 g for 60 min twice and 30 min twice, respectively), thus separating the desired particles from the secondary nucleation and impurities.

We labeled the particles with a fluorescent dye either during or after polymerization (to which we refer as either pre- or post-labeling). In the pre-labeling process, CAS (0.1 wt% based on swelling monomer) was first dissolved in the swelling monomer in the presence of the initiator. Then the same subsequent steps were followed as just mentioned and fluorescently labeled non-spherical particles were obtained in the end. In the post-labeling process, dried non-spherical (snowman or dumbbell-like) particles (~ 0.1 g) were first dispersed in a mixture (~ 5 ml) of acetone/pentanol (1:4 by weight) containing 1 mM of RAS by sonication, and then stirred gently overnight in a sealed glass vial (~20 ml in volume) at room temperature. Then the acetone was removed by evaporation at 50 $^{\circ}$C for 2 h. The labeled particles were washed two times with pentanol, one time with methanol, and three times with deionized water, respectively, by centrifugation. After drying under a N_2 stream, the fluorescent non-spherical particles were stored in a dark glass vial.

To transfer the particles to an apolar solvent, we modified the transfer approach from Espinosa et al. [25] A small amount of non-spherical particles (about 0.01 g) was first dispersed in pentanol then sedimented by a Hettich Rotina 46S centrifuge, and the supernatant was removed. Subsequently, they were transferred to hexane (containing 50 mM of the surfactant Span 85) as an apolar intermediate solvent and then further to decalin or CHB containing 50 mM of the surfactant Span 85 as well aided by sonication and centrifugation. After this procedure had been repeated four times, the solvent was considered completely exchanged. For the particle transfer to formamide, the intermediate solvent was skipped, and the surfactant was not necessary. Again the system was washed four times.

5.2.3 Characterization of the Non-Spherical Particles

SEM (scanning electron microscopy) imaging was performed using a field-emission scanning electron microscope (SEM XL FEG30). The samples were prepared by placing a droplet of suspension onto a glass slide and allowing the solvent to evaporate at room temperature. The samples then were sputter-coated with a layer of gold (Au) of 10 nm. The number-averaged re-polymerized radius (R_s) of the seed spheres and the radius (R_p) of the protrusions of the non-spherical particles and their standard deviations (σ_s, σ_p) were calculated on the basis of using TEM measurement software (iTEM, 5.0). The polydispersities (δ_s of the seed spheres and δ_p of the protrusions) of the colloid systems were defined as

$$\delta_s = \sigma_s / R_s \tag{5.1}$$

$$\delta_p = \sigma_p / R_p \tag{5.2}$$

The schematic model of the non-spherical particles is illustrated in Figure 5.2, which indicates the geometric relationships between R_s, R_p, and the contact angle (θ) of the protrusion on the re-polymerized seed sphere. The radius ratio (α) of the protrusion and re-polymerized seed sphere was defined as

$$\alpha = R_p / R_s \tag{5.3}$$

Fluorescence images were obtained using a Nikon confocal scanning laser microscope (CSLM, Nikon C1) with a Leica 63× oil confocal immersion lens with a numerical aperture of 1.4. The fluorescent dyes were excited at around 543 nm (RAS) and 408 nm (CAS), and their images were observed at emission wavelengths of around 605 nm (RAS) and 450 nm (CAS), respectively. The fluorescent samples were made using capillaries with a dimension of 0.2 mm × 2.0 mm (VitroCom, UK) cross section and a length of 5 cm, the two ends of the capillary were sealed with an epoxy glue. When imaging the phase separation process, we sealed the swollen seed spheres in the same sized glass capillaries which were glued using wax. Optical microscopy was performed with a Leica 63× lens and images were recorded with a Nikon (D90) digital camera.
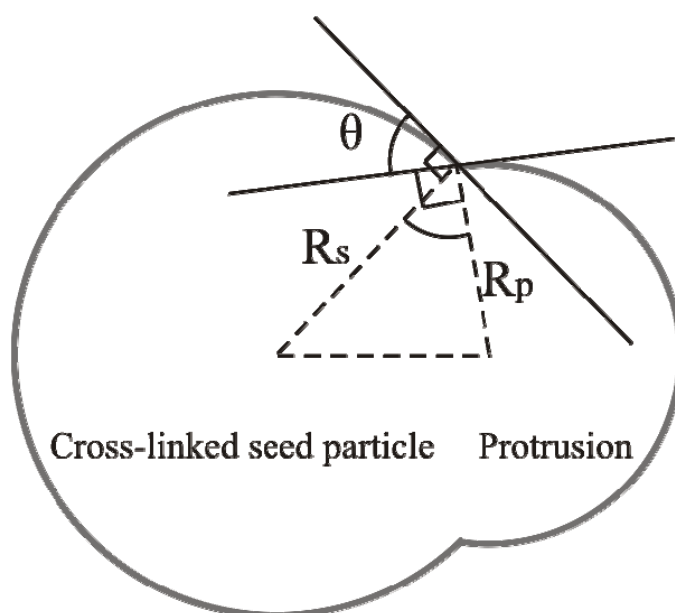
Figure 5.2. Schematic model of a non-spherical particle.

5.3 RESULTS AND DISCUSSION

5.3.1 Homogeneously Cross-linked Seeds

Initially, a series of homogeneously cross-linked PMMA spheres with cross-link densities of 1%, 2%, 5%, and 10% based on monomer mass and with a diameter around one micrometer were used as seeds. The seed particles were dispersed in an aqueous solution stabilized by 1 wt% (based on total emulsion mass) of PVP, these spheres were swelled and subsequently, re-polymerized. The growth of the seed spheres with 1% cross-link density (batch 1 in Tab. 5.1) produced a snowman-like structure with a relatively small protrusion, a contact angle of $33^{o}\pm3^{o}$ and a low polydispersity; (δ_s, δ_p) are 5.6% and 5.8% (see Fig. 5.3a). The figure illustrates that these non-spherical particles were monodisperse both in size and shape. When the cross-link density of the seed spheres was increased from 1% to 2% (batch 2) and further to 5% (batch 3), the degree of phase separation in the snowman particles increased, as seen from the contact angle that increased from $33^{o} \pm 3^{o}$ to $56^{o} \pm 6^{o}$ and $58^{o} \pm 7^{o}$, respectively (see
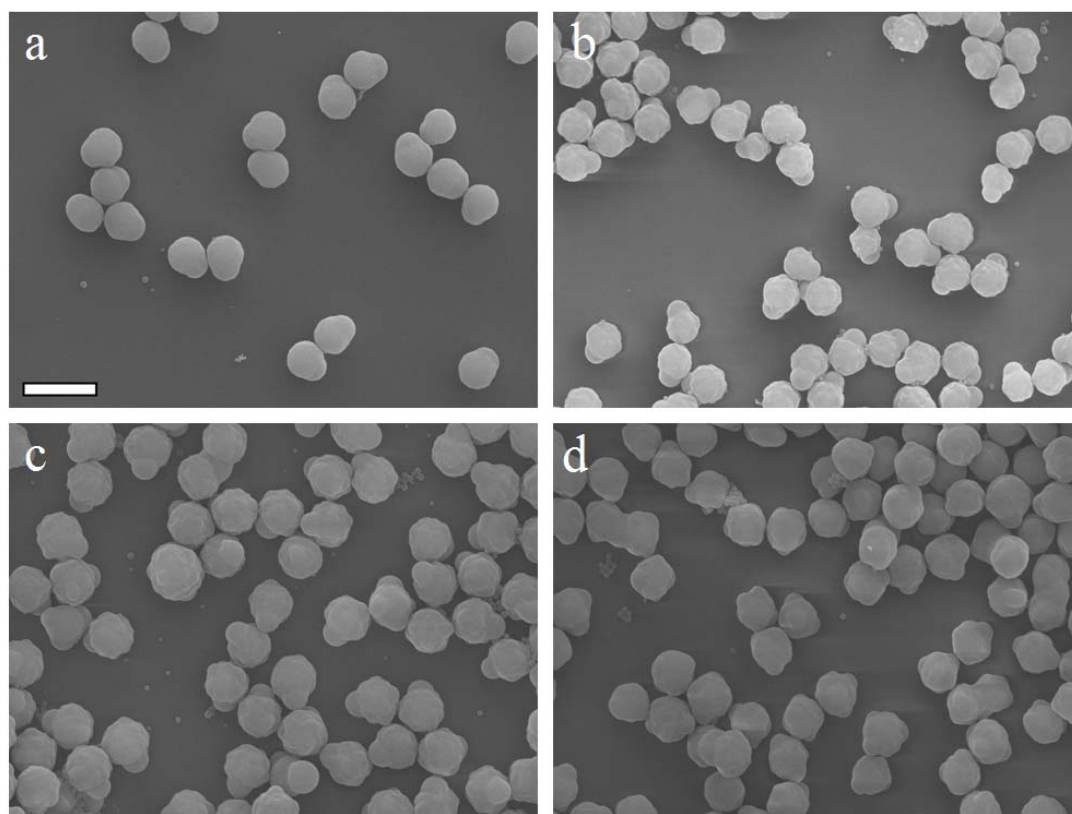
Figure 5.3. SEM micrographs of non-spherical PMMA particles made using homogeneously cross-linked PMMA spheres as seeds with different cross-link densities a) 1% b) 2% c) 5% d) 10%. The scale bar is 2 μm and the swelling monomer was kept the same amount for all four synthesis (4 g, details see batches 1-4 in Tab. 5.1).

Fig. 5.3). On the other hand, the size of the protrusions decreased, corresponding to α decreasing from 0.797 to 0.636. This may be caused by a combination of two factors: One is that the highly cross-linked seeds tend to absorb less swelling monomer, directly resulting in smaller protrusions. The other is that the highly cross-linked network has a higher viscosity, which slows the diffusion of the swelling monomer from the seed to a growing protrusion, leaving the seed larger. These two factors together led to α deceasing. In addition, and unfortunately, the seed part of the colloids became rather rough (Fig. 5.3b and c). Increasing the cross-link density of the seeds even further to 10% (batch 4) resulted in the formation of non-spherical particles with multiple protrusions (see Fig. 5.3d). This is probably caused by the highly cross-linked polymer network of the seeds. Upon heating the system, contraction takes place at the outer shell of the seeds prior to the inner part of the seeds. Strong compressive stress from the inner part of the seeds protruded the swelling monomer at various locations of the surface of the seeds. Although it is not the focus of the present research, it is of interest here to point out that particles with a controllable roughness have been used as a colloidal model system as well (see e.g. ref. [33]). For instance, it has recently become clear that by controlling particle roughness, the depletion effect, which is nice way to achieve attractions between smooth particles, can be effectively switched off if the particles roughness fulfills certain criteria (see e.g. ref. [34, 35]).

5.3.2 Core-Shell Cross-linked Seeds

Since our experiments on homogeneously cross-linked PMMA spheres met with only modest success, we decided to try seeds with the cross-linker concentrated in an outer shell. This could combine a higher swelling capacity of the uncross-linked core with a stronger elastic retraction force of the cross-linked shell. Such particles were made by starting the addition of cross-linker some time after the polymerization of the monomer has started, as shown in our
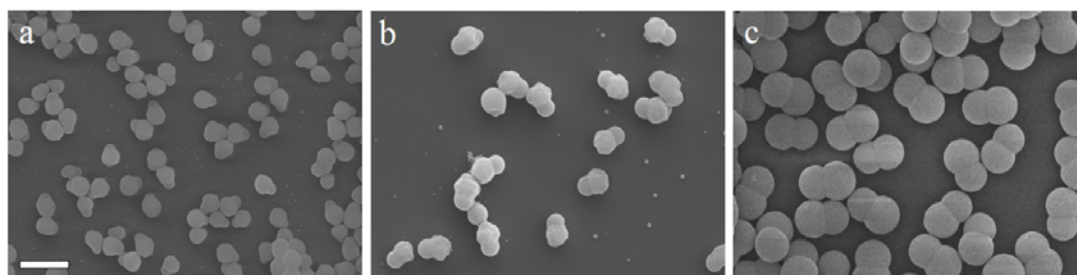
Figure 5.4. SEM micrographs of non-spherical PMMA particles made using dye-labeled PMMA spheres with different cross-linking structure as seeds (cross-link density was 2 wt%). The seeds were prepared with different addition start times and total addition times (in all cases the addition was finished after 3.5 h of reaction): a) 0 h - 3.5 h (batch 5 in Tab. 1); b) 0.33h - 3.1 h (batch 6); c) 1.5 h - 2 h (batch 7), the scale bar is 2 μm.
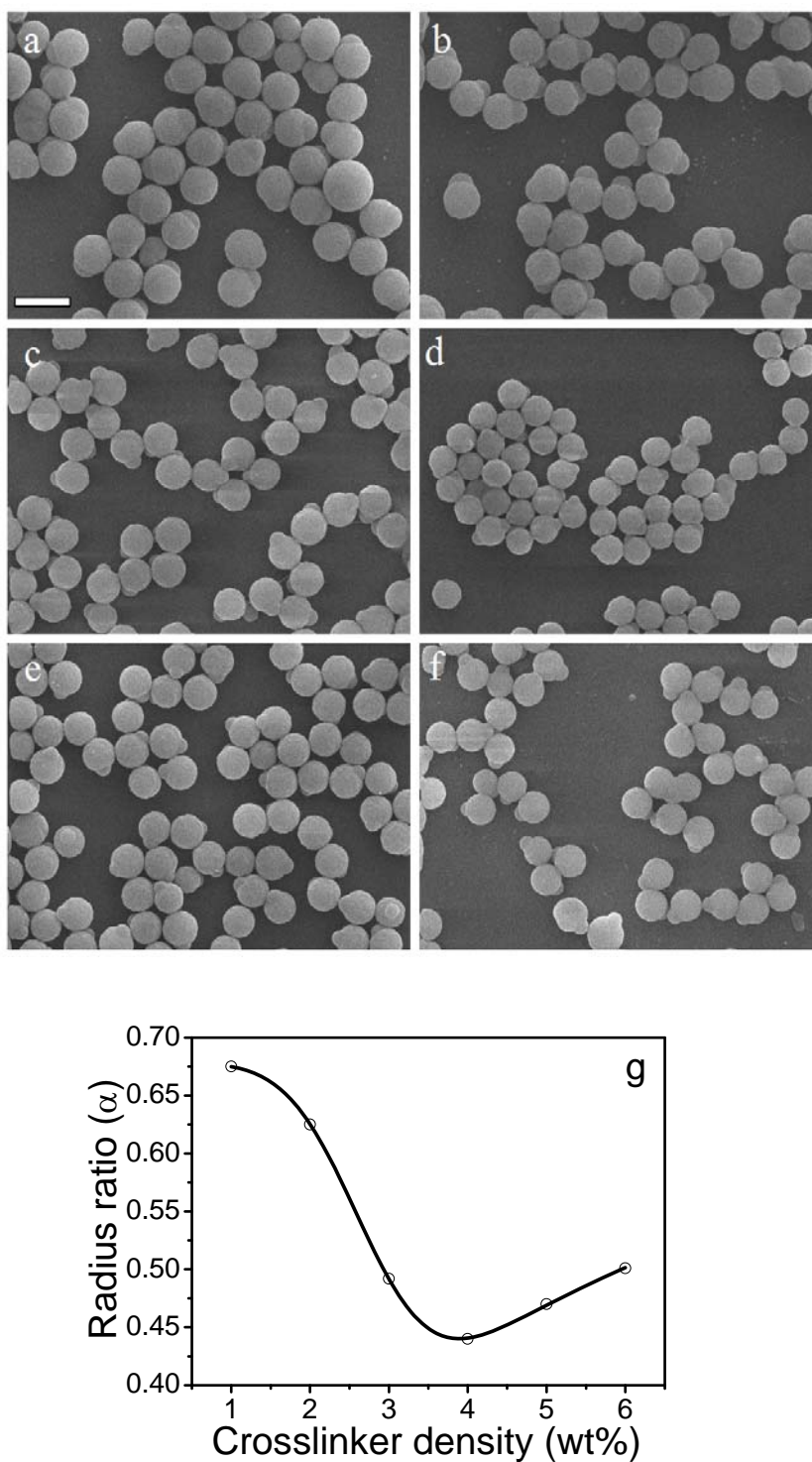
Figure 5.5. SEM micrographs of non-spherical PMMA particles made using core-shell cross-linked PMMA spheres as seeds with different cross-link densities a) 1 wt% (batch 8 Tab. 5.1); b) 2 wt% (batch 9); c) 3 wt% (batch 10); d) 4 wt% (batch 11); e) 5 wt% (batch 12); f) 6 wt% (batch 13), and the corresponding radius ratio (α) on non-spherical particles as a function of the cross-link density of core-shell cross-linked PMMA seeds summarized in g), in which open circles are experimental values and the solid line is a guide to the eye. The scale bar is 2 μm.

previous work. [29] There, we also discovered that the swelling ratio of core-shell cross-linked PMMA spheres was indeed much higher than for homogeneously cross-linked PMMA. [29] Therefore, we hypothesized that the core-shell cross-linked seeds might form bigger protrusions. In agreement with our expectations, using a later addition start time, which produced a thinner cross-linked shell, led to a bigger final protrusion (see Fig. 5.4). Note that the time at which addition was complete was kept constant (3.5 h), as was the total amount of cross-linker (2 wt% based on monomer mass, other details were listed in Tab. 5.1). This resulted in an increasingly thin shell with an increasingly high cross-link density. Figure 5.4 shows that the contact angle of the protrusion on the seed increased from $57^o \pm 7^o$, $66^o \pm 5^o$ to $70^o \pm 3^o$ as the time window of cross-linker addition was narrowed (batch 5-7). Additionally, α increased from 0.635, 0.779 to 0.956, implying the growth of the protrusion relative to the seed. It is worth pointing out that there is no significant difference of contact angles between non-spherical particles derived from dyed and un-dyed seeds.

In order to investigate the effect of the cross-link density of the shell on the morphology of the non-spherical particles, a series of core-shell cross-linked PMMA particles was prepared keeping the addition start and end times constant. These were used as seeds to prepare the non-spherical PMMA particles. Results are presented in Figure 5.5 (batch 8-13). It is seen that while the size of the protrusion became smaller as the cross-link density was increased, its contact angle became larger. Figure 5.5g presents the tendency of the radius ratio (α) as a function of the cross-link density of the core-shell cross-linked shells of the seeds. At first, α decreased with increasing cross-link density of the shells, which can be explained by a reduction of the swelling as the rigidity of the shell is increased. When the density of the polymer network was further increased, the apparently stronger elastic force expelled a large volume of the swelling monomer from the cores leading to bigger protrusions relative to the seeds. Note that, the radii of the re-polymerized seeds relative to the original seeds increased as the cross-link densities increased from 4 wt% to 6 wt% (from 1.004 to 1.290 and further to 1.313; this has not been fully understood yet).

5.3.3 Effect of the Swelling Monomer Content

Clearly, the size of the protrusion relative to the seed particle can be controlled through the cross-link density of the shell, but so far only in a relatively narrow range. If the protrusion could be stimulated to grow further, the snowman particles would transform into dumbbell (with equal sized lobes) or even 'inverted' snowman particles (protrusion is larger than seed). We show that this is possible by simply increasing the amount of swelling monomer. For these experiments we picked out the core-shell cross-linked PMMA seeds with 2 wt% cross-link density in which the cross-linker was added between 1.5 and 3.5 h of the reaction.
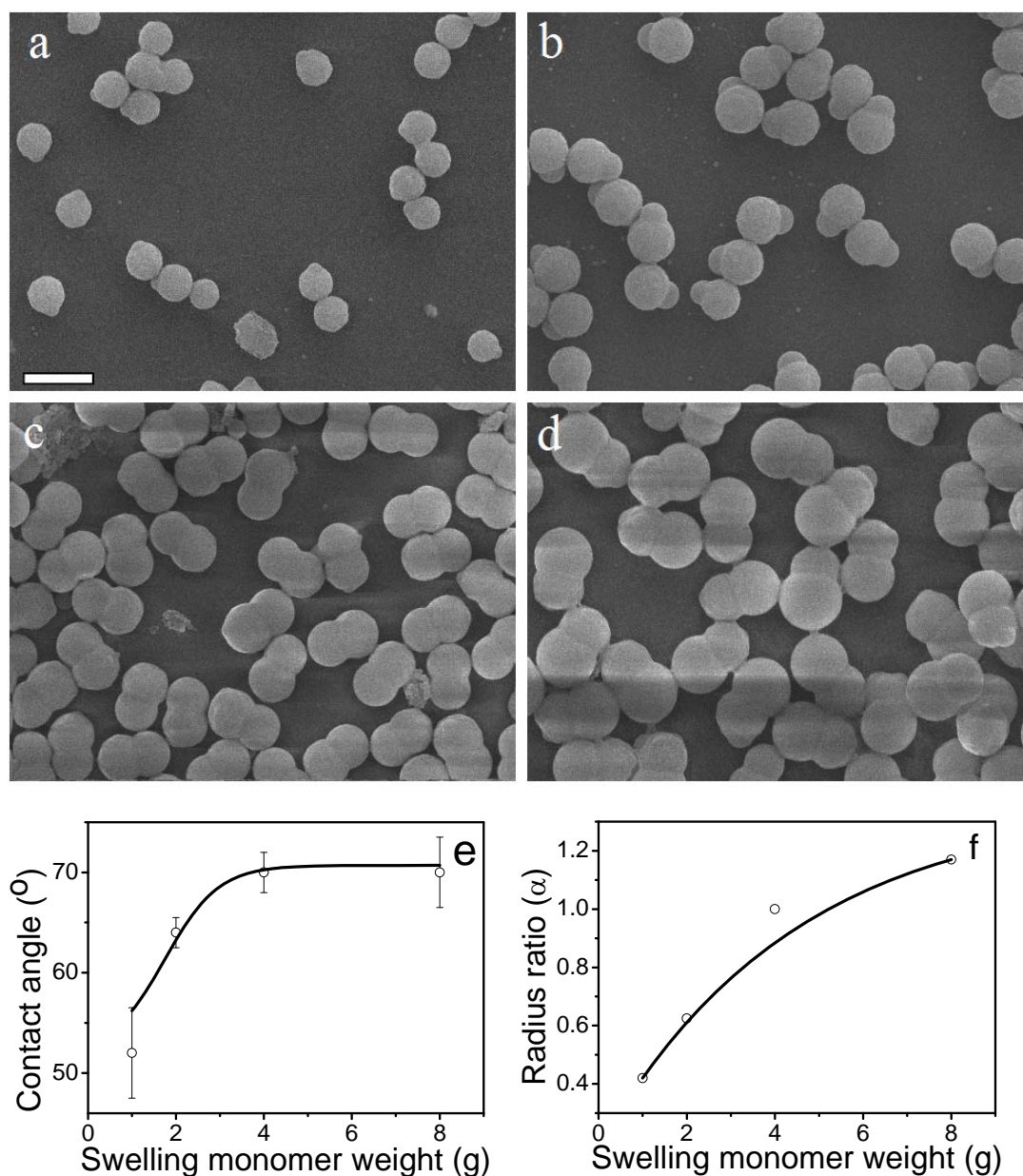
Figure 5.6. SEM micrographs of non-spherical PMMA particles swelled by different amounts of MMA, which changed the geometries of the resulting particles (seeds are core-shell cross-linked (the addition of the cross-linker started at 1.5 h and ended at 3.5 h of the reaction) PMMA spheres with 2 wt% cross-link density) a) 1 g (batch 14 in Tab. 5.1); b) 2 g (batch 9); c) 4 g (batch 15); d) 8 g (batch 16);, and the corresponding contact angle (θ) and radius ratio (α) of non-spherical particles as a function of swelling monomer mass (open circles are the experimental data points and the solid lines are a guide to the eye) are in e) and f). The scale bar is 2 μm.

Typical systems are shown in Figure 5.6a-d, and the detailed contact angle and radius ratio as a function of swelling monomer weight have been summarized in Figure 5.6e and f. Apart from a large increase in size ratio, the contact angle also increased up to a cross-linker content of 4 g (batch 15 in Tab. 5.1). When the amount of swelling monomer increased to 8 g (batch

16), the inverted snowman (protrusion is bigger than seed) like particles were obtained. Meanwhile, a small secondary lobe was present occasionally, opposite to the main protrusion on the seed particles surface (see Fig. 5.6d), which aided us to distinguish between the new-formed protrusions and original seeds. To our knowledge, this is the first time the inverted snowman particles are reported. It gives the potential to fabricate inverted snowman shaped particles with an even bigger radius ratio (α) or cone-shaped particles in one step.

5.3.4 Effect of Other Parameters

In addition, the effect of the PVP concentration on the morphology of the non-spherical particles also was investigated by decreasing the concentration of PVP from 1 wt% to 0.5 wt%, and further to 0 wt% (based on the total suspension mass). When 0.5 wt% of PVP was used (batch 17), the obtained system contained more multi-mers than the system with 1 wt% of PVP did (see Fig. 5.7a). A similar phenomenon was described in a previous paper, [36] that is, a smaller amount of stabilizer led to decreased stability of the system. In that case, swollen seed spheres with liquid protrusions tended to self-assemble into regular colloidal clusters as less stabilizer was presented. However, dimers (consisting of two seed particles) and trimers (consisting of three seed spheres) prevailed due to the relatively short stirring time (~ 18 h) in our experiment in the case of 0.5 wt% of PVP. At low swelling ratios (the amount of swelling monomer was 2 g), the interfacial tension compressed the seed spheres to form clusters
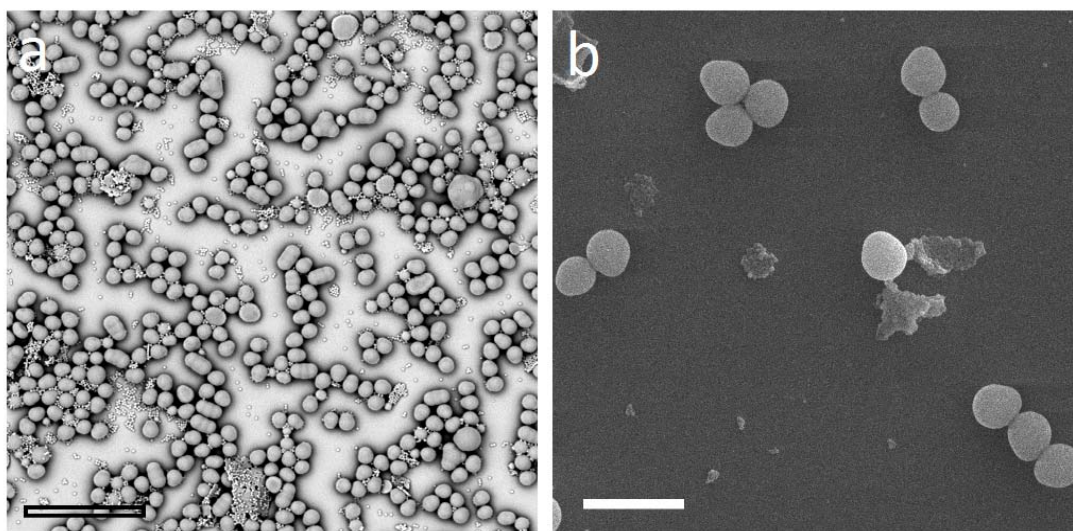
Figure 5.7. SEM micrographs of non-spherical PMMA particles were fabricated under various parameters a) 0.5 wt% of stabilizer (PVP, batch 17), b) EGDMA (2 wt% based on swelling monomer, batch 18) used as co-swelling monomer, core-shell cross-linked particles were used as seeds (the cross-link density is 2 wt%) and the amount of the swelling monomer were 2 g in a), 4 g in b), respectively. The scale bars are 10 μm and 2 μm in a) and b), respectively.

partially immersed in a liquid droplet. As expected, in the absence of PVP, the system was not able to stay stable any more.

Ethylene glycol dimethacrylate (EGDMA) has two unsaturated bonds and is therefore usually used as cross-linker to interconnect linear monomers, oligomers and polymers, leading to a cross-linked polymer network. The addition of EGDMA (2 wt% based on swelling monomer mass) in swelling monomer led to the formation of more branching and a larger volume of cross-linked polymer during polymerization. [29] This, in turn, led to particles of a high viscosity with a high degree of chain entanglement, and hence resulted in a smaller degree of phase separation (see Fig. 5.7b, batch 18). Compared to the previous sample (batch 15 in Fig. 5.6c) prepared under the same conditions except for the absence of EGDMA, the protrusions in Figure 5.7b were less distinct (radius ratio α = 0.76, contact angle is 29o ± 5o). This indicates that even a small amount of cross-linker has a strong effect on the formation of the protrusion.

5.3.5 Examples of Use in Real Space Model Studies

To make the non-spherical PMMA particles suitable for confocal microscopy studies, the particles were fluorescently labeled by either a pre- or post-labeling treatment as mentioned above. Results are shown in Figure 8a and b. The addition of a dye (CAS) in the swelling monomer did not have a significant effect on the formation of the resulting dumbbell shaped particles. Compared to the pre-labeling technique, the dye brought into the polymer phase via a post-labeling approach (for details see experimental part) was easily removed, because the dye was just physically absorbed by the particles. Just by rinsing the dyed particles which were produced by the post-labeling method with a good solvent for the dye (like ethanol), the dye could readily be removed. Subsequently, these non-fluorescent particles could be fluorescently labeled back by simply repeating the post-labeling treatment. In order to quantitatively study the phase behavior of these non-spherical particles in concentrated dispersions in 3D, light scattering needs to be reduced by dispersing the particles in a refractive index matching solvent (like decalin and/or CHB). Successful transfer of the particles from a polar to an apolar solvent (dielectric constant ε~2 like: hexane and decalin) or somewhat more polar but still not too polar solvent (~2 < ε < ~10) like cyclohexyl bromide (CHB) was achieved by modifying the approach developed by the group of Behrens, [25] in which a nonionic surfactant (Span 85) is used. In the solvent CHB, dumbbell particles behaved almost as hard particles, which was caused by not only the creation of sufficient charge on the PMMA to create enough particle repulsion, but also enough ions in the liquid to cause the Debye-Hückel screening length to be short compared to the particle size. The density difference between the solvent (CHB, $\rho \approx 1.33$ g/cm^3) and particles ($\rho \approx 1.18$ g/cm^3)
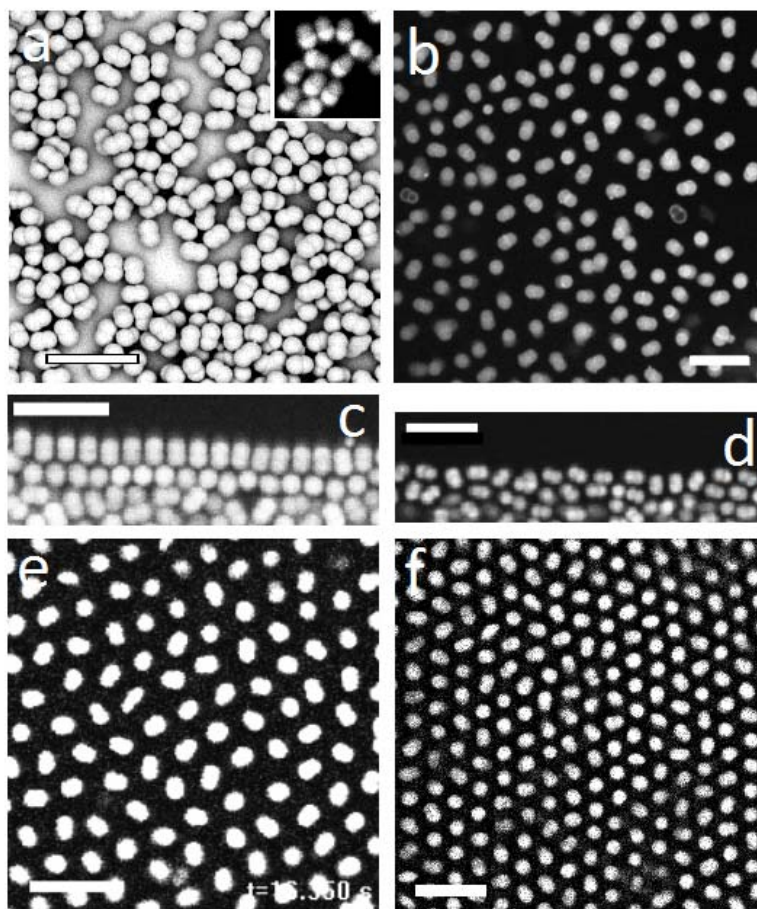
Figure 5.8. Scanning electron microscopy (SEM) and confocal micrographs of dyed
dumbbell particles: a) SEM micrograph of fluorescent dumbbell particles (CAS dye) labeled
during re-polymerization (pre-labeling), the inset is the corresponding confocal micrograph, b)
confocal micrograph of fluorescent dumbbell particles (RAS dye) labeled after
re-polymerization (post-labeling). Confocal micrographs of fluorescently labeled dumbbell
particles (stabilized by Span 85 of a concentration of 50 mM) sedimented at the interface of
air and CHB, c) a higher concentration of particles, d) a lower concentration of particles.
Confocal micrographs of dumbbell particles stabilized by Span 85 (50 mM), e) in hexane, f)
in decalin. All scale bars are 10 μm.

caused the particles to float up and gather at the interface of CHB and air. As a result, densely
packed dumbbell particles were observed at the interface (Figure 5.8c). Note that the particles
were aligned side-by-side as in Figure 5.8c. Alternatively, randomly oriented dumbbell
particles were observed at a lower volume fraction of the particles as shown in Figure 5.8d.
Unfortunately, only liquid and therefore short-ranged ordered structures were found in the
bulk in both cases. On the other hand, when the particles were dispersed in more apolar
solvents, such as hexane and decalin, the particles carried not only a significant amount of
electric charge but in addition the screening length was several micrometers long, as can be
seen from the long range repulsion in Figure 5.8e and f. Interestingly, the charged dumbbells

showed positional order but orientational disorder in both hexane and decalin, that is, they formed so-called plastic crystals, [37, 38] as shown in Figure 5.8e and f. This interesting structure is described in more detail elsewhere. [39]

We end with a demonstration of how the as-synthesized particles can be used in a second self-assembly step in which electric fields are used to direct the particles into strings and how a heating step makes the links between the anisotropic particles permanent according to a slight modification of a procedure recently developed in our group. [29, 32] Suspensions consisting of monodisperse non-spherical PMMA particles dispersed in the polar solvent formamide were introduced into a capillary cell with a pair of wires running through the length serving as electrodes. Upon application of a high frequency AC electric field, the induced dipole moment among the particles led to their assembly into strings parallel to the field, and particles were in a head-to-tail arrangement (E_{rms} = 0.05 V/μm, f = 1 MHz where E_{rms} is the root-mean-square electric field strength and f is the frequency). [38] The electric
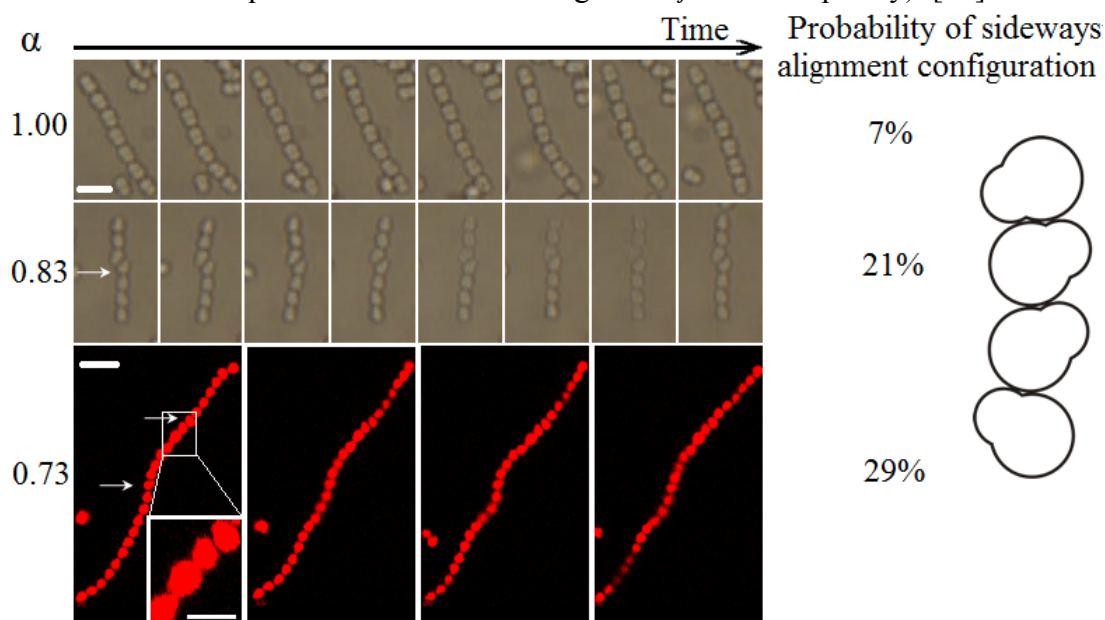
Figure 5.9. Time-lapse optical and confocal micrographs of semi-flexible colloidal polymer chains made of non-spherical PMMA particles with different radius ratios α in formamide. The arrows point out the rigid joints in the chains formed by a non-parallel alignment of two neighboring particles. All scale bars are 5 μm except in the inset where it is 2 μm.

field was maintained for 2 h and then switched off (details see supplementary information). We noticed that the capillary became rather hot during this time, but not so hot that it caused the boiling of formamide (boiling point is 210 ºC). After removing the field, more than 80% of the dispersion was converted to permanent strings with a broad distribution in lengths. The permanent bonding was probably caused by the high temperature, similar to the annealing process used to attach PMMA particles to each other in Ref. [29, 32, 40 and 41] The chains

were not rigid but semi-flexible, similarly to what was observed for strings of PVP coated PS sphere. [32] Figure 5.9 shows a time lapse of their Brownian movements. It is clearly seen that with decrease of α, a larger fraction of particles align sideways (see the frequency of sideways alignment configuration of non-spherical particles in Fig. 5.9). This tendency is in good agreement with computer simulation results. [42] Moreover, we observed that the chain was much more rigid at such points (shown by arrows in Figure 9). This is reminiscent of flexible polymer chains in which double bonds may be inserted to form local rigid connections and is presently under investigation.

5.4 CONCLUSIONS

In summary, we demonstrated a novel approach for fabricating homo-phase snowman or dumbbell shaped PMMA particles by seeded emulsion polymerization. The presented technique allows for precisely tuning the size of the newly formed polymer protrusions by localizing the cross-linker in an outer shell of the seed spheres, and adjusting the swelling monomer content. Moreover, making use of homogenously cross-linked seeds readily extended this method for making snowman shaped particles to a method for making particles with a tunable roughness. These anisotropic particles were made suitable for real space studies with confocal microscopy by fluorescent labeling and a transfer procedure to apolar index-matching solvents. Electric field driven assembly of these particles into permanently bonded, semi-flexible chains was demonstrated as well.

5.5 ACKNOWLEDGMENTS

5.6 SEPPLEMENTARY INOFRMATION

5.6.1 Electric Field

Fluorescently labeled non-spherical particles were dispersed in formamide (~0.5 wt%) with the help of sonication, aligned by an AC field in a electric capillary cell of 0.1 mm × 1.0 mm (VitroCom, UK) cross section with a desired length. A 50 V root-mean-square sinusoidal signal with a frequency of 1 MHz was applied to polarize the particles but not the double layer.

[24, 32, 40] When the electric field was maintained for five minutes, straight and stiff strings made of non-spherical particles were obtained, shown in supplementary figure 1. Upon increasing this time, the length of the strings increased. After switching off the electric field, the strings were still preserved and began to deform and move by thermal fluctuations. During the on-time of the electric field, the capillary cell was heated up, which probably resulted in a slight melting of the non-spherical particles causing them to connect each other.
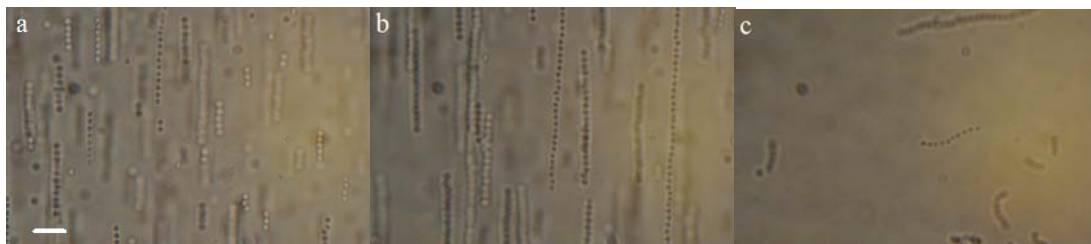
Supplementary Figure 5.1. Optical micrographs of polymer stings made of snowman like particles (α = 0.73). a) Electric field maintained for 5 minutes, b) electric field kept on for 110 minutes, c) electric field was off for 10 minutes. The scale bar is 10 μm.

5.7 REFERENCES

[1] Vroege, G. J.; Lekkerkerker, H. N. W. *Rep. Prog. Phys.* **1992**, *55*, 1241-1309.

[2] Perro, A.; Reculusa, S.; Ravaine, S.; Bourgeat-Lami, E.; Duguet, E. *J. Mater. Chem.* **2005**, *15*, 3745-3760.

[3] Glotzer, S.; Solomon, M. *Nat. Mater.* **2007**, *6*, 557-562.

[4] Yan, S.; Kim, S.; Lim, J.; Yi, G. *J. Mater. Chem.* **2008**, *18*, 2177-2190.

[5] Duguet, E.; Desert, A.; Perro, A.; Ravaine, S. *Chem. Soc. Rev.* **2011**, *40*, 941-960.

[6] Li, F.; Josephson, D. P.; Stein, A. *Angew. Chem. Int. Ed.* **2011**, *50*, 360-388.

[7] van Blaaderen, A. *Nature* **2006**, *439*, 545-546.

[8] Nagao, D.; van Kats, C. M.; Hayasaka, K.; Sugimoto, M.; Konno, M.; Imhof, A.; van Blaaderen, A. *Langmuir* **2010**, *26*, 5208-5212.

[9] Johnson, P. M.; van Kats, C. M.; van Blaaderen, A. *Langmuir* **2005**, *21*, 11510-11517.

[10] Solomon, M. J.; Zeitoun, R.; Ortiz, D.; Sung, K. E.; Deng, D.; Shah, A.; Burns, M. A.; Glotzer, S. C.; Millunchick, J. M. *Macromol. Rapid Commun.* **2010**, *31*, 196-201.

[11] Alargova, R. G.; Bhatt, K. H.; Paunov, V. N.; Velev, O. D. *Adv. Mater.* **2004**, *16*, 1653-1657.

[12] Ho, C. C.; Keller, A.; Odell, J. A.; Ottewill, R. H. *Colloid Polym. Sci.* **1993**, *271*, 469-479.

[13] Nagao, D.; Hashimoto, M.; Hayasaka, K.; Konno, M. *Macromol. Rapid Commun.* **2008**, *29*, 1484-1488.

[14] Fresnais, J.; Berret, J. –F.; Frka-Petesic, B.; Sandre, O.; Perzynski, R. *Adv. Mater.* **2008**, *20*, 3877-3881.

[15] Zoldesi, C. I.; Imhof, A. *Adv. Mater.* **2005**, *17*, 924-928.

[16] Sheu, H. R.; El-Aasser, M. S.; Vanderhoff, J. W. *J. Polym. Sci., Part A: Polym. Chem.* **1990**, *28*, 629-651.

[17] Mock, E. B.; De Bruyn, H.; Hawkett, B. S.; Gilbert, R. G.; Zukoski, C. F. *Langmuir* **2006**, *22*, 4037-4043.

[18] Mock, E. B.; Zukoski, C. F. *Langmuir* **2010**, *26*, 13747-13750.

[19] Kim, J. -W.; Larsen, R. J.; Weitz, D. A. *J. Am. Chem. Soc.* **2006**, *128*, 14374-14377.

[20] Kegel, W. K.; van Blaaderen, A. *Science* **2000**, *287*, 290-293.

[21] van Megen, W.; Underwood, S. M. *Nature* **1993**, *362*, 616-618.

[22] Bryant, G.; Williams, S. R.; Qing, L.; Snook, I. K.; Perez, E.; Pincet, F. *Phys. Rev. E* **2002**, *66*, 060501.

[23] Bosma, G.; Pathmamanoharan, C.; De Hoog, E. H. A.; Kegel, W. K.; Van Blaaderen, A.; Lekkerkerker, H. N. W. *J. Colloid Interface Sci.* **2002**, *245*, 292-300.

[24] Yethiraj, A.; van Blaaderen, A. *Nature* **2003**, *421*, 513-517.

[25] Espinosa, C. E.; Guo, Q.; Singh, V.; Behrens, S. H. *Langmuir*, **2010**, *26*, 16941-16948.

[26] El Masri, D.; van Oostrum, P.; Smallenburg, F.; Vissers, T.; Imhof, A.; Dijkstra, M.; van Blaaderen, A. *Soft Matter* **2011**, *7*, 3462-3466.

[27] Leunissen, M. E.; Christova, C. G.; Hynninen, A. -P.; Royall, C. P.; Campbell, A. I.; Imhof, A.; Dijkstra, M.; van Roij, R.; van Blaaderen, A. *Nature* **2005**, *437*, 235-240.

[28] Bartlett, P.; Campbell, A. I. *Phys. Rev. Lett.* **2005**, *95*, 128302.

[29] Peng, B.; van der Wee, E.; Imhof, A.; van Blaaderen, A. *Langmuir* **2012**, *28*, 6776-6785.

[30] Sheu, H. R.; El-Aasser, M. S.; Vanderhoff, J. W. *J. Polym. Sci., Part A: Polym. Chem.* **1990**, *28*, 653-667.

[31] Kegel, W. K.; Breed, D.; Elsesser, M.; Pine, D. J. *Langmuir* **2006**, *22*, 7135-7136.

[32] Vutukuri, H. R.; Demirors, A.; Peng, B.; van Oostrum, P.; Imhof, A.; van Blaaderen, A. *Angew. Chem. Int. Ed.* **2012**, *51*, 11249-11253.

[33] Kraft, D. J.; Ni, R.; Smallenburg, F.; Hermes, M.; Yoon, K.; Weitz, D. A.; van Blaaderen, A.; Groenewold, J.; Dijkstra, M.; Kegel, W. K. *Proc. Natl. Acad. Sci. U. S. A.* **2012**, *209*, 10787-10792.

[34] Badaire, S.; Cottin-Bizonne, C.; Stroock, A. D. *Langmuir* **2008**, *24*, 11451-11463.

[35] Zhao, K.; Mason, T. G. *Phys. Rev. Lett.* **2008**, *101*, 148301.

[36] Kraft, D. J.; Vlug, W. S.; van Kats, C. M.; van Blaaderen, A.; Imhof, A.; Kegel, W. K. *J. Am. Chem. Soc.* **2009**, *131*, 1182-1186.

[37] Marechal, M.; Dijkstra, M. Phys. *Rev. E* **2008**, *77*, 10.

[38] Demirors, A. F.; Johnson, P. M.; van Kats, C. M.; van Blaaderen, A.; Imhof, A. *Langmuir* **2010**, *26*, 14466-14471.

[39] Peng, B.; van Blaaderen, A.; Imhof, A. In preparation.

[40] Leunissen, M. E.; Vutukuri, H. R.; van Blaaderen, A. *Adv. Mater.* **2009**, *21*, 3116-3120.

[41] Vutukuri, H. R.; Stiefelhagen, J.; Vissers, T.; Imhof, A.; van Blaaderen, A. *Adv. Mater.* **2012**, *24*, 412-416.

[42] Smallenburg, F. Ph. D. thesis, **2012**.

6

Direct Observation of the Formation of Liquid Protrusions on Polymer Colloids and their Coalescence

ABSTRACT

Monodisperse non-spherical PMMA particles where a central core particle has grown two extra 'lobes' or protrusions placed opposite each other on the central sphere were successfully synthesized by swelling and subsequent polymerization of cross-linked poly (methyl methacrylate) (PMMA) spheres with swelling monomers (methyl methacrylate and the cross-linker Ethylene glycol dimethacrylate EGDMA). The use of large (~ 3 μm) seed particles allowed for real-time monitoring of the swelling and de-swelling of the cross-linked polymer network by using optical microscopy. A large number of small droplets of swelling monomers formed simultaneously on the surface of the seed particles, and fused together until under certain conditions two protrusions remained on opposite sides of the seed particles. The yield of such particles could be made as high as 90% with the spread in the angle between the protrusions being 180° and the polydispersity in their size: 7.0%. Stirring accelerated the transfer of the swelling monomers to the seed particles, which speeded up swelling as well. Stirring was also found to have the function of inducing the swollen seed particles to self-assemble into a wide variety of n-mers, consisting of a certain number, n, of swollen seed particles. The formation of these structures is guided by the minimization of the interfacial free energy between the seed particles, liquid protrusions and aqueous phase, but stirring time and geometrical factors influence it as well. By inducing polymerization the structures could be made permanent. Some control over the topology as well as overall size of the clusters was achieved by varying the stirring time before polymerization. Unfortunately, for n larger than 3 unique clusters were not really found and even for $n = 2$ separation of the clusters will not be easy. 3D models of possible particle structures that could be rotated in 3D were used to identify all projections of the structures obtained by scanning electrical microscopy (SEM). These models also revealed that the seed particles inside the central coalesced body were slightly compressed after polymerization. By extending the synthesis of the monodisperse particles with $n = 1$ (particles with opposite protrusions) to (slightly) different monomers

and/or different cores, an important class of patchy particles could be realized.

6.1 INTRODUCTION

Colloidal particles a few nanometers to a few micrometers in size are of great interest not only to the field of soft matter but also to that of condensed matter and materials science in general, because they can be used as ideal model systems in which they represent scaled up versions of atoms and ions, leading amongst other into insight into crystal nucleation and growth, the glass transition, and the influence of the range of particle-particle interactions on the phase behavior. To date, most studies of using colloids as model system focused on spherical particles or particles with simple shapes, such as rods and plates, which is mainly caused by the convenient preparation methods of these kinds of particles providing both high quantity and quality (uniform in size and shape). [1-8] Recently, the prospect of using colloidal particles as advanced building blocks for creating functional materials has been a powerful driving force to develop new colloidal synthesis routes for colloids of more complexity and with self-assembly and functionality in mind. These more complex building blocks are expected to facilitate and expand the range of possible colloidal structures, and are promising candidates to generate new functionalities. [9-12] Therefore, a reproducible synthesis with a high yield of non-spherical colloidal particles with a good size distribution and shape uniformity is important, but also a huge challenge.

During the last decade, intensive efforts led to sophisticated techniques for synthesizing non-spherical colloidal particles, although some old methods already available were also rediscovered. These techniques encompass, but are certainly not limited to: arrested self-assembly by drying particles in emulsion droplets [13-16] and seeded emulsion polymerization. [17-36] These methods draw from the diverse fields of chemistry, physics, biology, engineering and materials science, and, especially in combination, provide a powerful arsenal for the fabrication of new special building blocks. Among these methods mentioned, seeded emulsion polymerization method received much recent attention because it is a relatively easy process, can provide for high yields and is often reproducible. Bradford, *et al.* [17] first described this seeded emulsion polymerization in 1962, then, Sheu *et al.* [26, 27] developed this technique in detail about how the heating monomer-swollen cross-linked polystyrene spheres at a few micrometer size scale caused a phase-separation of the swelling monomer (styrene) from the cross-linked seed particles in the form of a liquid protrusion which could then be polymerized. Then, various extensions made this technique applicable to particles of different size and with chemical and/or physical anisotropies. [20-25, 28-36]

However, it is worth pointing out that most of these approaches were based on the use of cross-linked seed particles of polystyrene (PS) only and most focused on the case of a single protrusion.

The seeded emulsion polymerization method induced more complex shapes such as linearly trimeric, cone-shaped particles and water molecule-shaped particles by repeated swelling and polymerization, [24, 33] all of which are basically by variations of the swelling of seed particles follow by a phase separation. [17-19, 26, 27] As mentioned, after two cycles of this procedure, linearly trimeric PS particles were usually obtained, [24, 33] but sometimes particles of other shapes appeared. [24] The factors that influence these differences in morphology are not well understood and addressed in the present paper, although here the focus is on trying to achieve regular particles in a single step instead of multiple. Recently, in a somewhat different use of the seeded emulsion polymerization procedure, more or less making it into the process of Pine *et al.* [13-16] used with particles in emulsions was reported by Kraft *et al.* [20, 21] They found that the cross-linked PS spheres with a liquid protrusion could assemble by mildly aggregating these particles into regular colloidal clusters by coalescence of the wetting layer. By controlling the amount of protrusions with respect to the seed particles different geometries could be obtained. [20] Subsequent polymerization yielded a wide variety of regular *n*-mers that ranged from cluster-like particles up to the size of colloidosomes. Here, we decided to test in more detail the mechanism generally believed behind the formation of the liquid protrusion which is that: the relaxation of over-swollen cross-linked seed spheres causes the extrusion of a great number of tiny liquid droplets consisting of swelling monomer; which by lowering the combined surface tension fuse into a single protrusion in the end. [25, 27, 28, 35]

This study resulted in a straightforward preparation of linearly trimeric particles (LTP) in one step in which two protrusions are on opposite sides of the micron-sized cross-linked poly (methyl methacrylate) (PMMA) seed particles. Particles with liquid protrusions on opposite sides of seeds, called 'hamburger-type' particles by these authors, were also made by Okubo [37, 38] and others [39] in a related procedure. In this procedure, uncross-linked polymer (mostly PS) seed particles were swollen in a polar solvent by a non-polar solvent (*e.g.,* alkanes) which was also a bad solvent for the PS. Under certain conditions, LTP also resulted, which could turn the seed particles into anisotropic shapes by heating these particles close to the glass transition temperature of the seeds, which would then change shape induced by surface tension effects. In our case, we presented a different one step synthetic strategy to just mentioned Okubo's method to yield these LTP. Our method is mainly based on the seeded emulsion polymerization. A relatively large sized (~ 3 μm in diameter) cross-linked PMMA

spheres are used as seeds to absorb swelling monomer form the medium. The direct observation (by optical microscopy) of LTP formation reveal the fusion of tiny droplets which spontaneously takes place once the swelling monomers saturated seed particles start shrinking during a very short time. Due to the geometry, all the small protrusions on a single seed particle merge into two primary protrusions. This state will subsequently remain for a relatively long time span (> 5 days). These observed swelling and de-swelling processes of cross-linked PMMA networks testify to the applicability of the predicted formation mechanism of Sheu's PS system [26, 27] to our PMMA system. Moreover, during the swelling process, the coalescence of PMMA seed particles with liquid protrusions upon collision, induced by stirring, are inevitable. We also studied the mild aggregation of cross-linked PMMA seeds with liquid protrusions induced by stirring. Unfortunately, we did not find unique clusters of *n*-mers, where *n* is the number of seed particles, but more complex collections of isomers compared to other studies. [20, 21] The subsequent polymerization of the system can largely preserve the as-synthesized morphologies of the particles. In addition, aided by a method develop in our group, [41] dying LTP is possible. Subsequently, an adaptation of solvent swap approach recent published by Behrens group [42] is employed to disperse these LTP from polar to apolar, yet refractive index matching solvent (decalin), which makes these particles suitable for quantitative confocal microscopy studies in concentrated system. We observe a positionally order but orientationally disorder system, namely, plastic crystal.

6.2 MATERIALS AND METHODS

6.2.1 Materials

Methyl methacrylate (MM, Aldrich) was passed over an inhibitor removal column (Aldrich) at room temperature. After the inhibitor had been removed, MM was stored in a refrigerator at +4 $^{\circ}$C, and not longer than one month. Azo-bis-isobutyronitrile (AIBN, Janssen Chimica) was re-crystallized from ethanol before use. Ethylene glycol dimethacrylate (EGDMA, Sigma) was used as the cross-linker. Polyvinylpyrrolidone (PVP, K-90, Fluka) with an average molecular weight of 360,000 g/mol was used as the stabilizer. Methanol (Biosolve, Chemical grade) was used as the solvent in dispersion polymerization performed. Hydroquinone (Fluka) was used as the inhibitor. (*cis+trans*)Decahydronaphthalene (decalin, Fluka, Chemical grade) was used as index matching solvent for PMMA. Sorbitan trioleate (Span 85, Sigma, Chemical grade) served as the phase transfer agent. The fluorescent monomers (rhodamine b isothiocyanate)-aminostyrene (RAS) was prepared following a similar method described in

our previous work and chapter 5. [35] De-ionized water was used in all experiments and was obtained from a Millipore Direct-Q UV3 reverse osmosis filter apparatus.

6.2.2 Synthesis of Spherical Uncross-Linked Template Particles

Monodisperse spherical uncross-linked PMMA template particles were prepared using dispersion polymerization. [40, 41] In detail, a mixture consisting of 1 g of stabilizer (PVP) and 20.5 g of solvent (methanol) blended with 2.5 g of monomer (MM) containing 1 wt% (based on monomer) of initiator (AIBN) at first. Then, all of them were charged into a 250 ml round bottom flask equipped with a Teflon-coated stir bar and a condenser at room temperature. A de-oxygenation process was carried out for at least 0.5 h by bubbling nitrogen through the reaction mixture. Then, the flask was immersed in a silicon oil bath at 55 ^{o}C and stirred at 100 rpm. The temperature was maintained for 24 h before cooling back to room temperature. The obtained particles were rinsed three times with methanol and two times with de-ionized water by using a centrifuge (Hettich Rotina 46 S centrifuge, at 315 g for 15 min), and ultimately, dispersed in a 1 wt% PVP (K-90) aqueous solution at a particle weight fraction of 0.7%. The resulting template particle radius was determined by static light scattering (SLS) to be 980 nm with a polydispersity of 2.8% (for details, see supplementary information).

6.2.3 Synthesis of Spherical Cross-Linked Seed Particles

In this step, 20 ml template particle (0.7 wt%) aqueous suspension was charged into a round bottom flask. In a separate container, 2 g of swelling monomer (MM) containing 2 wt% (0.04 g, based on swelling monomer) of cross-linker (EGDMA) was mixed with 1 wt% (0.02 g, based on monomer) of initiator (AIBN), and then dispersed dropwise into 20 ml of 1 wt% of PVP aqueous solution under vigorous stirring. Later, this suspension was fed dropwise into the flask containing the template particles suspension under a gentle stirring (~ 100 rpm). All samples were swollen overnight under constant stirring at 100 rpm. Subsequently, nitrogen was bubbled through the reaction system for at least 30 min to purge the system of oxygen. The addition of a water soluble inhibitor (hydroquinone, 0.5 wt% based on swelling monomer) prevented secondary nucleation at an early stage of the reaction in the aqueous phase. After addition of this inhibitor the flask was heated to 70 ^{o}C and kept at this temperature for 8 h. Then, the samples was cooled down to room temperature and purified by washing it four times with de-ionized water using a centrifuge (Hettich Rotina 46 S, at 140 g for 15 min), and finally stored in a 1 wt% PVP aqueous solution with a mass fraction of 0.7%. The obtained seed particles were monodisperse in size (1480 nm in radius and 2.5% polydispersity measured by SLS, for details, see supplementary information).

6.2.4 Synthesis of Non-Spherical Particles

The cross-linked seed particles were used to synthesize non-spherical particles. The preparation procedure of non-spherical particles was similar to that of the cross-linked seed particles except for the amount of swelling monomer being 4 g with a 0.5 wt% (based on swelling monomer) of cross-linker (EGDMA) and 1 wt% (based on swelling monomer) of initiator (AIBN). Finally, the samples were dispersed in de-ionized water for characterization.

6.2.5 Dying Non-Spherical Particles

Post-dying the non-spherical particles was based on our previous work in chapter 5. [35] In brief, the suspension of non-spherical particles was first dried under a N_2 stream. The obtained dried particles (~ 0.1 g) were dispersed in a 5 ml solution of 1mM RAS in pentanol by sonication, and stirred (~ 100 rpm) overnight in a sealed glass vial at room temperature. Then, the labeled particles were separated by a centrifuge (315 g, 15 min) and washed once with ethanol and twice with de-ionized water. After drying under a N_2 stream, the fluorescent non-spherical particles were stored in a glass vial in the dark at room temperature.

6.2.6 Solvent Swap

To change the solvent from high polarity to very low, a modification of the procedure developed by the Behrens group [42] was carried out: A small amount of dried non-spherical particles (~ 0.01 g) was dispersed in de-ionized water and sedimented by using a Hettich Rotina 46 S centrifuge (140 g, 10 min) and the supernatant was removed. The non-spherical particles were first transferred from water to pentanol which acts as an intermediate solvent and then further to decalin with the help of the non-ionic surfactant (Span 85, 50 mM). After this last step had been repeated four times, the solvent was considered to be completely replaced.

6.2.7 Characterization

In order to determine the size and polydispersity of the spherical particles, static light scattering (SLS) was performed on a highly dilute suspension ($\Phi < 1 \times 10^{-6}$) in de-ionized water with home-built equipment using a He-Ne laser as a light source (632.8 nm, 10 mW). [41] The logarithm of the scattering intensity was plotted against the scattering vector $k = 4\pi n_r \sin(\theta/2)/\lambda$, where n_r is the solvent refractive index, θ is the scattering angle, and λ is the wavelength in vacuum. The SLS profiles were compared with the theoretical curves calculated with the full Mie solution for the scattering form factor for particles with a core-shell or homogeneous structure. Polydispersity was accounted for in the calculation by integrating over a Gaussian size distribution taking into account the size-dependent scattering intensity. [43]

Taking advantage of the relatively large size (in a micron-sized scale) of the particles presented in this chapter, the swelling behavior and the particle morphologies in preparations were easily recorded in real time with an optical microscope equipped with a 63× objective. These pictures were captured with a digital Nikon camera (D90), while the polymerized particles were examined using a scanning electron microscope (SEM, Phenom). The samples were sputter coated with 5 nm platinum prior to imaging. Confocal scanning laser microscopy (CSLM) was used to record the phase behavior of the fluorescent non-spherical particles in the absence of interference from the refractive index mismatch between solvents and samples. A Nikon confocal scanning laser scan head (Nikon C1) was operated in fluorescent mode on a Leica (DM IRB) inverted microscope. A Leica 63 × oil confocal immersion lens with a numerical aperture of 1.4 was used for measurement. The fluorescent dye was excited at around 543 nm and the images were collected at emission wavelengths of around 605 nm.

6.3 RESULTS AND DISCUSSION

6.3.1 Sample Preparation

Recently, seeded emulsion polymerization techniques have been successfully employed in the fabrication of various types of anisotropic polymer particles. Typically, cross-linked polymer spheres suspended in an aqueous environment are swollen with hydrophobic monomers, such as methyl methacrylate or styrene. Upon relaxation of the stretched polymer network, the strongly swollen polymer sphere phase separates, yielding a mildly swollen polymer sphere carrying a liquid protrusion consisting of swelling monomer. This relaxation can be enhanced by temperature elevation as well as a long swelling time. [23, 26, 27] The resulting particles were reported to be mainly dimers, [23, 25-32, 34, 35] but also popcorn-like [27, 35] and, after merging of the liquid protrusions on different seed particles with a single protrusion, also colloidal molecule-like shapes were seen. [20, 21] As mentioned before, the work of Okubo *et al.* [37-39] on the swelling and wetting of apolar solvents for polymer seed particles dispersed in polar liquids is closely related to the liquid protrusions. The only difference being that protrusions made from a monomer usually can be made more permanent by polymerization.

Sheu *et al.* [26, 27] proposed that multiple liquid protrusions formed on highly cross-linked seed particles (PS). They supposed that this could be attributed to in-homogeneities of the network, which tend to localize contraction forces during swelling. Until now, the number and position of multiple protrusions was mostly uncontrolled and research focused on this topic was rare. [24, 26, 27, 35]

We first followed (with slight modifications, for details, see the experimental section) the

procedure which was originally from Sheu's work [26] for preparing dumbbell-like PMMA particles instead of PS. The cross-link density of the seed particles was controlled at 2 wt% based on the mass of the monomers. The process of absorption and then the release of swelling monomers caused a phase separation between the swelling monomers and seed particles, forming liquid protrusions. Subsequently, heating induced polymerization of the monomers and also enhanced the phase separation leading to the growth of the protrusions. Surprisingly, PMMA seed particles with two newly-formed identical lobes or protrusions (also called 'hamburger-like' particles by others [37-39]) were obtained after rinsing away the impurities (see Fig. 6.1b). It is worth pointing out the two new-formed lobes were always located opposite from each other on the surface of a seed particle, which is why we denote these as: linearly trimeric (LT) particles, where the 'trimeric' here does not refer to the number of seeds, but to the number of separate shapes visible. Note that LT structure was independent of the swelling monomer composition; it appeared even if only a pure monomer (MM) instead of a mixture of monomer and cross-linker was used. This feature demonstrates the potential that our approach could be extended as a more universal method for preparing such LT-structured polymer particles with more chemical and/or physical anisotropies. For instance, by slightly modifying the procedure in which small quantities of other monomers are used in the swelling would result in particles where the charge density on the opposite lobes would be different from that of the seed particle. From computer simulations and theory it is clear that the self-assembly behavior of such particles is quite interesting. [44, 45] For self-assembly studies, it is quite important to be able to synthesis particles in bulk as for instance methods that rely on 2D methods will give a much lower yield of particles. [45]

6.3.2 Plastic Crystals

Colloidal hard dumbbells were computationally predicted to form a plastic crystal at aspect ratios lower than 0.4. [46, 47] Our group recently observed such plastic crystals in soft dumbbell systems (in 2D and 3D); these plastic crystals could be switched to full crystals by virtue of an electric field. [35, 48] Drawing inspiration from Espinosa's work, [42] the as-synthesized LT PMMA particles were efficiently transferred from a polar (water) to non-polar solvent (hexane or decalin) by means of a non-ionic surfactant (span 85) while keeping the Debye-Hückel screening length larger than the particle size. Soft plastic crystals made of the LT particles (LTP) were observed in two dimensions as shown in Figure 6.1c. The orientations of the LT PMMA particles are disordered, while the positions are ordered. Therefore, due to the long screening length of each particle in Figure 6.1c, plastic crystals made of LT particles in 3D, are feasible as well and will be described in a forthcoming chapter.
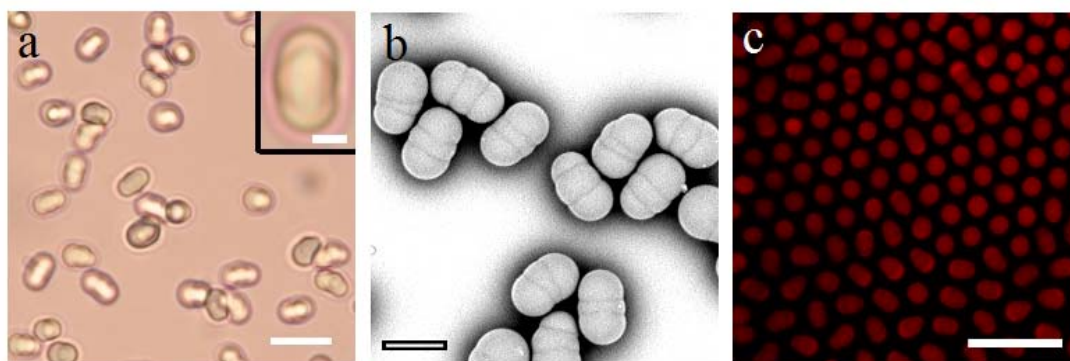
Figure 6.1. a) Light microscopy image of swollen seed particles (two identical liquid protrusions are attached on the opposite sides of a seed particle); the scale bar is 10 µm and the inset one is 2 µm. b) Scanning electron microscopy (SEM) image of typically obtained hamburger-like PMMA particles; the scale bar is 5 µm. c) Confocal microscopy image of a two-dimensional plastic crystal of hamburger-like PMMA particles dispersed in a refractive index matching solvent (decalin) stabilized by span 85 (50 mM); the scale bar is 20 µm.

6.3.3 Stirring Effect

During the swelling of seed particles, stirring was discovered to play a significant role on the formation of LTP, which is most likely caused by the fact that monomer droplets are also present and are sped up by the stirring to end up in/on the seed particles. As shown in Figure 6.2a and b, in the absence of stirring, swelling monomers diffused to the polymer phase much more slowly. Even after a day, there was no obvious change in the morphology of the particles. On the other hand, stirring efficiently accelerated the transfer of the swelling monomers; Figure 6.2c and d clearly demonstrate this fact.

6.3.4 Formation Exploration

To elucidate the formation mechanism of the LT-shaped particles, imaging of swollen particles as a function of time was tried. In order to directly observe the formation of liquid protrusions, a capillary (50 mm × 2 mm × 0.2 mm) was initially half filled with a suspension of seed particles. After half an hour, the density difference between the seed particles and solvent (water) forced the particles to sediment to the bottom of the capillary, where they stayed roughly stationary (due to the big size of the particle ~ 1.5 µm in radius) when was in the absence of stirring. Subsequently, the emulsion containing swelling monomers stabilized by PVP was fed carefully and slowly into the capillary (filled the other half capillary) consisting of seed particle suspension using a 1 ml syringe, so as to not significantly disturb the locations of the seed particles. The swelling monomers emulsion was comprised of a large number of tiny droplets of swelling monomers which were not visible under an optical

microscope, but could be observed by light scattering and swelling monomer form these small droplets were efficiently absorbed by the seed particles. On the other hand, due to the density difference between the swollen seed particles, the water phase and the big swelling monomer droplets, the swollen seed particles preferred to sediment to the bottom of the capillary while bigger swelling monomer droplets floated to the top of the capillary. Therefore, it was easier to accurately observe the swelling behavior of the seed particles directly at the place where is near the bottom of the capillary without too much disturbance from the big swelling monomers droplets. The summarized optical micrographs and corresponding schematic cartoons are shown in Figure 6.3.
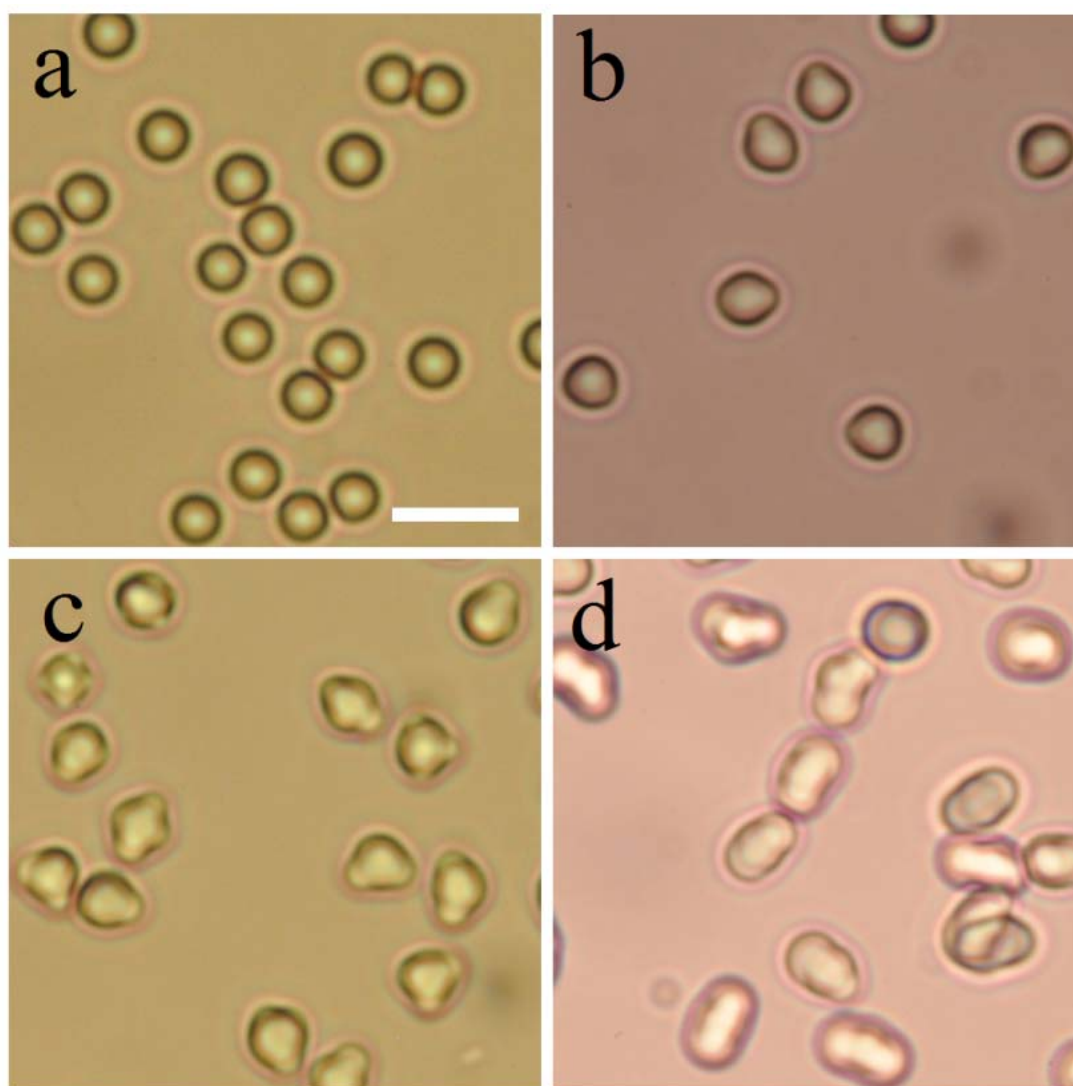
Figure 6.2. Optical microscopy images of swollen seed particles, without stirring at a) 0 min; b) a day, and with stirring at c) 0 min; d) 10 min. The scale bar is 10 μm.

Once the emulsion of swelling monomers was mixed with the seed particles dispersant, numerous small swelling monomers droplets were gradually absorbed by the seed particles in

which the swelling monomers swelled the cross-linked polymer network, resulting in expansion of the seed particles in the early stage of swelling. Then, shrinkage [27] of the cross-linked polymer network took place, leading to many tiny droplets comprised of swelling monomers to protrude out. The tiny droplets tended to fuse so as to lower their surface energies. As a result of the continued fusion among the small swelling droplets on the surface of a seed particle, only three primary liquid protrusions are visible in the third image in Figure 6.3. Two of these are located closer to each other than to the third one. When the liquid protrusions grew bigger, the two closer protrusions merged into a bigger one leaving only two. Interestingly, these non-identical liquid protrusions grew to an identical size over time and did so for almost all particles (~ 79%) at this stage. In the last optical image in Figure 6.3, a spherical seed particle with two identical liquid protrusions aligned linearly is presented. Polymerization afterwards did not influence this LT-shaped morphology (see Fig. 6.1).
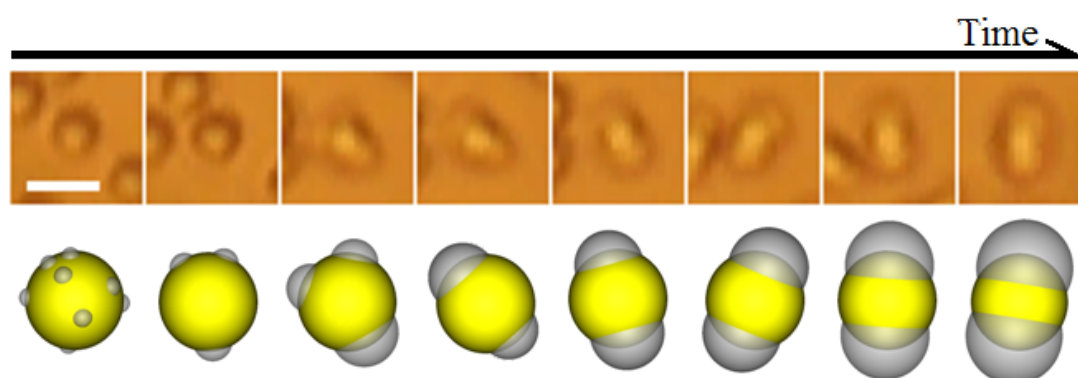
Figure 6.3. Time-lapse optical microscopy and corresponding schematic images (the seed particles and newly-formed protrusions are marked yellow and gray in color, respectively) of the formation and growth of the bi-liquid protrusions on the surface of a cross-linked (2 wt%) PMMA seed particle. The total time scale is about 15 min and the scale bar is 5 μm.

In our previous work in chapter 5, [35] small PMMA particles (around 1 μm in diameter) with the same cross-link density were used as seeds to prepare non-spherical particles via the seeded emulsion polymerization technique. During the stirring and subsequent polymerization stage, just one single protrusion was visible on each seed particle. Hence, it can be concluded that the formation of LTP is geometry (size)-dependent, since it mainly took place on the relatively large-sized seeds (*e.g.,* 1.5 μm in radius). Kraft *et al.* [14] introduced a synthetic method for assembling colloidal spheres into clusters by making use of liquid protrusions on the surfaces of cross-linked PS seed particles. They mentioned that they never observed more than one protrusion on small seed particles (PS, 222 nm in diameter), while for the big seed particles (PS, 1.88 μm in diameter) sometimes secondary protrusions were found, which were significantly smaller than the primary protrusions. They believed that the formation of more

than one protrusion was unfavorable in terms of surface energy, and the protrusions on the surface of a seed particle coalesced over time. Clearly, for a larger surface area per particle both the chance of getting multiple protrusions and the time they take to fuse will go up. To confirm it, our swelling systems were kept stirring under gentle stirring (~ 100 rpm) for five days. As a result, seed particles with only a single liquid protrusion attached prevailed, which implies that the LTP is only a transient state, with longer coalescence time, the distribution of protrusion number shifted to a lower number range. As expected, by refraining from stirring we noticed that once the LTP were dominant, these LT- structures were preserved for a longer time span (at least five days), giving ample time to freeze them in by polymerization. It may be that charges on the protrusions and/or a deformation of the central seed may delay the coalescence of the two opposing protrusions into one, a configuration with a lower free energy. Further research is necessary to determine the optimal conditions of the synthesis of the LTP which were also found by Okubo *et al.* [37, 38] under certain conditions when they did not swell seeds with monomers, but with apolar liquids. [37, 38]

6.3.5 Clusters

As mentioned above, stirring was crucial in our system. Without constant gentle stirring, the saturation of the swelling monomers among the cross-linked polymer network took up a relatively long time period. Alternatively, fast stirring (faster than 100 rpm) tended to cause the swollen seed particles to flocculate in the form of the visual agglomerations. On the other hand, after the formation of LT structures on the seed surfaces, constant gentle stirring induced the self-assembly by coalescence of the liquid protrusions on different colloids. [20-22] In principle, the more liquid droplets are present on the surface of the seed particles if they coalesce, the larger the number of combinations of colloidal structures that will be obtained. Specifically, for seeds with a single protrusion attached, all obtained colloidal structures with a given number of seed particles have an identical geometry. [20, 21] When a secondary identical liquid droplet is 'added' to the surface of a seed particle, the combinatory potential of such a colloid increases exponentially, not only due to the fusion of liquid droplets on the same seed particle, but also that of those on different seeds. Clusters made up of two seed particles are shown in Figure 6.5. Already here it is clear that the structures obtained are not unique, although the small number could still possibly be purified if a suitably sensitive technique would be used.

To reveal in more detail the internal structures of the clusters obtained, we tried to overlap images of the clusters (n = 2, 3, where n is the number of the seed particles contained in a cluster) based on the observation of a large number of such clusters from SEM with projections of 3D models. The 3D models were constructed according to the contacting angle

(θ), bond angle α (for $n = 2$), β (for $n = 3$), the radius of the seed particles (R_s), individual (R_i) and coalesced protrusions (R_c), and the distance between two seeds centers (L) (see the schematic models in Fig. 6.4). Specifically, the bond angle α and β in a cluster can be calculated via

$$\alpha = \cos^{-1}\left(1 - \frac{L^2}{2\left(R_c^2 + R_s^2 - 2R_c R_s \cos\theta\right)}\right), \tag{6.1}$$

$$\beta = \cos^{-1}\left(1 - \frac{L^2}{2\left(R_c^2 + R_s^2 - 2R_c R_s \cos\theta\right)}\right), \tag{6.2}$$

By only rotating these models, *i.e.*, changing the view point, we could reproduce all observed colloidal clusters. Good agreement between models and experiments required that the seed particles interpenetrated slightly (see Fig. 6.5). Similarly, for the trimeric clusters ($n = 3$) the seed particles partially overlapped inside the center in the coalesced protrusion body. However, the sizes of the overlap fractions varied with the sizes of the coalesced protrusions. The perspective images in Figure 6.5 clearly show, from left to right, a tendency to increase the overlapped fraction, which is mainly caused by the decrease in size of the coalesced protrusions. However, also a deformation of the seed particles to conform more to the surface tension of the monomer protrusions could partially explain these results. This would be similar to the work of Okubo *et al.* [37, 38] who observed organic solvents in/onto seed particles and investigated on how these liquid deformed the spherical seeds to anisotropic shapes. The smaller the coalesced protrusion are, the more severe the interpenetration and/or deformation forms. This 'soft' behavior can be understood by considering that the polymer network of the seeds was only cross-linked by 2% w/w cross-linker, and that the swelling monomers inherently are good solvents for polymer. Again, the configurations of dimers were maintained after polymerization, as seen from the optical microscopy and SEM images in Figure 6.5. Moreover, the bond angle α increased when less liquid contributed to the coalesced central body (α are 144° and 162° for the cases in Fig. 6.5-1 and 2, respectively). When the coalesced central body was composed of two liquid protrusion units, the two seed particles, as well as their protrusions, aligned linearly ($\alpha = 180°$), which is shown in Figure 6.5-3. It possible that the volume of the coalesced protrusions is too small in this case, restricting the movement of the seed particles inside the fused protrusions as was seen before in the work of Kraft *et al.* [21] Additionally, the total volumes of the liquid protrusions obtained using the 3D models for each configuration was roughly equal for the clusters with a given n, namely, the total volume of liquid protrusions only depended on how many seed particles (n) were contained in the clusters.
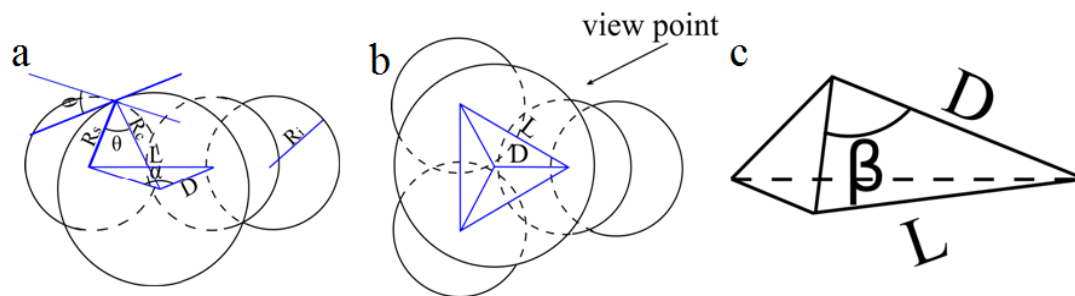
Figure 6.4. Schematic representations of (a) a dimeric cluster (comprising of two seed particles, and corresponding to the case in Fig. 6.5-2); (b) a trimeric cluster (comprising of three seed particles, and corresponding to the case in Fig. 6.6-2); (c) shows the geometric pyramid structure from the panel. Where L is the distance between the centers of two seeds, θ is the contact angle, α (for clusters which comprise two seeds) and β (for clusters which comprise three seeds) are the bond angles, R_s, R_i and R_c correspond to the radius of the seed particles, individual and coalesced protrusions, respectively.
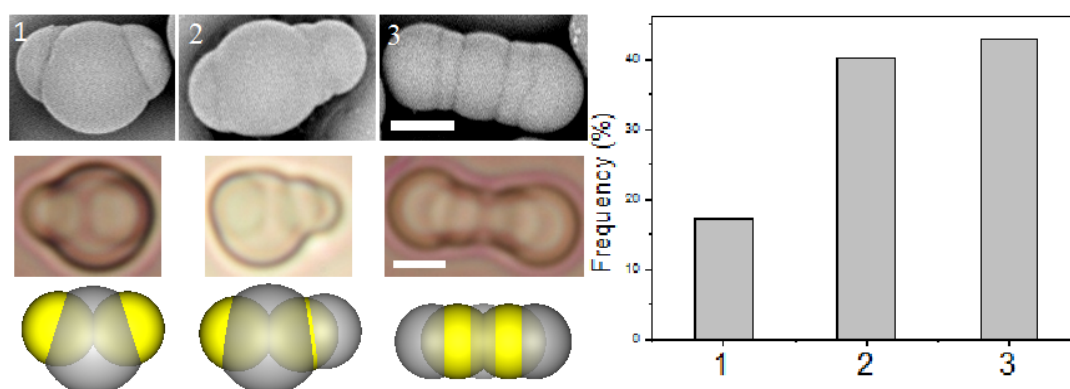
Figure 6.5. Colloidal PMMA clusters comprising of two seed particles before (optical microscopy images) and after (SEM images) polymerization, and their representations (after polymerization. The seed particles and newly-formed protrusions are marked yellow and gray in color, respectively). The bar graph shows their relative abundance. The scale bars are 3 μm.

Although the total volume of liquid protrusions for each n clusters was fixed, the coalesced protrusion size was variable, and mainly depended on the number of liquid protrusions that fused to form it. For $n = 3$, six distinct combinations were found and listed in Figure 6.6. In order to not confuse bond angle (α) in dimeric clusters ($n = 2$), we define the bond angle β for clusters (only applicable for the first four samples in Fig. 6.6) with three seeds as the angle between the center of the coalesced (largest) protrusions and any two seed particles (for more details, see Fig. 6.4). The bond angles in the clusters comprising three seeds show a gradual increase as the size of the coalesced droplet grows from left to right in the first four samples in Figure 6.6 (from 104° to 110°). This means the sizes of the centrally coalescent bodies of the clusters could be adjusted by the number of fused liquid entities, and directly affects the

variation of the bond angles as well. From the fact that the overlap fractions increased when fewer liquid protrusions participated in the centrally coalesced bodies, it can be inferred that the seed particles were less mobile when fewer liquid protrusions join in before polymerization. The subsequent polymerization caused shrinkage of the newly formed central polymer body according to the density increase from liquid monomer to solid polymer network, and, ultimately, resulted in a higher overlap fraction of seeds inside the central body.
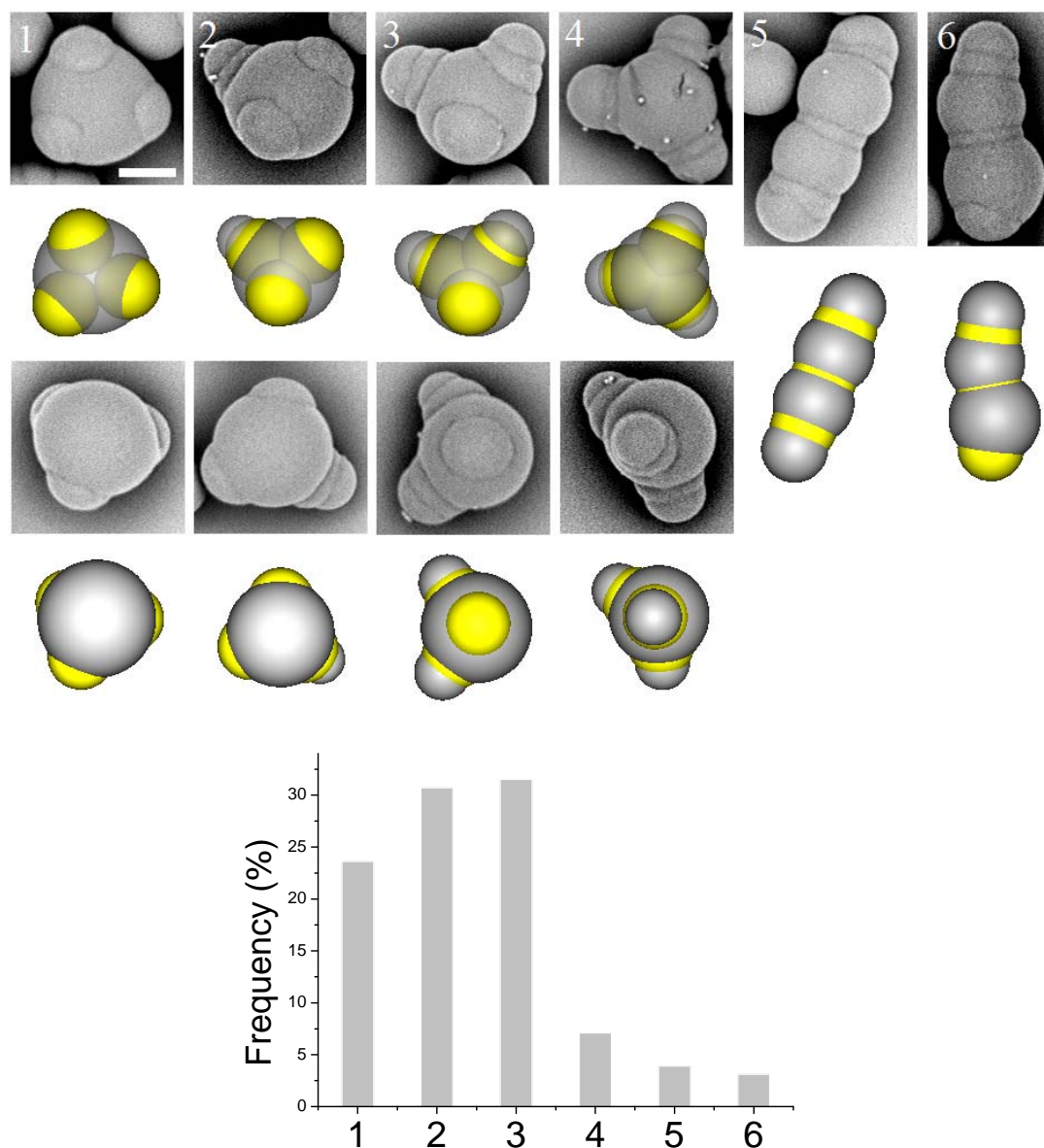
Figure 6.6. Colloidal PMMA clusters comprising three seed particles (SEM images) and their respective 3D model representations and relative abundance. The scale bar is 3 μm.

Inspecting image 6 in Figure 6.6, one individual and two coalesced protrusions are present from the top to bottom of the cluster. The first coalesced protrusion from the top comprised of two liquid protrusion units, which is not large enough to let two attached seed particles move

freely, while the bottom one comprised three liquid protrusion units, which indicates a small deviation of bond angle away from linear alignment (bond angle is 162°). One can roughly deduce a critical number of protrusion units, a larger number than which would lead to a non-linear alignment of the seeds, while a smaller number only induces a linear alignment of the seeds. It turns out that in our case this critical number equals 2. This is in good accordance with the case in Figure 6.5-2. A statistical analysis of the morphologies of the clusters consisting of three seed particles was carried out based on measuring more than 200 experimental (SEM) images, and the results are shown in Figure 6.6. It clearly shows that the most favorable configurations of clusters ($n = 3$) are the first three cases (see Fig. 6.6-1, 2 and 3), and that these are mainly dominated by the interfacial tension between the swelling monomers droplets and the aqueous phase. In comparison, clusters 5 and 6, which both exhibit a linear configuration, were rare due to their high surface energies.

In principle, the landscape of clusters undergoes an explosive increase for $n > 3$. However, in absolute number these clusters were rarely present because of the relatively short stirring period and the low stirring speed. The five typical configurations for the clusters comprised of four seed particles ($n = 4$) are shown in Supplementary Figure 6.3. Due to the significantly lower number of SEM images for $n = 4$ clusters, the statistics could not be determined. However, an apparent tendency is that the size of the individual protrusions on the seed particles decreased when the number of individual protrusions increased.

6.4 CONCLUSIONS

Monodisperse PMMA particles with two opposing protrusions on the central seed particles were fabricated via a one step seeded emulsion polymerization by using 2 wt% cross-linked PMMA spheres as seeds, despite of the fact that this configuration is only metastable. The formation of such non-spherical particles was recorded in real time by optical microscopy. At a certain point in time the monomer swelling the seed could be kept in the swollen particle and numerous tiny monomers droplets were extruded out onto the surface of the swollen seeds. Driven by the surface energy and geometry, fusion of the swelling monomers droplets took place, and finally only two primary liquid droplets were left, attached to the surface of the seed particles. At this stage a monodisperse system of linear-trimeric particles could be obtained. Such particles with opposing lobes are interesting for self assembly studies as has already been shown in computer simulations. [44] This synthesis route provides an easier method with a significantly higher yield than for instance trimeric patchy particles made by oblique evaporations or other 2D methods. [45] Stirring enhanced further coalescence of the liquid protrusions, either between protrusions on the same particles or between those on

different particles. This led to the formation of complex colloidal clusters which were unfortunately not unique for clusters build up from the same amount of seeds. The subsequent polymerization of the liquid protrusions kept the configurations more or less identical. 3D modeling of the obtained clusters offered insight into the internal structures of clusters. These plentiful 'isomeric' colloidal molecules are interesting candidates for chemical and physical research.

6.5 ACKNOWLEDGMENTS

Bas Kwaadgras is acknowledged for fruitful discussions.

6.6 SUPPLEMENTARY INFORMATION

6.6.1 Characterization of Seed Particles
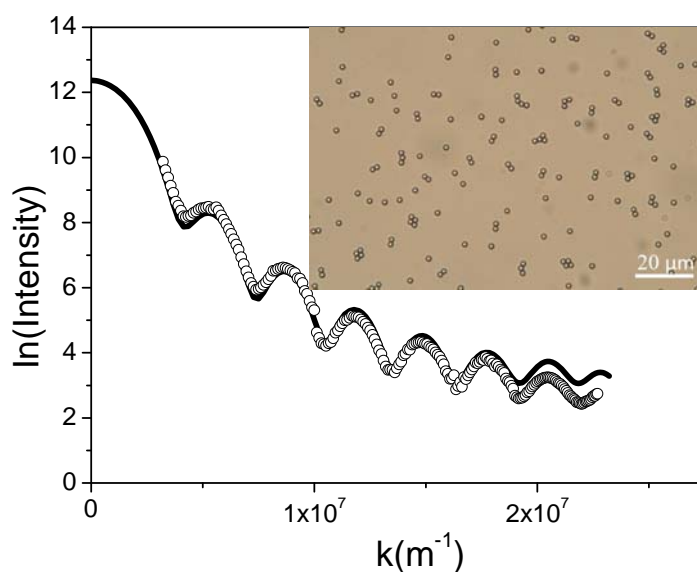
Supplementary Figure 6.1. Experimental data (open circles) and theoretical fit (solid line) of the uncross-linked template PMMA spheres measured in water. The curve was calculated using Mie theory (radius is 980 nm and polydispersity is 2.8%). The inset is the optical microscopy image of a sample dried on a glass slide.
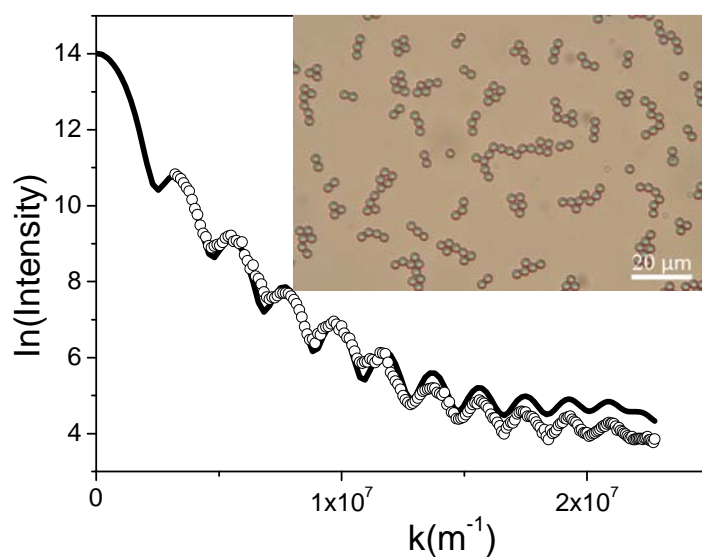
Supplementary Figure 6.2. Experimental data (open circles) and theoretical fit (solid line) of the cross-linked seed particles measured in water (with 2 wt% cross-link density). The curve was calculated using Mie theory (radius is 1480 nm and polydispersity is 2.5%). The inset is the optical microscopy image of a sample dried on a glass slide.

6.6.2 Clusters of *n* = 4
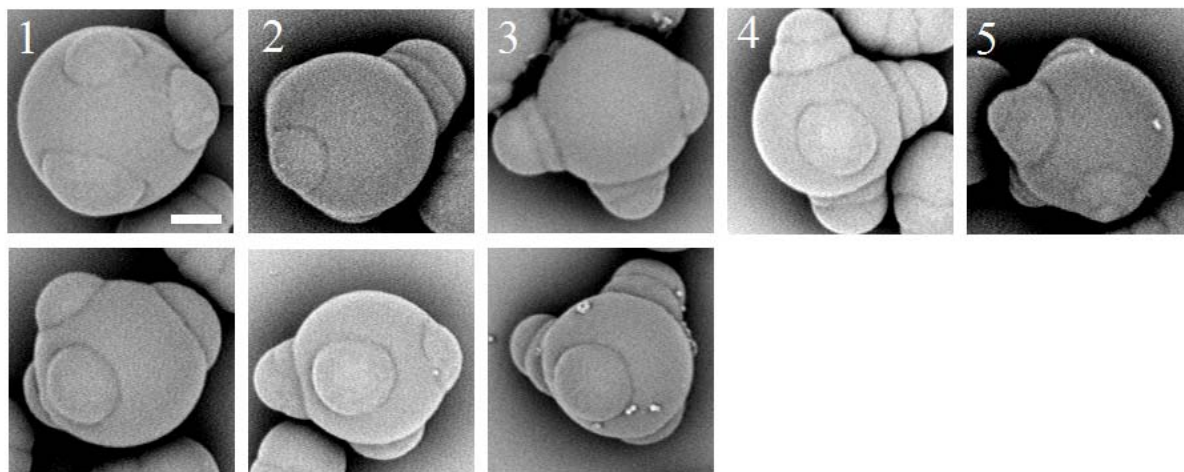
Supplementary Figure 6.3. SEM images of colloidal PMMA clusters comprising four seed particles (*n* = 4); the scale bar is 2 μm.

6.7 REFERENCES

[1]   van Blaaderen, A.; Wiltzius, P. *Science* **1995**, *270*, 1177-1179.

[2]   van Blaaderen, A. *Progr. Colloid Polym. Sci.* **1997**, *104*, 59-65.

[3]   Yetheraj, A.; van Blaaderen, A. *Nature* **2003**, *421*, 513-517.

[4] van Megen, W.; Underwood, S. M. *Nature*, **1993**, *362*, 616-618.

[5] Leunissen, M. E.; Christova, C. G.; Hynninen, A. P.; Royall, C. P.; Campbell, A. I.; Imhof, A.; Dijkstra, M.; van Roij, R.; van Blaaderen, A. *Nature* **2005**, *437*, 235-240.

[6] Shevchenko, E. V.; Talapin, D. V.; Kotov, N. A.; O'Brien, S.; Murray, C. B. *Nature* **2006**, *439*, 55–59.

[7] Kuijk, A.; van Blaaderen, A.; Imhof, A. *J. Am. Chem. Soc.* **2011**, *133*, 2346-2349.

[8] van der Beek, D.; Lekkerkerker, H.N.W. *Langmuir* **2004**, *20*, 8582-8586.

[9] Glotzer, S.C.; Solomon, M. J. *Nature Mater.* **2007**, *6*, 557-562.

[10] Duguet, E.; Desert, A.; Perro, A.; Ravaine, S. *Chem. Soc. Rev.* **2011**, *40*, 941-960.

[11] Perro, A.; Reculusa, S.; Ravaine, S.; Bourgeat-Lami, E.; Duguet, E. *J. Mater. Chem.* **2005**, *15*, 3745-3760.

[12] Yan, S.; Kim, S.; Lim, J.; Yi, G. *J. Mater. Chem.* **2008**, *18*, 2177-2190.

[13] Manoharan, V. N.; Elsesser, M. T.; Pine, D. J. *Science* **2003**, *301*, 483-487.

[14] Yi, G. -R.; Manoharan, V. N.; Michel, E.; Elsesser, M. T.; Yang, S. -M.; Pine, D. J. *Adv. Mater.* **2004**, *16*, 1204-1208.

[15] Cho, Y. -S; Yi, G. -R; Lim, J. -M.; Kim, S. -H.; Manoharan, V. N.; Pine, D. J.; Yang, S. -M. *J. Am. Chem. Soc.* **2005**, *127*, 15968-15975.

[16] Cho, Y. -S.; Yi, G. -R.; Kim, S. -H.; Pine, D. J.; Yang, S. -M. *Chem. Mater.* **2005**, *17*, 5006-5013.

[17] Bradford, E. B.; Vanderhoff, J. W. *J. Polym. Sci., Part C*, **1962**, *3*, 41-46.

[18] Okubo, M.; Katsuta, Y.; Matsumoto, T. *J. Polym. Sci., Polym. Lett. Ed.* **1980**, *18*, 481-486.

[19] Skjeltorp, A. T.; Ugelstad, J.; Ellingsen, T. *J. Colloid Interface Sci.* **1986**, *113*, 577-582.

[20] Kraft, D. J.; Vlug, W. S.; van Kats, C. M.; van Blaaderen, A.; Imhof, A.; Kegel, W. K. *J. Am. Chem. Soc.* **2009**, *131*, 1182-1186.

[21] Kraft, D. J.; Groenewold, J.; Kegel, W. K. *Soft Matter* **2009**, *5*, 3823-3825.

[22] Kraft, D. J.; Hilhorst, J.; Heinen, M. A. P.; Hoogenraad, M. J.; Luigjes, B.; Kegel, W, K. *J. Phys. Chem. B* **2011**, *115*, 7175-7181.

[23] Kim, J. -W.; Larsen, R. J.; Weitz, D. A. *J. Am. Chem. Soc.* **2006**, *128*, 14374-14377.

[24] Kim, J.-W.; Larsen, R. J.; Weitz, D. A. *Adv. Mater.* **2007**, *19*, 2005-2009.

[25] Kim, J. -W.; Lee, D.; Shum, H. C.; Weitz, D. A. *Adv. Mater.* **2008**, *20*, 3239-3243.

[26] Sheu, H. R.; El-Aasser, M. S.; Vanderhoff, J. W. *J. Polym. Sci., Part A: Polym. Chem.* **1990**, *28*, 629-651.

[27] Sheu, H. R.; El-Aasser, M. S.; Vanderhoff, J. W. *J. Polym. Sci., Part A: Polym. Chem.* **1990**, *28*, 653-667.

[28] Mock, E. B.; De Bruyn, H.; Hawkett, B. S.; Gilbert, R. G.; Zukoski, C. F. *Langmuir* **2006**, *22*, 4037-4043.

[29] Mock, E. B.; Zukoski, C. F. *Langmuir* **2010**, *26*, 13747-13750.

[30] Ge, J.; Hu, Y.; Zhang, T.; Yin, Y. *J. Am. Chem. Soc.* **2007**, *129*, 8975-8975.

[31] Nagao, D.; Hashimoto, M.; Hayasaka, K.; Konno, M. *Macromol. Rapid Commun.* **2008**, *29*, 1484-1488.

[32] Nagao, D.; van Kats, C. M.; Hayasaka, K.; Sugimoto, M.; Konno, M.; Imhof, A.; van Blaaderen, A. *Langmuir* **2010**, *26*, 5208-5212.

[33] Park, J.-G.; Forster, J. D.; Dufresne, E. R. *Langmuir* **2009**, *25*, 8903-8906.

[34] Park, J. -G.; Forster, J. D.; Dufresne, E. R. *J. Am. Chem. Soc.* **2010**, *132*, 5960-5961.

[35] Peng, B.; Vutukuri, H. R.; van Blaaderen, A.; Imhof, A. *J. Mater. Chem.* **2012**, 22, 21893-21900.

[36] Kegel, W. K.; Breed, D.; Elsesser, M.; Pine, D. J. *Langmuir* **2006**, *22*, 7135-7136.

[37] Fujibayashi, T.; Okubo, M. *Langmuir* **2007**, *23*, 7958-7962.

[38] Fujibayahsi, T.; Tanaka, T.; Minami, H.; Okubo, M. *Colloid Polym. Sci.* **2010**, *288*, 879- 886.

[39] Hosseinzadeh, S.; Saadat, Y.; Abdolbaghi, S. *Colloid Polym. Sci.* **2012**, *290*, 847-853.

[40] Shen, S.; Sudol, E. D.; El-Aasser, M. S. *J. Polym. Sci. Part A: Polym. Chem.* **1993**, *31*, 1393-1402.

[41] Peng, B.; van der Wee, E.; Imhof, A.; van Blaaderen, A. *Langmuir* **2012**, 28, 6776-6785.

[42] Espinosa, C. E.; Guo, Q.; Singh, V.; Behrens, S. H. *Langmuir*, **2010**, *26*, 16941-16948.

[43] Bohren, C. F.; Huffman, D. R.; *Absorption and scattering of light by small particles*; John Wiley and Son: New York, **1983**.

[44] Bianchi, E.; Kahl, G.; Likos, C. N. *Soft Matter* **2011**, *7*, 8313-8323.

[45] Chen, Q.; Bae, S. C.; Granick, S. *Nature* **2011**, *469*, 381-384.

[46] Vega, C.; Monson, P. A. *J. Chem. Phys.* **1997**, *107*, 2696-2697.

[47] Marechal, M.; Dijkstra, M. *Phys. Rev. E* **2008**, *77*, 061405.

[48] Demirors, A. F.; Johnson, P. M.; van Kats, C. M.; van Blaaderen, A.; Imhof, A. *Langmuir* **2010**, *26*, 14466-14477.

<div align="right">

7

</div>

Colloidal Clusters made using Emulsions and Dumbbell Particles: Experiments and Simulations

ABSTRACT

In this chapter, we use water-in-oil emulsion droplets to self-assemble (SA) different types of hydrophilic spherical, symmetric and asymmetric (size ratio 0.73) dumbbell (db)-shaped particles that are strongly attached to the water-oil interface into clusters of N particles ($N <$ 15) by slow and complete evaporation of the water phase. In addition, we investigate if the structures formed can be predicted by a simple computer simulation scheme in which the complex and continuously changing shape of the drying liquid interface is not taken into account directly. We find that the single and symmetric dumbbell shaped particles are well predicted for $N <$ 8 by a two-step simulation in which single droplets with N particles that interact through hard interactions only are considered. In the first step, the particles are confined to a spherical shrinking shell and after long time self-diffusion of the particles has stopped, the pressure increased steeply; in a second step, the second moment of the particle mass distribution is minimized. For the asymmetric db's, it is experimentally found that the larger bulb of the db dominates the structure formation, indicating that minimization of the second moment of the mass distribution is not a general guiding principle in this type of SA. The experimental results for the spheres, which lead to unique clusters for each N, are very similar to results presented in literature. Those for the symmetrical db's indicate that for smaller N ($N <$ 8) the clusters are still well defined (with at most two isomers formed), and that for N values of 3 and 5 chiral clusters are found which are each other's mirror image. Such structures are interesting in the exploration of chirality both in fundamental studies and in photonic materials. For the asymmetric db's interesting enantiomers form for $N = 2$, but already for $N > 2$ the number of different types of clusters quickly becomes intractably large and the uniqueness of the SA procedure is lost. Nevertheless, if the small bulbs are ignored, the structures formed resemble exactly those of single spheres ($N <$ 13) and thus are still interesting in cases where the effects of the smaller bulbs can be used as a tunable disturbance.

7.1 INTRODUCTION

In the last decade, there has been an important increase in the complexity of colloidal building blocks that have been developed with self-assembly (SA) steps in mind. [1-4] An important reason for this increase is the realization that with more complex, anisotropic building blocks come significantly more possible structures and symmetries that can be realized, increasing the ability to realize and optimize materials properties. [1-4] In addition, these particles are also interesting in model studies that answer questions that cannot be easily addressed with spheres, such as the importance of rotational aspects of particle motions in glass formation or crystallization. Emulsion droplets of a water phase in oil, the focus of this chapter, or vice versa are a powerful platform for the self-assembly (SA) of colloidal particles. [5] Velev *et al.* [6] pioneered shells of many particles (>>10) that could be generated using droplets and that are now generally called 'colloidosomes'. [7] These approaches used methods to destabilize the particles after/during the shell formation, to stabilize the integrity of the shells itself. Manoharan *et al.* [8] investigated the limit of small numbers, *N*, of particles adsorbed to droplets (*N* < 15) where the particles stayed stable while the oil was slowly and completely evaporated. Surprisingly, this procedure, which has now been performed with quite a number of different particles, leads at least for relatively small *N* to regular clusters where all clusters of the same *N* have the same shape. [9-13] It was noted already by Manoharan *et al.* [8] that the structures of the packings of particles in the clusters seem to minimize the second moment of the mass distribution of each *N*-mer. After the clusters with unique shapes for each *N*-mer have formed they can be separated in pure form by centrifugation in a density gradient. The method of Manoharan *et al.* has been extended to binary systems, [14] the use of more monodisperse emulsion droplets made by shear by Zerrouki *et al.* [15], combined with the 'over-swelling' method used in emulsion and dispersion polymerization to arrive at anisotropic particles [16] and to clusters of particles with a smaller size (< 200 nm) from smaller emulsion droplets by the group of Wittemann. [11-13] The extension to smaller particle sizes such that the clusters are still in the colloidal domain, *i.e.* are still affected significantly by Brownian motion, [12] is important as it allows for a next SA step which can still be driven and controlled by minimization of the free energy. As already mentioned, the regular clusters are also interesting for model studies: Edmond *et al.* used clusters of micron-sized particles dispersed in concentrated dispersions of spherical particles to probe the rotational diffusion of these tracers as a function of volume fraction of the host particles. [17]

Despite the strong interest and the general character of this method, there have not been many theoretical investigations into the mechanism and into the reasons behind the fact that

the second moment of the mass distribution seems to be minimized. Lauga and Brenner [18] have shown that the resulting unique structure of each N-mer can be correctly predicted by minimization of the complex oil-water surface free energy of the interface during the drying process by considering individual droplets with different numbers of particles attached to the interface. They considered a range of contact angles between the particles and the liquids and found good agreement with the experimentally observed clusters. It has not yet been explained why this evaporation driven SA procedure leads to minimization of the second moment of the particle mass distribution for each N-mer. Unfortunately, the calculations to minimize the ever changing surface between the particles are quite involved and thus slow and not so easily adapted to more complex starting particles.

The present chapter has a double focus: By using dumbbell (db) shaped polymethylmethacrylate (PMMA) particles that are both sterically and charge stabilized and that can be made in high purity and yield relatively easily. [21] We extended the cluster generating method of Manoharan *et al.* [8] using the evaporation of emulsion droplets to particles with an anisotropic shape. We are specifically interested in finding out if regular and thus unique structures would still be formed for each N-mer, and if so, whether the second moment of its still minimized. For our experimental studies, we used our recently developed 'over-swelling' seeded-growth procedure to make both symmetric and asymmetric PMMA db's (also referred to as 'snow-man' particles). [19] However, it is important to point out that several well developed other methods are also available to synthesize db shaped particles, *e.g.* for silica, [20] or for particles with a snow-man morphology where the protrusions are composed of different materials, *e.g.* by starting the synthesis with core-shell particles, see for instance ref. 21. It is even possible to have snow-man shaped particles were an inner spherical core is free to move inside the outer shell. [22] Particles like these have the important property that, if arranged into clusters or strings, [23] they can form enantiomeric structures or structures with a certain handedness like helices. [24] The movable cores can ultimately be manipulated with external fields as has already been shown in recent studies for the separate db's. [22] Although it has been shown [19] that the PMMA particles we used can be made fluorescent and are thus interesting for real-space studies using confocal microscopy, we chose to focus in this work solely on characterizing the clusters obtained by scanning electron microscopy (SEM) as this technique has a significantly higher resolution, even although the polymer particles are easily damaged by an electron beam.

The second focus of this chapter is on exploring an as simple as possible simulation procedure which correctly predicts the structures formed. The parameter space for possible structures that can be made using the evaporation driven SA method, if it is performed not

starting with spheres but colloids with an already more complex shape, [1-4] is huge and it would be quite efficient if optimized conditions could be found for desirable structures by simulations. As mentioned already, a full calculation minimizing the surface area which drives the SA is not a simple and quick procedure, especially not for clusters of particles with more complex shapes. Independently, Schwartz *et al.* [25] were motivated also to try to capture the essential physics of the process in a simulation scheme without addressing the deforming liquid interface, but instead these researchers focused also on obtaining the distributions of the number of clusters formed. Here we made the simulation even simpler by focusing on what cluster structure results from single droplets with N particles attached to its surface. We mimicked the SA process by a two-step simulation in which single droplets with N particles that interact through hard interactions only are considered. In the first step the particles are confined to a spherical shrinking shell and after the long time self-diffusion of the particles has stopped and the pressure increases steeply, the second moment of the particle mass distribution is minimized in a second step. In order to test this methodology we also experimentally investigated clusters generated by single particles, as it is known from literature that small differences in the structures of the unique clusters can result from, probably, differences in the interaction potential between the particles under different conditions. [8-15]

This chapter is built up as follows: After discussing the experimental and simulation methods we used to make and predict the clusters, we present and discuss results first for clusters generated from colloidal spheres and compare these with published results, next for symmetric dumbbells where unique structures were also found similarly to the clusters of spheres, however, with some of these consisting of enantiomers, and lastly for the asymmetric db's, where uniqueness is quickly lost if the whole particles are considered, but the structures are still recognizable and unique if one focuses on the placement of the larger bulbs only. Finally, we draw conclusions on the use of the evaporation driven SA for db-shaped particles and on how well the structures can be predicted by a simple simulation scheme.

7.2 MATERIALS AND METHODS

7.2.1 Materials

Methyl methacrylate (MMA, Aldrich, chemical grade) was passed over an inhibitor removal column (Aldrich). After the inhibitor had been removed, MMA was stored in a refrigerator at 4 ℃ and not longer than one month. Azo-bis-isobutyronitrile (AIBN, Janssen Chimica) was re-crystallized from ethanol before use. Ethylene glycol dimethacrylate (EGDMA,

Sigma-Aldrich, chemical grade) was used as the cross-linking agent. Polyvinylpyrrolidone (PVP, Fluka, chemical grade) with an average molecular weight of 360,000 g/mol (K-90) was used as the stabilizer. Hydroquinone (Fluka, chemical grade) was used as the inhibitor. Sorbitan monooleate (Span 80, Aldrich, chemical grade), methanol (Biosolve, chemical grade), dodecane (Aldrich, ≥ 99%) and glycerol (Sigma-Aldrich, ≥ 99.5%) were used as supplied. Deionized water was used in all experiments and was obtained from a Millipore Direct-Q UV3 reverse osmosis filter apparatus.

7.2.2 Particles Preparation

The spherical PMMA (poly methyl methacrylate) particles were prepared by dispersion polymerization following an adaption that mentioned in ref. 26 and had a radius of 0.69 μm and polydispersity of 3%. In detail, the solvent mixture of methanol (30.6 g) and water (6.14 g) containing 4.1 wt% PVP stabilizer was prepared first. Then, two thirds of this mixture, all of the monomer (2.5 g of MMA) and initiator (0.025 g of AIBN) were blended homogeneously under a constant stirring at ~ 200 rpm in a 250 ml flask. Nitrogen was bubbled through this mixture for at least 30 min. Then, this flask was immersed in a silicon oil bath and maintained at 55 ^{o}C under stirring at 100 rpm. 1 wt% (based on monomer mass) of cross-linker was mixed with the remaining one third of solvent-stabilizer mixture, and slowly fed into the flask from the beginning of the reaction at a constant addition rate for 10 h. After the addition was complete, the reaction mixture was maintained at 55 ^{o}C for 24 h before cooling down to room temperature. The obtained particles were rinsed three times with methanol and then de-ionized water. Finally they were dispersed in de-ionized water.

The asymmetric and symmetric dumbbells were fabricated by an 'over-swelling' method as reported in ref. 19 Firstly, the cross-linked seed PMMA particles were prepared by dispersion polymerization in a methanol and water mixture, as described above, then the swelling of seed particles took place in aqueous solution which contained swelling monomer droplets (MMA) in the presence of the initiator AIBN and the steric stabilizer PVP (1 wt% based on total mass), the second aqueous solution contained seed particles (~ 0.7 wt%) stabilized by PVP (1 wt% based on total mass). After 18 h of gentle stirring, it allows the cross-linked seed particles to over-swell and to phase separate to form a protrusion. Re-polymerization was carried out at 70 ^{o}C under an N_2 atmosphere for 8 h before cooling. The radius ratio could be precisely controlled by varying the amount of monomer (MMA, for details see ref. 19). The final particle suspension was washed about 4 times with de-ionized water using a centrifuge to remove the second nucleation and impurities. The symmetric dumbbells with a radius of 0.71 μm (polydispersity of 2.2 %) and a contact angle of 54°±3°, and asymmetric dumbbells with R_s (radius of seeds in asymmetric dumbbells) of 0.71 μm (polydispersity of 2.3%), R_p (radius

of polymer protrusion) of 0.52 μm (polydispersity of 3.7%) and a contact angle of 48.5°±3° were used in our experiments. SEM images of the particles obtained are shown in Figure 7.1a-c.

Clusters of these three particles were produced from water-in-oil emulsions. 1 ml of an aqueous dispersion of particles (1 wt% based on water mass) was mixed with 20 ml of dodecane with a stabilizer (Span 80, 0.5 wt% based on the dodecane mass) and emulsified by shearing at 3500 rpm for 3 minutes. Clusters were formed by self-organization of the spherical or non-spherical particles during the slow evaporation of water at 90 °C for 3 h. The obtained clusters were carefully washed with hexane (sedimented at 1 g for 12 h and re-dispersed under a ~ 300 rpm stirring) and dried under N_2 fluid. Ultimately, the clusters were re-dispersed in water (20 ml) by gently shaking by hand.

7.2.3 Density Gradient Separation

A linear density gradient method was performed by using two solvents with different densities and viscosities, which are water and glycerol. A homemade two-column type gradient forming device was used to prepare a 30 wt% -70 wt% glycerol aqueous solution. 10 ml of the cluster suspension was loaded on top of 100 ml of linear density gradient and centrifuged (Hettich Rotina 46 S) at 2000 rpm for 12 minutes. Isolated cluster bands that consisted of clusters of equal numbers of particles were formed. These fractionated uniform clusters were picked out by a pipette and glycerol was rinsed out by repeated centrifugation (at 1 g). Samples were finally dispersed in water for further characterization.

7.2.4 Sample Observation

In order to better understand the state of dispersion of the particles at the water-oil interface, we observed the sample with an optical microscope (Leica) equipped with a 63× objective at room temperature. After the evaporation and SA procedure had finished and the clusters washed, the detailed configuration of the clusters collected on a glass slide was determined by performing scanning electron microscopy (SEM) with a FEI Phenom scanning electron microscope. Samples were dried onto a glass slide at room temperature and sputter-coated with a layer of gold (Au) of 5 nm. None of the images shown were post-processed.

7.2.5 Simulation Methods

We tried to mimic the behavior of the colloidal particles in an emulsion droplet during the evaporation of the solvent by a simplified two-step procedure. In the experimental setup, the particle-particle and particle-wall interactions are difficult to determine and will probably change during the evaporation process. We assumed that the particles were confined to a spherical cavity that shrinks during the evaporation of the droplets. As a first approximation,

we modeled the particles and the droplet interface by hard interactions. As a result, no deformations of the wall from its spherical shape occurred, which is justified in the first stage of the evaporation process, *i.e.*, before packing constraints become important.

We simulated both spherical and dumbbell particles. In both cases, our unit of length was taken to be R_s, the diameter of the largest sphere size. The dumbbells are modeled as two partially overlapping hard spheres with diameter ratio $q = R_p / R_s$, at a fixed distance d ($d = \sqrt{R_s^2 + R_p^2 - 2R_s R_p \cos\theta}$, for details see Fig. 7.1d) between the centers. For both systems, the center of mass of each sphere was confined to a spherical simulation box with hard walls. During the simulations, the pressure was slowly increased from $P^* = PR_s^3 / k_B T = 1$ to 20 to mimic the evaporation of the droplet. At $P^* = 20$, the particles no longer have enough freedom of movement to rearrange, but still vibrate. To fix the structure, the pressure was then rapidly increased to $P^* = 100$, effectively leading to a fully jammed state.

In our simulations, we considered two different regimes for the particle wettability. In the non-wetting regime (contact angle $\cos\theta = 1$), the particles could move freely within the spherical cavity under the constraint that the particles did not overlap with each other or the droplet interface. We chose to also investigate this limit for two reasons: first, to see how much it matters if the particles are confined to an interface or not, but also because this limit has been observed for instance for sterically stabilized PMMA particles in apolar solvents (see *e.g.* refs. 27-28) and it is also relevant when there are so many particles that they cannot occupy the surface area, a limit not covered experimentally in this paper (see *e.g.* ref. 29). For finite wettability ($-1 < \cos\theta < 1$), the particles are attached to the droplet interface by a strong adsorption free energy, for particles used in the present study at least thousands of $k_B T$, [30] which we modeled by confining the center of mass of the particles to a thin spherical shell with thickness $d_s = 0.1 R_p$ at the droplet surface, where R_p is the diameter of the smallest sphere in the system. We found that the final structure of the cluster is not affected by the shell thickness d_s, provided that $d_s << R_p$.

Manoharan *et al*. [8] suggested that after reaching this spherical packing stage, further evaporation of the droplet induces a reorganization of the particles due to the attractive Van der Waals interactions, which reduces the second moment of the mass distribution in the system. To model the second stage of the evaporation process, we used the jammed spherical clusters obtained from the spherical compression simulations, removed the spherical confinement, and used a standard Monte Carlo scheme to minimize M_2. In this simulation, the total energy of the system was taken to be proportional to M_2, with a dimensionless proportionality constant α that is increased slowly to anneal the cluster to a local potential

energy minimum:

$$\beta U(r_s^N) = \alpha \sum_{i=1}^{N} m_i |r_i - r_0|^2 / R^2 \tag{7.1}$$

with $\beta = 1/k_B T$, k_B Boltzmann's constant, T the temperature, R the sphere diameter, and N the number of spheres in the cluster. In the case of dumbbell particles, each sphere was counted separately in the summation. The (dimensionless) mass m_i is only important if multiple sphere sizes appear in the system, and was taken to be 1 for the largest sphere size in the system. The strength of the potential α was increased from 100 to 1000, at which point no further reorganization is observed. The system is then quenched at $\alpha = 10000$ to remove any further vibrations. For the results presented below, both the compression and annealing parts of the simulation consisted of $8 \cdot 10^6$ Monte Carlo cycles. We also performed simulations with lower compression and annealing rates, but found similar results for the final clusters.
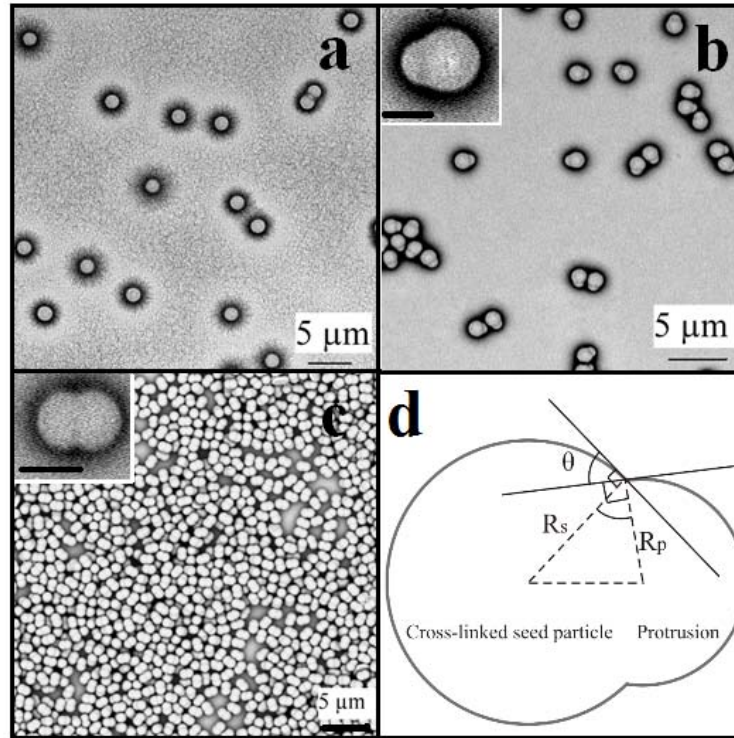
Figure 7.1. Scanning electron microscopy (SEM) images and schematic model image of the three different colloidal building blocks. (a) SEM micrograph of the spherical building blocks (radius of 0.69 μm and polydispersity of 3%). (b) SEM micrograph of the asymmetrical dumbbell particles ($R_s = 0.71$ μm 2.3% in polydispersity; $R_p = 0.52$ μm, 3.7% in polydispersity; and $\theta = 49°\pm3°$); the scale bar in the inset image is 1 μm. (c) SEM micrograph of symmetric dumbbell particles ($R_s = 0.71$ μm, 2.2% in polydispersity and $\theta = 54°\pm3°$); the scale bar in the inset image is 2 μm. (d) Schematic diagram of dumbbell particles; where R_s and R_p are the radius of the seed and protrusion part of the dumbbell, respectively, and θ is the contact angle of the dumbbell.

7.3 RESULTS AND DISCUSSION

7.3.1 Clusters of Single Spheres

As a test for our method, we first apply it to clusters of spherical particles, with cluster sizes $4 \leq N \leq 14$. We present the results of the packing before and after minimizing M_2 for both wettable and non-wettable particles, as well as the corresponding experimental images, in Table 7.1. As expected, the experimentally observed clusters $N \leq 12$ match with the simulated wettable particles after M_2 minimization. For larger clusters ($N > 12$), no clear match between simulations and experiments can be found. Nonetheless, it is clear that for sufficiently small clusters, our method provides a good indication of the types of structures that can be expected in clusters formed by evaporation of emulsion droplets with spherical particles. In literature some differences are reported between different particle systems that have been used to perform this self-assembly method. Although in nearly all cases the reported structures observed for different N are almost unique, there are some differences. This is another reason why we also performed cluster formation on single spheres for our particle and solvent combination. Actually, almost all configurations from literature are identical with our experimental results for spheres; differences only show up at clusters with $N = 11$ in Manoharan and Yi *et al.*'s paper, [8, 9] or sometimes, other isomeric clusters present at $N = 7$, 8, 11 for Cho's system [10] and $N = 5, 6, 8$ for Wagner's system. [13]

7.3.2 Clusters of Symmetric Dumbbells

In order to judge if we can expect the presence of chirality with a certain cluster structure, we apply the theory developed to describe the symmetry of molecules to these colloidal clusters. Chiral molecules necessarily belong to point groups C_1, C_n and D_n (or, rarely, to T, O, I), that is, groups that have only proper symmetry axes. All other point groups, that is, those that have alternating (improper) axes (S_n), including reflection planes and inversion centers, planes of symmetry (σ) or a center of symmetry (i) are associated with achiral molecules. [31]

Our symmetric dumbbells are characterized by the following average parameters: radius of 0.71 μm, polydispersity of 2.2 % (see Fig. 7.1c). As mentioned in the methods section the clusters of different N were purified by density gradient centrifugation, see Figure 7.2 for an example (and also see Supplementary Figure 7.2, SI-7.2). Close-ups of the clusters found for different N are shown in Figure 7.3 and compared with those found from computer simulations. According to the chirality considerations mentioned above, the clusters from the symmetric dumbbells lack chirality when $N = 2$ (because they have a symmetry plane σ), 4 (because they have a symmetry plane σ), 6 (because of a S_3 alternative axis, or a center of
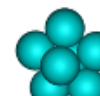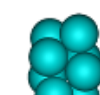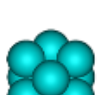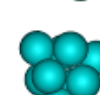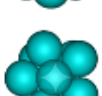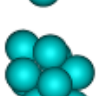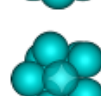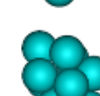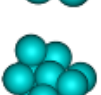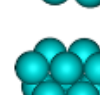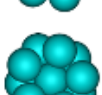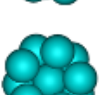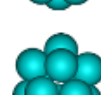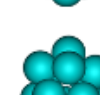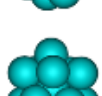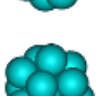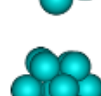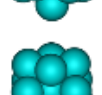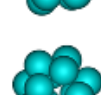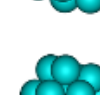
| N | Non-wettable | | Wettable | | Obser- |
	before	after	before	after	ved
4	a	a	a	a	a
5	a	b	a	b	b
6	a	a	a	a	a
7	a	b	a	b	b
8	a	b	a	b	b
9	a	b	a	b	b
10	a	b	a	b	b
11	a	b	c	d	d
12	a	a	b	b	b
13	a	b	c	d	e
14	a	b	c	d	e

Table 7.1. Structures found from simulations of spherical particles in evaporation droplets, and experimental results. The first column shows the number of particles N. The next two columns show the results if the particles are not confined to the droplet interface, both before and after minimizing M_2. The fourth and fifth column show the configurations resulting from fixing the particles to the droplet interface. The last column shows the experimental results. The letters denote structures that are the same for the same cluster size. The scale bar is 2 μm.

symmetry i for the one shown as inset in Fig. 7.3) and 7 (because of a symmetry plane σ) (see Fig. 7.3). On the other hand, the trimer and pentamer are chiral colloidal clusters, in which a C_3-axis and no symmetry elements are present, respectively. We find good agreement between the experimentally observed clusters and the structures predicted using the simulation method where the particles are adsorbed to the interface, which applies best to our experiments. Ofcourse, at the moment it is not yet possible to separate the stereoisomers from each other, but mostly this is similar to molecular chiral mixtures as well and provides an interesting avenue for research. Especially if these kinds of chiral clusters could be made from *e.g.* optically active materials their handedness is also of interest for photonic applications.
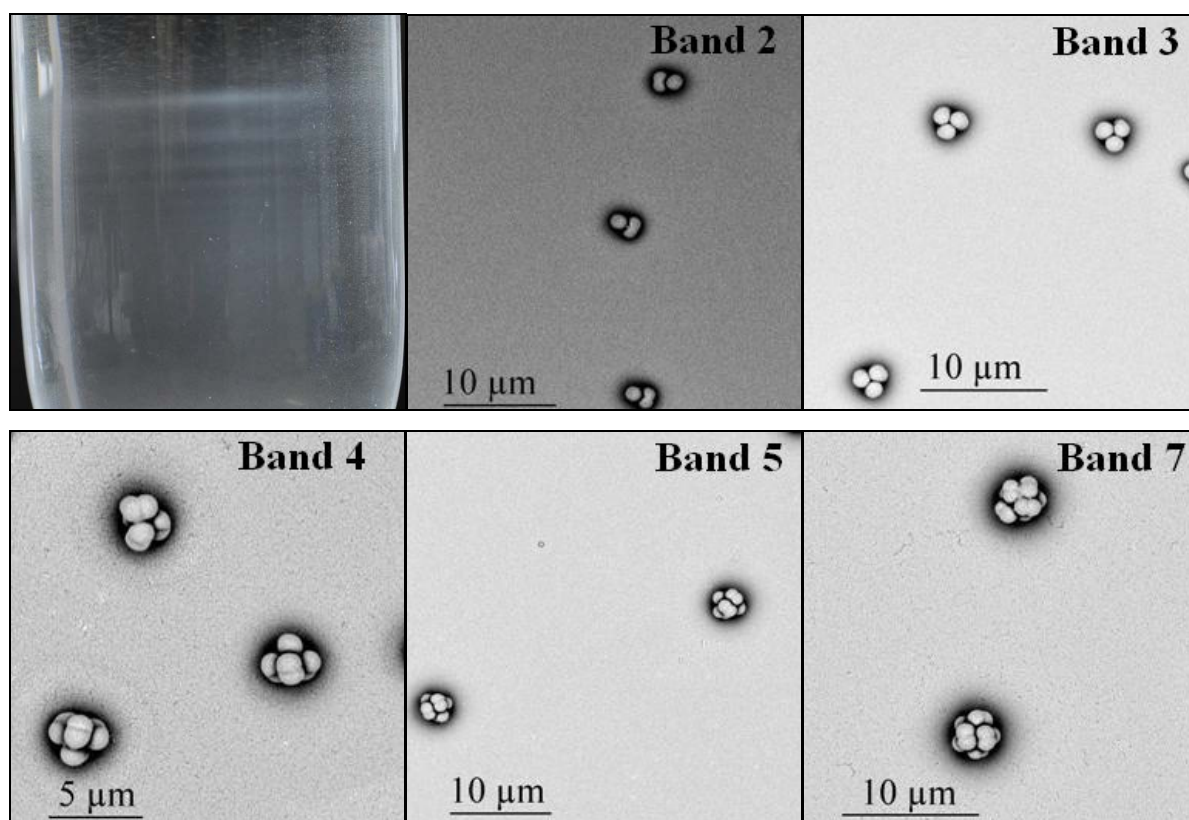

Figure 7.2. The density gradient separation of the clusters applied to clusters of symmetric dumbbells. The top left image is the tube containing the distinct bands of cluster with a given *N*. The others are SEM images of different bands.

Unfortunately, the mostly unique structures that can be made from the symmetric db's do not have nice names like their counterparts that are made from spheres. It is interesting, though, to see in how far the structures resemble those made of spheres if the db's had been made from two touching spheres. In other words, which clusters of *N* dumbbells correspond to clusters of 2*N* spheres? For small clusters (*N* < 5), the clusters formed by the symmetric dumbbells indeed are the same as those formed by 2*N* spheres. While the configurations partly coincide at *N* = 5, for larger sizes, the relevant clusters from spheres are totally
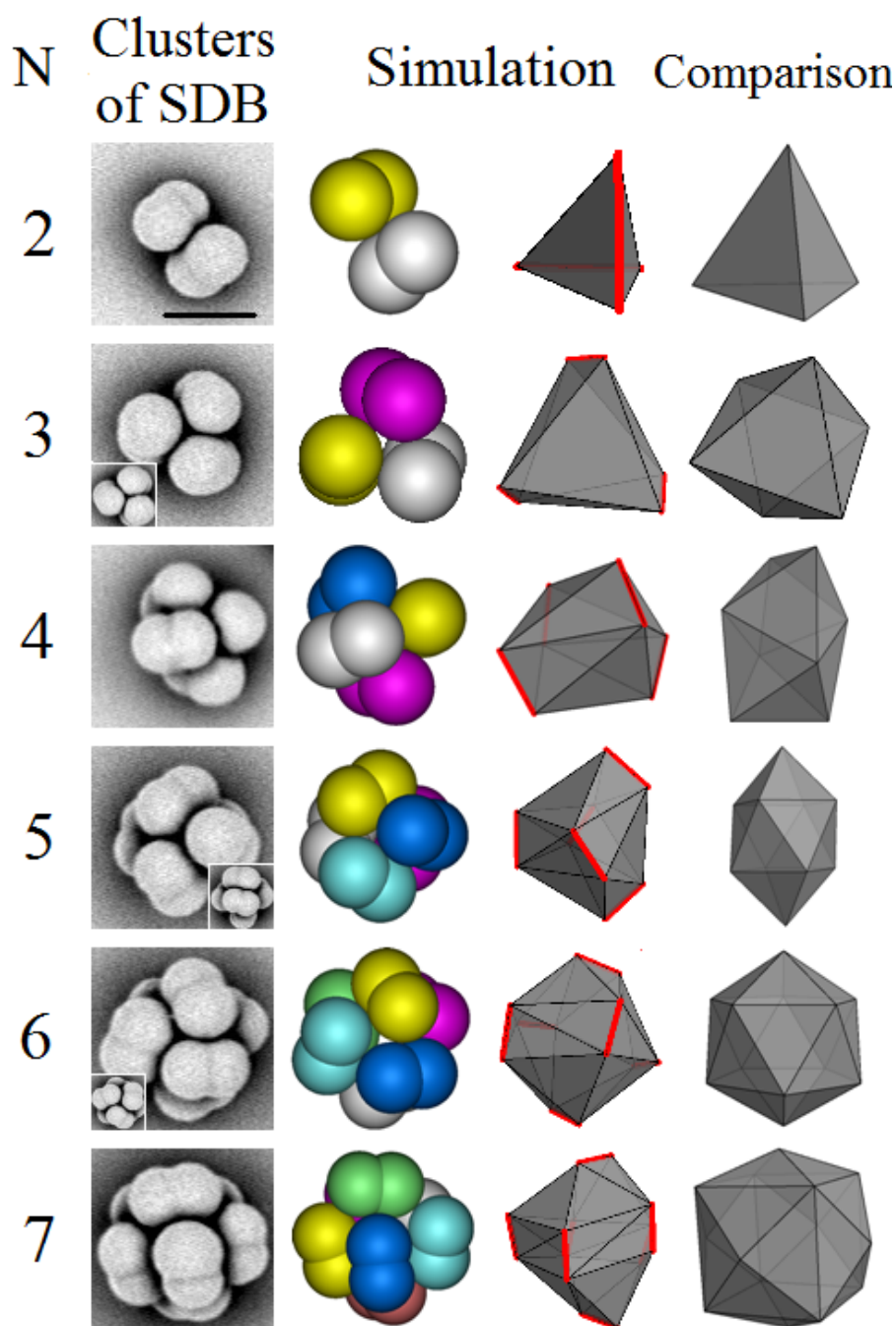
Figure 7.3. Cluster configurations for the spherical db particles (0.71 μm in radius and 2.2% in polydispersity). The first column denotes the cluster size N; the second column of images shows experimental SEM micrographs of clusters of size N; the insets show enantiomeric clusters ($N = 3$ and 5) or isomeric clusters ($N = 6$); the third and fourth columns show the corresponding simulations packing results and their schematic packing models (the red lines stand for dumbbells and each dumbbell connected with its neighbors by drawing black lines), respectively; The fifth column shows the corresponding SEM micrographs of clusters of spheres with $2n$ when the dumbbells are regarded as two independent spheres; The second two columns show the corresponding clusters from the computer simulations. The scale bars are 2 μm.

dissimilar. This is caused by the unpliancy of the dumbbell, which prevents a closer packing of dumbbells as is possible for spheres. It should of course be mentioned that although the structures below $N = 5$ would besimilar in those of spheres and db's, if the compositions of the db halves were different, the number of different stoichiometries that would result from clusters of mixtures of two particles would be far greater than if the *n*-mers were built up of asymmetrically composed db's.

7.3.3 Clusters of Asymmetric Dumbbells

Monodisperse asymmetric dumbbells with average parameters: R_s of 0.71 μm with a polydispersity of 2.3%, R_p of 0.52 μm with a polydispersity of 3.7%, and contact angle of 49° $\pm3^o$ were used as packing units. Here, details on size parameter(s) of the asymmetric db's refer also to schematic image (Fig. 7.1d). All distinct structures of the clusters observed for the lower number of particles ($N = 2, 3, 4$) are summarized in Figure 7.4. We observed two configurations for both $N = 2, 3$. According to theory of the symmetry of molecules referred to before, [31] for the dimeric clusters the absence of any symmetry elements directly predicts a pair of enantiomeric colloidal clusters, and the enantiomers should occur with equal probability. (see Fig. 7.4a) For the trimeric clusters, two isomers are present, because these have a plane of symmetry. Hence, they are achiral. However, these two configurations do not have the same yield: the one in which the protrusions have a heterogeneous orientation is the favorable configuration (the yield is 76% based on around 100 counts), compared to the other, with homogeneously oriented protrusions (the yield is 24%) (see Fig. 7.4b). A ratio of 1:3 is expected if the up-down orientation of the dumbbells would be random.

For increasing N, the number of configurations of clusters increased dramatically, in both the experiments and simulations. For $N = 4$, we observed eight configurations (see Fig. 7.4c). The top left configuration in Fig. 7.4c, which is also predicted by the simulations, is a diastereomeric cluster (having a S_4 alternative axis). The bottom left cluster is achiral (with an *i* symmetry center). Three pairs of chiral colloidal tetramers are displayed in Fig. 7.4c that are mirror images of each other. Surprisingly, if the protrusions were removed from the tetramer cluster, all the configurations of the asymmetric dumbbells are superposable on a common cluster that is structurally identical to the tetramer formed of spheres. One can conclude that the asymmetric dumbbell packing leads to bigger-bulb-dependent clusters, while the smaller bulb simply attaches to the bigger bulb with a relatively free orientation. Since the particles were confined to lie horizontally in the interface of a spherical droplet, and they always stay at the interface that way this restriction causes the loss of one rotational degree of freedom. Indeed, we never observed the small bulb hiding in the center of the clusters.
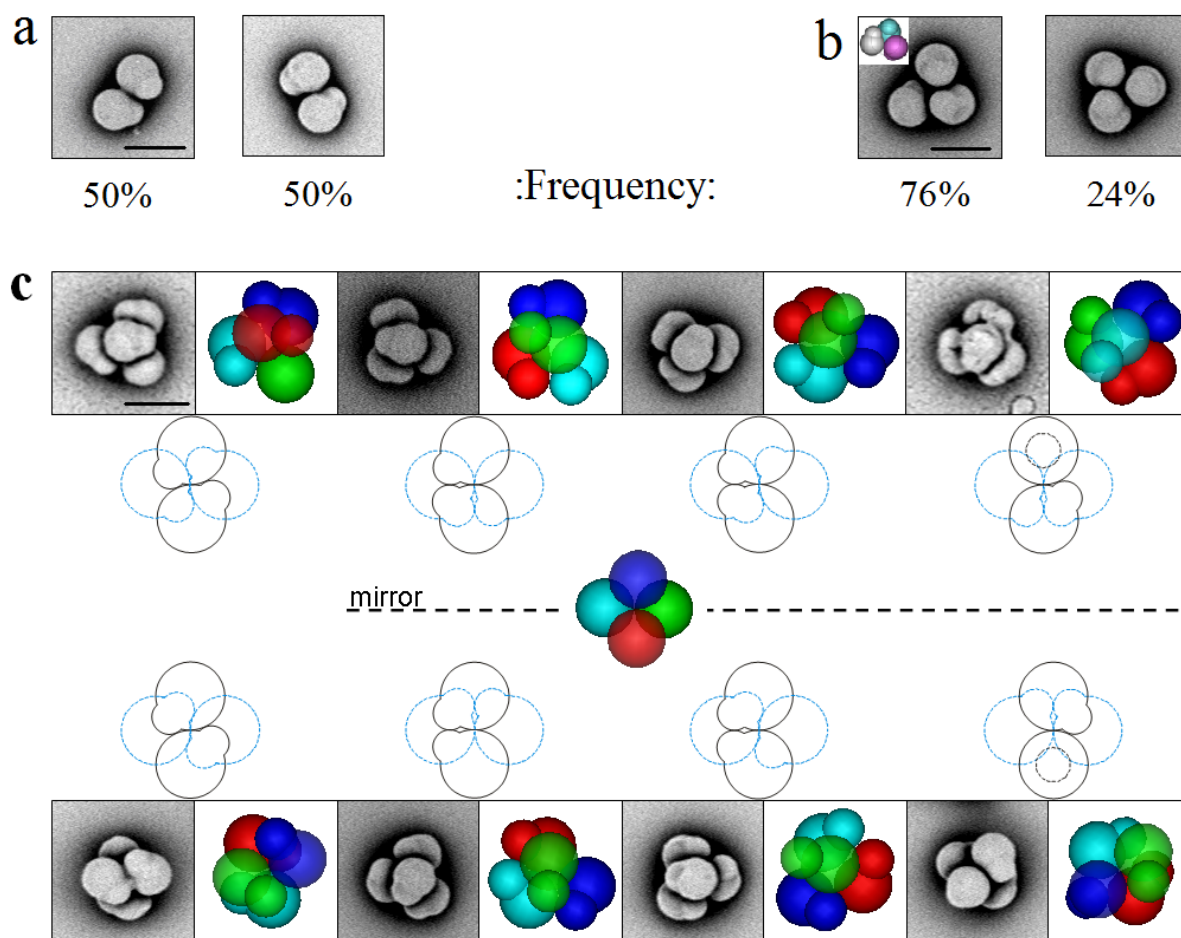
Figure 7.4. Simple cluster structures with $N = 2, 3, 4$ made of the asymmetric dumbbells (size ratio of 0.73, overlap see Fig. 7.1b and d). Some shrinkage and deformation of the particles occurred during drying and exposure to the electron beam, but the structures are still recognizable. (a) The experimental frequencies of the clusters for $N = 2$ are given next to the SEM micrographs of the pair of chiral clusters. (b) The experimental frequencies of clusters at $N = 3$ are given next to SEM micrographs of the two structures of clusters found. The inset is the result of a computer simulation, which matches the observed cluster configuration. (c) The first and last rows show SEM micrographs and translucent schematic images of the clusters observed in simulations for $N = 4$, while the second and third rows are 2D perspective views of each corresponding cluster. Note that the large spheres are always in the same configuration. All scale bars are 2 μm.

The landscape underwent a quantitative change for $N > 4$, where there were too many configurations to catalog experimentally. We therefore show some typical examples of the experimental observations and simulation results in Figure 7.5. We again observed that the large spheres are arranged in the same configurations as those seen in clusters of spherical particles, while the directions of the small protrusions are more or less random. These variations break the symmetry of the main frame of the clusters, which could for instance be exploited by changing the composition of the smaller bulbs. In this case, the index contrast of.
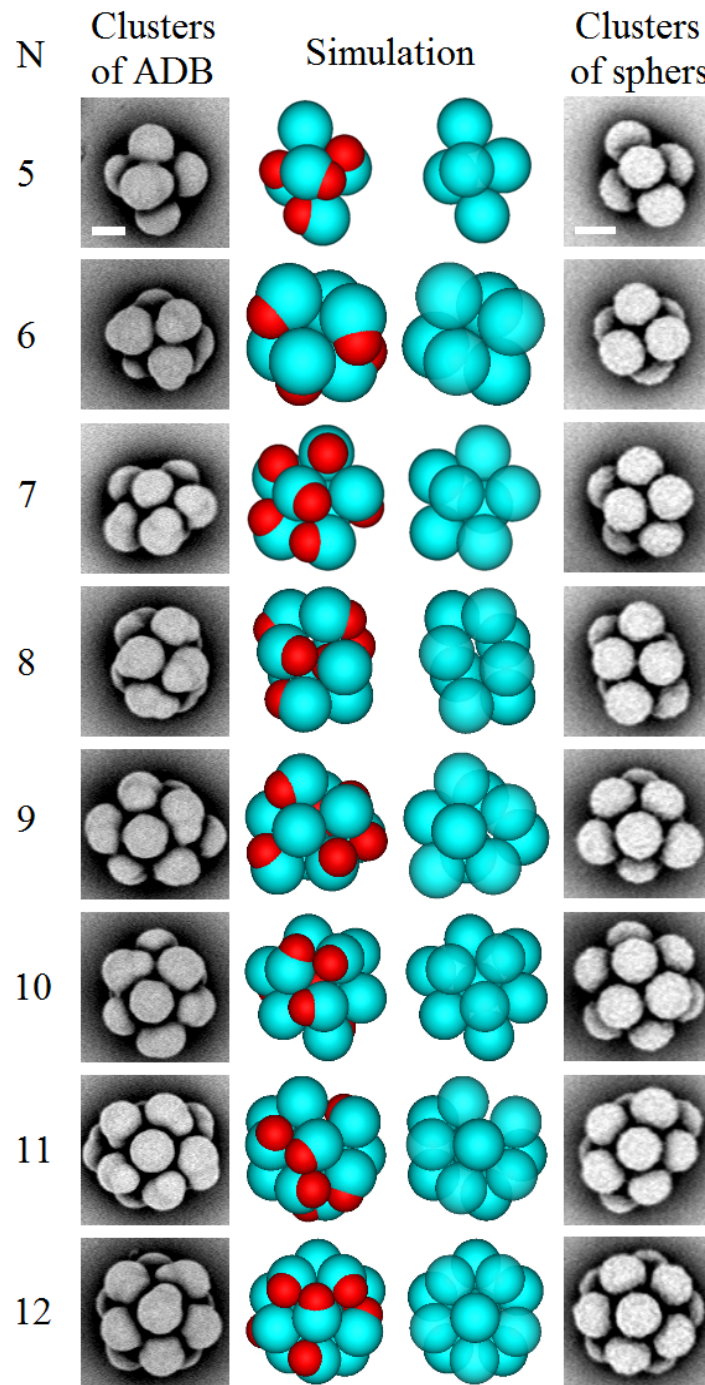
Figure 7.6. Cluster configurations for asymmetric dumbbells of $N > 4$. The first columns indicates clusters of size N, while the second and fifth columns show the cluster configurations of the asymmetric dumbbells (size ratio of 0.73) and spheres, respectively, as determined by SEM. All the clusters of spheres for a specific cluster size N have identical configurations, while the configurations shown for clusters of the asymmetric dumbbells are typical configurations taken from the many corresponding examples found both in the experiments and simulations (third column). The fourth column lays out the configurations of clusters in which the small protrusions were removed from the simulation results, and which resemble the cluster configurations in the last column. All scale bars are 1 μm.

the smaller part of the db could be used to add more or less randomness to the scattering signal if the clusters would be placed on a photonic lattice. Also the inter cluster interactions could be randomized depending on the properties of the composition of the smaller bulb.

When applying the same simulation method to this system of asymmetric building blocks, the configurations found directly after the compression step, *i.e.* before the M_2 minimization step, did not agree with the experimental snapshots for either wettable or non-wettable particles. Clear differences in the positions of the large spheres could be seen, and the small spheres generally still had a limited freedom of movement before M_2 minimization, rather than being mechanically arrested due to contact with other spheres as seen in the experimental snapshots. When minimizing the second moment of the mass distribution, the resulting configuration is influenced by the mass ratio m_p/m_s of the seed (big) and protrusion (small) spheres. Of course, as the minimization of M_2 is only an empirical model for the final stages of droplet evaporation, for which no strong theoretical basis has been given, the "mass" in this context is not physically linked to the real mass of the sphere. Simply letting the mass of each sphere scale with its volume, such that $m_p / m_s = R_p^3 / R_s^3$, generally led to configurations where the smaller spheres preferentially resided in the center of the cluster, which deviates from the experimental observations. Reducing the effect of the positions of the small spheres on M_2 yielded much better agreement with the experimental observations. The resulting clusters were independent of the exact mass ratio, as long as $0 < m_p / m_s << R_p^3 / R_s^3$: all that appeared to be required is a strong preference for the large spheres to be near the center of the cluster, and a weak contribution of the small spheres to prevent any freedom of movement in the final configuration. For all clusters sizes, the structure of the large spheres in the final configuration agrees with those seen in experiments, with the positions of the small particles varying between different simulation runs and experimental snapshots.

As was already mentioned, from Figure 7.4 it is quite clear that if one neglects the smaller bulbs in the structure, the cluster structures found experimentally for $N < 13$ are equal to those of the clusters of the single spheres and indicate that the principle of minimizing the second moment of the mass distribution is not a general rule in this kind of SA processes as it leads to incorrect structures if this minimization was followed for these particles.

7.4 CONCLUSIONS

In this paper we investigated the self-assembly of anisotropic dumbbell-shaped particles confined onto the interface of water emulsion droplets dispersed in an oil phase while the

water is evaporated. The symmetric db's did not consist of two spheres attached, but had a shape consisting of two equal overlapping spheres (radius of 0.71 μm with a polydispersity of 2.2% and a contact angle of $54^o \pm 3^o$).   The asymmetric dumbbells had a radius ratio of 0.73 with a contact angle of $49^o \pm 3^o$. We also investigated whether a simple simulation scheme could predict the structures formed. We used a two-step simulation in which single droplets with N particles were considered only and in which the interactions between the particles were assumed to be hard interactions only. In the first step the particles were confined to a shrinking spherical shell and after the pressure increased steeply the second moment of the particle mass distribution was minimized in a second step. The simulation procedure predicted structures of N-mers formed for both spheres, which were similar to literature results, and the symmetric db particles well for $N < 8$. However, for the asymmetric db's results were predicted well only if the minimization of the mass distribution was performed giving less weight to the smaller bulb. For the asymmetric db's it was found that the structures formed were identical those of spheres if the position of the smaller bulbs was ignored. If the whole particle was taken into account, the uniqueness of the structures formed was already lost after $N > 2$, while for $N = 2$ two chiral enantiomers were found. Probably because of the confinement to the liquid interface, the smaller bulbs were never found to point inwards. As the structures are still unique with respect to the larger bulb, the use of anisotropic db's could be interesting for studies for which the small bulbs can generate a kind of randomness on the properties. Our results also indicate that minimization of second moment of the mass distribution is not a general rule for this kind of SA.

For the symmetric db's unique structures were found (at least for $N < 8$) both in the experiments and the simulations. Several of the structures were completely unique, while for others only two isomers were found; for $N = 6$ without chirality and for $N = 3$ and $N = 5$ with chirality. The chiral structures are interesting as they are not present in clusters from single spheres. Chiral structures also are interesting for photonic applications as they interact differently with light. Also, the unique structures found for the db's indicate that for db's with bulbs composed of different materials or with a movable core, this procedure of SA is an interesting additional step to include complexity.

Witteman and coworkers have shown [11-13] that the evaporation driven SA onto the interface of droplets still works with particles with a size of about 150 nm. However, as all particles with a size above ~ 10 nm are still expected to adhere strongly, with respect to the thermal energy, to an oil-water interface, there still is quite some room for performing this SA scheme with significantly smaller nano-particles. If for instance quantum dots or metal nanoparticles are used there is even room to repeat the whole procedure several times, using

different building blocks, while still ending up with clusters in the colloidal domain. This would make it possible to use the resulting complex particles in colloidal crystallization or to have them undergo any other SA procedure.

7.5 ACKNOWLEDGMENTS

We would like to thank Frank Smallenburg for performing all of the simulation work discussed in this chapter.
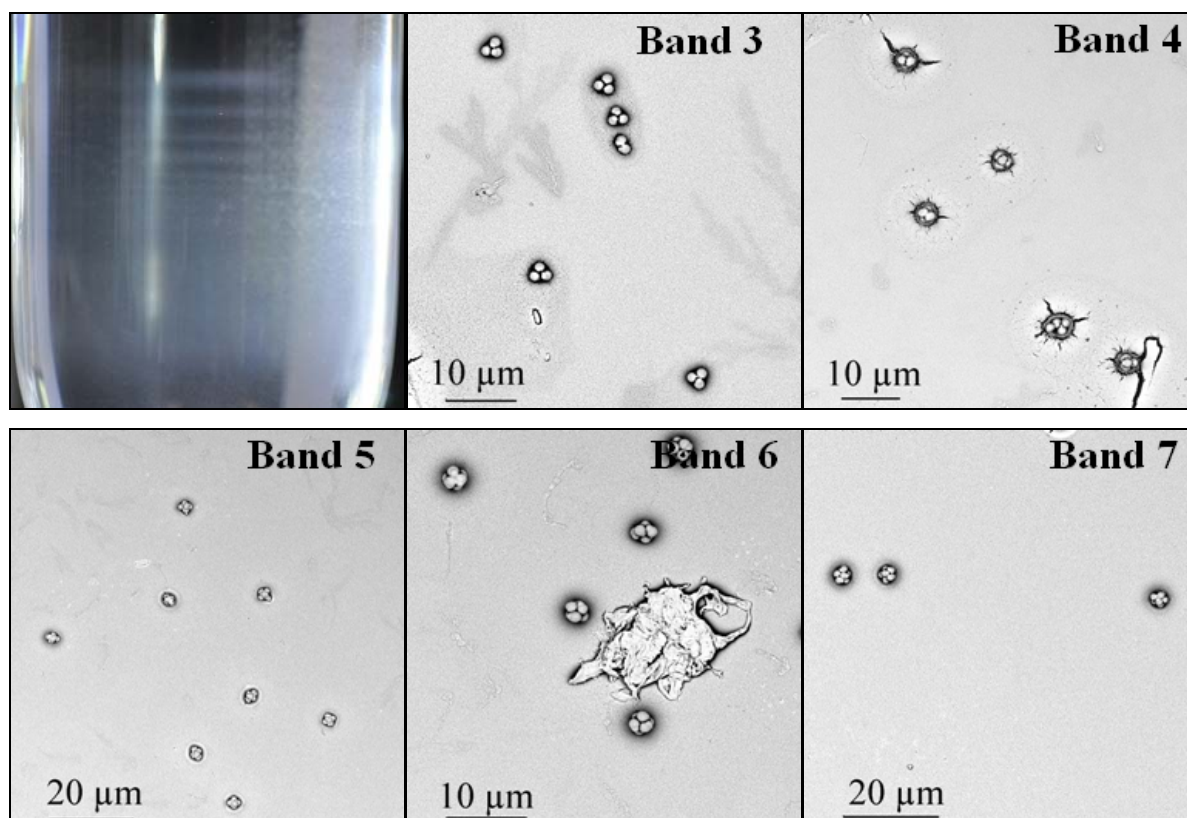
7.6 SUPPLEMENTARY INFORMATION

7.6.1 Particles at Interface
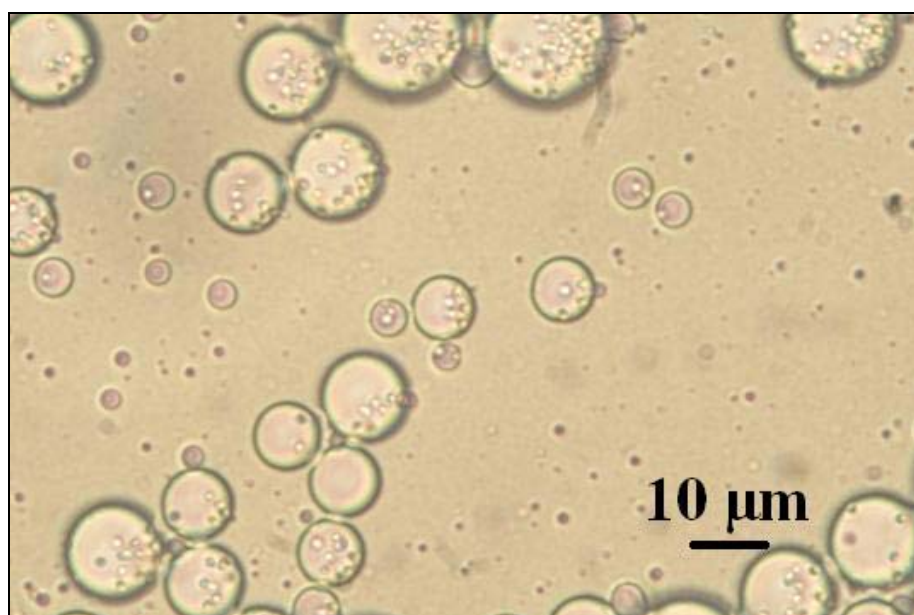
Supplementary Figure 7.1. Optical microscopy image of the asymmetric dumbbells particles which were all found adsorbed, as expected, at the water/oil interface (before heating), not dispersed in the oil.

7.6.2 Density Gradient Separation

Clusters from Asymmetric Dumbbells

Supplementary Figure 7.2. The density gradient separation of the clusters of asymmetric dumbbells. The top left image is the tube containing the distinct bands of cluster with a given *N*. The rest are SEM images of different bands.

7.7 REFERENCES

[1] van Blaaderen, A. *Science* **2003**, *301*, 470-471.

[2] Glotzer, S. C.; Solomon, M. J. *Nat. Mater.* **2007**, *6*, 557-562.

[3] Li, F.; Josephson, D. P.; Stein, A. *Angew. Chem. Int. Ed.* **2011**, *50*, 360-388.

[4] Duguet, E.; Desert, A.; Perro, A.; Ravaine, S. *Chem. Soc. Rev.* **2011**, *40*, 941-960.

[5] McGorty, R.; Fung, J.; Kaz, D.; Manoharan, V. N. *Mater. Today* **2010**, *13*, 34-42.

[6] Velev, O. D.; Furusawa, K.; Nagayama, K. *Langmuir* **1996**, *12*, 2374-2384.

[7] Dinsmore, A. D.; Hsu, M. F.; Nikolaides, M. G.; Marquez, M.; Bausch, A. R.; Weitz, D. A. *Science* **2002**, *298*, 1006-1009.

[8] Manoharan, V. N.; Elsesser, M. T.; Pine, D. J. *Science* **2003**, *301*, 483-487.

[9] Yi, G. -R.; Manoharan, V. N.; Klein, S.; Brzezinska, K. R.; Pine, D. J.; Langes, F. F.; Yang, S. -M. *Adv. Mater.* **2002**, *14*, 1137-1140.

[10] Cho, Y. -S.; Yi, G. -R.; Kim, S. -H.; Pine, D. J.; Yang, S. -M. Chem. Mater. 2005, 17, 5006-5013.

[11] Wagner, C. S.; Lu, Y.; Wittemann, A. *Langmuir* **2008**, *24*, 12126-12128.

[12] Hoffmann, M.; Wagner, C. S.; Harnau, L.; Wittemann A. *ACS Nano* **2009**, *3*, 3326-3334.

[13] Wagner, S. C.; Fischer, B.; May, M.; Wittemann, A. *Colloid Polym. Sci.* **2010**, *288*, 487-498.

[14] Cho, Y. -S.; Yi, G. -R.; Lim, J. -M.; Kim, S. -H.; Manoharan, V. N.; Pine, D. J.; Yang, S. -M. *J. Am. Chem. Soc.* **2005**, *127*, 15968-15975.

[15] Zerrouki, D.; Rotenberg, B.; Abramson, S.; Baudry, J.; Goubault, C.; Leal-Calderon, F.; Pine, D. J.; Bibette, J. *Langmuir* **2006**, *22*, 57-62.

[16] Kraft, D.; Vlug, W.; van Kats, C.; van Blaaderen, A.; Imhof, A.; Kegel, W. *J. Am. Chem. Soc.* **2009**, *131*, 1182-1186.

[17] Edmond, K. V.; Park, H. J.; Elsesser, M. T.; Hunter, G. L.; Pine, D. J.; Weeks, E. R. *Chaos* **2011**, *21*, 041103.

[18] Lauga, E.; Brenner, M. *Phys. Rev. Lett.* **2004**, *93*, 238301.

[19] Peng, B.; Vutukuri, H. R.; van Blaaderen, A.; Imhof, A. *J. Mater. Chem.* **2012**, *22*, 21893-21900.

[20] Johnson, P.; van Kats, C.; van Blaaderen, A. *Langmuir* **2005**, *21*,11510-11517.

[21] Nagao, D.; van Kats, C. M.; Hayasaka, K.; Sugimoto, M.; Konno, A.; Imhof, A.; van Blaaderen, A. *Langmuir* **2010**, *26*, 5208-5212.

[22] Okada, A.; Nagao, D.; Ishii, H.; Konno, M. *Soft Matter* **2012**, *8*, 3442-3445.

[23] Nagao, D.; Sugimoto, M.; Okada, A.; Ishii, H.; Konno, M.; Imhof, A.; van Blaaderen, A. *Langmuir* **2012**, *28*, 6546-6550.

[24] Zerrouki, D.; Baudry, D. J.; Pine, D. J.; Chaikin, P.; Bibette, J. *Nature* **2008**, *455*, 380-382.

[25] Schwarz, I.; Fortini, A.; Wagner, S. C.; Wittemann, A.; Schmidit, M. *J. Chem. Phys.* **2011**, *135*, 244501.

[26] Peng, B.; van der Wee, E.; Imhof, A.; van Blaaderen, A. *Langmuir* **2012**, *28*, 6776-6785.

[27] Leunissen, M. E.; van Blaaderen, A.; Hollingsworth, A. D.; Sullivan, M. T.; Chaikin, P. M. *Proc. Natl. Acad. Sci. USA* **2007**, *104*, 2585-2590.

[28] Leunissen, M. E.; Zwanikken, J.; van Roij, R.; Chaikin, P. M.; van Blaaderen, A. *Phys. Chem. Chem. Phys.* **2007**, *9*, 6405-6414.

[29] Velev, O. D.; Lenhoff, A. M.; Kaler, E. W. *Science* **2000**, *287*, 2240-2243.

[30] Pieranski, P. *Phys. Rev. Lett.* **1980**, *45*, 569-572.

[31] Eliel, E. L. W.; Wilen, S. H.; Mander, L. N. *Stereochemistry of Organic Compounds* **1994**, New York: John Wiley & Sons, Inc.

8

Plastic Crystals of Long-Ranged Repulsive Dumbbell-Shaped Colloids

ABSTRACT

A novel experimental long-ranged soft PMMA (poly methyl methacrylate) dumbbell dispersion in an apolar solvent was studied. Deep insight into the structure is possible due to the refractive index matching between the particles and solvent. The projected displacements of the position and orientation of the dumbbells were recorded and quantitatively analyzed in 2D. High crystalline order was not only exhibited by the average position of the particles, but also by their position in individual images. The orientations were completely disordered, which is associated with the full angle (360°) rotation of the dumbbells in 3D. This structure is a so-called plastic crystal. A random *hcp* (hexagonal close packed) structure was found in this plastic crystal of dumbbells by studying the 3D structure. Additionally, a high-frequency AC electric field was used to influence the orientation of the plastic crystals, and some control was achieved, which provides a possibility to develop a switchable photonic crystal under an external field.

8.1 INTRODUCTION

Recently, the prospect of using anisotropic particles as building blocks for colloid science has governed an increasing amount of attention, because their anisotropy in chemical and/or physical aspects has a high potential both for applications and fundamental research, which goes beyond that of spheres, [1-6] especially with respect to the phase behavior of anisotropic particles, which is richer than that of spherical particles. [7-12] Fluorescently labeled poly (methyl methacrylate) (PMMA) and silica are two frequently used materials for phase behavior study in real space, because they can be easily refractive index matched with solvents and, consequently, the problems arising from scattering are eliminated and van der Waals interaction can be ignored. [13-19] Most of the particles were sterically stabilized and, combined with the refractive index-matching with solvents, this made them an ideal hard-sphere model system. Moreover, the utilization of an external field, for example electric field, enormously enhances the amount of control over the structure, the rheological and the optical properties of the colloid system. [11, 12, 20-23]

Based on recent progress in the synthesis of non-spherical particles, like dumbbells, [11, 20, 24] rods [12, 21] and polyhedron-shaped particles, [25] exploring their phase behavior in experiment is highly desired. [11, 12, 20-22 25-27] Kuijk *et al.* [12, 21, 26] have successfully synthesized rod-shaped silica particles with a tunable aspect ratio. Elaborate phase behavior results of such rods under the influence of gravity and/or an electric field were also investigated. For short rods or long rods in the low volume fraction domain, an isotropic phase was usually obtained, but an electric field could assist the formation of crystals of such rod systems. Demirörs *et al.* [11, 27] reported the phase behavior of soft silica dumbbells by tailoring the interactions, and also by using an electric field. A detailed phase diagram was presented through tuning the strength of electric field and the aspect ratio of the dumbbells. Unfortunately, not a plastic crystal but a plastic glass was obtained in the presence of gravity and a plastic crystal (exhibiting positional order but orientational disorder) was not found. [11] This is probably related to either the charge density of the particles or the big contrast in density between the particles and solvents. [28] Indeed, gravity cannot readily be neglected due to the density mismatching between the silica particles and the solvents. PMMA, however, is much easier to density match than silica, especially for many model studies that use large (micrometer-sized) particles. [29-31] Studies on the phase behavior of anisotropic PMMA particles are highly desired.

On the basis of the recent development of the seeded emulsion polymerization method, [32-36] PMMA non-spherical particles have been successfully fabricated in polar solvents.

The morphology of such particles could be readily tuned through adjustment of various experimental parameters, like swelling ratio, the cross-linked structure of the seeds, the concentration of stabilizer, *etc*. [20] With the aid of a non-ionic surfactant (Span 85), [37] the transfer of these anisotropic PMMA particles from the polar environment to an apolar solvent was realized. In apolar solvents, the particles exhibited a long range repulsion and, interestingly, their positions were ordered, while they lacked orientational order, [20] thus forming a so-called plastic crystal. Plastic crystals are regarded to have high potential in photonic applications, because an external field can be used to switch the structure dramatically, as recent works have demonstrated. [27, 38, 39] Additionally, a plastic crystal of hard dumbbells was predicted and studied computationally by Vega *et al.* [40] and Marechal *et al.* [41] Phase behavior of long-ranged soft plastic crystals still have not been reported or predicted in detail yet, and work on this is highly desired and would be interesting.

Here, we present a plastic crystal of long-ranged soft PMMA dumbbells dispersed in a refractive index-matching, yet close density-matching solvent decalin. The thick double layer allows dumbbell particles to repel each other and giving rise to a plastic crystal structure which shows positional order but orientational disorder. A computer algorithm for rod systems is introduced to track the position and orientation trajectories of the dumbbells. The results demonstrate that the dumbbells have a long-ranged positional ordering but incomplete orientational ordering. Preliminary 3D analysis indicates the dumbbell system has a random *hcp* (hexagonal close packed) structure. Furthermore, high-frequency electric AC fields (1 MHz) trapped the translation and rotation of the dumbbell particles, providing a possible way towards smart materials with novel photonic applications.

8.2 MATERIALS AND METHODS

8.2.1 Materials

Methyl methacrylate (MMA, Aldrich, chemical grade) was passed over an inhibitor removal column (Aldrich). After the inhibitor was removed, MMA was stored in a refrigerator at around +5 $^{\circ}$C for no longer than one month. Azo-bis-isobutyronitrile (AIBN, Aldrich, chemical grade) was re-crystallized in ethanol before use. Ethylene glycol dimethacrylate (EGDMA, Sigma-Aldrich, chemical grade) was used as the cross-linker during the synthesis of the PMMA spheres. Polyvinylpyrrolidone (PVP, Fluka) with an average molecular weight of 360,000 g/mol (K-90) was used as the polar stabilizer in the synthesis of the anisotropic particles. Hydroquinone (Fluka) was used as an inhibitor. The fluorescent monomer rhodamine b isothiocyanate (RITC) was stored in the refrigerator at around – 20 $^{\circ}$C and used

as supplied. Sorbitan trioleate (Span 85, Sigma, chemical grade), methanol (Biosolve, chemical grade), decahydronaphthalene (mixture of *cis* + *trans*, decalin, Fluka, 98%) and hexane (Biosolve, chemical grade) were used as supplied. High purity water (resistivity 18 MΩ·cm^{-1}) was obtained from a Millipore Direct-Q UV3 reverse osmosis filter apparatus.

8.2.2 Procedure for Non-Spherical Particles Synthesis

An adaption of the preparation strategy based on the approach in ref. 42 and our modification there of as described in chapter 2 [31] was carried out. In brief, monodisperse homogeneously cross-linked PMMA particles in the micron size range were fabricated through a successive addition of cross-linker (at the beginning of the reaction) in order to not significantly disturb the sensitive nucleation stage during the polymerization, which was described in detail in ref. 31. For convenient observation of the particles with confocal microscopy, relatively large PMMA spheres (~ 1.6 μm in diameter) were prepared by simply decreasing the concentration of the stabilizer (PVP) used in chapter 2. In addition, the total addition time was extended to 10 h to produce fully cross-linked spherical seed particles (also see chapter 4). The detailed recipe is listed in Table 1. The obtained PMMA spheres were uniform in size (diameter = 1.61 μm, polydispersity = 3%, determined by TEM measurement).

Table 1. Recipe for Homogeneously Cross-Linked PMMA Spheres[a]

	PVP (g)	Methanol (g)	De-ionized Water (g)	MM (g)[b]	EGDMA (wt%)[c]
Reaction Flask	1.00	16.4	4.10	2.5	
Syringe[d]	0.50	8.2	2.05		1

[a] polymerization was carried out at 55 °C for 24 h.

[b] MM contained 1wt% of AIBN.

[c] based on MM mass.

[d] addition start and total addition times were 0 and 10 h, respectively.

Before carrying out further experiments, these particles were rinsed twice with methanol, and three times with 1 wt% PVP aqueous solution by means of sonication and centrifuge (315 g for 15 min). Finally, the particles were stored in 1 wt% PVP aqueous solution with a mass fraction of 0.7 %, in a refrigerator at + 4 °C no longer than a week. This particle suspension needed to be dispersed homogeneously with sonication before use.

The preparation of dumbbell-shaped PMMA particles was based on our previous method. [20] In brief, 22 g of monomer oil-in-water emulsion (stabilized by 1 wt% PVP) consisting of 2 g of swelling monomer (MMA) was prepared in the presence of an initiator (AIBN) (1 wt% based on the swelling monomer mass) by homogenizing with an IKA MS2 minishaker at

2500 rpm for 5 min. Then this emulsion was added slowly to 20 ml of seed suspension (0.7 wt%) under a slow stirring (< 100 rpm). After the particles were allowed to swell overnight, protrusions formed, and these were made polymerized by elevation of the temperature (70 $^{\circ}$C) in a N_2 atmosphere for 8 h. The obtained particle suspension was washed 4 times with de-ionized water to separate the desired dumbbell-shaped particles from the secondary nucleations and impurities.

The obtained dumbbell-shaped PMMA particles were fluorescently labeled via a post-labeling process which can be found in detail in chapter 4 and 5. Typically, dried dumbbell-shaped particles (~ 0.1 g) were first dispersed by sonication in a mixture (~ 5 ml) of pentanol containing 1 mM of RITC, and then stirred gently (~ 100 rpm) overnight in a sealed glass vial (~ 20 ml in volume) at room temperature. After a short sonication step (~ 2 min) to disperse the particles, these labeled particles were washed twice with pentanol, once with methanol, and twice with de-ionized water, respectively, by centrifugation. After drying under a N_2 stream, these dried, fluorescently labeled dumbbell-shaped particles were stored in a glass vial in the dark at room temperature.

The transfer of fluorescent dumbbell particles from polar to apolar solvent was achieved via a modification of the approach of Espinosa's *et al.* [37] A small number of dried dumbbell particles was first dispersed in pentanol which was the intermediate solvent, and subsequently in decalin with the help of a non-ionic surfactant (span 85, 50 mM), aided by sonication and centrifugation. After this procedure was repeated four times, the solvent was considered completely exchanged.

8.2.3 Characterization of the Non-spherical Particles

The size and polydispersity of the dumbbell shaped PMMA particles were determined with a field-emission scanning electron microscope (SEM XL FEG30). A dilute suspension of particles in de-ionized water was prepared and a droplet of it was placed onto a glass slide, allowing the solvent to evaporate at room temperature, and the glass slide was adhered to a SEM stub with a conductive carbon film. The sample was sputter coated with a layer of platinum (Pt) of 5 nm. The number-averaged radius (R) of the seed particles and dumbbell-shaped particles and their standard deviations (σ) were calculated on the basis of using TEM measurement software (iTEM, 5.0). The polydispersity (δ) of the colloid systems was defined as $\delta = \sigma / R$.

The phase behavior of the fluorescent dumbbell shaped particles was investigated in real space by using a Nikon confocal microscope with a Leica 63 × oil confocal immersion lens with a numerical aperture of 1.4. The fluorescent dye (RITC) was excited at around 543 nm and its images were observed at around 605 nm. The fluorescent samples were made using

capillaries with a dimension of 0.2 × 2.0 mm cross section with a length about 5 cm (VitroCom, UK). The capillary was filled with a dispersion of particles at a volume fraction around 0.03. The capillaries were sealed with no. 68 UV-curing optical adhesive (Norland) under a UV lamp prior to observation. Measurements were performed in a temperature controlled room at $21 \pm 1 \ {}^{\circ}$C.

To investigate the electric field induced behavior of the dumbbells in decalin, 0.1 × 1 mm (cross section) capillaries were used. Two 50 μm diameter nickel alloy wires (Goodfellow, U.K.) ran lengthwise on the opposite sides of the 1 mm gap through a capillary. The capillaries were sealed with no. 68 UV-curing optical adhesive (Norland) under a UV lamp. Subsequently, up to 340 V root-mean-square sinusoidal signal with a frequency of 1 MHz was applied. Measurements on the alignment in this field were performed after 5 min.

The positional coordinates and orientational order parameters of the dumbbell particles in confocal microscopy images were obtained developed in our group for rod tracking. [44] This method is an extension of that of the method described by Crocker and Grier [43] for 2D systems that was extended to 3D for spheres by van Blaaderen *et al.* [19], Since the shape of our particles is not actually rod-like but similar to a rod with low aspect ratio, we expected this algorithm to perform reasonably well for our dumbbell shaped particles as well, which will also be discussed in the following part of this paper. For a full 3D analysis of the rotation of anisotropic particles this code is still being tested.

8.3 RESULTS AND DISCUSSION

The formation mechanism of dumbbell- or snowman-shaped PMMA particles has been demonstrated in our previous paper [20] and other published papers [32, 35]. The cross-linked polymer network absorbed swelling monomer from the media and over-swelled, then the entropy-driven shrinkage of the swollen particles induced the formation of protrusions consisting of swelling monomers. Coalescence of small protrusions took place with time. Finally a single or multiple protrusions appeared, mainly depending on the cross-link density and structure of the seeds. [45, also see chapter 6] Of course, the size of the seeds and aging time also affected the morphology of the swollen seeds (see chapter 6). Subsequent polymerization led to the solidification of protrusions and also enhanced the phase separation. The obtained non-spherical particles were monodisperse in size and shape (D = 2.0 μm and polydispersity = 2.2%, and L = 0.98 μm, polydispersity = 4.6%, where L is the distance between centers of the two spherical parts, D is the diameter of the single spherical part (see also the schematic model in the inset in Figure 8.1b), as shown in Figure 8.1a.

Transferring of particles from polar to apolar environment by using the non-ionic

surfactant Span 85 has been successfully applied to spherical PMMA particles. [31] The application of this technique to non-spherical PMMA particles, which have a similar synthesis procedure to PMMA spheres in polar environments, is therefore a straightforward step. A typical example is shown in Figure 8.1b. The dumbbell-shaped particles can be regarded as two overlapping spheres. Therefore, their aspect ratio varies between 0 and 1. In this case, it is about 0.5 (also see the model in the inset of Figure 8.1b). Interestingly, the positions of the dumbbell particles were highly ordered, while orientational order was absent. They were arranged in a so-called plastic crystal.

When the van der Waals attractions are negligible due to the fact that particles have long range repulsions and the refractive index is matched between the solvent and the particles, the interactions of these soft particles can be described with a screened Coulomb potential only, which is given as follows:

$$\frac{U(r)}{k_B T} = \begin{cases} \dfrac{Z^2 \lambda_B}{(1+\kappa D/2)^2} \dfrac{\exp[-\kappa(r-D)]}{r}, & r \geq D \\ \\ \infty, & r < D \end{cases} \qquad (8.1)$$

where k_B is Boltzmann's constant, T the absolute temperature, D the diameter of the particle, Z the charge of the ion, and κ is the inverse Debye screening length:

$$\kappa^{-1} = (8\pi\lambda_B \rho)^{-1/2} \qquad (8.2)$$

where ρ is the ion density and λ_B is Bjerrum length of the suspending medium with dielectric constant ε_m:

$$\lambda_B = \frac{e^2}{4\pi\varepsilon_m \varepsilon_0 K_B T} \qquad (8.3)$$

where e is the elementary charge and ε_0 is the permittivity of vacuum.

Compared with polar solvent system, the ion density of apolar solvent is extremely lower than that of a polar solvent, which will lead to an increase in Debye screening length (κ^{-1}). Since κ is in terms of Coulomb potential in the exponential, as κ gets smaller the potential becomes longer ranged. It will lead to a significant dissociation. Although the origin of the ions is uncertain, it is known that the surfactant micelles (non-ionic surfactant Span 85) can stabilize the ions and effectively screen the particles' surface charge. [37] The inter-particle repulsion is directly visible in the confocal image given in Figure 8.1b.

Compared with the case of silica dumbbells in cyclohexyl bromide in Demirörs' thesis, [11] the PMMA dumbbells in decalin take advantage of refractive index matching and a closer density matching. [46] Thus, the 3D real-space observation can be achieved and gravity
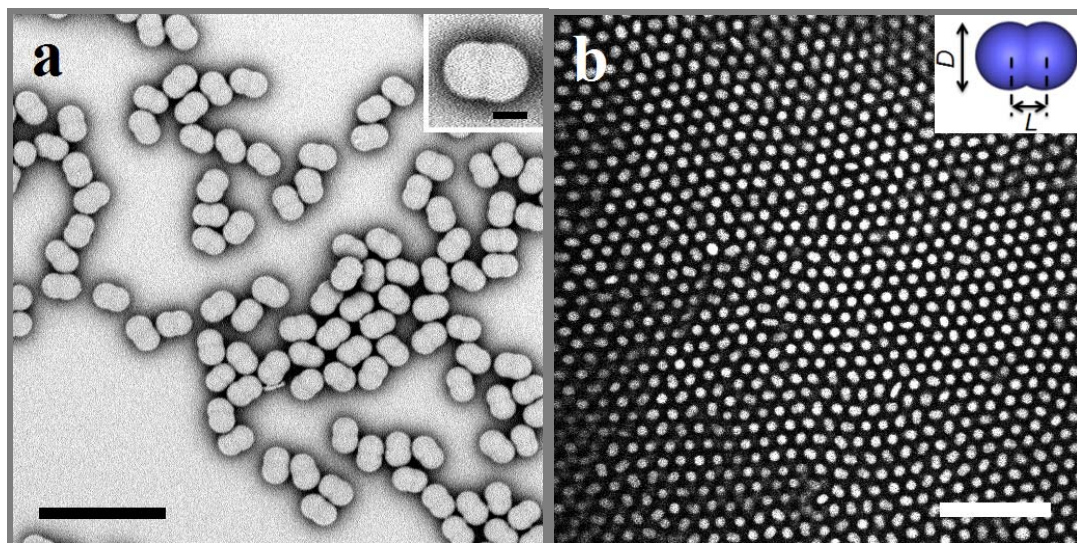
Figure 8.1. a) Scanning electron microscopy (SEM) images of synthesized dumbbell-shaped PMMA particles (D ≈ 2 μm); b) dumbbell-shaped particles dispersed in decalin with the help of Span 85, developing a plastic crystal. The inset shows a schematic model of these particles. The scale bars are 10 μm in a), 20 μm in b) and 1 μm in the inset in panel a.

effects play a smaller role. After a short time span (~ 10 min), an ordered hexagonal structure formed in large domains, as shown in Figure 8.1b. Algorithms to find the position and orientation of the rods in 2D are well developed in our group. Algorithms consist of five steps, which have been briefly described in Kuijk's thesis [12] and in detail in an upcoming publication. [44] It is worthwhile to point out that the algorithm for 2D works well for dilute systems. Since rods in a dilute system move fast compared to the scanning speed, 3D imaging of such a system is not possible without fixing the rods or slowing down their velocities, for instance by polymerization of the medium and freezing the rods [47, 48] or using more viscous apolar solvents. [49] Therefore, we mainly focused analyzing the 2D dynamics and structure.

The 2D algorithm analyzed a single frame of PMMA dumbbells dispersed in decalin. The backbones of the dumbbells were identified and we checked the validity with the original image, as shown in Figure 8.2b. Clearly, the identification is in good agreement with experimental images, except occasionally, the algorithm believed two dumbbells were overlapping, while actually only a single dumbbell was present. This is probably caused by misidentifying the dumbbell as two rods, which will affect some calculations shown later in this paper. When the orientations were discarded, a reconstruction of the center of mass of the dumbbells based on the 2D algorithm identification results was achieved and is shown in Figure 8.2c. An ordered hexagonal lattice was observed, and the positional order in this dumbbell system was confirmed by the Fourier transform (see the inset in Figure 8.2c). In

Figure 8.2d, the orientations of the dumbbells were distinguished by marking them in a series of colors, which is mapped in the inset of Figure 8.2d. In order to quantitatively judge the orientational order of this system, a nematic order parameter for a 2D system is introduced, defined as:

$$S_{2d} = \frac{1}{N} \sum_{i=1}^{N} \cos(2\theta_i) \tag{8.4}$$

where θ_i is the angle between the ith dumbbell's major axis and the nematic director. This nematic order parameter S_{2d} takes a value between 0, for a completely disordered phase, and 1, for a perfectly oriented phase. For the case in Figure 8.2a and its reproduction in Figure 8.2d,
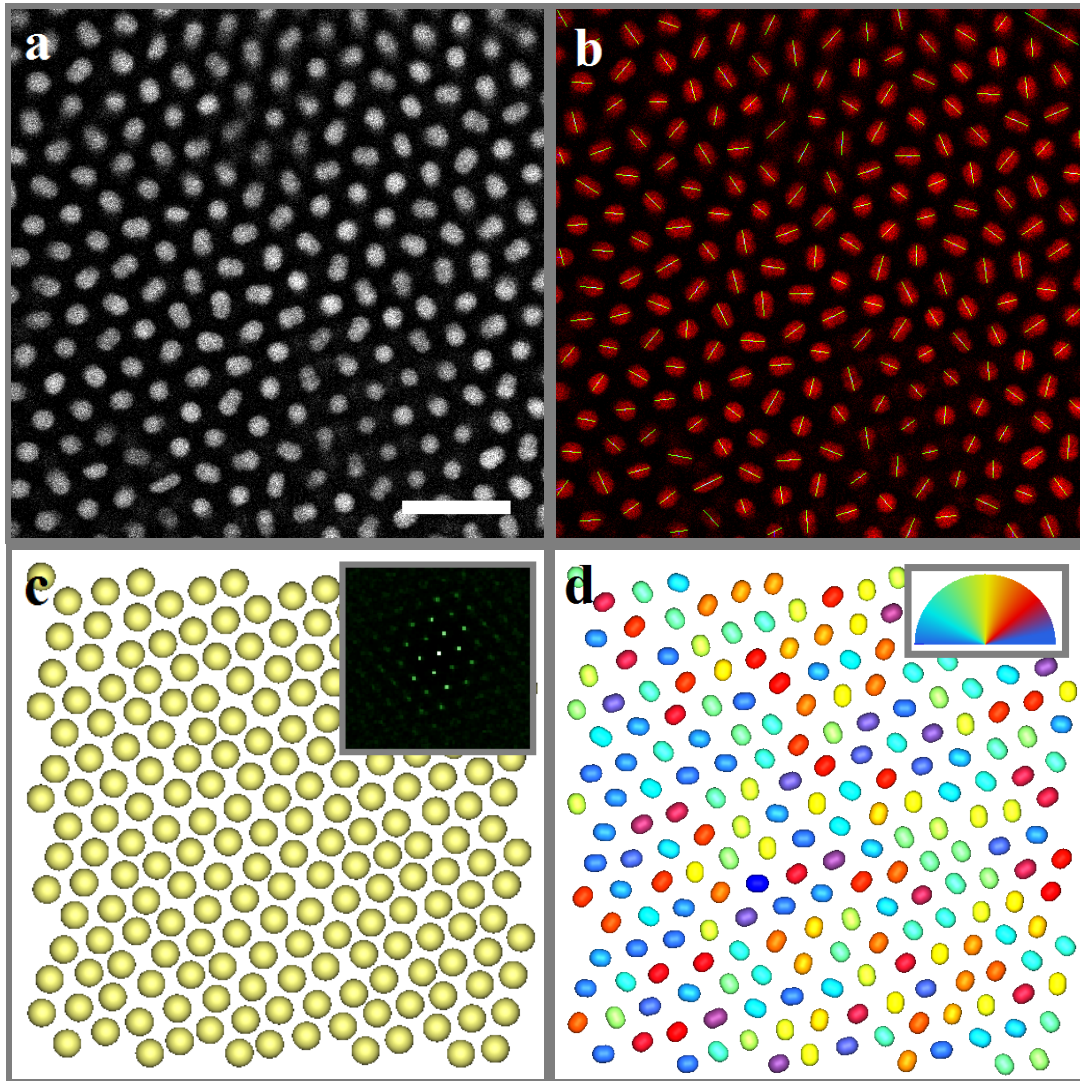
Figure 8.2. a) A confocal microscopy snapshot of a two-dimensional plastic crystal; b) overlay of backbones and confocal image; c) reconstruction of the positions of the particles in their plastic crystal configuration using spheres as components. The inset is its corresponding Fourier transform; d) reconstruction of the plastic crystal using rods as building blocks. Different colors denote different orientations, the inset illustrates the color legend for the orientation. The scale bar is 10 μm.

the nematic order parameter S_{2d} is 0.015 which clearly demonstrates an orientational disorder of the system. Moreover, the two-dimensional radial distribution function of centers of mass for the dumbbells in Figure 8.2a was calculated and plotted as a red line in Figure 8.3. Compared with a perfect (111) plane of a *fcc* (face-centrered cubic) structure, the experimental peaks fit well with those from that theoretical model.

The positional order of the plastic crystal system was also recorded in time at a plane far away from the top and bottom layers of plastic crystals. For a 500-frame movie taken 0.85 second apart, an average radial distribution function of the plastic crystal was calculated, as given in Figure 8.3 in the blue line. This averaged radial distribution function is much smoother and fits even better to a perfect (111) plane of an *fcc* crystal than that from a single frame. From the picture of the radial distribution function, information about the distance between two building blocks can be acquired as well, which turns out to be, approximately two times the diameter of the dumbbell. Note, a small peak is present r ≈ 0, which stems from the aforementioned misidentification of the algorithm that we used. Some overlapped identifications of dumbbell took place occasionally, and the positions of such dumbbells would be considered very closely spaced, which led to this invalid peak.
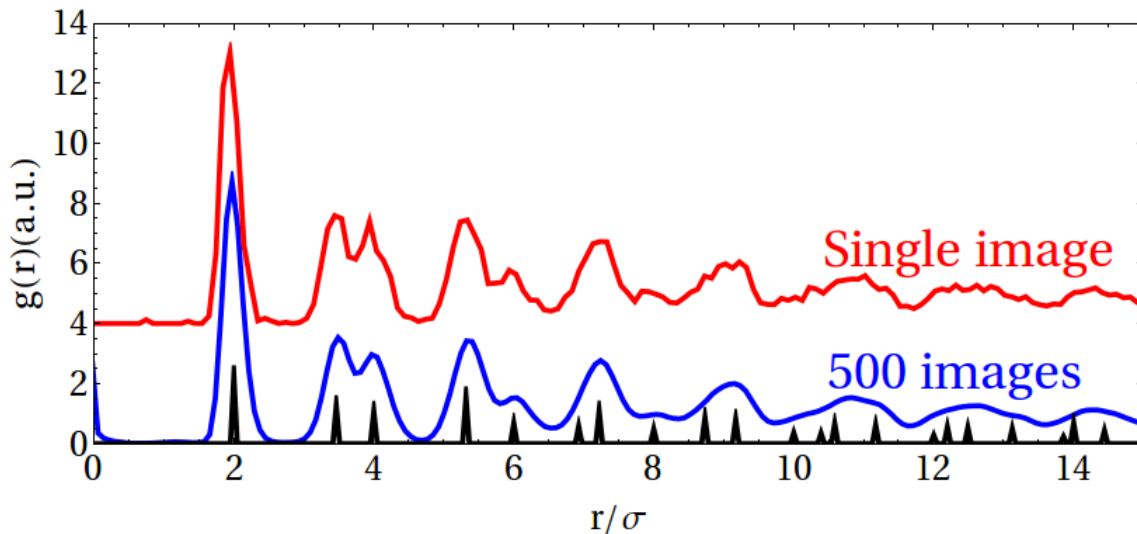
Figure 8.3. 2D Radial distribution function of plastic crystals, obtained from a single image (contains around 200 particles) in red and averaged from 500 images (425s) in blue. The equivalent from the theoretical model for the *fcc* (face-centered cubic) (111) plane is shown in black peaks.

The particle tracking process not only provided the projected positions of the dumbbells, but also the projected orientations. We took the x-axis as the nematic director, and then calculated the angle between the dumbbell major axis and the nematic director. The distribution of angles thus obtained is plotted in Figure 8.4. Here, the azimuthal angle takes on a value within the range of 0° to 180°. Moreover, an average nematic order parameter of this

500-frame movie was also calculated based on Eq. 8.4, which was 0.04. Clearly, the dumbbells are randomly orientated, such that at any instant there are equally many oriented in every direction. Although this result of projected orientation angle does not contain the rotation of the particles in 3D, it reflects that the particles can freely rotate.
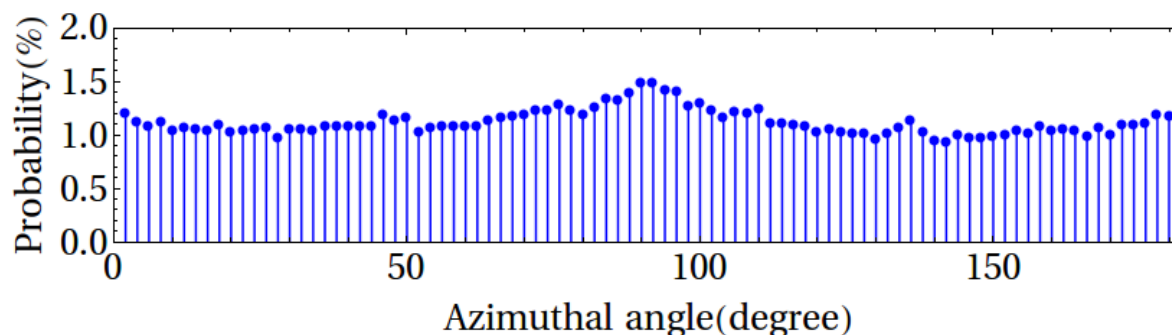

Figure 8.4. Projected in-plane angle distribution of a plastic crystal over 500 frames (425 s).

In addition, a series of frames (500) of plastic crystals, which were record at the same plane but different times (over 425 s) was superimposed, showing a very regular hexagonal ordering of the dumbbells, given in Figure 8.5a. The fact that the particles look spherical indicates that they can all freely rotate, which also implies that there may be no correlation between each particle. Moreover in Figure 8.5b, the average value of these slices is shown. A perfect hexagonal ordering was observed and illustrates the crystalline of the system, and also demonstrates particles being 'confined' to their average positions, only moving around these average positions. The Fourier transform confirms the positional order as well in the inset in Figure 8.5b. Furthermore, the trajectories of this plastic crystal over 500 frames were plotted too, as shown in Figure 8.5c. Again, the trajectory of single particles shows that they moved randomly around their average position, confined in the hexagonal lattice. Combining the
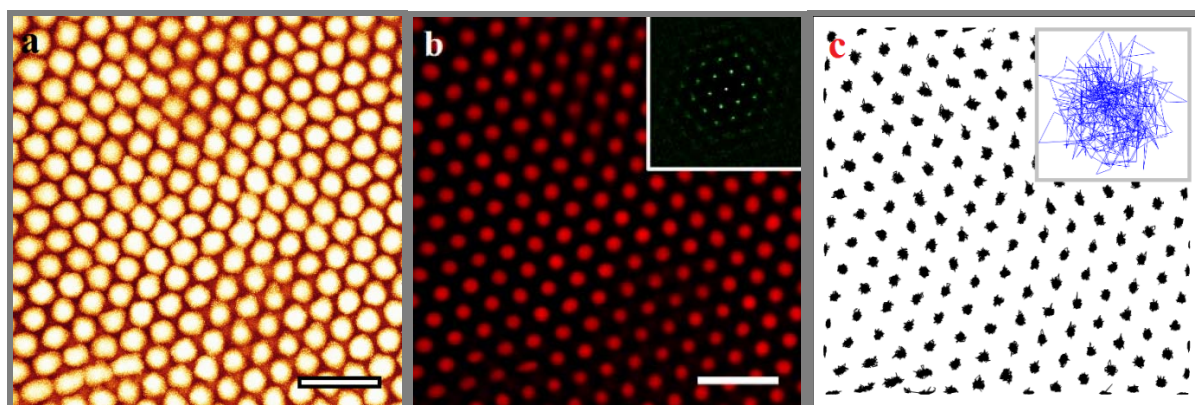
Figure 8.5. a) Superimposed confocal image of plastic crystals over 500 images (425 s); b) The average confocal image of plastic crystal over 500 frames (425 s), the Fourier transform in the inset is shown; c) the trajectories of plastic crystals over 500 images collected in 425 s. The scale bars are 10 μm.

conclusion of positional order and the fact that is orientational disorder, we conclude that a plastic crystal has been obtained in this dumbbell system.

Based on the success in 2D analysis of plastic crystals, characterization and an analysis of these crystals in 3D are desired. The result is demonstrated in Figure 8.6 (note, the images were recorded from the place which was far from the top and bottom layers of crystals). Reconstruction was achieved based on coordinates from the 3D algorithm and 3D experimental scanning, in which a mixture of *fcc* (face-centered cubic) and *hcp* (hexagonal close packed) structure was observed (see Fig. 8.6a). In Figure 8.6a, the grey circles point out the *hcp* domains in which the third layer was placed directly over the first plane, giving rise to an ABA series, while the white circles include the *fcc* domains in which the three layers are staggered relative to each other, giving rise to an ABC sequence. For clarity, unit cells of *fcc* and *hcp* structures was given in Figure 8.6b. A clear ABC packing corresponds to an *fcc* structure, while ABAB packing corresponding to an *hcp* structure. The side view (XZ-plane) of this plastic crystal exhibits a similar result as just mentioned (see Fig. 8.6b). In summary, random-hexagonal close packed (*r-hcp*) structure was found for plastic crystal of dumbbells in 3D.
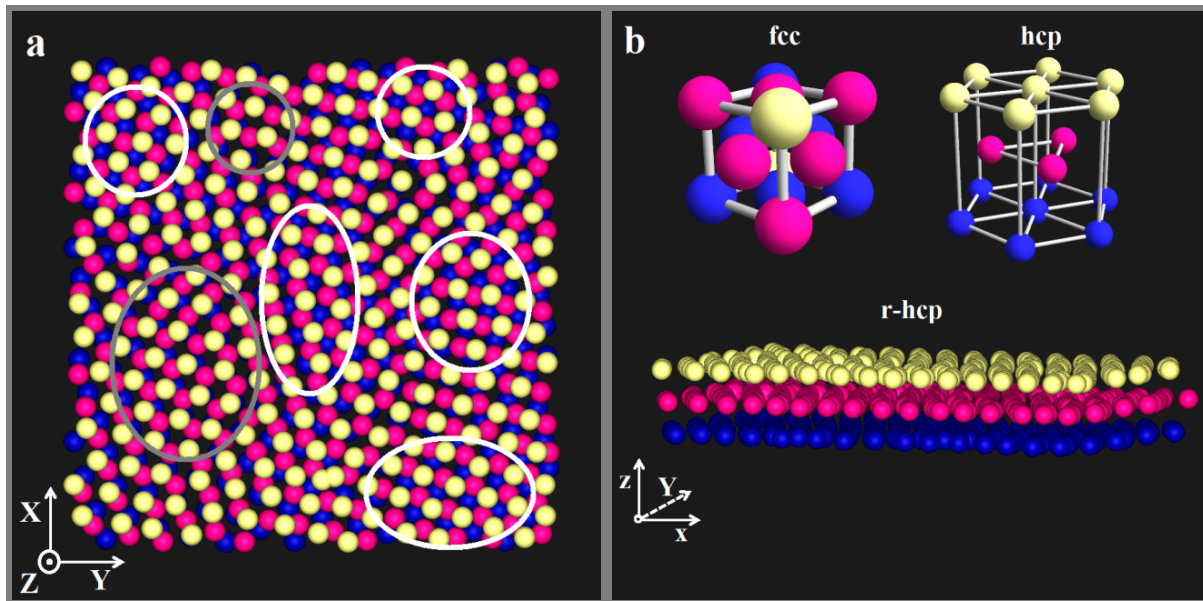
Figure 8.6. 3D reconstruction of plastic crystals, a) view at XY-plane; b) view from the XZ-plane, the insets illustrate unit cells of *fcc* (face-centered cubic) and *hcp* (hexagonal close packed) structure.

It would be useful if the orientational order could be controlled externally, for example by an electric field. When PMMA dumbbell particles are dispersed in decalin, the contrast of dielectric constant between the colloid ($\varepsilon \approx 2.6\ \varepsilon_0$) and solvent ($\varepsilon \approx 2.2\ \varepsilon_0$) [46] unfortunately is rather small, but with a strong enough field can induce a dipole moment. In our experiments,

an electric field with a frequency of 1 MHz was used to prevent polarization of the double layer. When no electric field was applied, the dumbbells were randomly oriented (see Fig. 8.2 and previous statements), while, when the electric field was turned on, the dumbbells oriented with their long axis parallel to the field direction at the field strength of 340 V/mm, as shown in Figure 8.7a. In Figure 8.7b, the orientations of the dumbbell were marked with the same color coding as before, and most of the particles' color are now close to the color yellow, which indicates the direction of the electric field.
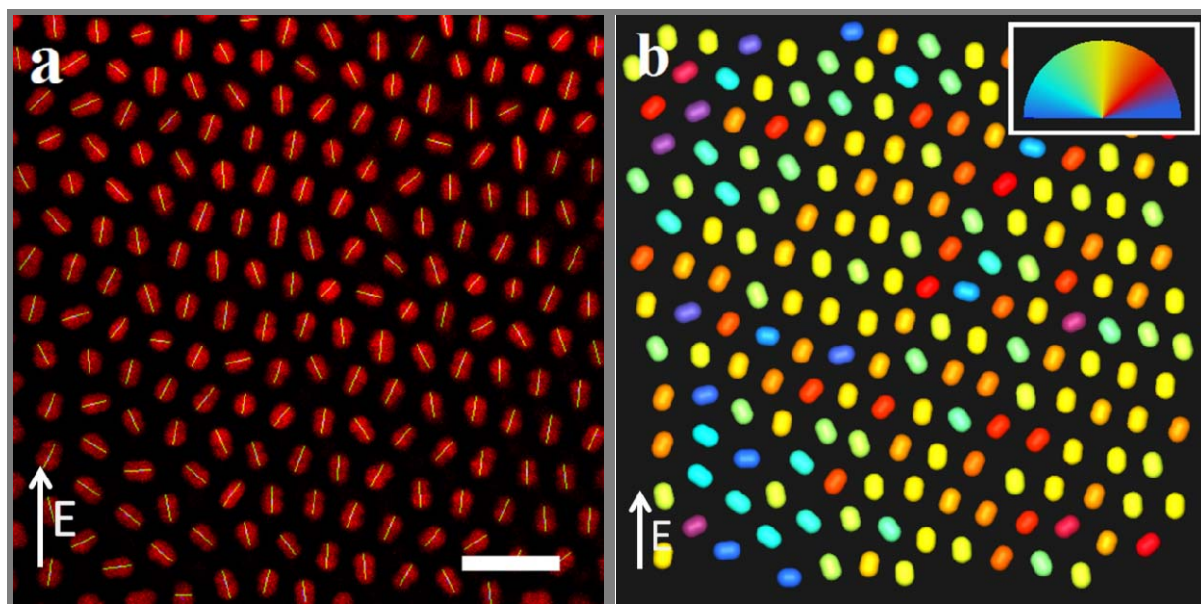
Figure 8.7. a) Overlay of backbones and confocal image. An external electric field of 340 V_{rms}/mm was applied to the sample in the vertical direction, as shown. The scale bar is 10 µm. b) Reconstruction of the plastic crystals using rods as building blocks. Different colors denote different orientations, the inset provides a color legend of orientation. Most dumbbells were aligned along the direction of the E-field.

The degree of alignment of the system was quantified by calculating the nematic order parameter from 200 images (170s) using Eq. 8.4. Note that here, θ is the angle between the dumbbell's long axis and the electric field direction. In our case, the nematic order parameter was 0.49, which demonstrates some ordering present in the system. In Figure 8.8, the distribution of orientations as a function of the azimuthal angle was plotted. A peak is present at around 100°, which again confirms the statement about partial ordering in the dumbbell system under the influence of a high-frequency electric field. As mentioned before, the dipole moments can be controlled by tuning the strength of the applied electric field. Unfortunately, limitations of the apparatus prevented further elevation of the electric field strength.
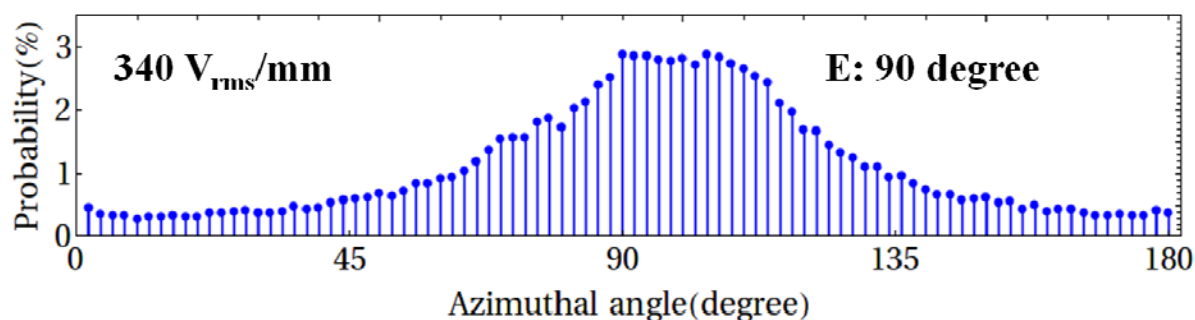
Figure 8.8. Projected in-plane angle distribution of plastic crystals with an external electric field of 340 V_{rms}/mm over 200 frames (170 s). The direction of electric field was at 90°.

8.4 CONCLUSIONS

Long ranged soft plastic crystals of PMMA dumbbells were successfully prepared in an apolar ($\varepsilon \approx 2.2\ \varepsilon_0$), refractive index matching, yet almost density matching solvent decalin in 3D. A computer algorithm for 2D rod systems was used to track the positional and orientational trajectories of this long-ranged soft dumbbell system, which confirmed the formation of a plastic crystal (positionally ordered but orientationally disordered) in 2D. Moreover, 3D positional analysis of this crystal was also carried out, and a random hexagonal close packed structure (*r-hcp*) was found. Additionally, modest control in orientational order in this dumbbell system has been achieved by means of a high-frequency E-field, thus providing a potential for photonic applications.

8.5 ACKNOLEDGEMENTS

8.6 REFERENCES

[1]   Glotzer, S. C.; Solomon, M. J. *Nature Mater.* **2007**, *6*, 557-562.

[2]   Duguet, E.; Desert, A.; Perro, A.; Ravaine, S. *Chem. Soc. Rev.* **2011**, *40,* 941-960.

[3]   Yan, S.; Kim, S.; Lim, J.; Yi, G. *J. Mater. Chem.* **2008**, *18*, 2177-2190.

[4]   Xia, Y.; Gates, B.; Yin, Y.; Lu, Y. *Adv. Mater.* **2000**, *12*, 693-713.

[5]   Perro, A.; Reculusa, S.; Ravaine, S.; Bourgeat-Lami, E.; Duguet, E. *J. Mater. Chem.* **2005**, *15*, 3745-3760.

[6]   Hu, J.; Zhou, S.; Sun, Y.; Fang, X.; Wu, L. *Chem. Soc. Rev.* **2012**, *41*, 4356-4378.

[7]   Vroege, G. J.; Lekkerkerker, H. N. W. *Rep. Prog. Phys.* **1992**, *55*, 1241-1309.

[8]   Li, F.; Josephson, D. P.; Stein, A. *Angew. Chem. Int. Ed.* **2011**, *50*, 360-388.

[9]   van Blaaderen, A. *Science* **2003**, *301*, 470-471.

[10] van Blaaderen, A. *Nature* **2006**, *439*, 545-546.

[11] Demirors, A. F. Thesis, Utrecht University, **2010**.

[12] Kuijk, A. Ph.D. Thesis, Utrecht University, **2012**.

[13] Jenkins, M. C.; Egelhaaf, S. U. *Adv. Colloid Interface Sci.* **2008**, *136*, 65-92.

[14] Prasad, V.; Semwogerere, D.; Weeks, E. R. *J. Phys.: Condens. Matter* **2007**, *19*, 113102.

[15] Yethiraj, A. *Soft Matter* **2007**, *3*, 1099-1155.

[16] Besseling, R.; Isa, L.; Weeks, E. R.; Poon, W. C. K. *Adv. Colloid Interface Sci.* **2009**, *146*, 1-17.

[17] van Blaaderen, A. *Prog. Colloid Polym. Sci.* **1997**, *104*, 59-65.

[18] van Blaaderen, A.; Imhof, A.; Hage, W.; Vrij, A. *Langmuir* **1992**, *8*, 1514-1517.

[19] van Blaaderen, A.; Wiltzius, P. *Science* **1995**, *270*, 1177-1179.

[20] Peng, B.; Vutukuri, H. R.; van Blaaderen, A.; Imhof, A. *J. Mater. Chem.* **2012**, *22*, 21893-21900.

[21] Kuijk, A.; van Blaaderen, A.; Imhof, A. *J. Am. Chem. Soc.* **2011**, *133*, 2346-2349.

[22] Vutukuri, H. R.; Demiror, A. F.; Peng, B.; van Oostrum, P. D. J.; Imhof, A.; van Blaaderen, A. *Angew. Chem. Int. Ed.* **2012**, *51*, 11249-11253.

[23] Gast, A.; Zukoski, C. *Adv. Colloid Interf. Sci.* **1989**, *30*, 153-202.

[24] Johnson, P. M.; van Kats, C. M.; van Blaadere, A. *Langmuir* **2005**, *21*, 11510-11517.

[25] Vutukuri, H. R.; Stiefelhagen, J.; Vissers, T.; Imhof, A.; van Blaaderen, A. *Adv. Mater.* **2012**, *24*, 412-416.

[26] Kuijk, A.; Byelov, D. V.; Petukhov, A. V.; van Blaaderen, A.; Imhof, A. *Farad. Discuss.* **2012**, 159, 181-199.

[27] Demirors, A. F.; Johnson, P. M.; van Kats, C. M.; van Blaaderen, A.; Imhof, A. *Langmuir* **2010**, *26*, 14466-14471.

[28] Liu, B.; Peng, B.; Besseling, T. H.; Imhof, A.; van Blaaderen, A. In preparation.

[29] Yethiraj, A.; van Blaaderen, A. *Nature* **2003**, *421*, 513-517.

[30] Royall, C. P.; Dzubiella, J.; Schmidt, M.; van Blaaderen, A. *Phys. Rev. Lett.* **2007**, *98*, 188304.

[31] Peng, B.; van der Wee, E.; Imhof, A.; van Blaaderen, A. *Langmuir* **2012**, *28*, 6776-6785.

[32] Sheu, H. R.; El-Aasser, M. S.; Vanderhoff, J. W. *J. Polym. Sci., Part A: Polym. Chem.* **1990**, *28*, 629-651.

[33] Mock, E. B.; De Bruyn, H.; Hawkett, B. S.; Gilbert, R. G.; Zukoski, C. F. *Langmuir* **2006**, *22*, 4037-4043.

[34] Mock, E. B.; Zukoski, C. F. *Langmuir* **2010**, *26*, 13747-13750.

[35] Kim, J. -W.; Larsen, R. J.; Weitz, D. A. *J. Am. Chem. Soc.* **2006**, *128*, 14374-14377.

[36] Nagao, D.; Hashimoto, M.; Hayasaka, K.; Konno, M. *Macromol. Rapid Commun.* **2008**, *29*, 1484-1488.

[37] Espinosa, C. E.; Guo, Q.; Singh, V.; Behrens, S. H. *Langmuir* **2010**, *26*, 16941-16948.

[38] Ge, J.; Yin, Y. *Angew. Chem. Int. Ed.* **2011**, *50*, 1492-1522.

[39] Ge, J.; Yin, Y. *Angew. Chem. Int. Ed.* **2007**, *46*, 7428-7432.

[40] Vega, C.; Monson, P. A. *J. Chem. Phys.* **1997**, *107*, 2696-2697.

[41] Marechal, M.; Dijkstra, M. *Phys. Rev. E* **2008**, *77*, 061405.

[42] Shen, S.; Sudol, E. D.; El-Aasser, M. S. *J. Polym. Sci., Part A: Polym. Chem.* **1993**, *31*, 1393-1402.

[43] Crocker, J. C.; Grier, D. G. *J. Colloid Interface Sci.* **1996**, *179*, 298-310.

[44] Besseling, T. H.; Hermes, M.; van Blaaderen, A. In preparation.

[45] Peng, B.; van Blaaderen, A.; Imhof, A. In preparation.

[46] Leunissen, M. E.; van Blaaderen, A.; Hollingsworth, A. D.; Sullivan, M. T.; Chaikin, P. M. *Pro. Natl. Acad. Sci. USA* **2007**, *104*, 2585-2590.

[47] Shereda, L. T.; Larson, R. G.; Solomon, M. J. *Phys. Rev. Lett.* **2010**, *105*, 228302.

[48] Wu, Y. L. Ph.D. Thesis, Utrecht University, **2007**.

[49] Mukhija, D.; Solomon, M. *J. Colloid Interface Sci.* **2007**, *314*, 98-106.

Site-Specific Growth of Polymer on Bullet-Shaped Silica Rods

ABSTRACT

Bullet-shaped silica colloids were used as seeds for the growth of polymer (polymethylmethacrylate (PMMA) and polystyrene (PS)) in dispersion polymerization. After modifying the silica surface, the polymer was found to anchor exclusively at the flat tip of the rods, rather than at the other surfaces with a higher curvature. A series of experiments was performed suggesting that it is the combination of a surface chemical heterogeneity and the lower curvature that directs the polymer towards this location. The perfect tendency of the rods to attach end-on to the polymer was confirmed and used to produce hedgehog-shaped hybrid particles, in which several silica rods stand out perpendicularly from the surface of a PMMA particle. In this dispersion polymerization the rods functioned as the stabilizer rendering the addition of the usual polymeric stabilizer unnecessary. The synthetic methods developed break the symmetry of the rod-shaped particle in the direction of the anisotropy allowing the anisotropy to be directed e.g. by external fields.

9.1 INTRODUCTION

Considerable attention has been paid in recent years to colloidal particles that combine an anisotropic shape with a composite structure, because they combine the properties of different materials in one particle and allow anisotropy in materials properties. This leads to potential applications that are hard to achieve by either material alone or with spherically-shaped particles, such as the fabrication of optical, electronic, and sensing devices to the utilization as fillers for the paint and coating industries. [1-6] In addition, if the symmetry of the particles can be broken in the direction of the anisotropy the resulting particles can in principle be pointed in specific directions with an external electric field. For instance, in the case of photo-catalytic rod-like particles that split water in its elemental components this would allow much more easy separation of the oxygen and hydrogen produced by such systems. [7-9] Furthermore, the anisotropic interactions between such particles could be put to use in new collective assembly strategies, such as amphiphilic behavior seen in particles composed of parts with different hydrophilicity or surface roughness and liquid crystalline behavior. [10-13] Many efforts have been devoted to the synthesis of anisotropic hybrid particles, including self-assembly of small clusters of spherical particles, [14-16] oriented surface modification of spheres placed on a substrate or interface, [17-20] or directed nucleation on the surface of primary particles. [21-23] Oriented surface modification has also been used to provide silica rods with gold tips. [24] Such so-called Janus rods have also been made by combining conventional lithography with nanorod synthesis [25] and by electroplating in an anodic alumina membrane. [26] Also, reactive ion etching of polymer rods out of a multilayer polymer film using colloidal particles as masks [27] has been demonstrated. These multistep procedures yield well-defined rods, but in small quantities.

Recently, our group developed a method to produce monodisperse rod shaped silica colloids by droplet-induced directional growth of silica by the hydrolysis and condensation of a silica precursor. [28] The cylindrical particles grow out of water-in-oil emulsion droplets containing polyvinylpyrrolidone (PVP) and end up having one rounded end, where the silica growth started, and one flat end to which the droplet remained stably attached. This remarkable manner of attachment is exemplified by the fact that the rods could be elongated by further additions of silica precursor [23]. Indeed, He *et al.* [29, 30] produced amphiphilic silica rods in this way by post-addition of a second organo-silica precursor.

After the rods were removed from their original reaction mixture the water droplets are gone and there is only the slight anisotropy of the shape on both ends of the rod. We recently checked in nematic and smectic liquid crystal phases formed by these bullet-shaped particles

if the asymmetry in the ends give rise to directionality of the rods. This turned out not to be the case as could by nicely demonstrated by particles for which the fluorescence intensity was not constant over the length of the rods. [31] However, when we used these particles, after surface modification with a silane coupling agent containing the monomer of PMMA, as seeds in a typical dispersion polymerization (of methylmethacrylate (MMA) or styrene (St)), we found that the polymer bulbs that formed at the ends of the rods became attached exclusively at the end where once the water droplet had been. Interesting hybrid organic-inorganic colloids with anisotropic properties in the direction of the length of the rod can be produced in this manner. We investigated the cause of the preferred attachment by tuning the shape and surface chemistry of the rods and now are able to control the attachment site. Furthermore, we show that the silica rods can also replace the usual polymeric steric stabilizer in dispersion polymerization by collectively attaching head-on to the surfaces of growing PMMA particles, as in a Pickering emulsion. Particles with a unique hedgehog-like (or porcupine-like) architecture were produced in this way.

9.2 MATERIALS AND METHODS

9.2.1 Materials

In the synthesis of silica rods: tetraethyl orthosilicate (TEOS, 98%, Aldrich) was used as the precursor for the silica rods. Ammonia (NH_3, 29 wt% solution in water, Merck) was used as the catalyst. Poly(vinylpyrrolidone) (PVP, K-30, Aldrich) with an average molecular weight of 40,000 g/mol, 1-pentanol ($\geq$ 99%, Sigma), ethanol (chemical grade, Baker), and sodium citrate dehydrate ($\geq$ 99%, Sigma) were used as received. De-ionized water was used in all experiments and was obtained from a Millipore Direct-Q UV3 reverse osmosis filter apparatus.

In the preparation of hybrid particles: Methyl methacrylate (MMA, Aldrich) was passed over an inhibitor removal column (Aldrich) at room temperature. After the inhibitor had been removed, MMA was stored in a refrigerator at +4 ^{o}C for not longer than 1 month. Styrene (St, Fluka) was passed through a homemade activated alumina filled column to remove the inhibitor and used immediately. Azo-bis-isobutyronitrile (AIBN, Janssen Chimica) was re-crystallized from ethanol before use. Divinylbenzene (DVB, 80%, technical grade, Aldrich) was used as the cross-linking agent. Poly(vinylpyrrolidone) (PVP, K-90, Fluka) with a molecular weight of 360,000 g/mol and PHSA-*g*-PMMA (a poly(12-hydroxystearic acid) (PHSA) grafted PMMA copolymer) were used as stabilizers. The PHSA-*g*-PMMA stabilizer, dissolved in a mixture of ethyl acetate and butyl acetate, was homemade and its synthesis is

described by Antl *et al.* [32] Rodamine b isothiocyanate (Aldrich) was used as fluorescent dye. 1-Octanethiol (≥ 98.5%, Aldrich), methanol (chemical grade, Biosolve), acetone (chemical grade, Baker), hexane (chemical grade, Biosolve), dodecane (> 99%, Sigma-Aldrich), sulfuric acid (95%, Fisher), and hydrogen peroxide (35% in water, Merck) were used as received.

3-(Trimethoxysilyl) propyl methacrylate (TPM, 98%, Aldrich) was used as the coupling agent between silica rods and PMMA. Hydrofluoric acid (HF, 48 wt% in H$_2$O, Sigma-Aldrich) was diluted to about 5 wt% with de-ionized water and then used to selectively etch the silica rods.

9.2.2 Procedure for Silica Rods Synthesis

The silica rods were synthesized using the method in a previous paper. [28] Typically, bullet-shaped rods with a length of 737 nm and a diameter of 384 nm were prepared as follows: 80 g of PVP (K-30) was dissolved in 800 ml of 1-pentanol by sonication until all PVP was dissolved, and placed in a 1 L glass flask. Then, 80 ml of ethanol, 40 ml of de-ionized water and 8 ml of 0.18 M sodium dihydrate aqueous solution were added to the PVP/pentanol mixture. The flask was shaken by hand for 2 min. Subsequently, 16 ml of ammonia was added, and the flask was shaken again by hand. Then, 8 ml of TEOS was added to the mixture, and briefly shaken to mix the content. The flask was left to rest and the reaction was allowed to proceed for 36 h. The length of the rods can be readily tuned by using various amounts of water. The details can be found in ref. [28]. After the reaction the silica rods were thoroughly cleaned by centrifugation and re-dispersion in ethanol by sonication 4 times, and finally dried with a nitrogen stream at room temperature.

The morphology of the rods can be easily tuned by growing silica layers in a precise way using the so-called Stöber method. [33] For the 15 nm thick silica layer, 0.4 g of silica rods was dispersed by sonication in a mixture consisting of 40 ml ethanol, 1.3 ml water and 1.6 ml of ammonia. Then, 0.2 ml of TEOS was added. The reaction was allowed to proceed for 24 h. For the rods with two rounded ends, ~ 150 nm in thickness of silica layer was grown on the original silica rods. This process can be achieved through a multi-step growth of silica layers using in total 7 ml TEOS. The final products were washed three times with ethanol and dried at room temperature.

In one experiment the rods were treated with a piranha solution (sulfuric acid and hydrogen peroxide at a 3:1 v/v ratio) to clean their surface from organic residues. First, the dried rods (~ 0.05 g) were dispersed in sulfuric acid (~ 9 ml) by sonication. Then, hydrogen peroxide (~ 3 ml) was added to the suspension of rods, and the dispersion was stirred overnight. The next day, the rods were separated by centrifugation and rinsed with de-ionized water until the pH was close to 7. Finally, the rods were dried at room temperature for further use.

9.2.3 Procedure for TPM Coating

To provide a basis for the PMMA to react to, the silica rods were treated with the coupling agent 3-(trimethoxysilyl) propyl methacrylate (TPM). Typically, 0.3 g of dried rod-like silica particles were dispersed in 5 ml of ethanol after which 1 ml of ammonia and 3 ml of TPM were added. The mixture was sonicated for 1 min to disperse the rods. The mixture was then stirred for 3 h at a moderate stirring rate (~100 rpm) at room temperature. After this procedure, the suspension was transferred to a 50 ml round bottom flask and vacuum distilled at room temperature to promote the condensation reaction as Philipse *et al.* [34] described. After about 20 min, 1-2 ml bright, gel-like suspension remained at the bottom of the flask, and the distillation was stopped. This TPM grafted silica (named TPM-SiO$_2$) was purified by 3 cycles of centrifugation/re-dispersion in ethanol. The final samples were dispersed in ethanol and stored at +4 ^{o}C for no longer than one week.

9.2.4 Procedure for Hybrid Polymer-Silica Particles Synthesis

Hybrid PMMA-silica particles were synthesized through the co-polymerization of TPM grafted silica rods with methyl methacrylate (MMA) in a polar medium. Typically, a mixture containing 0.4 g PVP (K-90), 0.051 g TPM-SiO$_2$ rods, and 4.1 g methanol was prepared. Then, MMA containing 1 wt% of initiator (AIBN) was added. This reaction mixture was deoxygenated for 1 h by bubbling nitrogen through the mixture. Subsequently, the flask with this mixture was placed into a pre-heated silicone oil bath and maintained at 55 ^{o}C, and stirred at 100 rpm for 24 h before cooling down to room temperature. The obtained particles were rinsed three times with methanol using a centrifuge (Hettich Rotina 46 S, at 315 g for 20 min). The products were stored in methanol for further purification to remove the free polymer particles by sedimentation. By simply scaling up the reaction (*e.g.*, five times the initial quantities), the yield of the rods increased, while the quality remained the same, and the result is shown in Supplementary Figure 9.1a (SF-9.1a).

Hybrid PS-silica particles were synthesized in a similar way to that of PMMA-silica particles. In detail, 0.1 g PVP (K-90), 0.05 g TPM-SiO$_2$, and 4.1 g ethanol mixed homogeneously by sonication for 1 min, and then, St (~0.24 g) containing 1.2 wt% of initiator (AIBN) was added to the mixture. A de-oxygenation (N$_2$ bubbling through the mixture for around 1 h) was carried out prior to the co-polymerization. Co-polymerization took place at 70 ^{o}C, and maintained for 24 h. The products were washed with ethanol at 315 g for 20 min (Hettich Rotina 46 S) three times to remove the un-boned stabilizer and monomer, and stored in ethanol for further purification to remove the free polymer particles. The result is shown in SF-9.1b.

Based on the recipe just mentioned, a variety of hybrid particles was successfully prepared by making use of silica rods that had undergone diverse treatments.

To selectively remove the silica from hybrid particles, hydrofluoric acid (HF) was used and diluted to about 5 wt% with de-ionized water first. Then, HF aqueous solution was added in excess to the suspension of hybrid particles (~ 0.1 wt% in water), and kept stirring (~ 100 rpm) for 30 min. Subsequently, the particles were rinsed three times with de-ionized water to purify the residue of the hybrid particles, and the final product was stored at room temperature for characterization.

In the chemical-stabilizer-free dispersion polymerization, the procedure was similar to the dispersion polymerization just described. Typically, 0.05 g of TPM-SiO$_2$ rods was dispersed in 4.1 g of methanol. Then, various amounts of MMA containing 1wt% (based on the monomer mass) of AIBN were fed into the dispersion of rods under constant stirring (~ 100 rpm). After 1 h of deoxygenation, the flask was immersed into the silicone oil bath at 55 $^{\circ}$C and maintained for 24 h. After the reaction was complete, the un-reacted MMA were removed by three rinse cycles with methanol, and the obtained product was stored in methanol for observation.

9.2.5 Purification of the Hybrid Particles from the Polar Solvent

The synthesis of hybrid particles also results in a number of free PMMA particles. In order to purify the hybrid particles, a mixture of glycerin and water was used in combination with a centrifuge (Hettich Rotina 46 S), to separate the hybrid particles from the mixed system. An empirical weight ratio (α) between glycerin and water was used, calculated by:

$$\alpha = \frac{\rho_g \rho_w - \rho_m \rho_g}{\rho_m \rho_w - \rho_g \rho_w} \tag{9-1}$$

where ρ_g, ρ_w and ρ_m are the density of glycerin (2.61 g/cm^3), water (0.997 g/cm^3) and mixture of glycerin and water at 25 $^{\circ}$C, respectively. Considering the density of PMMA of about 1.18 g/cm^3, we selected the density of the mixture (ρ_m = 1.20 g/cm^3) to be slightly higher than PMMA. The separation was carried out with a Hettich Rotina 46 S centrifuge, at 800 g for 5 hours. After the third purification, the particles dispersed in methanol and centrifuged three times to remove the remainder of the glycerin/water mixture. Ultimately, the obtained particles were stored in methanol for further use.

9.2.6 Procedure for Dying the Particles

The as-synthesized hybrid particles were labeled with a fluorescent dye. First, an amount of hybrid particles (~ 0.1 g) was collected through a centrifugation process and the supernatant was removed. Then, the hybrid particles were dispersed by sonication in 5 ml of pentanol

containing 1 mM of Rodamine b isothiocyanate (RITC) in a 20 ml glass vial. The suspension was stirred at 100 rpm for 2 days at room temperature. Subsequently, the labeled particles were washed twice with pentanol, once with methanol, and three times with de-ionized water, respectively, by centrifugation. After drying under a nitrogen stream at room temperature, the fluorescently labeled hybrid particles were stored in a dark glass vial for further observation.

In order to minimize interference from light scattering, refractive index matching between the particles and solvent is desired. However, due to the fact that the particles are made of two types of material, full refractive index matching is impossible. Considering the refractive index of silica (1.45) and PMMA (1.49), we chose a mixture of glycerin and water (roughly 9:1 in weight) [35] to refractive index match with the silica rods.

In fact, the following confocal scanning laser microscopy observation indicated that the dye only partly penetrated into the particles, developing core-shell fluorescently labeled particles (see the inset in Figure 9.2d).

9.2.7 Characterization

To determine the details (size, polydispersity and morphology and internal structure) of the particles, transmission electron microscopy (TEM) was performed with a Philips Tecnai 10 (accelerating voltage $\leq$ 100 kV). A diluted sample suspension was deposited on a copper grid coated with a polymer membrane which was carbon coated, and the sample was allowed to dry at room temperature. Tomographic reconstructions were made by taking TEM images at angles ranging from -70° to +70° with intervals of two degrees and aligned using gold markers. The software used for alignment and reconstruction is the IMOD package made by the Boulder laboratory in Colorado. [36, 37] For the Tomogram generation the SIRT algorithm was used with 70 iteration steps and a radial filter cut-off of 0.4 and falloff of 0.05.

Scanning electron microscopy (SEM) was carried out with a Philips XL30FEG microscope to observe the surface morphology and shape of the particles. The samples were prepared by placing a drop of dispersion on a grid and allowing the solvent to evaporate at room temperature. The samples then were sputter-coated with a layer of platinum (Pt) about 3 nm.

Confocal scanning laser microscopy (CSLM) was used to help assessing the structure of the fluorescently labeled hybrid particles. The dried fluorescently labeled particles ($\sim$ 0.01 g) were dispersed in the mixture of glycerin of water ($\sim$ 1 g, 9:1 in weight) in a small vial (contents $\sim$ 1 ml) with the help of sonication bath. To be able to use the cell in the CSLM setup, the bottom of the vial was removed and replaced with a thin cover glass, which was glued to the vial using epoxy glue. A Nikon confocal scanning laser can head (Nikon C1) was operated in fluorescence mode on a Leica (DM IRB) SP2 inverted microscope. Measurements were performed with a Leica 100 $\times$ oil confocal immersion lens with a numerical aperture of

1.4. The fluorescent particles were excited at around 543 nm, and their images were observed at emission wavelengths of around 605 nm.

9.2.8 Theoretical Calculation

The theoretical strategy that we used to simulate the behavior of bullet-shaped particles adsorbed to the flat interface of two liquids is the method of Ref 8 and 9. This technique is called triangular tessellation technique in which the surface of the particle is approximated by a large number of triangles. This approximation can be improved upon by reducing the triangle size. The liquid-liquid interface is assumed to be flat.

In this model, the adsorption free energy of system is only in terms of the contributions of surface-area and contact line, which is written as

$$V(z,\phi) = \gamma_{12}(A - S_{12}) + \gamma_{1c}S_1 + \gamma_{2c}S_2 + \tau L, \tag{9-2}$$

where S_1 is the surface area of the particle above the interface, namely, in phase 1, while the S_2 is the surface area of the particle below the interface; A is the total surface area of the interface and S_{12} is the cross section of the particles at the interface. γ_{12}, γ_{1c} and γ_{2c} are the surface tensions between phase 1 and 2, and particle; τ is the line tension and L is the length of contact line, respectively. The adsorption energy in Eq. 9-2 depends on z (the position of the interface with respect to the center of the particle) and ϕ (the polar angle, which measures the angle between the particle's rotational symmetry axis and the interface normal, ranging from 0 to π). The schematic model can be found in Figure 9.1.
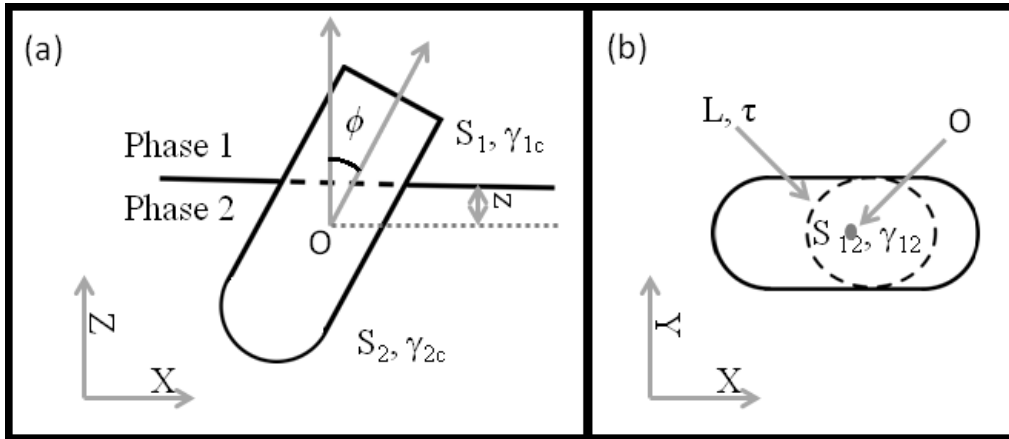
Figure 9.1. A side and top view of a bullet-shaped particle adsorbed at a flat liquid-liquid interface, which show the parameters used in our model. The center of particle (point O) is located at a distance z to the interface of phase 1 and phase 2. The polar angle ϕ is the angle between the interfacial normal and the rotational symmetry axis of the particle. The interface has a total area of A with its corresponding interfacial tension γ_{12}. The surface area of the particle consists of two parts, one of which is above the interface and denoted by S_1 with a surface tension of γ_{1c} between particle and phase 1, the other of which below the interface is

denoted by S_2 with a surface tension of γ_{2c} between particle and phase 2. S_{12} (the area enclosed by the dashed line in b)) is the cross section of particles at the interface. The dashed circle in b) is the contact line with a circumference of L and corresponding line tension τ. a) The XZ-plane cross section of the particle and interface. b) The XY-plane cross section of the particle and interface.

We define the state when the particle is fully immersed in phase 1 as a reference state. In this case, the relative free energy is written as

$$F(z,\phi) = V(z,\phi) - \gamma_{12}A - \gamma_{1c}S_1 = (\gamma_{1c} - \gamma_{2c})(S_1 - S) - \gamma_{12}S_{12} + \tau L, \qquad (9\text{-}3)$$

where S is the total surface area of the particles ($S = S_1 + S_2$). When the particle is completely encompassed by phase 1, $F(z,\phi)$ is zero. The γ_{1c} and γ_{2c} can be replaced by using Young's equation [40]

$$\gamma_{12}\cos\theta = \gamma_{1c} - \gamma_{2c}, \qquad (9\text{-}4)$$

then, the Eq. 3 is rewritten to

$$F(z,\phi) = \gamma_{12}[(S_1 - S)\cos\theta - S_{12}] + \tau L, \qquad (9\text{-}5)$$

The detailed description about the calculation can be found in refs. 38 and 39.

9.3 RESULTS AND DISCUSSION

Several batches of silica rods were synthesized following the method from our previous work (details can be found in 'materials and methods', MAM). [28] A typical monodisperse silica rod system with a diameter (D) of 327 nm and length (L) of 1.2 μm is shown in the inset in Figure 9.2a. The 3D reconstruction of the particle shape, achieved by electron tomography, [36, 37] clearly shows the bullet-like shape and the difference between the two ends of the rods, one of which is hemispherical while the other is almost flat. In order to use these particles as seeds their surfaces were first modified with the silane coupling agent trimethoxysilyl propyl methacrylate (TPM). A typical one-pot dispersion polymerization of monomer in a polar medium was then carried out: all the agents (TPM modified silica rods, PVP as a stabilizer, initiator, monomer (MMA or St) and solvent) were added to a flask and dispersed homogeneously under a nitrogen stream. Elevation of the temperature then initiated the polymerization. Details of the synthesis and purification are given in the MAM. Interestingly, the obtained hybrid particles exhibited a lollipop shape due to the exclusive attachment of the polymer bulbs to the less curved tips of the rods. Typical systems are shown in Figure 9.2b-d (for PMMA) and supplementary Figure 9.2 (SF-9.1b, for PSt). The growth location of polymer bulbs was independent of the aspect ratio (from 1.9 to 4) of the rods. The

ratio of monomer to seed particle also did not influence the growth location, but only the size of the polymer bulb. Although the recipe was not yet optimized to prevent secondary nucleation of PMMA which did not attached to the silica rods, these secondary nucleation can be easily removed by centrifugation. Upon increasing the reagents in the synthesis, the yield was readily scaled up and the obtained particles possessed a good uniformity in shape (see MAM and SF-9.2a).
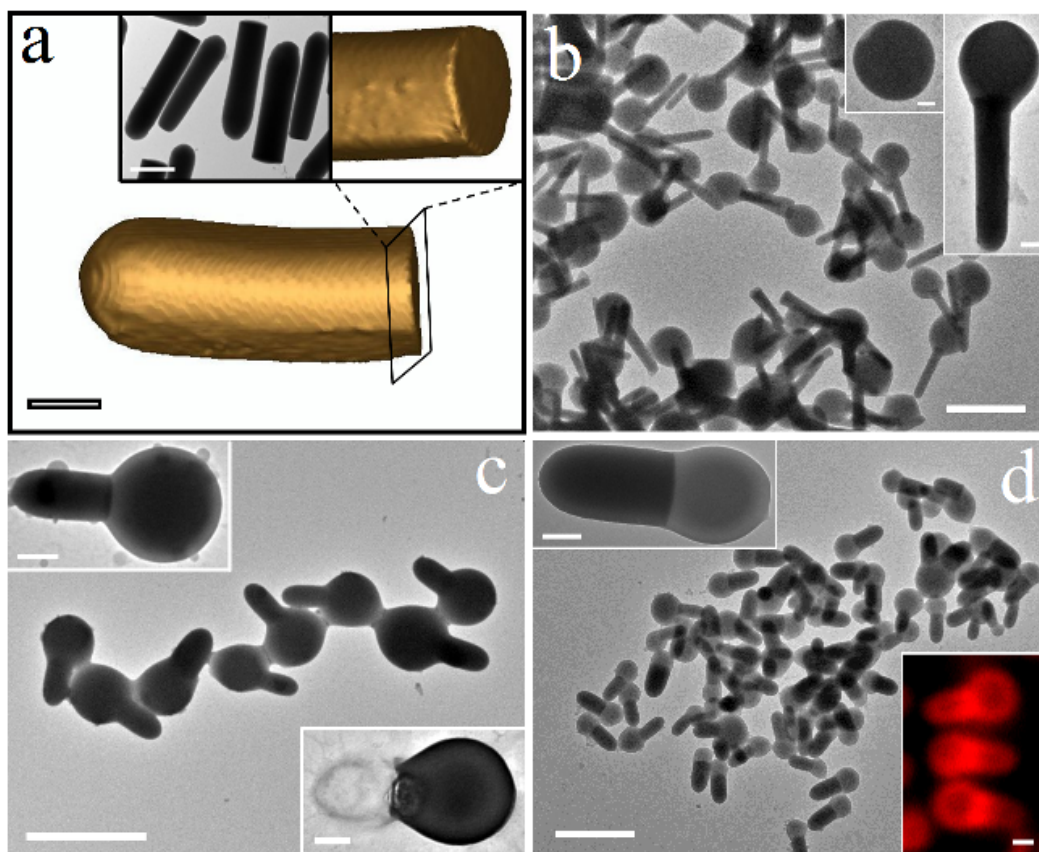
Figure 9.2. Transmission electron microscopy (TEM) images of the hybrid silica-PMMA particles. (a) 3D reconstruction using electron tomography of a single silica rod showing that the two ends have different curvatures. The inset is a close-up of the flat end and a TEM image of the silica rods ($L = 1.2$ μm and $D = 327$ nm). (b) TEM images of 'lollipop-shaped' particles made from long rods ($L = 1.3$ μm and $D = 225$ nm). The PMMA bulbs ($D = 940$ nm) only attached at the flat end of the rods. The insets show an occasional detached PMMA bulb carrying a clear indentation and a single hybrid particle at higher resolution. (c) TEM image of lollipop-shaped particles ($D_{PMMA} = 868$ nm) made from short rods ($L = 737$ nm μm and $D = 384$ nm) at a mass ratio of 9.7:1. The insets are a single particle at a higher resolution and the result of etching the silica seed with HF. (d) A similar result ($D_{PMMA} = 603$ nm) at the lower mass ratio between MMA and silica rods of 4.85:1. The lower inset shows the as-synthesized particles after fluorescent labeling in a solvent matching the refractive index of silica. The scale bar in (a) is 200 nm and 500 nm in the inset. Scale bars in (b-d) are 2 μm and 200 nm in the insets.

Selective etching of the silica with hydrofluoric acid indicated that a thin layer (~ 20 nm) of polymer also covered the rest of the silica rods (inset of Figure 9.2c). It is more likely, however, that this is PVP left over from the silica synthesis as the conditions at which PMMA completely wets that particles are quite different. [34] The particles could be labeled with Rhodamine b isothiocyanate (RITC) and dispersed in a solvent mixture matching the refractive index of silica (for details see MAM). A confocal fluorescence micrograph shows that both the rod and the bulb became labeled at the surface (inset of Figure 9.2d), suggesting a thin PMMA film might indeed be covering the whole rod.

9.3.1 Formation Exploration

We monitored in more detail the formation of the PMMA bulbs at the flat ends in the sample of Figure 1c by taking samples at different times during the preparation. The samples were quenched in a large amount of room-temperature solvent to prevent further growth. TEM images of these samples are shown in Figure 9.3 (also see SF-9.2 and 3). It is clear that PMMA nuclei are already present on the flat end of the silica early in the reaction (see SF-9.2). A little while later these nuclei were seen to have merged (see SF-9.3), after which a PMMA bulb grows until the monomer runs out, all the while increasing its contact angle at the edge of the silica particle without much 'spilling over' around the flat site onto the length of the rod. To investigate why the PMMA prefers so strongly to attach to the flat ends several additional experiments were performed. The commonly used surface coating with TPM strongly promotes the nucleation of dispersion-polymerized PMMA on silica, but it is expected to cover the whole silica surface. That the TPM treatment is necessary is seen from an experiment in which this step was omitted: no association between the PMMA and silica was observed at all and separate PMMA spheres were formed instead (see SF-9.4). A surface treatment with TPM (or similar compound) is what allows spherical silica seeds to be partially wetted by PMMA so that they can be decorated with one or more polymer bulbs. [2, 21, 42-44] SF-9.5 shows such a result using our exact synthesis protocol. Alternatively, if the silica surface is wetted completely by the PMMA, the silica becomes covered with a complete and uniform layer: this is shown by SF-9.6 where a dispersion polymerization in apolar medium (hexane/dodecane) was used in conjunction with a comb-graft stabilizer of polyhydroxystearic acid grafted onto PMMA (for details see MAM) similarly as already described by our group for the coating of silica spheres. [41]

Two reasons can be put forward to explain the attachment of PMMA to the flat silica ends: The first is a lower surface free energy for nucleation of a spherical monomer-swollen PMMA droplet to a flat surface as compared to a rounded surface. Clearly, the contact area will be smaller in the former case. A second possible explanation is that the surface chemistry of the

flat silica end differs from that of the rest of the surface. During the silica synthesis this end remained in contact with the water droplet containing a high concentration of PVP and sodium citrate, [28] and could therefore contain a different amount of organic residues. For example, from elemental analysis and porosimetry we know that a few percent of PVP is actually incorporated into the silica. [31] It is conceivable, then, that the flat silica end contains more PVP than the other surfaces. This quantity is too small, however, to detect with analytical methods.
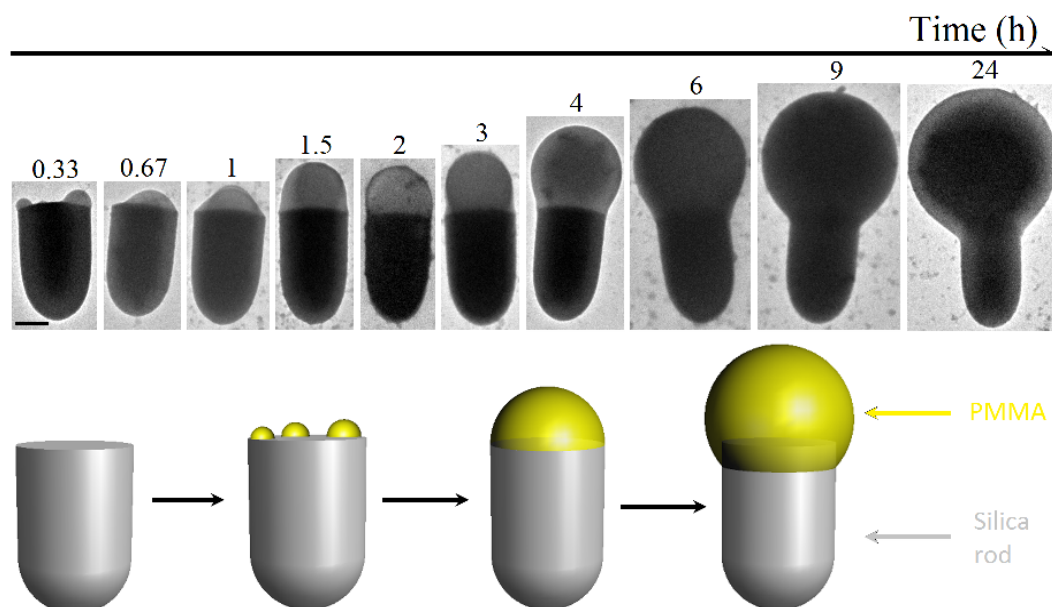
Figure 9.3. TEM images taken at intervals of the attachment and growth of a PMMA bulb onto the flat end of the silica rods. The lower row is a cartoon of the process. The scale bar is 200 nm.

The surface chemistry of the rods can be made more uniform by coating them over with an additional thin layer of silica with the usual seeded Stöber growth method (for experimental details see MAM). [33] When a 15 nm coating was applied, the edges of the silica rods also became slightly rounded, but their original shape was largely preserved. After the usual TPM treatment this thin silica coating was already enough to direct part of the PMMA toward the sides of the silica rods (see Fig. 9.4 and SF-9.7). A further increase of the silica coating to ~150 nm led to two ends with nearly the same curvature. This time PMMA formed a single bulb, but it attached to the silica rod side-on. This experiment suggests that it is mainly the surface heterogeneity that causes the location of the PMMA attachment. However, since the thickness of the silica coating still seems to influence the PMMA distribution a shape effect cannot be excluded.

A way to remove any surface heterogeneity with little change in the shape of the silica seeds is a 24-hour treatment with piranha solution. This is expected to remove any organic

residue and result in a uniform hydroxylated silica surface. However, we found that most, but not all, PMMA was still attached to the ends of the silica rods (see SF-9.8). Alternatively, a calcination step at 500 °C is expected to certainly remove all organics. After further re-hydroxylation and TPM coating steps the PMMA this time attached to the edge of the rods (see SF-9.9). Although the calcination also caused the silica edge to become slightly rounded the particle shape was largely preserved. The most likely explanation for the PMMA attachment location therefore seems to be a different surface chemistry of the flat ends as the
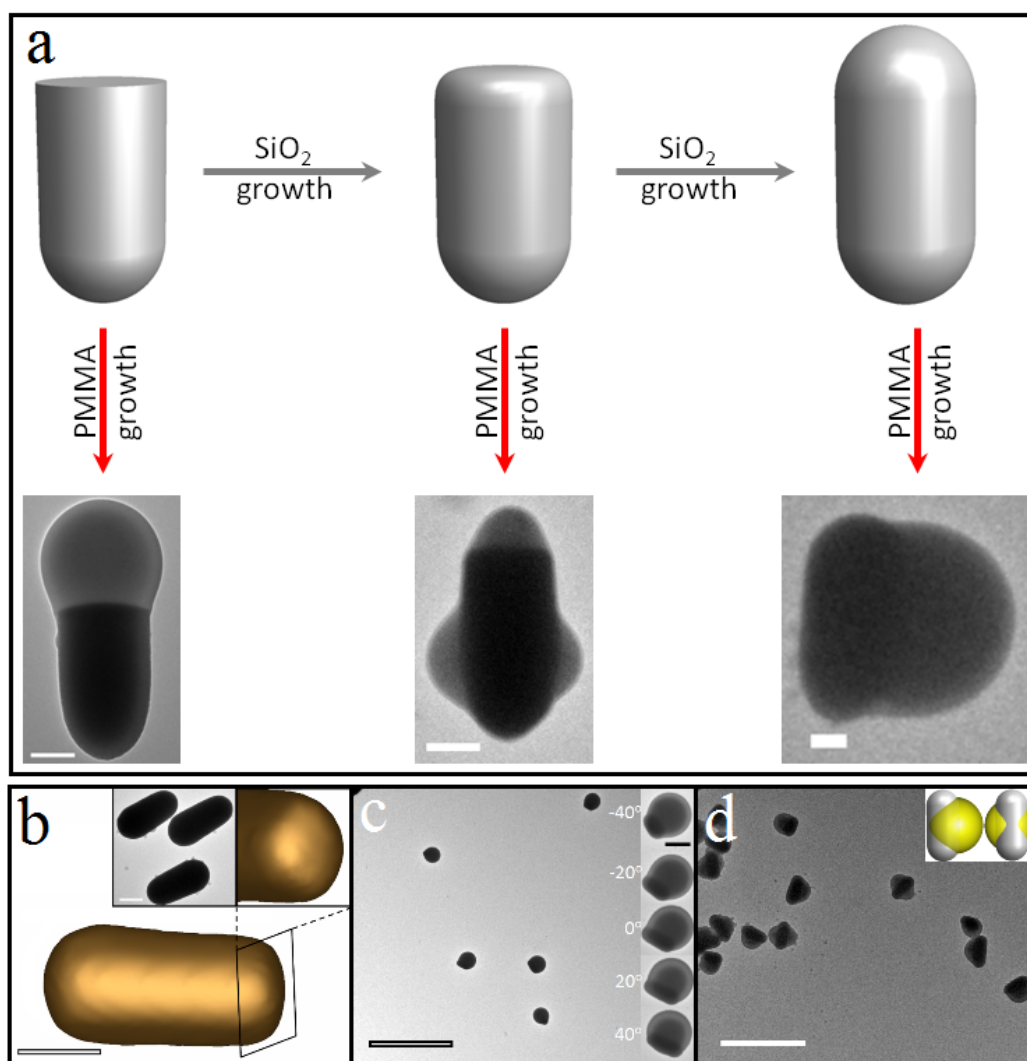
Figure 9.4. (a) Attachment of the PMMA bulb to silica rods that have been coated with an additional layer of 0, 15, and 150 nm of silica. The silica/MMA mass ratio was 9.7:1. (b) 3D electron tomography reconstruction of a single silica rod with two rounded ends due to a 150 nm coating. (c) TEM images of rods (two identical ends, $L = 1.7$ μm, and $D = 0.78$ μm) with a PMMA bulb ($D = 2.04$ μm) attached to the side of each rod. The insets are a single hybrid particle observed from different viewing angles at high resolution. (d) TEM images of hybrid particles made at a lower mass ratio of 4.85:1. The insets are schematic images of these hybrid particles at different viewing angles. The scale bar is 200 nm, 500 nm, 10 μm and 5 μm in a), b), c) and d), and 500 nm and 1 μm in the insets of b) and d), respectively.

dominant effect, with perhaps some additional influence of the particle shape. Moreover, these experiments present useful ways to manipulate the morphology of hybrid organic-inorganic particles.

9.3.2 Applications

The 'perfect' (meaning 100% effective) site-specific attachment of the as-synthesized silica rods to PMMA suggests that they could serve to stabilize these polymer particles by a mechanism similar to that in a Pickering emulsion. [45] In recent years work has shown that rod and disk shaped particles can also efficiently stabilize emulsion droplets or foam bubbles, by attaching side-on to them. [46-48] On the other hand, our silica is expected to attach with the flat end of the bullet attached to the PMMA, which would be quite unique. Therefore, we
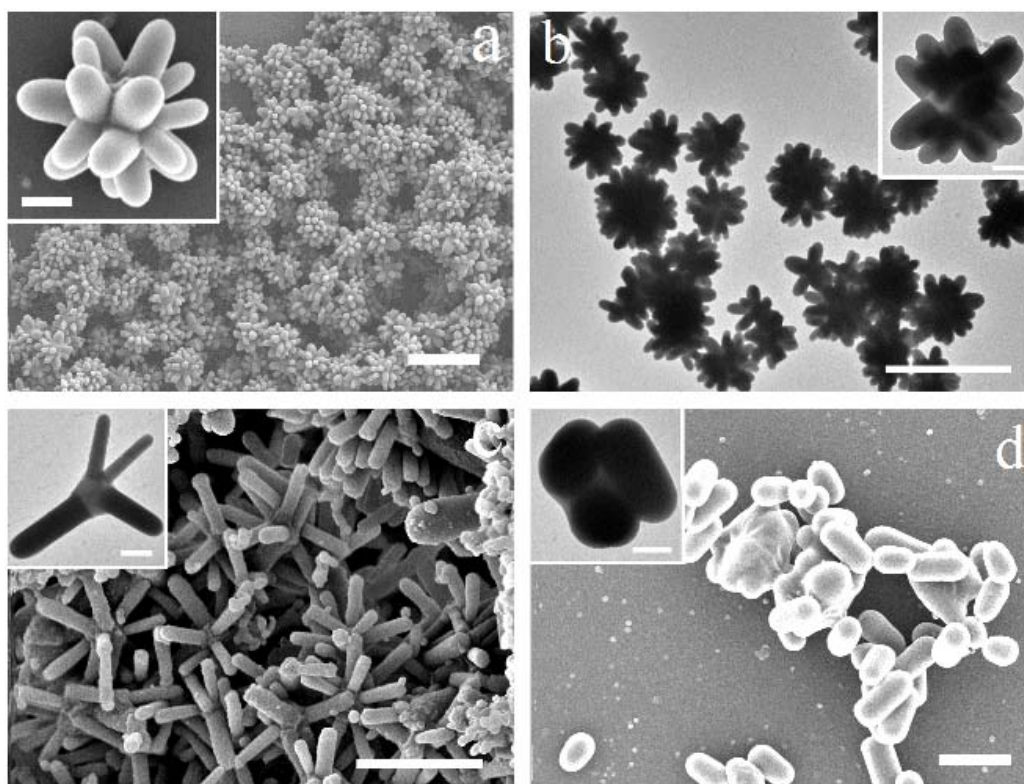
Figure 9.5. PMMA particles stabilized by silica rods instead of PVP; a) SEM and b) TEM image of short rods (aspect ratio of 1.9) stabilizing PMMA colloids prepared at a mass ratio silica to MMA of 1:4.85; c) SEM image of long rods (aspect ratio of 4.2) stabilizing the PMMA at a mass ratio of 1:2.43. The inset is a TEM image; d) SEM image of rods (aspect ratio of 2.2, coated with extra silica to produce two rounded ends) stabilizing PMMA at a mass ratio of 1:0.97. The inset is a TEM image. The scale bars are 5 μm in a) and b) and 2 μm in c) and d), and in the insets 500 nm, respectively.

again performed a dispersion polymerization of MMA in the presence of TPM-modified silica rods, but this time omitted PVP as the steric stabilizer. First, rods with a flat tip and an aspect

ratio of 1.9 were used at a silica:MMA at a weight ratio of 1:4.85. Nearly monodisperse hedgehog-shaped hybrid particles were obtained, as shown in Figure 9.5a and b. From these images, one can indeed distinguish that only the flat ends attach to the PMMA phase, as expected, and cover the whole PMMA surface. The fact that the PMMA is present as separate particles shows that the silica successfully played its role as a shape-anisotropic steric stabilizer. A similar result was obtained with longer rods (Fig. 9.5c), but a smaller amount of PMMA (silica/MMA = 1:2.43 in mass) could be stabilized. Also, fully in accordance with our observations made before for the attachment of PMM onto rods with two rounded ends (Fig. 9.5d), the stabilized quantity of monomer further declined to one fifth the amount of the short rod system (silica/MMA = 1:0.97), and all the rods were attached side-on.

9.3.3 Theoretical Support

We roughly estimated the adsorption free-energy of a bullet-shaped rod at a flat liquid-liquid interface shown in Figure 4a and b by using a triangular tessellation technique (see MAM for the method used). [43, 44] According to Eq. 9-5, for certain shaped particle, the interfacial tension (γ_{12}) of phase 1 (PMMA) and 2 (methanol), and the contact angle (θ) are necessary for the free energy calculation. In order to use this model, certain assumptions have been made: 1) the PMMA is regarded as a liquid-like phase at the reaction temperature (55°), and the interfacial tension γ_{12} is supposed the surface tension between PMMA and methanol; 2) Due to fact that methanol is completely wettable with solid PMMA, [49, 50] the interfacial tension is examined in the range of 0.1 to 0.0001 N/m; [49, 51] 3) the contact angle (θ) between TPM-SiO$_2$, PMMA and methanol is not significantly changed during the solidification of PMMA, and when PVP is present in the system; 4) The line tension is neglected according to its small value ($|\tau| \approx 10^{-11}$ N/m). [52, 53]

The contact angle of 115° ($\pm 10^{o}$) is obtained based on the TEM images of samples shown in Figure 9.2b and c. The adsorption energy minimized with respect to z as a function of the orientational angle ϕ of the particle is plotted in Figure 9.6. It is seen that a horizontal orientation has a lower energy than a perpendicular one, but the two states are separated by a large energy barrier. Even if a very small value of interfacial tension γ_{12} is adopted, *e.g.*, 0.0001 N/m, [51] the free-energy barrier over which the state from metastable switches to minimum state is still significant (744 k_BT). In our case, according to the minimum adsorption free-energy, the side-on configuration of silica particles attached to the PMMA phase is more favorable than that of the flat end-on configuration. However, the flat end-on configuration is a metastable state, minimum separated from the global minimum by a high energy barrier (several hundred k_BT). This means that once the PMMA attaches to the flat end, thermal fluctuations are insufficient to change that situation. Even when very low interfacial tensions
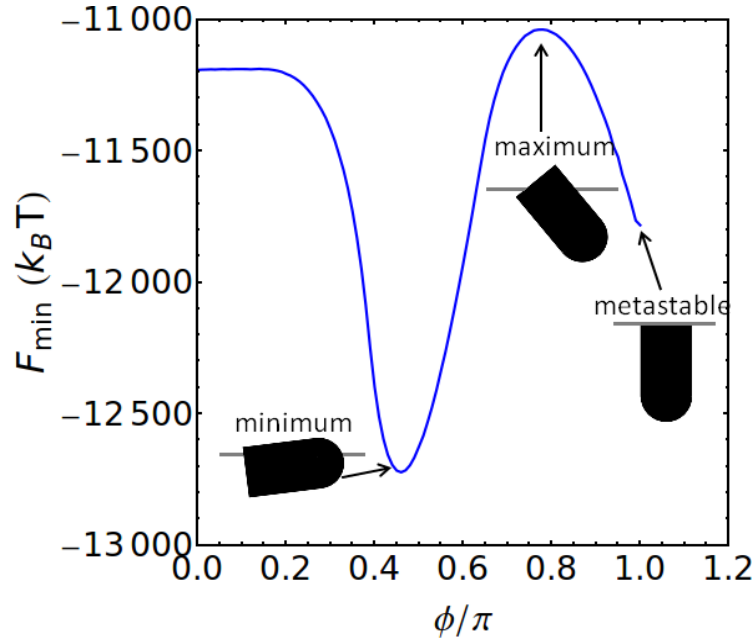
Figure 9.6. The minimum adsorption free-energy curve (F_{min}) with $\theta = 115°$ and supposed interfacial tension of 0.0001 N/m for the bullet-shaped particle ($L = 737$ nm and $D = 384$ nm) adsorbed at the interface of two liquids. The polar angle between the interfacial normal and the rotational symmetry axis of the colloids is denoted by ϕ (also see Fig. 9.1). The insets are schematic images of the configuration of the particle at the interface.
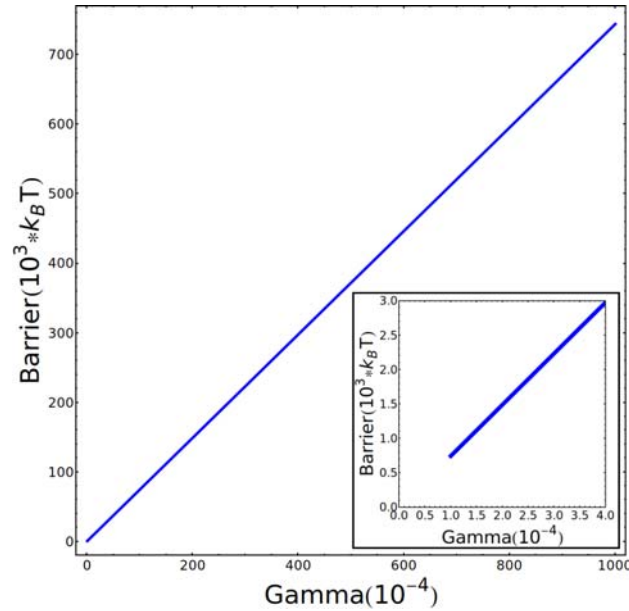

Figure 9.7. The surface free-energy barrier between the maximum and the metastable minimum as a function of interfacial tension γ_{12}, based on the simulation. The contact angle is 115°.

(down to 0.1 mN/m) are assumed (see Fig. 9.6). We also plot the adsorption energy barrier as a function of interfacial tension in Figure 9.7. It clearly shows that the energy barrier is

linearly changed with interfacial surface tension. However, our simulation cannot explain why the PMMA attaches there in the first place. We therefore conclude that the surface chemistry of the flat end is more favorable for PMMA nucleation. In other words, it implies that the surface chemical heterogeneity of the silica rod induces the PMMA nuclei preferential attaching to the flat tip of silica rod, and the high energy barrier restricts the location of PMMA bulbs only there. It is expected from these results that a site specific attachment also will occur on liquid droplets.

9.4 CONCLUSIONS

In conclusion, variously shaped hybrid silica-polymer particles were prepared via a typical dispersion polymerization of methylmethacrylate or styrene in the presence of bullet-shaped colloidal silica rods. At an early stage of the reaction the polymer nuclei preferentially attached to the flat end of the silica rods, after which they grew to form a single spherical bulb there. Upon modification of the rods by growing extra silica layers or by treatment with piranha solution or calcination, the location of polymer attachment could be changed from head-on to side-on. These experiments supplemented with a theoretical calculation show that the attachment location is mainly driven by a different surface chemistry of the flat end of the silica rods, while the geometry mainly acts to trap the polymer there. We also used this preferred attachment to produce PMMA particles from which multiple silica rods protrude perpendicularly like the spines of a hedgehog. The broken symmetry in terms of material properties of our particles along the length direction also means that it will be possible to direct the individual particles with external fields.

9.5 ACKNOWLEDGMENTS

9.6 SUPPLEMENTARY INFORMATION

9.6.1 Composite Particles
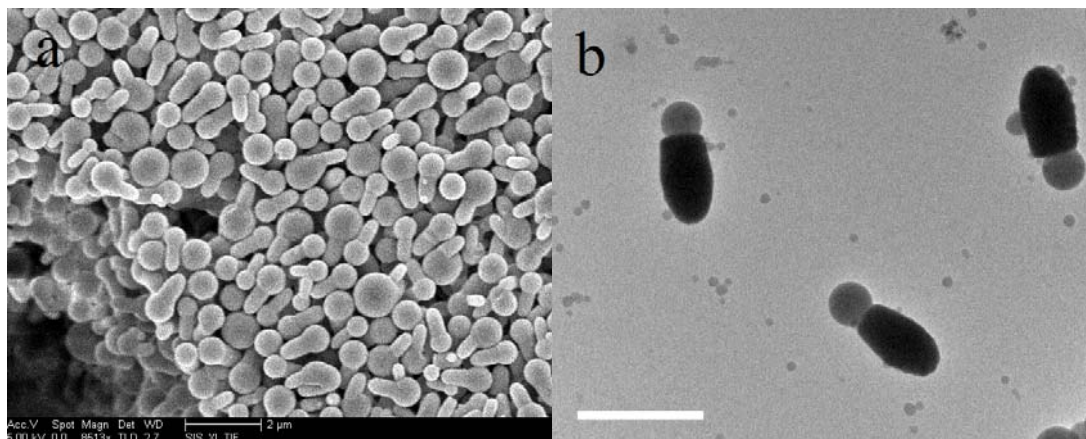
Supplementary Figure 9.1. a) Scanning electron microscopy (SEM) image of non-spherical hybrid silica-PMMA particles prepared in bulk by using the monomer (methyl methacrylate, MMA) and rods at a weight ratio of 4.85:1. This is scaling up by five times the recipe mentioned in the experimental section. The scale bar is 2 μm. b) Transmission electron microscopy (TEM) image of lollipop-shaped hybrid particles prepared by using styrene and rods at a weight ratio of 4.85:1.

9.6.2 Initial Stage of Reaction
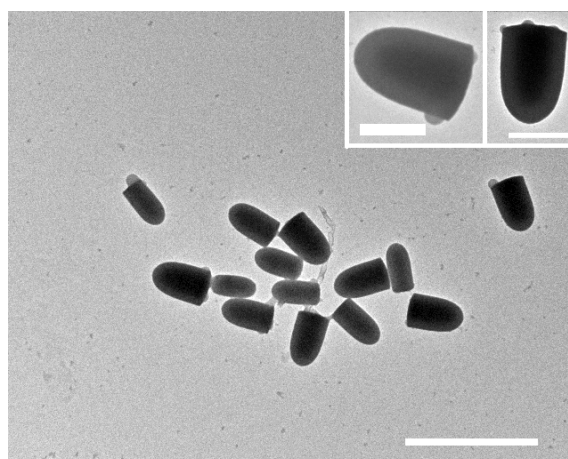
Supplementary Figure 9.2. TEM image of hybrid particles obtained 20 minutes after the start of the polymerization of MMA in the presence of silica rods as seeds. It clearly indicates the primary nuclei of monomer were preferentially, but not exclusively, attached to the flat ends of the silica rods. The scale bar is 2 μm and the insets 500 nm.
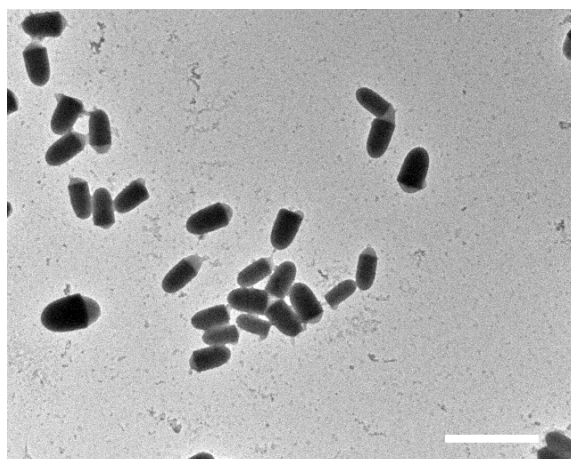
Supplementary Figure 9.3. TEM image of hybrid particles obtained 40 minutes after the start of the polymerization of MMA in the presence of silica rods as seeds. Most of the PMMA bulbs are located to the flat surface of the rods. The scale bar is 2 μm.

9.6.3 Absence of TPM
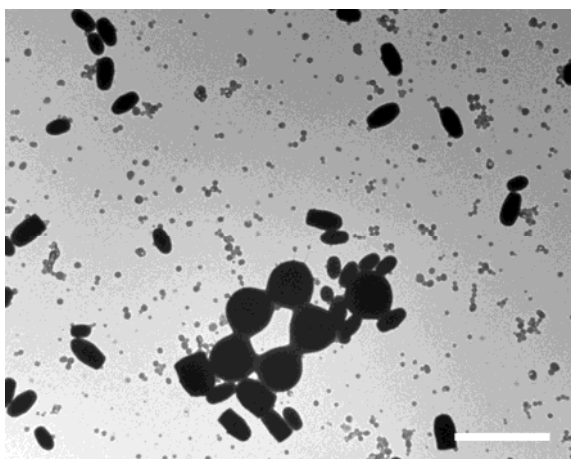
Supplementary Figure 9.4. TEM image of a system prepared with bare silica rods (without TPM treatment) and monomer (MMA). Clearly, the PMMA did not attach to the rods. The scale bar is 2 μm.

9.6.4 Silica Spheres as Seeds
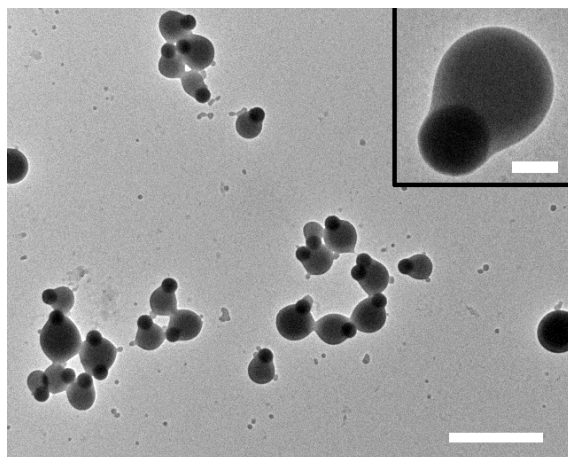
Supplementary Figure 9.5. Transmission electron microscopy (TEM) image of snowman-shaped silica-PMMA particles, made by using TPM-SiO$_2$ spheres instead of the silica rods. It indicates that the TPM modified silica surface was partly wetted with PMMA. The scale bar is 2 μm and the inset 200 nm.

9.6.5 Manipulation of Contact Angle
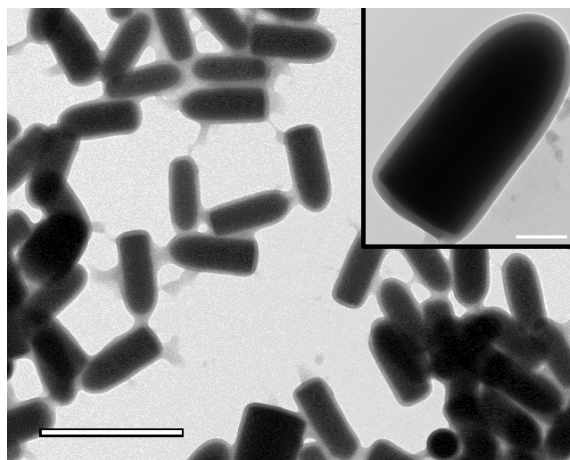
Supplementary Figure 9.6. TEM image of core-shell PMMA-silica particles prepared in apolar solvent (mixture of hexane and dodecane, the recipe is originally from ref. [32]), the scale bar is 2 μm and the inset 200 nm.

9.6.6 Shape and Surface control of Silica Rods
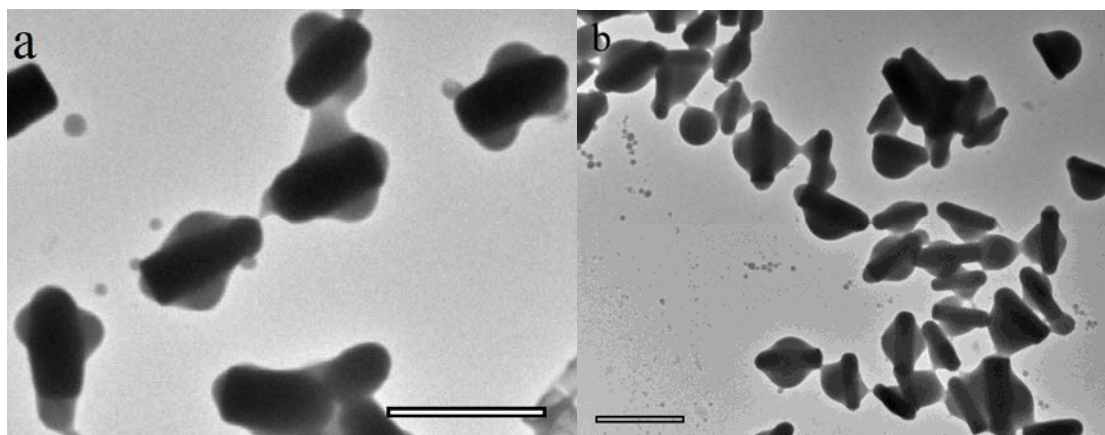
Supplementary Figure 9.7. TEM images of PMMA attached silica rods that have been coated with an additional layer of 15 nm of silica. a) short rods (aspect ratio is about 2.4); b) long rods (aspect ratio is about 3.8). The silica/MMA mass ratio was 9.7:1. The scale bars in a) and b) are 1 and 2 μm, respectively.
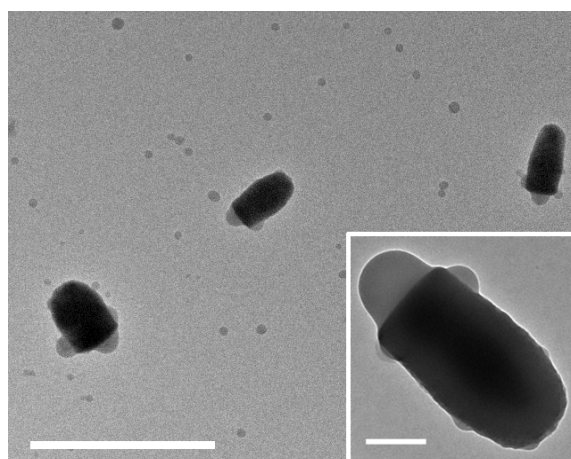
Supplementary Figure 9.8. TEM image of lollipop-shaped hybrid particles by using piranha-cleaned silica rods. Most of the PMMA is at the flat end of the silica rods, but small secondary PMMA bulbs are also present. The scale bar is 2 μm and the inset 200 nm.
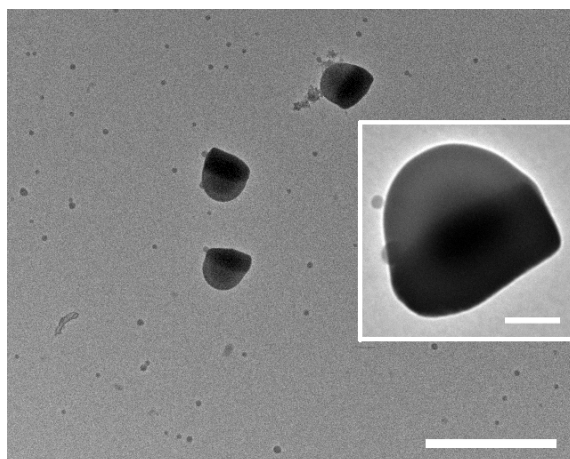
Supplementary Figure 9.9. TEM images of PMMA bulbs attached to the silica rods side-on, after the silica rods had calcined at 500 °C for 2 h. The silica/MMA mass ratio was 9.7:1. The scale bar is 2 μm, and in the inset 200 nm.

9.7 REFERENCES

[1]   Glotzer, S.; Solomon, M. *Nat. Mater.* **2007**, *6*, 557-562.

[2]   Duguet, E.; Desert, A.; Perro, A.; Ravaine, S. *Chem. Soc. Rev.* **2011**, *40*, 941-960.

[3]   Hu, J.; Zhou, S.; Sun, Y.; Fang, X.; Wu, L. *Chem. Soc. Rev.* **2012**, *41*, 4356-4378.

[4]   Perro, A.; Reculusa, S.; Ravaine, S.; Bourgeat-Lami, E.; Duguet, E. *J. Mater. Chem.* **2005**, *15*, 3745-3760.

[5]   Yan, S.; Kim, S.; Lim, J.; Yi, G. *J. Mater. Chem.* **2008**, *18*, 2177-2190.

[6]   Bourgeat-Lami, E. In *Hybrid Materials*, Kikelbick G.; Wiley-VCH Verlag GmbH & Co. KGaA, Weinheim, **2007**; Chapter 2, page 87.

[7]   Chen, X.; Shen, S.; Guo, L.; Mao S. S. *Chem. Rev.* **2010**, *110*, 6503-6570.

[8]   Kubacka, A.; Fernandez-Garcia, M.; Colon, G. *Chem. Rev.* **2012**, *112*, 1555-1614.

[9]   Amirav, L.; Alivisatos, A. P. *J. Phys. Chem. Lett.* **2010**, *1*, 1051-1054.

[10] Kim, J. -W.; Larsen, R. J.; Weitz, D. A. *J. Am. Chem. Soc.* **2006**, *128*, 14374-14377.

[11] Kim, J. -W.; Lee, D.; Shum, H. C.; Weitz, D. A. *Adv. Mater.* **2008**, *20*, 3239-3243.

[12] Kraft, D. J.; Ni, R.; Smallenburg, F.; Hermes, M.; Yoon, K.; Weitz, D. A.; van Blaaderen, A.; Groenewold, J.; Dijkstra, M.; Kegel, W. K. *Proc. Natl. Acad. Sci. USA* **2012**, *109*, 10787-10792.

[13] Vroege, G. J.; Lekkerkerker, H. N. W. *Rep. Prog. Phys.* **1992**, *55*, 1241-1309.

[14] Yin, Y.; Lu, Y.; Xia, Y. *J. Am. Chem. Soc.* **2001**, *123*, 771-772.

[15] Yin, Y.; Lu, Y.; Gates, B.; Xia, Y. *J. Am. Chem. Soc.* **2001**, *123*, 8718-8729.

[16] Zerrouki, D.; Baudry, J.; Pine, D; Chaikin, P.; Bibette, J. *Nature* **2008**, *455*, 380-382.

[17] Paunov, V. N.; Cayre, O. J. *Adv. Mater.* **2004**, *16*, 788-791.

[18] Lu, Y.; Xiong, H.; Jiang, X.; Xia, Y. *J Am. Chem. Soc.* **2003**, *125*, 12724-12725.

[19] Correa-Duarte, M. A.; Salgueirino-Maceira, V.; Rodriguez-Gonzalez, B.; Liz-Marzan, L. M.; Kosiorek, A.; Kandulski, W.; Giersig, M. *Adv. Mater.* **2005**, *17*, 2014-2018.

[20] Ohnuma, A.; Abe, R.; Shibayama, T.; Ohtani, B. *Chem. Commun.* **2007**, 3491-3493.

[21] Perro, A.; Duguet, E.; Lambert, O.; Taveau, J. C.; Bourgeat-Lami, E.; Ravaine, S. *Angew. Chem. Int. Ed.* **2009**, *48*, 361-365.

[22] Ohnuma, A.; Cho, E. C.; Camargo, P. H. C.; Au, L.; Ohtani, B.; Xia, Y. *J. Am. Chem. Soc.* **2009**, *131*, 1352-1353.

[23] Sacanna, S.; Rossi, L.; Pine, D. J. *J. Am. Chem. Soc.* **2012**, *134*, 6112-6115.

[24] Chaudhary, K.; Chen, Q.; Juarez, J. J.; Granick, S.; Lewis, J. A. *J. Am. Chem. Soc.* **2012**, *134*, 12901-12903.

[25] Qin, L.; Park, S.; Huang, L.; Mirkin, C. A. *Science* **2005**, *309*, 113-115.

[26] Wang, Y.; Hernandez, R. M.; Bartlett, D. J.; Bingham, J. M.; Kline, T. R.; Sen, A.; Mallouk, T. E. *Langmuir* **2006**, *22*, 10451-10456.

[27] Li, X.; Wang, T.; Zhang, J.; Zhu, D.; Zhang, X.; Ning, Y.; Zhang, H.; Yang, B. *ACS Nano* **2010**, *4*, 4350-4360.

[28] Kuijk, A.; van Blaaderen, A.; Imhof, A. *J. Am. Chem. Soc.* **2011**, *133*, 2346-2349.

[29] He, J.; Hourwitz, M. J.; Liu, Y.; Perez, M. T.; Nie, Z. *Chem. Comm.* **2011**, *47*, 12450-12452.

[30] He, J.; Yu, B.; Hourwitz, M. J.; Liu, Y.; Perez, M. T.; Yang, J.; Nie, Z. *Angew. Chem. Int. Ed.* **2012**, *51*, 3628-3633.

[31] Kuijk, A. Ph. D. thesis, **2012**.

[32] Antl, L.; Goodwin, J. W.; Hill, R. D.; Ottewill, R. H. *Colloids and Surface* **1986**, *17*, 67-78.

[33] Stöber, W.; Fink, A.; Bohn, E. *J. Colloid Interface Sci.* **1968**, *26*, 62-69.

[34] Philips, A. P.; Vrij, A. *J. Colloid Interface Sci.* **1989**, *128*, 121-136.

[35] Dassanayke, U.; Fraden, S.; van Blaaderen, A. *J. Chem. Phys.* **2000**, *112*, 3851-3858.

[36] Kremer, J. R.; Mastronarde, D. N.; McIntosh, J. R. *J. Struct. Biol.* **1996**, *116*, 71-76.

[37] Mastronarde, D. N. *J. Struct. Biol.* **1997**, *120*, 343-352.

[38] de Graaf, J.; Dijkstra, M.; van Roij, R. *Phys. Rev. E* **2009**, *80*, 051405.

[39] de Graaf, J.; Dijkstra, M.; van Roij, R. *J. Chem. Phys.* **2010**, *132*, 164902.

[40] Young, T. *Phil. Trans. R. Soc. Lond.* **1805**, *95*, 65-87.

[41] Kegel, W. K.; van Blaaderen, A. *Science* **2000**, *287*, 290-293.

[42] Bourgeat-Lami, E.; Lang, J. *J. Colloid. Interface Sci.* **1998**, *197*, 293-303.

[43] Bourgeat-Lami, E.; Lang, J. *J. Colloid. Interface Sci.* **1999**, *210*, 281-289.

[44] Nguyen, D.; Ravaine, S.; Bourgeat-Lami, E.; Duguet, E. *J. Mater. Chem.* **2010**, *20*, 9392-9400.

[45] Pickering, S. U. *J. Chem. Soc., Trans.* **1907**, *91*, 2001-2021.

[46] Noble, P. F.; Cayre, O. J.; Alargova, R. G.; Velev, O. D.; Paunov, V. N. *J. Am. Chem. Soc.* **2004**, *126*, 8092-8093.

[47] Bon S. A. F.; Colver, P. J. *Langmuir* **2007**, *23*, 8316-8322.

[48] Zhou, W.; Cao, J.; Liu, W.; Stoyanov. S. *Angew. Chem. Int. Ed.* **2009**, *48*, 378-381.

[49] Dann, J. R. *J. Colloid Interface Sci.* **1970**, *32*, 302-319.

[50] Zdziennicka, A. *Colloid Surface A.* **2010**, *367*, 108-114.

[51] Zisman, W. A. *Contact angle wettability and adhension*, in: Advances in Chemistry Series, vol. 43, American Chemical Society, Washington, DC, **1964**, pp. 1-51.

[52] Rowlinson, J. S.; Widom, B. *Handbook of Surface and Colloid Chemistry*. Dover Publication (Midneola), 1st edition, **2003**.

[53] Amirfazli, A.; Neumann, A. W. *Adv. Colloid Interface Sci.* **2004**, *110*, 121-141.

Summary

The main subject of this thesis is the structure control of polymer particles, in particular, poly(methyl methacrylate) (PMMA) particles, by dispersion polymerization. This structure control, ranging from control over surface morphology and internal structure to shape manipulation of polymer particles, was attempted through copolymerization of monomers with various types of materials, such as cross-linkers, dyes, and silica spheres and rods. The obtained spherical and nonspherical particles were applicable as model systems for exploiting phase behaviors in the presence or absence of external fields (such as electric and gravity fields), and for various other applications.

Spherical particles are extensively used for experimental studies, because of their mature synthetic strategies. Using uniform spherical particles to start with, a number of diverse monodisperse anisotropic (in shape or composite) particles can be developed. In **Chapter 2**, we first described a simple approach in which the 'problematic' reagents (for example, cross-linker and dyes) were maintained at a low concentration level either before or after the sensitive nucleation stage of the dispersion polymerization, which ultimately, led to a core-shell or homogeneous structure merely depending on the addition start time of problem reagent. The obtained PMMA particles in polar environments were up to micron-sized and fluorescently labeled, providing a possibility of studying their phase behavior in 3D with the aid of confocal scanning laser microscopy (CSLM), because due to the scattering of the system being effectively eliminated as well as the use of fluorescent dyes, one can directly observe them on a single-particle level to obtain insight into colloidal structures and dynamics or even concentrated dispersions and study their phase behavior in real space. PMMA is much easier to refractive index and density match than other materials (for example silica and polystyrene PS). The successful transfer of these polar environment favoring PMMA particles to apolar solvents (hexane, decahydronaphthalene (decalin) and cyclohexyl bromide) with the help of a nonionic surfactant (Span 80) gave rise to a detailed observation of a gradual change from a core-shell to a homogeneous structure which was further confirmed by swelling experiments with a good solvent (tetrahydrofuran (THF)), because the disturbance from scattering was largely eliminated by combining PMMA with refractive index matching solvents (decalin, cyclohexyl bromide). In addition, the particle size ranging from sub-micron to micron, was precisely adjusted by simply tuning the concentration of cross-linker (ethylene glycol dimethacrylate, EGDMA) in the range from 1 to 10 wt% with respect to the monomer

(methyl methacrylate, MMA) and the weight ratio of the polar solvents methanol and water. Finally, these PMMA particles could be permanently bound into flexible strings by application of a heating step in a high frequency electric field.

The cross-linker (EGDMA) density used in Chapter 2 is not higher than 10 wt%. In **Chapter 3**, initially, a higher concentration (> 10 wt% with respect to monomer mass) of EGDMA was copolymerized with monomer (MMA) aiming for highly cross-linked PMMA particles. Particles with several primary dimples and a rough surface were obtained, which led us to switch to using an alternative cross-linker, divinylbenzene (DVB), commonly used in the preparation of cross-linked polystyrene (PS) systems. We found that the DVB instantaneously copolymerized with monomer after the nucleation stage, giving rise to a rigid cross-linked shell. The transformation in density from liquid (MMA) to solid (PMMA) induced by polymerization caused an 'outward shrinkage' of the system. Finally [[By using 'finally', it appears as if you present a new result here, but I think you mean to say that this outward shrinkage could result in a void being produced. Suggestion: 'This shrinkage could lead to a void in each particle']], a void was produced. By varying the cross-linker density and addition start time of DVB, the sizes of both the voids and the particles were precisely controlled. Subsequently, we employed this simple one-step manner more generally, ranging from various types of polymerization methods (surfactant-free emulsion, dispersion and precipitation polymerization) and diverse kinds of materials (polystyrene, poly(*N*-isopropylacrylamide) and PMMA) to differently shaped (snowman, dumbbell, inverted-snowman, linear trimeric and multi-pod like) particle syntheses. In addition, the obtained hollow particles were robust enough to not collapse even when they were dried, and scaling up did not result in a reduction in uniformity in size and yield of particles.

In **Chapter 4**, we described a variety of circumstances under which a series of atypically shaped PMMA particles were produced. The experimental conditions used in this chapter were based on those in Chapter 2, but only a slight change in recipe resulted in a completely deviated outcome (non-spherical particles). After carrying out a comprehensive investigation, we summarized the empirical recommendations for preparing spherical particles with a smooth surface. These recommendations involved maintaining the concentration of cross-linker (EGDMA for PMMA system and DVB for PS) below a relatively low level during the polymerization; or narrowing the difference of solubility parameter between the polymer and solvent media and further influencing the polymerization locus away from the growing particles during the polymerization; or using either a high concentration or a longer stabilizer; or a combination of all of these. Benefiting from these experiences, spherical polymer particles with a smooth surface were successfully fabricated. Alternatively, dented

spheres or particles covered with nodules, or a combination of both were found. Based on the conclusions given in Chapter 2 and 3, a possible formation mechanism was proposed, which is probably useful for a better understanding of copolymerization in dispersion polymerization and for guiding researchers to design functional polymer particles that are more promising.

Inspired by the observation that the swelling ratio of core-shell cross-linked PMMA spheres was larger than that of homogeneously cross-linked particles, which we demonstrated in Chapter 2, a series of experiments were designed for the synthesis of snowman- or dumbbell-shaped particles in **Chapter 5**. Upon absorbing monomer (MMA) droplets from the monomer emulsion, the cross-linked particles were over-swollen and a subsequent heating step induced the excess monomer to phase-separate in the form of a protrusion, which can subsequently be solidified with a polymerization treatment. This method was called seeded emulsion polymerization. The initial trial focused on a system of homogeneously cross-linked particles which resulted in only nonspherical particles with either a single small protrusion or multiple protrusions. In order to yield dumbbell- or inverted snowman- (in which the protrusion is bigger than the seed) shaped particles, core-shell cross-linked PMMA particles were used as seeds. As we expected, dumbbell- and snowman-shaped particles were successfully synthesized. Subsequently, fluorescent labeling made these dumbbell particles good candidates for 3D imaging with CLSM. A similar transfer of dumbbell particles from a polar to an apolar solvent, aided by a surfactant Span 85, was successfully carried out, as we did in Chapter 2. We found that the dumbbell particles organized into a so-called plastic crystal where the particles are positionally ordered but orientationally disordered. These plastic crystals were discussed in detail in Chapter 9. Additionally, aided by a high-frequency AC electric field the resulting non-spherical particles were able to self-assemble into semi-flexible permanently bonded colloidal chains in a polar solvent (formamide). These chains are interesting as polymer model analogs at a visible colloidal scale.

An extension of seeded emulsion polymerization as mentioned in Chapter 5, was exploited in **Chapter 6** by using fully and highly cross-linked (2 wt%) PMMA particles as seeds. The large size (~3 μm in diameter) of the seeds allowed for real-time monitoring of the formation of liquid protrusions with optical microscopy. We observed the formation of two situated on opposite sides of the central seed particle, due to the fusion of small monomer droplets as well as geometry factors. This metastable configuration was easily permanently 'captured' through a subsequent polymerization treatment. We named these structured particles linear trimeric particles (LTPs). In addition, again aided by surfactant in combination with a dye, we could observe the real-space behavior of LTPs in an index matching solvent (decalin). Similarly, plastic crystals were found in this system as well. During the synthesis of LTPs, coalescence

of PMMA seeds with liquid protrusions upon collision, induced by external disturbance (stirring), was inevitable. We also studied the structure of clusters with different number of seed particles by 3D modeling. These colloidal clusters are interesting candidates for isomeric molecule modeling.

The dumbbell and snowman shaped PMMA particles described in Chapter 5 are ideal building blocks for packing experiments. **In Chapter 7**, a water-in-oil emulsion technique was applied for packing spherical and nonspherical particles. Due to the nature of dumbbell and snowman particles, they preferred staying at the interface between water and oil phase. The subsequent gradual loss of water caused by heating led to a close packing of particles. After separation, a variety of clusters was classified by n (where n is the number of particles in the packing unit). For clusters made from spheres, a unique structure was found corresponding to each n; for the dumbbell system, the configurations of clusters built of n dumbbells were similar to those of clusters with $2n$ spheres up to $n = 5$. Less or no similarity was found when n was greater than 5. For the system of snowman particles, the main frame of the clusters was determined by the big bulbs of the snowman particles, while the small bulbs were positioned more randomly. In addition, results from Monte Carlo simulations were consistent with these findings.

We continued the investigation of plastic crystals firstly demonstrated in Chapters 5 and 7, and exhibited detailed results in **Chapter 8**. In this chapter, we transferred the fluorescent PMMA dumbbells into an apolar ($\varepsilon \approx 2.2\ \varepsilon_0$), refractive index matching and density almost matching solvent (decalin) assisted by the nonionic surfactant we used earlier, Span 85. The dumbbells were far apart and a computer algorithm for rods was used to track both the projected position and orientation parameters of our dumbbell system in 2D. The results showed a high crystalline order not only exhibited by the average position of the particles, but also by their positions in individual images, while the orientations of the particles were completely disordered. This confirmed the formation of plastic crystals in 2D. Thanks to the refractive index matching, we were able to image many layers deep into the crystals. We found a random hexagonal close packing structure in 3D in these plastic crystals. Subsequently, a high-frequency AC electric field was used to align the orientation of the plastic crystals along the direction of the electric field. Modest control has been achieved, thus providing a potential for switchable photonic crystals.

In the end, we 'jumped' the research topic from the domain of dumbbell-, snowman- or similarly shaped particles to the area of composite particles in **Chapter 9**. We showed that a combination of geometrical and surface chemical anisotropy anchored growth of polymer on bullet-shaped silica rods. These bullet-shaped silica particles were used as seeds for the

growth of polymer in dispersion polymerization. After modifying the surface of the silica particles, the subsequent growth of polymer was observed to occur exclusively at the flat tip of silica rods. By carrying out a series of experiments and computer simulations, we discovered that this exclusive growth location is due to surface heterogeneity and low curvature. In addition, an extended use of this property was applied to achieve stabilizer-free dispersion polymerization with silica rods instead of a chemical stabilizer. All silica rods were found standing out perpendicularly from the surface of a PMMA particle, thus forming porcupine-like composite particles.

Samenvatting

Het voornaamste onderwerp van dit proefschrift is de structuurbeheersing van polymeerdeeltjes, in het bijzonder poly(methylmethacrylaat) (PMMA-)deeltjes, met behulp van dispersiepolymerisatie. Deze structuurbeheersing, uiteenlopend van het beheersen van de oppervlakmorfologie en de interne structuur tot het beïnvloeden van de vorm van de polymeerdeeltjes, hebben we nagestreefd met behulp van copolymerisatie van monomeren met verschillende materialen, met name crosslinker, kleurstof en silicabollen en -staafjes. De verkregen bolvormige en niet-bolvormige deeltjes waren toepasbaar als modelsystemen voor het exploiteren van fasegedrag in de af- of aanwezigheid van externe velden (zoals elektrische of gravitationele velden), en voor verscheidene andere toepassingen.

Bolvormige deeltjes worden op grote schaal gebruikt in experimenteel onderzoek vanwege de vergevorderde synthesestrategieën voor hun synthese. Met uniforme bolvormige deeltjes als beginpunt kunnen diverse monodisperse anisotrope (van vorm of samenstelling) deeltjes vervaardigd worden. In **Hoofdstuk 2** hebben eerst een eenvoudige aanpak beschreven waarmee de 'problematische' reactanten (bijvoorbeeld crosslinker en kleurstoffen) vóór ofwel na het gevoelige nucleatiestadium van de dispersiepolymerisatie op een laag concentratieniveau konden worden gehouden, hetgeen uiteindelijk leidde tot een kern-schil- of homogene structuur, afhankelijk van slechts het tijdstip waarop begonnen werd met het toevoegen van het probleemreactant. De verkregen PMMA-deeltjes in een polaire omgeving waren tot aan enkele microns in grootte en fluorescent gelabeld, zodat het mogelijk was om hun fasegedrag in 3D te bestuderen met behulp van confocale laserfluorescentiemicroscopie (CSLM) omdat, vanwege zowel het feit dat de verstrooiing in het systeem vrijwel weggewerkt was alsook het gebruik van fluorescente kleurstoffen, het mogelijk was om hen rechtstreeks op het niveau van enkele deeltjes te observeren en zodoende inzicht te krijgen in colloïdale structuren en dynamica of zelfs geconcentreerde dispersies en hun fasegedrag in positieruimte. Het index- en dichtheidsmatchen van PMMA is veel gemakkelijker dan van andere materialen (bijvoorbeeld silica en polystyreen (PS)). Door deze PMMA-deeltjes, die een polaire omgeving prefereren, over te plaatsen naar apolaire oplosmiddelen (hexaan, decahydronaftaleen (decaline) en cyclohexylbromide) met behulp van een niet-ionisch surfactant (Span 80) werd het mogelijk om de geleidelijke overgang van een kern-schilstructuur naar een homogene structuur nauwkeurig waar te nemen. Deze overgang

werd nader bevestigd door zwelexperimenten met een goed oplosmiddel (tetrahydrofuraan (THF)), omdat de verstoring door verstrooiing bijna geheel was weggewerkt door PMMA te combineren met brekingsindexmatchende oplosmiddelen (decaline en cyclohexylbromide). Bovendien werd de deeltjesgrootte, uiteenlopend van submicron tot micron, nauwkeurig versteld door simpelweg de concentratie crosslinker (ethyleenglycoldimethacrylaat, EGDMA) bij te stellen, in een bereik van 1 tot 10% (m/m) ten opzichte van het monomeer (methylmethacrylaat, MMA) en de gewichtsverhouding van de polaire oplosmiddelen methanol en water. Tenslotte konden deze PMMA-deeltjes permanent gebonden worden in flexibele kettingen door een verhittingsstap toe te passen in een hoogfrequent elektrisch veld.

De crosslinkerdichtheid (EGDMA) gebruikt in Hoofdstuk 2 is niet hoger dan 10% (m/m). In **Hoofdstuk 3** werd eerst een hogere concentratie (> 10% (m/m) ten opzichte van de monomeermassa) van EGDMA gecopolymeriseerd met een monomeer (MMA), met in hoge mate gecrosslinkte PMMA-deeltjes als doel. Deeltjes met enkele primaire kuiltjes en een ruw oppervlak waren het gevolg, hetgeen ons naar een alternatieve crosslinker deed overschakelen, namelijk divinylbenzeen (DVB), dat vaak wordt gebruikt voor de bereiding van polystyreen-(PS-)systemen. We ontdekten dat het DVB onmiddellijk copolymeriseerde met monomeer na het nucleatiestadium, resulterend in een harde gecrosslinkte schil. De verandering in dichtheid van vloeistof (MMA) tot vaste stof (PMMA), teweeggebracht door polymerisatie, zorgde voor een naar buiten toe gerichte krimp van het systeem. Uiteindelijk ontstond zo een holte in elk deeltje. Door de dichtheid van crosslinker en het tijdstip waarop begonnen werd met het toevoegen van DVB te variëren konden de groottes van zowel de holtes als de deeltjes nauwkeurig beheerst worden. Vervolgens gebruikten we deze éénstapsmethode algemener, uiteenlopend van diverse soorten polymerisatiemethoden (surfactantvrije emulsie-, dispersie- en bezinkselpolymerisatie) en verscheidene materiaalsoorten (polystyreen, poly(*N*-isopropylacrylamide) en PMMA) tot de synthese van deeltjes met diverse vormen (gelijkend op sneeuwpoppen, dumbbells, geïnverteerde sneeuwpoppen, lijnvormige trimeren of multi-pods). Bovendien waren de verkregen holle deeltjes stevig genoeg om niet in te storten, zelfs niet als ze werden gedroogd, en opschaling resulteerde niet in een vermindering van de gelijkmatigheid in grootte of de opbrengst van deeltjes.

In **Hoofdstuk 4** hebben we een veelvoud aan omstandigheden beschreven waaronder een reeks PMMA-deeltjes met atypisch vormen onstonden. De in dit hoofdstuk gebruikte experimentele condities zijn gebaseerd op die uit Hoofdstuk 2, maar slechts een kleine verandering in het recept leidde tot een geheel andere uitkomst (niet-bolvormige deeltjes). Na een veelomvattend onderzoek uitgevoerd te hebben, hebben we enkele empirische aanbevelingen samengevat voor het bereiden van bolvormige deeltjes met een glad oppervlak.

We bevolen aan om de concentratie crosslinker (EGDMA voor een PMMA-systeem en DVB voor PS) onder een bepaald niveau te houden; of het verschil in oplosbaarheidsparameter tussen het polymeer en het oplosmedium te verkleinen en zo de polymerisatielocus verder van de groeiende deeltjes weg te bewegen tijdens de polymerisatie; of om gebruik te maken van een hogere concentratie of een langere stabilisator; of een combinatie van de voorgaande opties. Profiterend van deze ervaring hebben we met succes gladde bolvormige polymeerdeeltjes gefabriceerd. Aan de andere kant vonden we ook deeltjes met kuiltjes of deeltjes bedekt met knoesten, of een combinatie van beide. Gebaseerd op de conclusies van Hoofdstuk 2 en 3 hebben we een mogelijk formatiemechanisme voorgesteld, dat waarschijnlijk nut kan hebben voor een beter begrip van copolymerisatie in dispersiepolymerisatie en voor het leiden van auteurs naar het ontwerpen van gefunctionaliseerde polymeerdeeltjes die meer veelbelovend zijn.

Geïnspireerd door de observatie dat de zwelverhouding van gecrosslinkte kern-schil-PMMA-deeltjes groter was dan die van homogeen gecrosslinkte deeltjes, hetgeen we lieten zien in Hoofdstuk 2, ontwierpen we een aantal experimenten voor de synthese van sneeuwpop- of dumbbellvormige deeltjes in **Hoofdstuk 5**. Door druppeltjes monomeer (MMA) te absorberen uit de monomeeremulsie werden de gecrosslinkte deeltjes overmatig opgezwollen en een daaropvolgende verhittingsstap deed het overtollige monomeer fasescheiden in de vorm van een uitstulping, die vervolgens kon worden verhard door een polymerisatiebehandeling. Deze methode heet gekiemde emulsiepolymerisatie. De eerste test focuste zich op een systeem van homogeen gecrosslinkte deeltjes, hetgeen resulteerde in alleen niet-bolvormige deeltjes met ofwel een enkele kleine uitstulping, ofwel meerdere uitstulpingen. Om deeltjes met een dumbbell- of geïnverteerde sneeuwpopvorm (waarin de uitstulping groter is dan het kiemdeeltje) te verkrijgen, werden gecrosslinkte kern-schil-PMMA-deeltjes gebruikt als kiem. Zoals verwacht werden de dumbbell- en sneeuwpopvormige deeltjes met succes gesynthetiseerd. Vervolgens maakte fluorescente labeling deze dumbbelldeeltjes goede kandidaten om te imagen met CLSM. We voerden met succes een overplaatsing soortgelijk aan degene die we in Hoofdstuk 2 toepasten, van een polair naar een apolair oplosmiddel met de hulp van het surfactant Span 85, uit, en ontdekten dat de dumbbelldeeltjes zich organiseerden in een zogeheten plastic kristal, waarin de deeltjes qua positie geordend zijn, maar qua oriëntatie niet. Deze plastic kristallen hebben we nauwkeurig beschreven in Hoofdstuk 9. Geholpen door een hoogfrequent wisselend elektrisch veld waren de niet-bolvormige deeltjes in staat om te zelfassembleren in semi-flexibele permanent gebonden colloïdale kettingen in een polair oplosmiddel (formamide). Deze kettingen zijn interessant als modelsystemen voor polymeren, op een zichtbare, colloïdale

schaal.

Een uitbreiding van gekiemde emulsiepolymerisatie, genoemd in Hoofdstuk 5, werd geëxploiteerd in **Hoofdstuk 6** door geheel en in hoge mate gecrosslinkte PMMA-deeltjes als kiem te gebruiken. De aanzienlijke grootte (de diameter was ongeveer 3 μm) van de kiemdeeltjes maakte het mogelijk om de vorming van vloeibare uitstulpingen realtime te observeren met optische microscopie. We zagen de vorming van twee uitstulpingen op tegenoverliggende kanten van het centrale kiemdeeltje, als gevolg van de fusie van kleine monomeerdruppeltjes en ook geometrische factoren. Deze metastabiele configuratie kon gemakkelijk permanent 'gevangen' worden door een opvolgende polymerisatiebehandeling. We noemden deze gestructureerde deeltjes lineaire trimerische deeltjes (LTDs). Nogmaals geholpen door een surfactant met een kleurstof konden we het gedrag van de LTDs in een index-matching oplosmiddel (decaline) in positieruimte observeren. Ook in dit systeem vonden we een plastic kristal. Door botsingen tussen de vloeibare uitstulpingen op de PMMA-deeltjes als gevolg van externe verstoringen (roeren) tijdens de synthese van de LTDs was samenklontering onvermijdbaar. We bestudeerden ook de structuur van deze clusters met verschillende hoeveelheden kiemdeeltjes, met behulp van 3D-modellen. Deze colloïdale clusters zijn interessante kandidaten voor isomerische molecuulmodellering.

De PMMA-deeltjes met een dumbbell- of sneeuwpopvorm, beschreven in Hoofdstuk 5, zijn ideale bouwblokken voor stapelingsexperimenten. In **Hoofdstuk 7** pasten we een water-in-olie-emulsietechniek toe voor stapeling van bolvormige en niet-bolvormige deeltjes. Als gevolg van de aard van dumbbell- en sneeuwpopvormige deeltjes bleven ze bij voorkeur op het grensvlak tussen de water- en de oliefase. Het daaropvolgende geleidelijke verlies van water door verhitting zorgde voor een dichte stapeling van deeltjes. Na scheiding classificeerden we een verscheidenheid aan clusters aan de hand van *n,* het aantal deeltjes in de clustereenheid. Voor clusters gemaakt van bollen vonden we voor elke waarde van *n* een unieke structuur; voor het dumbbellsysteem waren de configuraties van clusters opgebouwd uit *n* dumbbells vergelijkbaar met die van clusters van 2*n* bollen, voor *n* < 5. We vonden minder, of geen enkele, overeenkomst voor *n* > 5. Voor systemen van sneeuwpopdeeltjes werd de hoofdstructuur bepaald door de grote bollen van de sneeuwpopdeeltjes, terwijl hun kleine bollen zich meer willekeurig positioneerden. Tevens bleken de resultaten van de Monte Carlo-simulaties consistent met deze bevindingen.

We zetten het onderzoek van plastic kristallen, die we lieten zien in Hoofdstuk 5 en 7, voort en toonden gedetailleerde resultaten in **Hoofdstuk 8**. In dit hoofdstuk brachten we de fluorescente PMMA-dumbbells over naar een apolair ($\varepsilon \approx 2.2\ \varepsilon_0$), brekingsindexmatchend en bijna dichtheidsmatchend oplosmiddel (decaline), geholpen door het niet-ionische surfactant

dat we eerder gebruikten, Span 85. De dumbbells waren ver van elkaar verwijderd en we gebruikten een computeralgoritme voor staafjes om zowel de geprojecteerde posities in de individuele beelden alsook de oriëntatieparameters van ons dumbbellsysteem te volgen in 2D. De resultaten lieten een hoge mate van kristallijne orde zien, niet alleen wat betreft de gemiddelde posities van de deeltjes maar ook wat betreft hun posities in de individuele beelden, terwijl de oriëntaties van de deeltjes volledig wanordelijk waren. Hiermee bevestigden we de vorming van een plastic kristal in 2D. Dankzij het brekingsindexmatchen waren we in staat tot vele lagen diep in de kristallen te kijken. We vonden een willekeurig hexagonale dichte stapeling in 3D in deze plastic kristallen. Vervolgens werd een hoogfrequent wisselend elektrisch veld gebruikt om de oriëntatie van het plastic kristal uit te lijnen in de richting van het elektrisch veld. Een bescheiden beheersing werd bereikt, hetgeen dus een mogelijkheid vormt voor schakelbare fotonische kristallen.

Aan het eind sprongen we van het terrein van dumbbell-, sneeuwpop- of gelijksoortig gevormde deeltjes naar dat van composietdeeltjes in **Hoofdstuk 9**. We lieten zien dat een combinatie van geometrische en oppervlakchemische anisotropie de groei van polymeren op kogelvormige silicastaafjes verankerde. Deze kogelvormige silicadeeltjes werden gebruikt als kiemdeeltjes voor de groei van polymeer in dispersiepolymerisatie. Na het veranderen van het oppervlak van de silicadeeltjes zagen we dat de daaropvolgende polymeergroei uitsluitend plaatsvond op de platte uiteindes van de silicastaafjes. Door een reeks experimenten en computersimulaties uit te voeren, ontdekten we dat deze exclusieve groeilocatie het gevolg is van de heterogeniteit van het oppervlak en de lage kromming. Deze eigenschap pasten we ook toe om stabilisatorvrije dispersiepolymerisatie te bereiken met silicastaafjes in plaats van een chemische stabilisator. Alle silicastaafjes bleken loodrecht op het oppervlak van het PMMA-deeltje te staan, en het geheel vormde zo stekelvarkenachtige composietdeeltjes.

Acknowledgements

After four years' working and studying, and a half year struggling writing at Soft Condensed Matter group in Utrecht University, although it is hard to believe, this thesis is close to the end. Undoubtedly, I cannot bring this thesis into being alone. In this journey of four and a half years, many people help me in innumerable ways, and I take this opportunity to express my deepest gratitude to all of them who have helped me and directly or indirectly contributed to this thesis.

First, I am indebted to my supervisor, Alfons van Blaaderen. Thank you for offering me a Ph.D. position in your group and collaborating with you. Discussion with you always broadened my knowledge in both professional and universal domains. I am also grateful to your patience for reading all my manuscripts, and very useful guidance for how to write a scientific paper, which indeed deepened my cognition scope of this colorful scientific realm. At the end of last year (2012), it was my honor to company with your for three days visit around Shanghai in China. Also, my sincere gratitude goes to my daily supervisor, Arnout Imhof, thanks for offering me the opportunity to pursue my Ph.D. degree with you and such an interesting research topic, and for giving me endless support and enough freedom in pursing my research without any restrictions. The door of your office was always open for me to have a discussion, and your encouragement and inspiration always helped me fixing out the problem and out of the trouble over my four and a half years research life. Thanks for your patience with which you have read over and over again all my manuscripts and guidance to improve my English writing skill. Alfons and Arnout, for both of you, it has been a great honor for me to work under their supervision. I thank you both from the core of my heart. I cannot wish for better supervisors. I hope to keep collaborations with you in my future research.

Also, I would like to thank Majorlein for collaborating and contributing computer simulation results in two chapters in this thesis, and critical reading of my thesis. I also thank René, Laura and Marijn for many fruitful insight from the theoretical point of view and introductory talks with which I started to understand and explore the mechanism shielded behind the experimental phenomenon.

Next, I would like to express my gratitude to my officemates during the last four and a half years in Room 056, L.S. Ornsteinlaboratorium. Peter, Esther, Bas, Matthew, Linh, Henriëtte,

Rik, thanks for all keeping up with me with a very cozy atmosphere. With your accompany, I spend my most beautiful four and a half years abroad; with your help, this thesis could be smoothly going to the end; and with your pleasant conversation, I start to learn a totally different (for me) life, a Dutch way of life. I cannot wish for better roommates. A special thanks to Bas, with who I shared this office with the largest overlap in time, thanks for reading some of my manuscripts and critical commends both in science and language, and translating the summary of my thesis into Dutch, and also for your patience (at the beginning of my study) in explaining me the 'tedious' theory. I will not forget our first cooperative experiment in the preparation of chemical garden, although, it was failed in the end. We believe we can definitely success at our second trial.

Moreover, I would like to extend my gratitude to my collaborators inside and outside Soft Condensed Matter group in Utrecht University. Rao, thanks for our collaboration on flexible strings and sharing your knowledge. Ernest, thank you as my master student and for contributing your semi-flexible PMMA string results to our first paper. Johan, my dear friend, I appreciate for your great help in both of scientific and non-scientific life. Your shared experimental experience and advises did save me a lot of unnecessary exploration time in research. I am also thankful for your contributions to my Chapter 3, which will publish soon. In addition, your teaching in the decoration of my newly rented apartment is a precious wealth from which I benefit all my life. Ahmet, thanks for introducing me the density gradient method and sharing your knowledge about titanium particles synthesis. Anke, thank you for sharing your experience about silica rod preparation, which is extremely vital for one of my most important work presented in Chapter 9. Bart, thanks for your contribution on 3D imaging of silica rods and our collaboration also with Marlous on patched silica rods. Joost, I benefit a lot from your surface adsorption free energy calculation and your preciseness research style. You deserve a great thank for your patient introduction and explanation about your theory and models, and your proficiency of Mathematica always extricated me from troubles. Thijs, collaboration with you on plastic crystals was a nice experience. I thank for your shared calculation results, and for testing and further developing the algorithm of silica rods which was originally written by Michiel. Frank, the experience of our perfect collaboration cluster of dumbbell and snowman shaped particles was memorable. Hopefully, our work can publish soon.

A small Chinese subdivision of our group is obliged, our unforgettable memory is not only restricted in science, but also in normal life, a frequent party held in turn with Ran, Weikai, Tiansong, Da and their wives (if applicable) at various places is wonderful. Actually, we have successfully shifted the group lunch site from the canteen in Minneart to our coffee corner.

List of Publications

This thesis is based on the following publications:

- Bo Peng, Ernest van der Wee, Arnout Imhof and Alfons van Blaaderen, *Synthesis of Monodisperse, Highly Cross-Linked, Fluorescent PMMA Particles by Dispersion Polymerization*, *Langmuir* **2011**, *28*, 6776-6785. (Chapter 2)

- Bo Peng, Johan Stiefelhagen, Alfons van Blaaderen and Arnout Imhof, *A General Approach towards Monodisperse Hollow Polymer Particles with Tunable Structures,* submitted. (Chapter 3)

- Bo Peng, Alfons van Blaaderen and Arnout Imhof, *Surface Morphology Control of Cross-Linked Polymer Particles via Dispersion Polymerization*, submitted. (Chapter 4)

- Bo Peng, Hanumantha Rao Vutukuri, Alfons van Blaaderen and Arnout Imhof, *Synthesis of Fluorescent Monodisperse Non-Spherical Dumbbell-Like Model Colloids*, *Journal of Materials Chemistry* **2012**, *22*, 21893-21900. (Chapter 5)

- Bo Peng, Alfons van Blaaderen and Arnout Imhof, *Direct Observation of the Formation of Liquid Protrusions on Polymer Colloids and their Coalescence*, submitted to *ACS Applied Materials & Interface*. (Chapter 6)

- Bo Peng, Frank Smallenburg, Marjolein Dijkstra, Arnout Imhof and Alfons van Blaaderen, *Colloidal Clusters made using Emulsions and Dumbbell Particles: Experiments and Simulations*, submitted to *Journal of the American Chemical Society*. (Chapter 7)

- Bo Peng, Ahmet Demirörs, Thijs Besseling, Alfons van Blaaderen and Arnout Imhof, *Plastic Crystals of Long-Ranged Repulsive Dumbbell-Shaped Colloids*, in preparation. (Chapter 8)

- Bo Peng, Joost de Graaf, Bart de Nijs, Marjolein Dijkstra, René van Roij, Alfons van Blaaderen and Arnout Imhof, *Site-Specific Growth of Polymer on Bullet-Shaped Silica Rods*, submitted to *Angewandte Chemie International Edition*. (Chapter 9)

Other publications:

- Bo Peng, Min Chen, Shuxue Zhou, Limin Wu, Xiaohua Ma, *Fabrication of Hollow Silica Spheres using Droplet Templates Derived from a Miniemulsion Technique*, *Journal of Colloid and Interface Science* **2008**, *321*, 67-73.

• Hanumantha Rao Vutukuri, Ahmet Faik Demirörs, Bo Peng, Peter van Oostrum, Arnout Imhof and Alfons van Blaaderen, *Colloidal Analogues of Charged and Uncharged Polymer Chains with Tunable Stiffness*, *Angewandte Chemie International Edition*, **2012**, *51*, 11249-11253.

• Ziwei Deng, Haibao Zhu, Bo Peng, Hong Chen, Yuanfang Sun, Xiaodong Gang, Pujun Jin and Juanli Wang, *Synthesis of PS/Ag Nanocomposite Spheres with Catalytic and Antibacterial Activities*, *ACS Applied Materials & Interfaces* **2012**, *4*, 5625-5632.

Curriculum Vitae

Bo Peng was born on 9 February, 1983 in Dezhou, Shandong province, China. He graduated from Dezhou No. 2 middle school in 2001, after which he started him study on Marine Engineering at Dalian Maritime University. After one year study, he decided to shift focus to Chemistry, from which he obtained his bachelor's degree in 2005. In the same year, from September, he began his master study at Fudan University, and was majored in Material Chemistry and supervised by Prof. Limin Wu. As main part of the master project he worked on organic and inorganic composite ultrathin type fire-retardant coating for stainless steel, and preparation of high performs heavy-duty coating based on hybrid epoxy resin. Apart from coating research, he also contributed a paper on preparation of hollow silica spheres using droplet templates derived from a miniemulsion technique. In September 2008 he commenced his PhD position in the Soft Condensed Matter group headed by Prof. Alfons van Blaaderen at Utrecht University, the Netherlands, under supervision of Arnout Imhof and Alfons van Blaaderen. He presented his work as oral and poster contributions at several national and international conferences, including Physics@FOM, Dutch Polymer Day, Nanodirect Annual Meeting, Macro2010: 43rd IUPAC World Polymer Congress, the Jülich Soft Matter days, International Association of Colloid and Interface Scientists Conference. His research on the morphology and structure control of polymer and composite particles and their phase behavior is described in this thesis.